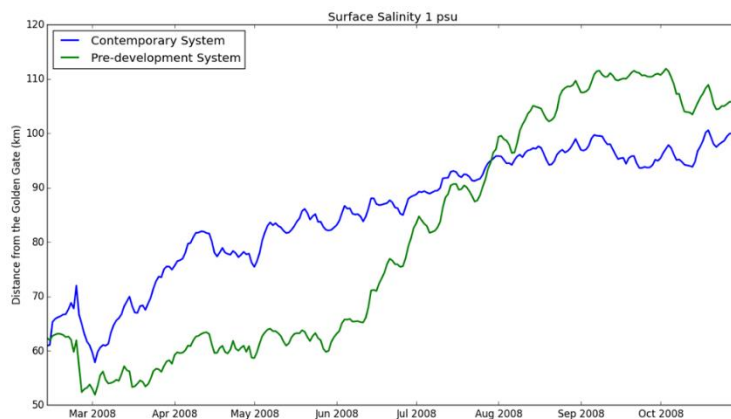
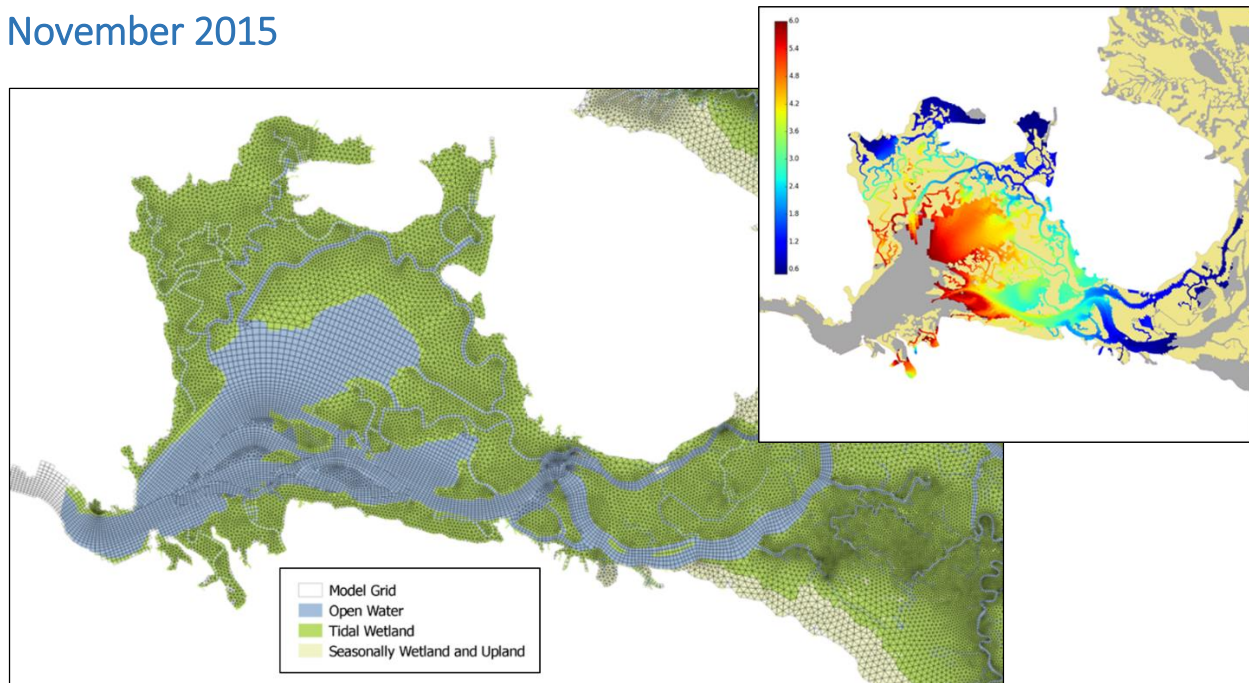


Hydrodynamic and Salt Transport Modeling of the Pre-Development Upper San Francisco Estuary

Phase 2 Technical Memorandum

MWD Task Order 01, Subtask 6, Agreement No. 143936

November 2015



Prepared For:
Metropolitan Water District of Southern
California
1121 L Street
Sacramento, CA 95814
Contact:
Paul Hutton, PhD, P.E.
phutton@mwdh2o.com
(916) 650-2620

Prepared By:
Resource Management Associates
4171 Suisun Valley Road, Suite J
Fairfield, CA 94534
Contact:
Stephen Andrews, PhD
steve@rmanet.com
(707) 864-2950

Executive Summary

Many changes have taken place in the Delta between the early 1800s and today, including channel deepening and straightening, levee construction, marsh removal, and inflow alterations in magnitude and timing, among others. In order to examine how these changes affected the physical characteristics of the estuary, 3-D hydrodynamic models of the system as it was in the early 1800s (the “pre-development” condition) and its current condition were constructed. The contemporary system model was created for the present-day channel configuration in the upper estuary and the present-day bathymetry. It was calibrated to observed flow and stage data from a network of continuous monitoring sites throughout the Bay and Delta. The pre-development system model was created to match the pre-development channel configuration in the upper estuary, as delineated by the San Francisco Estuary Institute (SFEI). SFEI and the University of California, Davis (UCD) collaborated to provide the historical data set for the model bathymetry. The pre-development model was calibrated by varying the marsh plain elevations in order to match sparse observed data points of tidal characteristics. These characteristics included tidal range in channels and marsh plain inundation depth and frequency, as well as broader metrics such as the extent of freshwater tidal habitat.

Model simulations were performed on the calibrated grids to examine calendar years 2006–2008. This period was chosen to represent recent hydrologic conditions associated with a relatively high flow year (2006) and a relatively low flow year (2008). Delta boundary flows were derived from observed and simulated data for the contemporary and pre-development systems, respectively. A simulation of pre-development boundary flows, provided by the California Department of Water Resources (CDWR), assumed contemporary unimpaired upstream hydrology to route runoff events through the Central Valley landscape as thought to exist prior to the land use changes of the past 150 years. A contemporary ocean water surface elevation record, shifted to account for sea level rise, was used for the pre-development simulation.

An isohaline analysis was performed to characterize the axial distance to the 2 psu bottom salinity location from the Golden Gate inlet (X2) as well as three additional surface isohalines. For both the pre-development and contemporary simulations, statistical regressions were developed to relate modeled isohaline locations to net Delta outflow. Results indicated only small differences in salinity response to outflow conditions, with the pre-development system X2 being slightly more sensitive to changes in net outflow than the contemporary system. When given the same inflows, results indicated that the X2 position in the contemporary and pre-development systems would be located within 5 km of each other 90% of the time.

Additional analyses were performed to examine the characteristics of the low salinity zone, differences in tidal prism upstream of Martinez, channel velocities, and source water distributions. Simulations of the low salinity zone show one that is more variable, with large tidal variations in spatial area, in the pre-development system. On average, the pre-development low salinity zone has the same volume as in the contemporary system, but has more area, exposing a greater amount of low salinity zone water to the photic zone.

An analysis of tidal prism upstream of Martinez showed only a small increase in tidal prism in the pre-development system. This finding is similar to that calculated by Gilbert (1917) in an analysis of the effects of marsh reclamation and hydraulic mining sedimentation. While the pre-development system has abundant marsh plain area available for inundation, dissipation of tidal energy over the marsh and through the sinuous channel network limits a significant increase in the volume of water that can be exchanged into the upper estuary. The contemporary system has 2% of the pre-development marsh plain area, but its straighter and deeper main channels help increase tidal prism.

An analysis of tidal velocities in channels showed the pre-development system to have relatively higher velocities on ebb tide than the contemporary system. This has implications for the transport of sediment and associated material into the estuary between the two systems. Finally, an analysis of source water showed the spatial extent of Sacramento River water to be significantly greater in the western, central, and south Delta regions in the contemporary system.

The analyses presented in this report quantitatively characterize differences that have taken place in the hydrodynamic and salinity environment of the San Francisco Estuary between the early 1800s and the present day. It is hoped these results will be used to inform management and restoration plans for today's estuary. A major product of this work, the calibrated 3-D hydrodynamic models of the pre-development and contemporary systems, will be useful to future investigations into different aspects of the physical systems.

Table of Contents

Executive Summary.....	i
Introduction	1
Motivation.....	1
Scope.....	2
Modeling Framework.....	3
Development and Calibration of the Contemporary San Francisco Estuary Model	6
Grid Development.....	6
Model Boundary Conditions	7
Calibration Simulations.....	12
Observed Data Sources.....	22
Calibration Results	24
Development and Calibration of the Pre-development San Francisco Estuary Model.....	35
Grid Development.....	35
Model Boundary Conditions	41
Historical Observed Data Sources.....	43
Calibration Simulations	45
Calibration Results	47
Simulation Runs for Analysis.....	53
Isohaline Analysis.....	59
Literature Review	59
Analysis Methods.....	62
Results.....	64
Isohaline Regression Analysis	64
Sacramento River and San Joaquin River X2 Regressions	72
X2 Regressions Using Net Delta Outflow Index	74
Delta Salinity Gradient Model: Regression Fit to Multiple Isohalines.....	78
Summary	86
Low-Salinity Zone Habitat Characteristics	87

Analysis Methods	87
Results	88
Upper Estuary Tidal Prism	92
Analysis Methods	92
Results	93
Channel Velocity Analysis	96
Analysis Methods	97
Results	98
Source Water Fingerprinting	101
Analysis Methods	101
Results	102
References	112
Appendix A: Specific Conductivity to Salinity Conversion Methods	117
Appendix B: Contemporary San Francisco Estuary Model Individual Flow Station Plots	119
Appendix C: Contemporary San Francisco Estuary Model Individual Stage Station Plots	150
Appendix D: Individual Isohaline Regression Plots	198

List of Figures

Figure 1 Contemporary San Francisco Estuary model grid.....	7
Figure 2 Contemporary San Francisco Estuary model grid bathymetry and boundary conditions.	11
Figure 3 Contemporary model river inflow boundary conditions, 2006–2008.....	13
Figure 4 Contemporary model river inflow boundary conditions, 2006–2008, log scale.	14
Figure 5 Contemporary model export flow boundary conditions, 2006–2008.....	15
Figure 6 Contemporary model inflow salinity boundary conditions, 2006–2008.....	16
Figure 7 Contemporary model stage boundary condition at Point Reyes, 2006–2008.	17
Figure 8 Contemporary model evaporation boundary conditions, 2006–2008.....	18
Figure 9 Contemporary model precipitation boundary conditions, 2006–2008.	19
Figure 10 Contemporary model net Delta outflow, 2006–2008.	20
Figure 11 Contemporary model total Delta NCD, 2006–2008.	21
Figure 12 Stations for contemporary Bay–Delta model flow and stage calibration.	23
Figure 13 USGS Polaris program salinity sampling locations. Map obtained from Polaris project page: http://sfbay.wr.usgs.gov/access/wqdata/overview/wherewhen/stnmap.html	24
Figure 14 USGS measured (left) and modeled (right) salinity transects for calibration period. ..	32
Figure 15 Continuation of Figure 14.	33
Figure 16 Continuation of Figure 14.	34
Figure 17 Comparison of observed X2 location based on USGS Polaris cruise data and model- predicted X2 location.	34
Figure 18 Pre-development model Phase 1 and Phase 2 upper estuary grid extents.	37
Figure 19 Pre-development model grid detail in north Delta.	38
Figure 20 Pre-development model grid detail in lower north Delta.	38
Figure 21 Pre-development model grid detail in the central Delta.....	39
Figure 22 Pre-development model grid detail in the south Delta.....	39
Figure 23 Pre-development model grid detail in Suisun Bay and Suisun Marsh.....	40
Figure 24 Pre-development model Suisun Bay and Marsh bathymetry.	40
Figure 25 Upper estuary section of the pre-development Delta grid. Boundary inflow locations are shown.	42
Figure 26 Pre-development model river inflows for calibration period in July 2008.....	46
Figure 27 Modeled pre-development Delta tidal range and point locations of historical observed data. Historical observed data sources are given in Table 7.	48
Figure 28 Modeled pre-development Delta tidal inundation frequency and point locations of historical observed data. Historical observed data sources are given in Table 7.	49
Figure 29 Spatial extent of modeled pre-development Delta tidal freshwater habitat (right) and historical habitat delineation map (left) from Whipple et al. (2012).	50

Figure 30 Modeled pre-development Delta marsh plain inundation depths and locations of historical observed data. Maximum modeled depths of water are shown for a spring tide period on the left and for a neap tide period on the right. Historical observed data sources are given in Table 7.....	51
Figure 31 Modeled higher high tide flooding patterns in the pre-development Delta (left) and conceptual representation from Whipple et al. (2012) (right).....	52
Figure 32 Modeled lower high tide flooding patterns in the pre-development Delta (left) and conceptual representation from Whipple et al. (2012) (right).....	52
Figure 33 Pre-development model river inflow boundary conditions, 2006–2008.	54
Figure 34 Pre-development model river inflow boundary conditions, 2006–2008, log scale.	55
Figure 35 Comparison of pre-development and contemporary Delta total net channel depletions, 2006–2008.	56
Figure 36 Comparison of pre-development and contemporary simulation net Delta outflow, 2006–2008.	57
Figure 37 Comparison of pre-development and contemporary simulation net Delta outflow, 2006–2008, log scale.	58
Figure 38 Contemporary (top) and pre-development (bottom) isohaline transect locations. Transect distances are given in km.....	63
Figure 39 Contemporary and pre-development simulation results of 2 psu daily-averaged bottom salinity. Average Sacramento and San Joaquin isohaline position is shown.....	67
Figure 40 Contemporary and pre-development simulation results of 1 psu daily-averaged surface salinity. Average Sacramento and San Joaquin isohaline position is shown.....	67
Figure 41 Contemporary and pre-development simulation results of 6 psu daily-averaged surface salinity. Average Sacramento and San Joaquin isohaline position is shown.....	68
Figure 42 Contemporary and pre-development simulation results of 2.64 mS/cm daily-averaged surface conductance. Average Sacramento and San Joaquin isohaline position is shown.....	68
Figure 43 Contemporary system simulation 2 psu bottom salinity regression and hydrodynamic model time series comparison (top) and regression fit (bottom). Model-calculated outflow at Martinez is used for the independent outflow variable, Q	69
Figure 44 Pre-development system simulation 2 psu bottom salinity regression and hydrodynamic model time series comparison (top) and regression fit (bottom). Model-calculated outflow at Martinez is used for the independent outflow variable, Q	70
Figure 45 X2 isohaline response to 2006 contemporary simulation net Delta outflows.	71
Figure 46 X2 isohaline response to 2006 pre-development simulation net Delta outflows.....	71
Figure 47 Contemporary system simulation San Joaquin River X2 regression and hydrodynamic model time series comparison. Model-calculated outflow at Martinez is used for the independent outflow variable, Q	73

Figure 48 Pre-development system simulation San Joaquin River X2 regression and hydrodynamic model time series comparison. Model-calculated outflow at Martinez is used for the independent outflow variable, Q .	74
Figure 49 Comparison of contemporary simulation NDOI (black line) and model-predicted outflow at Martinez (magenta line).	76
Figure 50 Comparison of pre-development simulation NDOI (black line) and model-predicted outflow at Martinez (magenta line).	76
Figure 51 Contemporary system simulation X2 regression and hydrodynamic model time series comparison. NDOI is used for the independent outflow variable, Q .	77
Figure 52 Pre-development system simulation X2 regression and hydrodynamic model time series comparison. NDOI is used for the independent outflow variable, Q .	77
Figure 53 Contemporary simulation S_0 calculated values and regression model fits for stations at 5 km intervals along the salinity transect.	82
Figure 54 Pre-development simulation S_0 calculated values and regression model fits for stations at 5 km intervals along the salinity transect.	83
Figure 55 Contemporary system simulation DSG regression and hydrodynamic model time series comparison. Model calculated flow at Martinez is used for the outflow variable, Q .	84
Figure 56 Pre-development system simulation DSG regression and hydrodynamic model time series comparison. Model calculated flow at Martinez is used for the outflow variable, Q .	84
Figure 57 Contemporary system simulation DSG regression and hydrodynamic model time series comparison. NDOI is used for the outflow variable, Q .	85
Figure 58 Pre-development system simulation DSG regression and hydrodynamic model time series comparison. NDOI is used for the outflow variable, Q .	85
Figure 59 Volume, area, and average depth of the low-salinity zone for the pre-development and contemporary model simulations in 2008.	89
Figure 60 Low tide (left) and high tide (right) low salinity zone variation in the pre-development estuary. Gray areas indicate water with depth average salinity outside of the 0.5–6 psu zone. Beige areas indicate dry cells.	90
Figure 61 Volume, area, and average depth of the low-salinity zone for the pre-development and contemporary model simulations as a function of X2 location. Analysis period is 2008. In the lower two plots, points indicate daily average values; the daily range for each variable is shown as a line.	91
Figure 62 Tidal flow at Martinez. Positive flows are defined as the ebb direction.	94
Figure 63 Water volume upstream of Martinez. Solid lines show water volume in areas with a maximum depth greater than 0.5 m. Dashed lines show shallow water volume.	95
Figure 64 Locations of cross-sections for channel velocity analysis.	97
Figure 65 Cross-sectionally averaged velocity time series at Cache Slough at Ryer Island.	100

Figure 66 Simulated majority water source distributions on 1 March 2008 for contemporary system (left) and pre-development system. Dry cells are colored beige. Cells having shallow water are lightly colored.....	103
Figure 67 Simulated majority water source distributions on 1 May 2008 for contemporary system (left) and pre-development system. Dry cells are colored beige. Cells having shallow water are lightly colored.....	104
Figure 68 Simulated majority water source distributions on 1 July 2008 for contemporary system (left) and pre-development system. Dry cells are colored beige. Cells having shallow water are lightly colored.....	105
Figure 69 Individual water source relative concentrations for the contemporary model simulation, 1 March 2008. Cells with less than 5% of a given source water are colored gray. .	106
Figure 70 Individual water source relative concentrations for the pre-development model simulation, 1 March 2008. Dry cells are colored beige. Cells having shallow water are lightly colored. Cells with less than 5% of a given source water are colored gray.	107
Figure 71 Individual water source relative concentrations for the contemporary model simulation, 1 May 2008. Cells with less than 5% of a given source water are colored gray.....	108
Figure 72 Individual water source relative concentrations for the pre-development model simulation, 1 May 2008. Dry cells are colored beige. Cells having shallow water are lightly colored. Cells with less than 5% of a given source water are colored gray.	109
Figure 73 Individual water source relative concentrations for the contemporary model simulation, 1 July 2008. Cells with less than 5% of a given source water are colored gray.....	110
Figure 74 Individual water source relative concentrations for the pre-development model simulation, 1 July 2008. Dry cells are colored beige. Cells having shallow water are lightly colored. Cells with less than 5% of a given source water are colored gray.	111
Figure 75 Contemporary system simulation 1 psu surface salinity regression and hydrodynamic model time series comparison (top) and regression fit (bottom). Model-calculated outflow at Martinez is used for the independent outflow variable, Q	198
Figure 76 Pre-development system simulation 1 psu surface salinity regression and hydrodynamic model time series comparison (top) and regression fit (bottom). Model-calculated outflow at Martinez is used for the independent outflow variable, Q	199
Figure 77 Contemporary system simulation 6 psu surface salinity regression and hydrodynamic model time series comparison (top) and regression fit (bottom). Model-calculated outflow at Martinez is used for the independent outflow variable, Q	200
Figure 78 Pre-development system simulation 6 psu surface salinity regression and hydrodynamic model time series comparison (top) and regression fit (bottom). Model-calculated outflow at Martinez is used for the independent outflow variable, Q	201

Figure 79 Contemporary system simulation 2.64 mS/cm surface EC regression and hydrodynamic model time series comparison (top) and regression fit (bottom). Model-calculated outflow at Martinez is used for the independent outflow variable, Q 202

Figure 80 Pre-development system simulation 2.64 mS/cm surface EC regression and hydrodynamic model time series comparison (top) and regression fit (bottom). Model-calculated outflow at Martinez is used for the independent outflow variable, Q 203

List of Tables

Table 1 Contemporary model river inflow boundary condition data sources. 9

Table 2 Contemporary model wind boundary condition data sources..... 10

Table 3 Contemporary model evaporation and precipitation boundary condition data sources. 10

Table 4 Contemporary model calibration simulation temporary barrier installation and removal dates..... 12

Table 5 Contemporary San Francisco Estuary model flow accuracy metrics. 26

Table 6 Contemporary San Francisco Estuary model stage accuracy metrics. USGS stations indicated with an asterisk had data measured relative to an arbitrary vertical datum and were shifted by constant values to match average computed values at that location. 28

Table 7 Historical observations of tidal range and marsh plain inundation characteristics. 44

Table 8 Individual isohaline regression fit statistics. Average Sacramento and San Joaquin isohaline position and hydrodynamic model calculated outflow at Martinez were used as inputs for the analysis..... 66

Table 9 Individual X2 regression fit statistics for the Sacramento River, San Joaquin River, and the averaged position. Estuary outflow is estimated as model-predicted outflow at Martinez. 73

Table 10 Individual X2 regression fit statistics for the Sacramento River, San Joaquin River, and the averaged position. Estuary outflow is estimated using NDOI..... 75

Table 11 Contemporary system simulation S_0 model fitting parameters. Aggregate fit parameters were calculated using stations 40–70..... 80

Table 12 Pre-development system simulation S_0 model fitting parameters. Aggregate fit parameters were calculated using stations 40–55..... 80

Table 13 Delta Salinity Gradient model regression fit statistics for the Sacramento River, San Joaquin River, and the averaged position. Estuary outflow is estimated using model calculated outflow at Martinez. 81

Table 14 Delta Salinity Gradient model regression fit statistics for the Sacramento River, San Joaquin River, and the averaged position. Estuary outflow is estimated using NDOI. 81

Table 15 Tidal prism comparison by month. 94

Table 16 Tidal velocity, period, and excursion statistics. Shorter periods and higher absolute maximum velocities associated with ebb tide are highlighted yellow to indicate ebb dominance. Shorter periods and higher absolute maximum velocities associated with flood tide are highlighted blue to indicate flood tide dominance. 99

Table 17 Source waters for inflows groups for fingerprinting analysis. 101

Table 18 Salinity conversion method sensitivity analysis. 118

Introduction

This technical memorandum summarizes Phase 2 of RMA's investigation into the hydrodynamics and salinity regime of the pre-development San Francisco Estuary system. The remainder of this section introduces and provides context and motivation for the study. The following sections detail the modeling framework used to investigate the physical environment of the pre-development and contemporary estuary systems, and the work done to calibrate each model. Throughout this memorandum, the terms "pre-development" and "natural" are used interchangeably. To compare the salinity regimes of the two systems, long term model simulations were performed and a statistical analysis of isohaline position dependence on net Delta outflow was conducted. Specifics of the simulation boundary conditions, isohaline analysis methods, and analysis results are presented in separate sections. Four additional aspects of the physical system, of relevance to conditions experienced by aquatic organisms, were chosen for further analysis: the characteristics of the low salinity zone habitat, the tidal prism of the upper estuary, maximum in-channel velocities, and source water distributions. The final sections of the report present the methods and results of these analyses.

Motivation

The San Francisco Estuary is the largest estuary on the Pacific Coast of the United States, and a watershed covering 40% of the area of California drains to the estuary (Kimmerer 2004). Many changes to the estuary and watershed have taken place since the gold rush period of the 1840s. These include Delta channel straightening and deepening, channel cross-cut construction, marsh plain removal, levee construction, island flooding, land use changes to the Central Valley and upper watersheds, dam construction, diversion installations, gate and barrier installation, sea level rise, and the effects of sediment flux from the hydraulic mining era on channel bathymetry. Recent work has attempted to quantify aspects of landscape change in the Delta and infer the effects of these changes on the ecological functions provided by the Delta (SFEI 2014). But very little has been done in the way of assessing hydrodynamic and salinity changes. The need for such an assessment is clear, and calls have been made for this investigation. In one example, Enright et al. (2013) mention "The northern reach of the San Francisco estuary contains hundreds of modified or disconnected terminal tidal sloughs where the current and temperature regime is probably considerably changed. A proper characterization of the change would require sophisticated modeling." The focus of this study is to quantitatively assess the impacts of changes in the San Francisco Estuary over the last 200 years using detailed hydrodynamic modeling. It is hoped this work will shift the focus from qualitative and anecdotal assessments of pre-development estuary function to the results of quantitative investigations.

Scope

This report represents the product of RMA's contribution to the second phase of a larger investigation of the pre-development San Francisco Estuary system. The project is a joint effort between RMA, Metropolitan Water District of Southern California (MWD), the San Francisco Estuary Institute (SFEI), the University of California, Davis (UCD), the California Department of Water Resources (CDWR), and individuals at California Polytechnic State University at San Luis Obispo, MWH, and independent consulting firms. In addition to performing the initial studies characterizing the ecology and physical habitats of the pre-development Delta, SFEI was responsible for translating historical observations into quantitative measurements of channel bathymetry and data points for model calibration (Whipple et al. 2012). UCD was responsible for creating the digital elevation model of the upper estuary (DEM). RMA was responsible for using the DEM to create a 3-D model representing the pre-development system, calibrating the model, and performing simulations to investigate the salinity and hydrodynamic regimes. CDWR was responsible for providing estimates of natural hydrology to be used as model boundary conditions. Their work relied on previous investigations of evapotranspiration of pre-development Central Valley vegetation (Howes et al. 2015) and the natural hydrology of the estuary watershed (Fox et al. 2015, MWH 2015). Progress of work done by SFEI, UCD, and CDWR are detailed in separate technical memorandums.

This work builds on the work that was done by RMA for Phase 1 of the pre-development estuary study (RMA 2014). A review of some of that work is covered herein where necessary. Specific Phase 2 task items that will be covered in this report include the expansion of the existing pre-development hydrodynamic model grid, calibration of the pre-development model to match historical observations, simulation of high flow and low flow water years for the pre-development and contemporary systems, an analysis of modeled salinity isohaline locations, and an analysis of additional hydrodynamic variables of interest.

Aspects of the physical system chosen for additional analysis focused on quantities of relevance to aquatic organisms or large scale marsh restoration, and were determined after discussions with experts on the San Francisco Estuary. An analysis of the volume, area, and depth characteristics of the low salinity zone was chosen because of its importance to fish and zooplankton. An analysis of tidal prism in the upper estuary was chosen because of its implications for large scale habitat restoration of the Delta. Differences in maximum channel velocities between the pre-development and contemporary systems were analyzed because of their implications for transport of sediment and associated material into and out of the estuary. Finally, a fingerprinting analysis of source water was performed because of its relevance to migratory fish.

Modeling Framework

The computational framework necessary for hydrodynamic modeling of the San Francisco Estuary includes several components: a model grid; a hydrodynamic model engine, along with the specified engine parameters; supporting methods for calculating time-dependent inputs to the engine which are not supplied natively; and boundary conditions.

The UnTRIM model (Casulli and Walters 2000; Casulli and Zanolli 2007) was chosen as the hydrodynamic engine for this work. UnTRIM uses the semi-implicit method to numerically solve the 3-D Reynolds-averaged Navier-Stokes equations for conservation of fluid volume and momentum to predict water velocities, water surface elevations, and scalar transport:

$$\frac{\partial u}{\partial x} + \frac{\partial v}{\partial y} + \frac{\partial w}{\partial z} = 0$$

$$\frac{\partial u}{\partial t} + u \frac{\partial u}{\partial x} + v \frac{\partial u}{\partial y} + w \frac{\partial u}{\partial z} - fv = -g \frac{\partial \eta}{\partial x} + \nu^h \left(\frac{\partial^2 u}{\partial x^2} + \frac{\partial^2 u}{\partial y^2} \right) + \frac{\partial}{\partial z} \left(\nu^v \frac{\partial u}{\partial z} \right)$$

$$\frac{\partial v}{\partial t} + u \frac{\partial v}{\partial x} + v \frac{\partial v}{\partial y} + w \frac{\partial v}{\partial z} + fu = -g \frac{\partial \eta}{\partial y} + \nu^h \left(\frac{\partial^2 v}{\partial x^2} + \frac{\partial^2 v}{\partial y^2} \right) + \frac{\partial}{\partial z} \left(\nu^v \frac{\partial v}{\partial z} \right)$$

$$\frac{\partial C}{\partial t} + \frac{\partial(uC)}{\partial x} + \frac{\partial(vC)}{\partial y} + \frac{\partial(wC)}{\partial z} = \frac{\partial}{\partial x} \left(K^h \frac{\partial C}{\partial x} \right) + \frac{\partial}{\partial y} \left(K^h \frac{\partial C}{\partial y} \right) + \frac{\partial}{\partial z} \left(K^v \frac{\partial C}{\partial z} \right)$$

where u , v , and w are the velocities in the x , y , and z directions, C is the scalar concentration, t is time, f is the Coriolis frequency, g is the acceleration of gravity, η is the free surface elevation, and ν and K are the eddy viscosities and diffusivities. Hydrostatic pressure is assumed in the vertical direction. This is not a requirement of the UnTRIM model, but the simplification is valid for the flow conditions modeled in this work and is applied for all simulations.

These equations are subject to the free surface boundary conditions:

$$\frac{\partial \eta}{\partial t} + \frac{\partial}{\partial x} \left[\int_{-h}^{\eta} u \, dz \right] + \frac{\partial}{\partial y} \left[\int_{-h}^{\eta} v \, dz \right] = 0$$

$$\nu^v \frac{\partial u}{\partial z} = \gamma_T (u_a - u), \quad \nu^v \frac{\partial v}{\partial z} = \gamma_T (v_a - v), \quad \text{at } z = \eta$$

where γ_T is the wind stress coefficient at the water surface, h is the water depth measured positive downward from a constant vertical datum, and u_a and v_a are the components of the wind velocity.

The bottom boundary condition is:

$$v^v \frac{\partial u}{\partial z} = \gamma_B u, \quad v^v \frac{\partial v}{\partial z} = \gamma_B v, \quad \text{at } z = -h$$

where γ_B is the bottom friction coefficient. In the implementation of UnTRIM for this project, the bed friction coefficient is specified as a function of the bed roughness height, following Gross (2009).

UnTRIM's numerical methods have evolved over the years from a 2-D, depth-averaged, Cartesian grid (TRIM) method (Casulli 1990) to the 3-D TRIM method (Casulli and Cheng 1992; Casulli and Cattani 1994) to its present 3-D unstructured grid method (Casulli and Walters 2000). Key attributes of the numerical method include the use of an unstructured orthogonal staggered Arakawa-C grid in the horizontal dimensions, z-layer vertical coordinates, a semi-implicit finite-difference/finite-volume approach, and the Eulerian-Lagrangian Method (ELM) for advection of momentum (Casulli 1990; Casulli and Walters 2000). The model allows for the relevant physical processes necessary for modeling estuarine transport and circulation to be taken into account; its accuracy has been verified for relevant test cases with analytical solutions (see for example, Casulli and Zanolli 2007).

UnTRIM is particularly well suited to wetting and drying simulations, allowing arbitrarily fast propagation of fronts, preserving non-negative water depth, and maintaining volume and scalar mass conservation to machine accuracy (Casulli 2009). The model was further extended to allow representation of subgrid scale bathymetry (Casulli and Stelling 2010), which allows bathymetry to be resolved at a higher resolution than the computational grid. This allows a more accurate representation of element volume and face area, leading to better estimates of fluid volume and momentum without requiring large increases in computational resources. A high-resolution flux-limiting method (Casulli and Zanolli 2005) is used for scalar transport; the specific limiter used in our applications is the Van Leer limiter (Van Leer 1974).

The UnTRIM model is provided as a computational engine with a Fortran-based application program interface (API) that allows users to supply engine parameters and customize their implementations of turbulence and boundary conditions. A vertical turbulence closure scheme was prescribed using the k- ϵ version of a Generic Length Scale (GLS) closure with stability functions from Kantha and Clayson (Rodi 1987; Umlauf and Burchard 2003; Kantha and Clayson 1994). Specific parameter values for the method were taken from Warner et al. (2005). No turbulence closure scheme was used in the horizontal.

Temperature was neglected in our applications as temperature gradients have a small effect on baroclinic pressure gradients relative to salinity gradients (Kimmerer 2004). Salinity was converted to water density in the model using the haline contraction coefficient

$0.78 \text{ kg m}^{-3} \text{ psu}^{-1}$. Wind forcing was considered and the wind drag coefficient was calculated using the method of Smith and Banke (1975). Bed friction was parameterized using a quadratic stress formula and specified bed roughness height, z_0 . The threshold minimum water depth for momentum equation to be solved was set at 1 cm for all simulations.

Development and Calibration of the Contemporary San Francisco Estuary Model

In order to accurately investigate differences between the pre-development and contemporary estuary systems, separate models must be developed for each. This section details the development and calibration of the contemporary San Francisco Estuary model. Both system models were developed using the same UnTRIM engine and modeling framework described in the previous section. The same approximate grid resolution was also used. The utility of this approach is that any impacts on the results due to numerical method and grid errors will be approximately the same for both simulations, removing this as a source of uncertainty in comparisons of model results. A calibrated contemporary system model also allows us to demonstrate that the modeling framework is sufficient to represent the relevant estuarine physics, as determined by comparison to an abundance of present-day data available for model evaluation.

Grid Development

An unstructured orthogonal grid of the present-day San Francisco Estuary and near-shore region was developed using the grid generation software, *Janet* (Lippert and Sellerhoff 2006) (Figure 1). The ocean boundary was chosen to be an arc approximately 50 kilometers from Golden Gate, in order to prevent reflection and interference of ocean stage boundary condition with the Pacific coast. The lateral extents of Delta channels were chosen to include tidally inundated areas and to approximately match the locations of data observation stations for use as boundary conditions, while extending far enough upstream to minimize tidal reflection from model boundaries. Flow-aligned quadrilateral elements were used for major channels and flow paths. Triangular elements were used for tidal flats, areas in between flow paths, transition areas between diverging or merging flow paths, and areas where there was no clear flow direction. Typical horizontal cell spacing was 150 m.

Subgrid bathymetry was set using a digital elevation model (DEM) of the San Francisco Estuary compiled from a large number of bathymetric surveys and integrated and distributed by CDWR (Wang and Ateljevich 2012). A large number of Delta channels are represented using 2 m resolution; the remainder of the DEM uses 10 m resolution. Modifications to the DEM were made to raise the land elevations within non-flooded Delta islands in order to prevent incorrect subgrid estimations of element volumes in cells adjacent to Delta levees. Subgrid bathymetry was set using 20 subedges per computational cell side.

A total of 54 layers were used to resolve the vertical scale; layer depths were 1 m for the surface layers (down to -20 m, NAVD88) and increased by 10% with depth. The resulting grid

consisted of 29,100 horizontal 2-D cells and approximately 300,000 active 3-D prisms during a typical simulation.

Model Boundary Conditions

The ocean water surface boundary condition was forced using time series data from the NOAA station 9415020 at Point Reyes. The station was chosen because of its proximity to the model ocean boundary and the results of previous simulations showing its use preserves important tidal constituent characteristics within the bay (Gross et al. 2009). Tidal elevations were prescribed without the use of a phase lag or amplification factor.

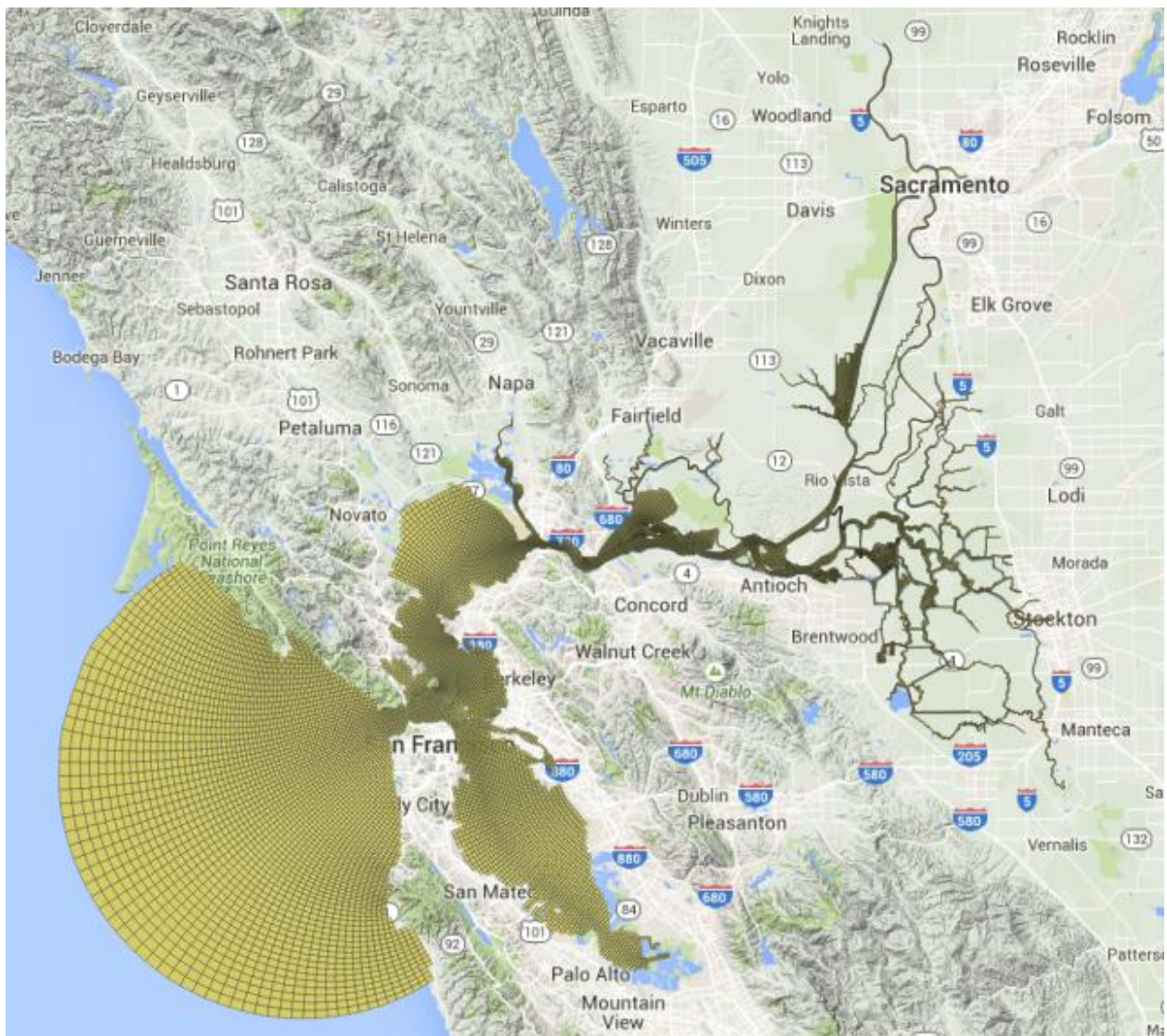


Figure 1 Contemporary San Francisco Estuary model grid.

Boundary conditions and hydraulic operations in the upper estuary were developed following those used in the RMA Bay-Delta Model (RMA 2005). Inflow boundary conditions were prescribed at the major riverine inflows to the estuary shown in Figure 2 and include the Sacramento, San Joaquin, Cosumnes, Mokelumne, Napa, and Calaveras Rivers, as well as the Yolo Bypass, Paradise Cut, and the Sacramento Regional Wastewater Treatment Plant discharge. The ocean boundary salinity was set to a constant 33.5 psu. River inflows were given time-varying salinities converted from measured specific conductivity measurements using the UNESCO equations (Fofonoff and Millard Jr. 1983). Boundary flow and specific conductivity time series data were obtained from nearby USGS and CDWR monitoring locations (Table 1). Major diversions from the Delta included those for the State Water Project (SWP), the Central Valley Project (CVP), Contra Costa Water District (CCWD) withdrawals at Old River and Victoria Canal, and the North Bay Aqueduct, and were prescribed at the locations shown in Figure 2 using data provided by CDWR.

While the UNESCO equations are useful for converting specific conductivity to salinity in waters where the majority of dissolved salts are ocean-derived, they may not be accurate in locations that are highly influenced by land-derived salts. In order to examine conversion errors, UNESCO-predicted salinities were compared to those predicted using the site-specific regressions suggested by CDWR (1986). Results are shown in Appendix A and focus on the area of the low salinity zone, because of its importance to this report's isohaline analysis. Conversion errors were generally between 5 and 10%, with the UNESCO equations generally predicting lower salinities for a given conductivity than the site specific equations. Because of the small differences in predicted salinity, the UNESCO conversion method was used for simplicity.

Wind speed and direction for calculation of the water surface stress was prescribed as constant within a local region surrounding each of the eight wind stations shown in Figure 2. Data were obtained from NOAA wind stations in the lower estuary and California Irrigation Management Information System (CIMIS) stations in the upper estuary (Table 2). Wind measurements from CIMIS stations taken at 2 m height were converted to 10 m height for use in the wind stress equations. Evaporation and precipitation were prescribed as constant within South Bay, Central and San Pablo Bays, and Suisun Bay based on adjacent CIMIS station data (Table 3, Figure 1). The total of local minor agricultural diversions, return flows, evaporation, precipitation, and groundwater seepage (collectively referred to here as net channel depletions, or NCD) was prescribed at 247 locations throughout the Delta based on data compiled by CDWR. NCD were applied at the closest 2-D element to the corresponding DSM2 computational nodes, at the bottom vertical layer. Hydraulic structure operations were prescribed at the Suisun Marsh Salinity Control Gates, the Delta Cross-Channel, Rock Slough, and seasonally for the south temporary Delta barriers at Old River at Tracy, Middle River, Grant Line Canal, and the head of Old River (Figure 1). Flows through each structure were implemented in the UnTRIM framework

by prescribing zero lateral flow between adjacent elements spanning the structure, calculating structure discharge using water surface elevations and weir and culvert equations (see for example, USACE 2010), and prescribing source/sink flows to the adjacent structure elements using an iterative method in order to avoid overshoots/undershoots in transferred volume.

The bed roughness heights (z_0) in the lower estuary and Suisun Bay were prescribed following Cheng et al. (1993) and Gross et al. (2009) as decreasing with the depth of the water column. z_0 values ranged from 0.1 mm at -10 m NAVD88 to 4 mm at 1 m NAVD88. The bed roughness height was prescribed as a constant 0.1 mm throughout the Delta and Suisun Marsh. This low value in the channels was required to balance the numerical diffusion of momentum inherent in the ELM method (Gross et al. 1999).

Table 1 Contemporary model river inflow boundary condition data sources.

River Inflow	Station Number and Name	Agency
Sacramento and American Rivers	11447650 Sacramento River at Freeport	USGS
San Joaquin River and Paradise Cut	11303500 San Joaquin River at Vernalis	USGS
Calaveras River	Mormon Slough at Bellota	USACE
Yolo Bypass High Flows	11453000 Yolo Bypass near Woodland	USGS
Yolo Bypass Toe Drain	Yolo Bypass at Lisbon Weir	CDWR
Mokelumne River	11325500 Mokelumne River at Woodbridge	USGS
Cosumnes River	11133500040 Cosumnes River at Michigan Bar	USGS
Napa River	11458000 Napa River at Napa	USGS

Table 2 Contemporary model wind boundary condition data sources.

Wind Region	Station Number and Name	Agency
Coastal Ocean	9415020 Point Reyes	NOAA
South Bay	9414523 Redwood City	NOAA
Central Bay	9414290 San Francisco	NOAA
San Pablo Bay	157 Point San Pedro	CIMIS
Suisun Bay	9415144 Port Chicago	NOAA
South Delta	47 Brentwood	CIMIS
Central Delta	140 Twitchell Island	CIMIS
North Delta	122 Hastings Tract	CIMIS

Table 3 Contemporary model evaporation and precipitation boundary condition data sources.

Evap/Precip Region	Station Number and Name	Agency
South Bay	171 Union City	CIMIS
Central and San Pablo Bays	157 Point San Pedro	CIMIS
Suisun Bay	123 Suisun Valley	CIMIS

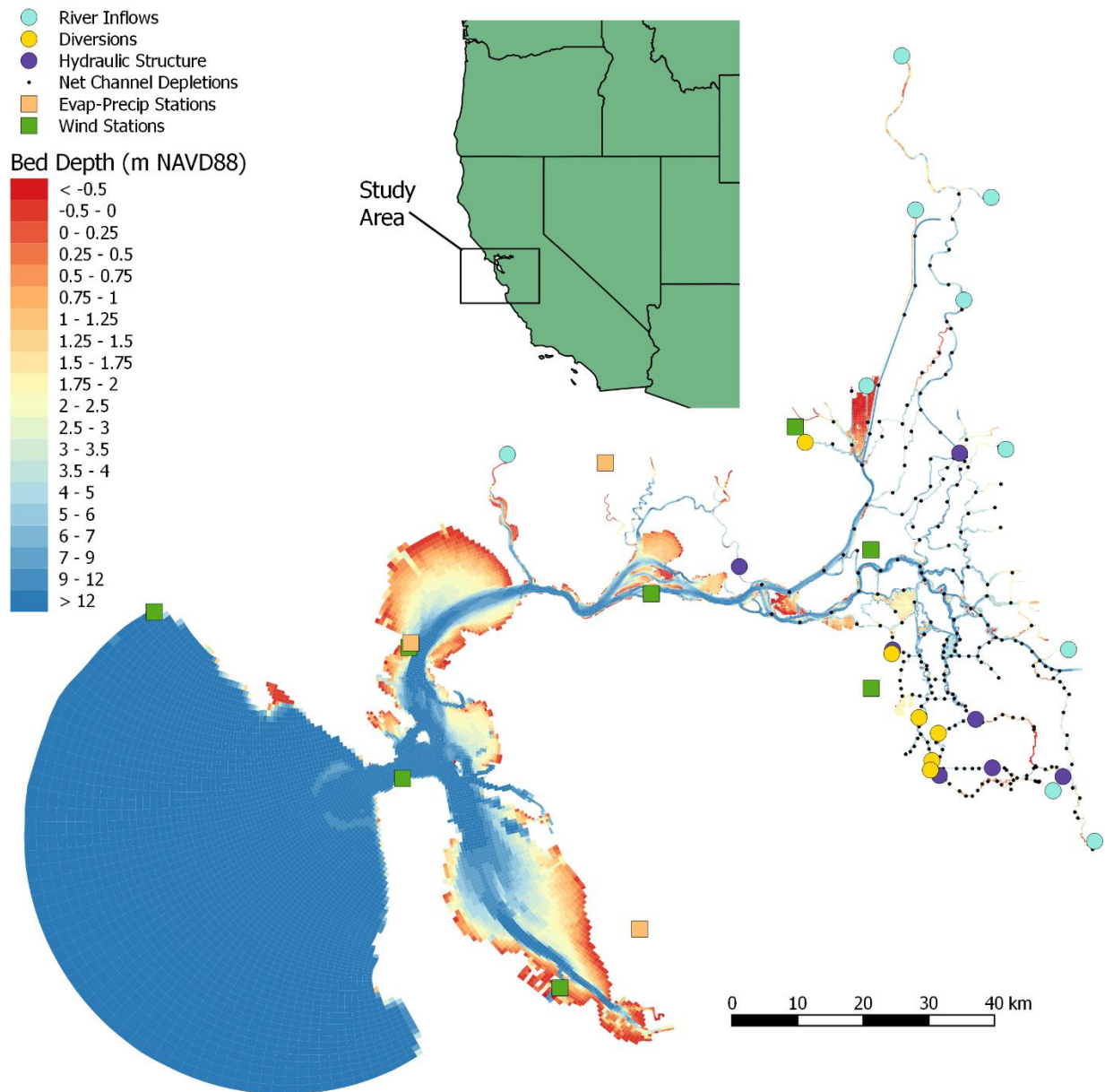


Figure 2 Contemporary San Francisco Estuary model grid bathymetry and boundary conditions.

Calibration Simulations

The calibration period for the contemporary San Francisco Estuary model was chosen as February 2006 through October 2008. The start date was chosen at high net Delta outflows in order to allow any effects due to incomplete knowledge of the initial 3-D salinity field to quickly wash out. The full three year period was chosen to encompass both a high flow year (2006) and a low flow year (2008) and coincide with the isohaline analysis time period. CDWR Water Year Hydrologic Classification Indices for the Sacramento Valley are listed as *wet*, *dry*, and *critical* for water years 2006, 2007, and 2008, respectively.

Stage, river inflow, export, and salinity boundary condition time series are shown in Figure 3 through Figure 7. Evaporation and precipitation boundary conditions are shown in Figure 8 and Figure 9. Net delta outflow for the simulation period is shown in Figure 10 and ranges from over 200,000 cfs in March 2006 to below 5,000 cfs in low flow periods during summer/fall 2007 and 2008. A time series of the total NCD for the Delta is shown in Figure 11. Table 4 gives the installation and removal dates of temporary barriers in the south Delta.

The initial condition water level was set at a constant value and all cells were given initial velocities of zero. The initial salinity field was prescribed based on Polaris cruise data and reset several hours after the start of the model simulation in order to allow the hydrodynamic effects of a “cold start” to dissipate before salinity was set.

Model calibration was carried out by making slight changes to the bed roughness heights, z_0 , from those suggested by Gross et al. (2009) and by modifying grid geometry to better capture flow splits and channel geometry in areas where problems were identified.

Table 4 Contemporary model calibration simulation temporary barrier installation and removal dates.

Year	Spring Head of Old River		Fall Head of Old River		Old River at Tracy		Middle River		Grant Line Canal	
	In	Out	In	Out	In	Out	In	Out	In	Out
2006	–	–	–	–	31 Jul	16 Nov	8 Jul	18 Nov	26 Jul	21 Nov
2007	26 Apr	22 May	18 Oct	10 Nov	23 Apr	7 Nov	10 Apr	20 Nov	11 May	8 Nov
2008	–	–	16 Oct	3 Nov	19 Jun	4 Nov	23 May	5 Nov	27 Jun	11 Nov

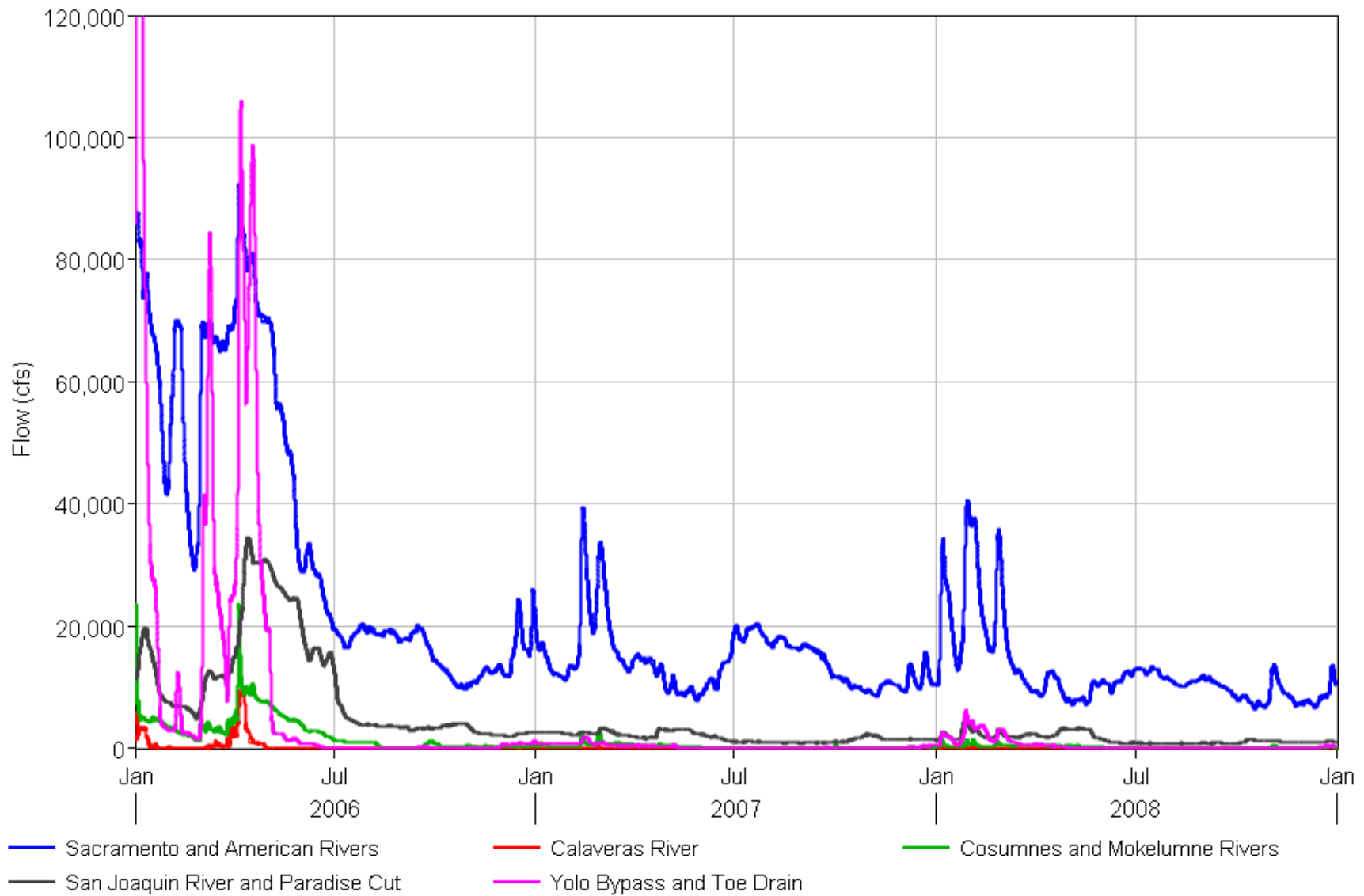


Figure 3 Contemporary model river inflow boundary conditions, 2006–2008.

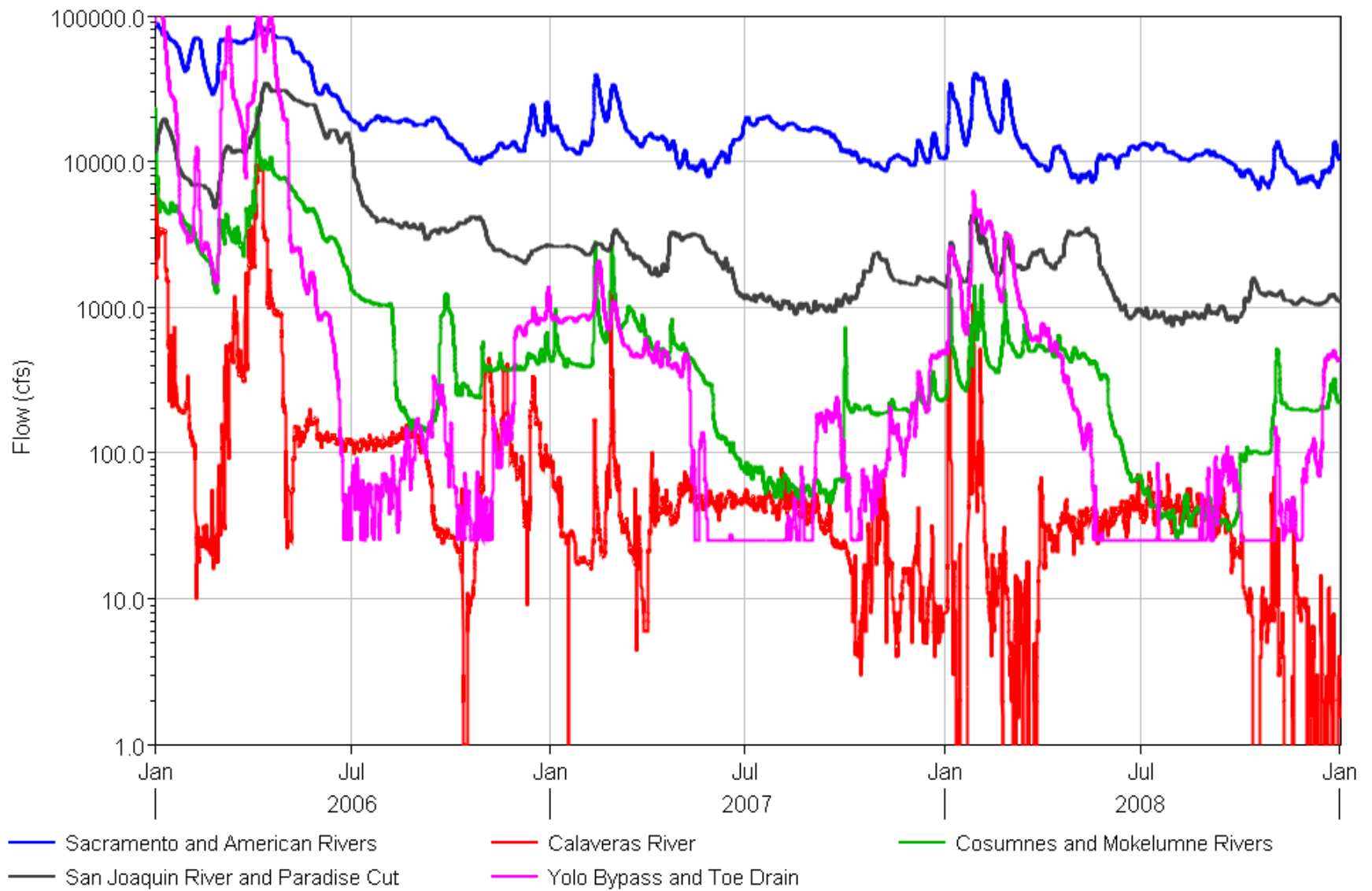


Figure 4 Contemporary model river inflow boundary conditions, 2006–2008, log scale.

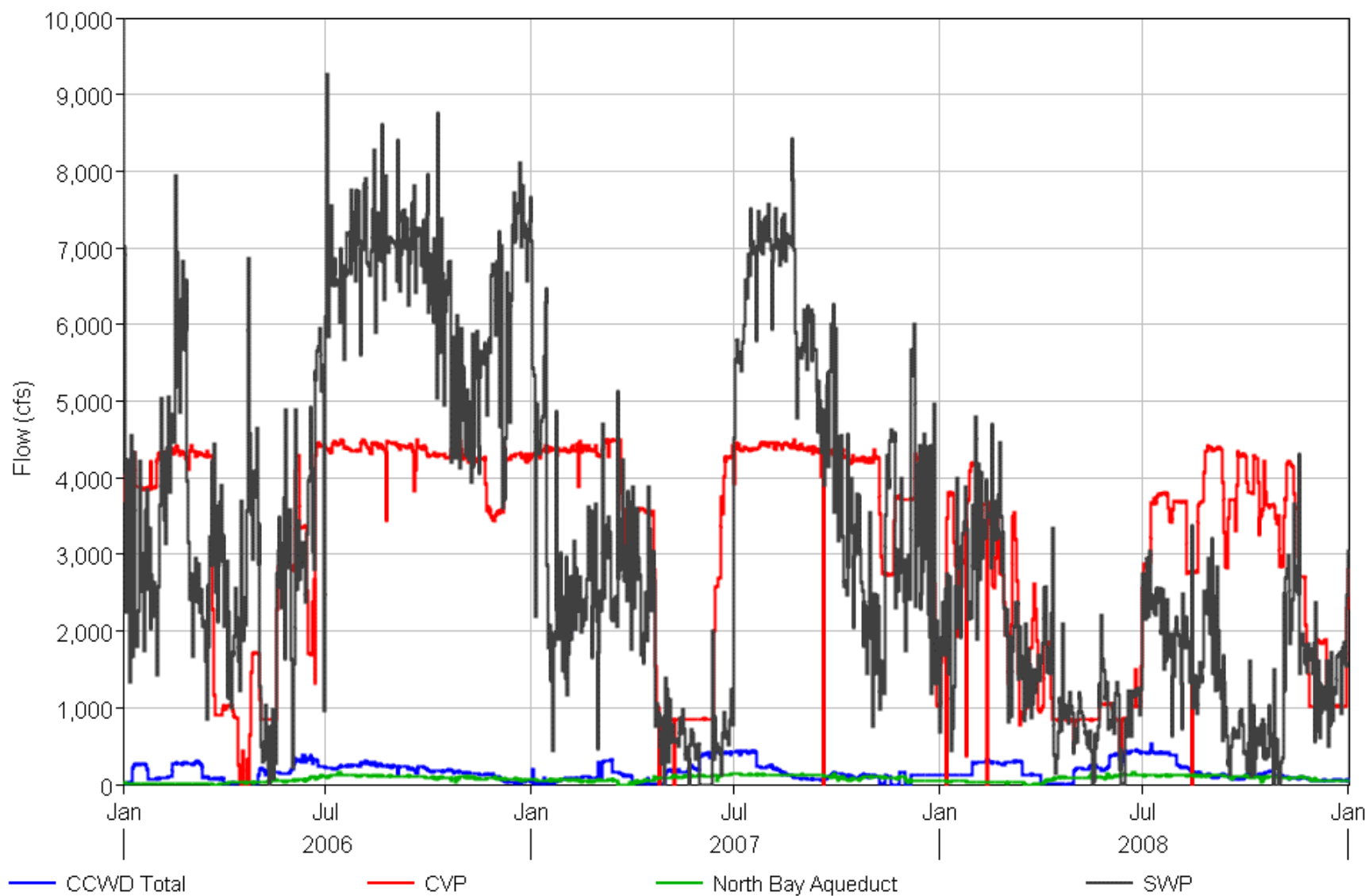


Figure 5 Contemporary model export flow boundary conditions, 2006–2008.

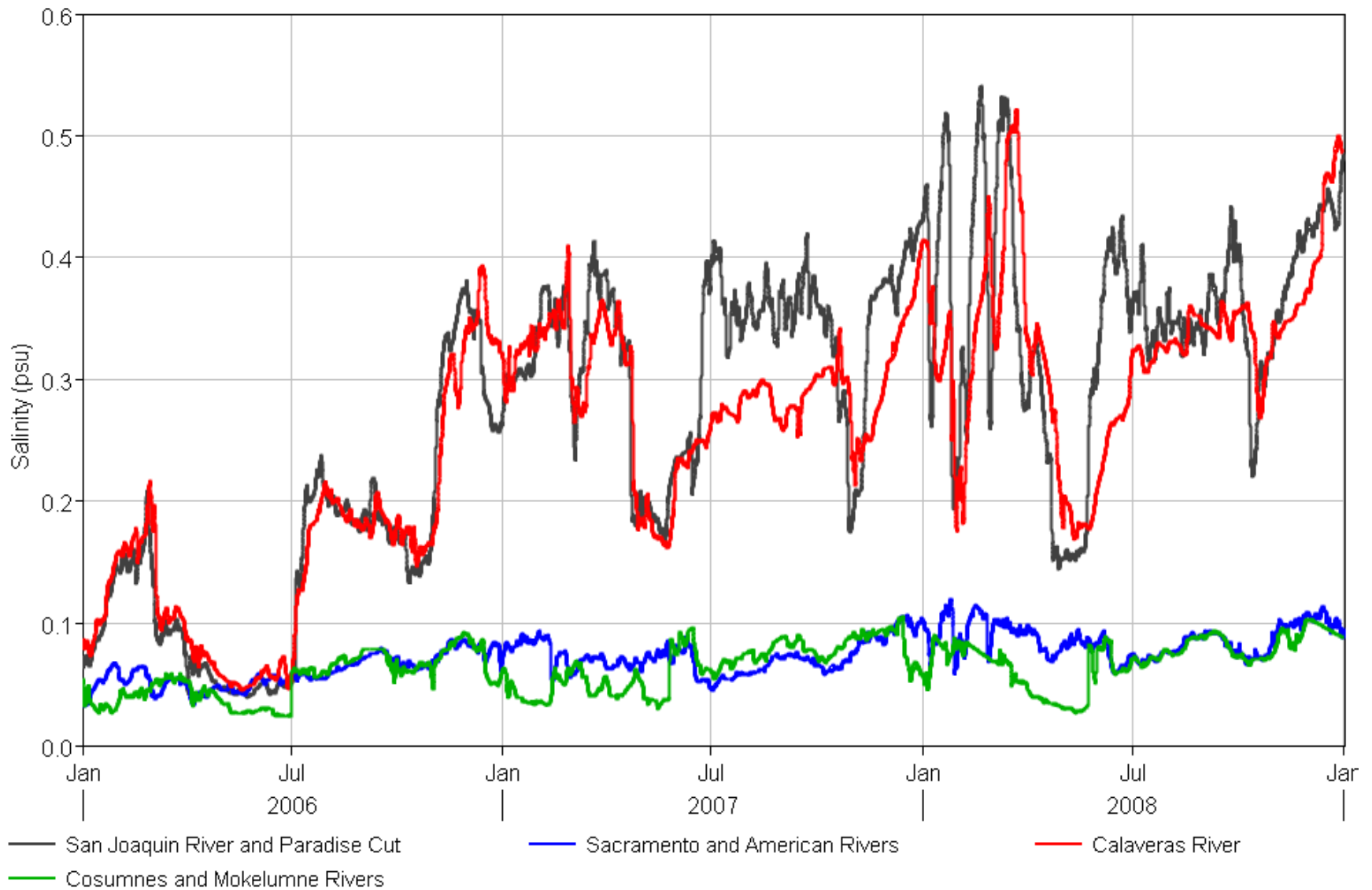


Figure 6 Contemporary model inflow salinity boundary conditions, 2006–2008.

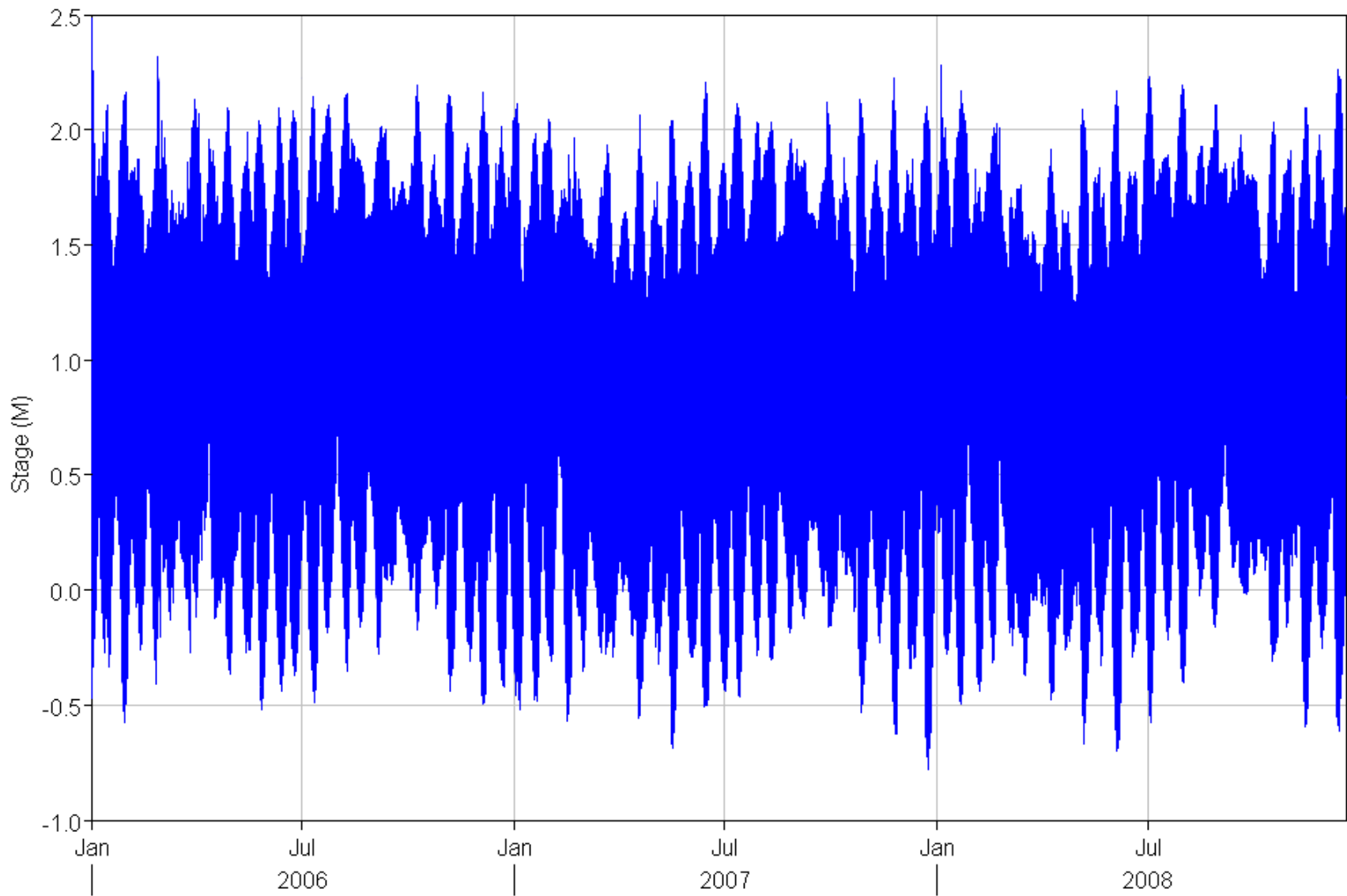


Figure 7 Contemporary model stage boundary condition at Point Reyes, 2006–2008.

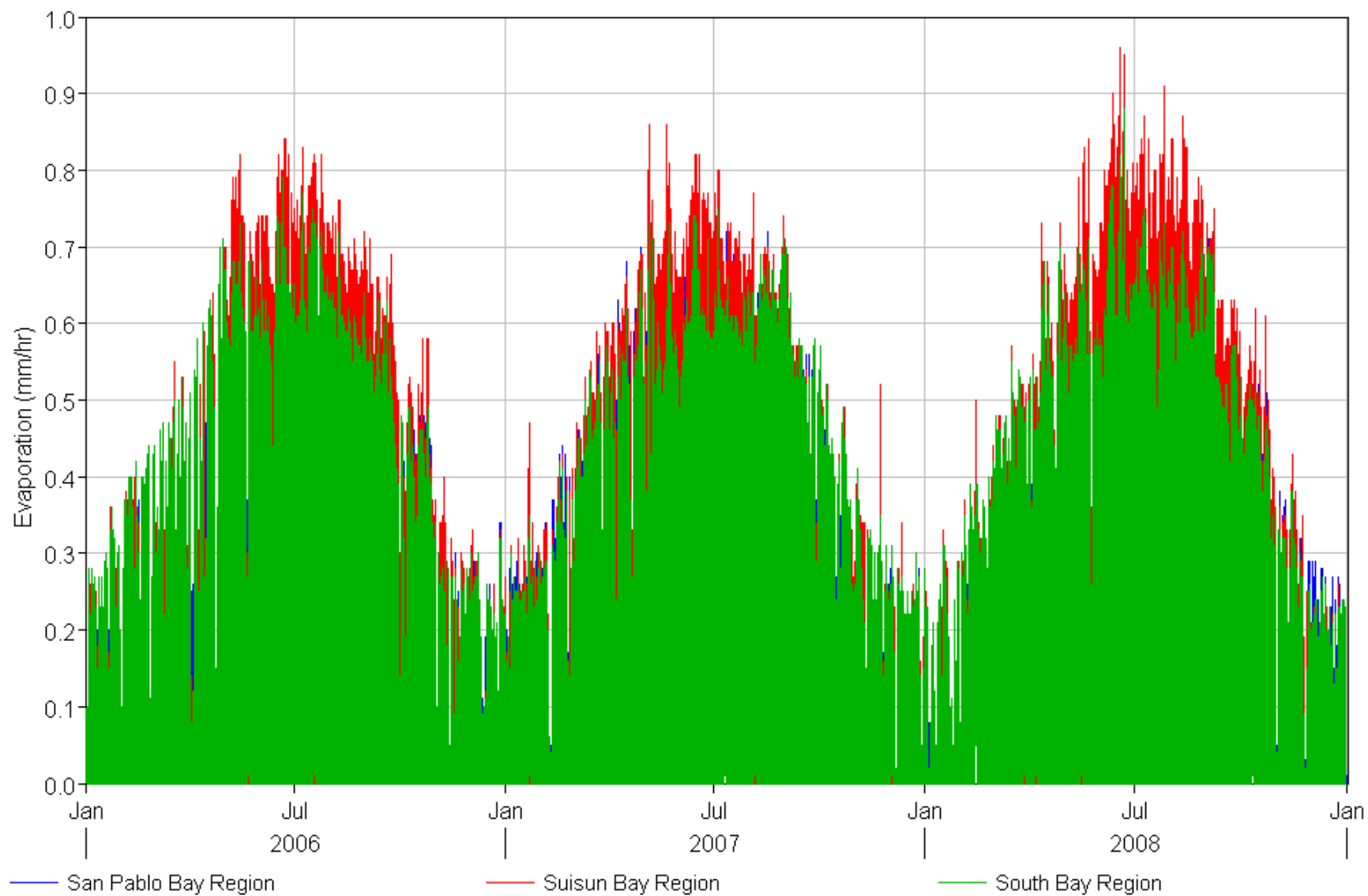


Figure 8 Contemporary model evaporation boundary conditions, 2006–2008.

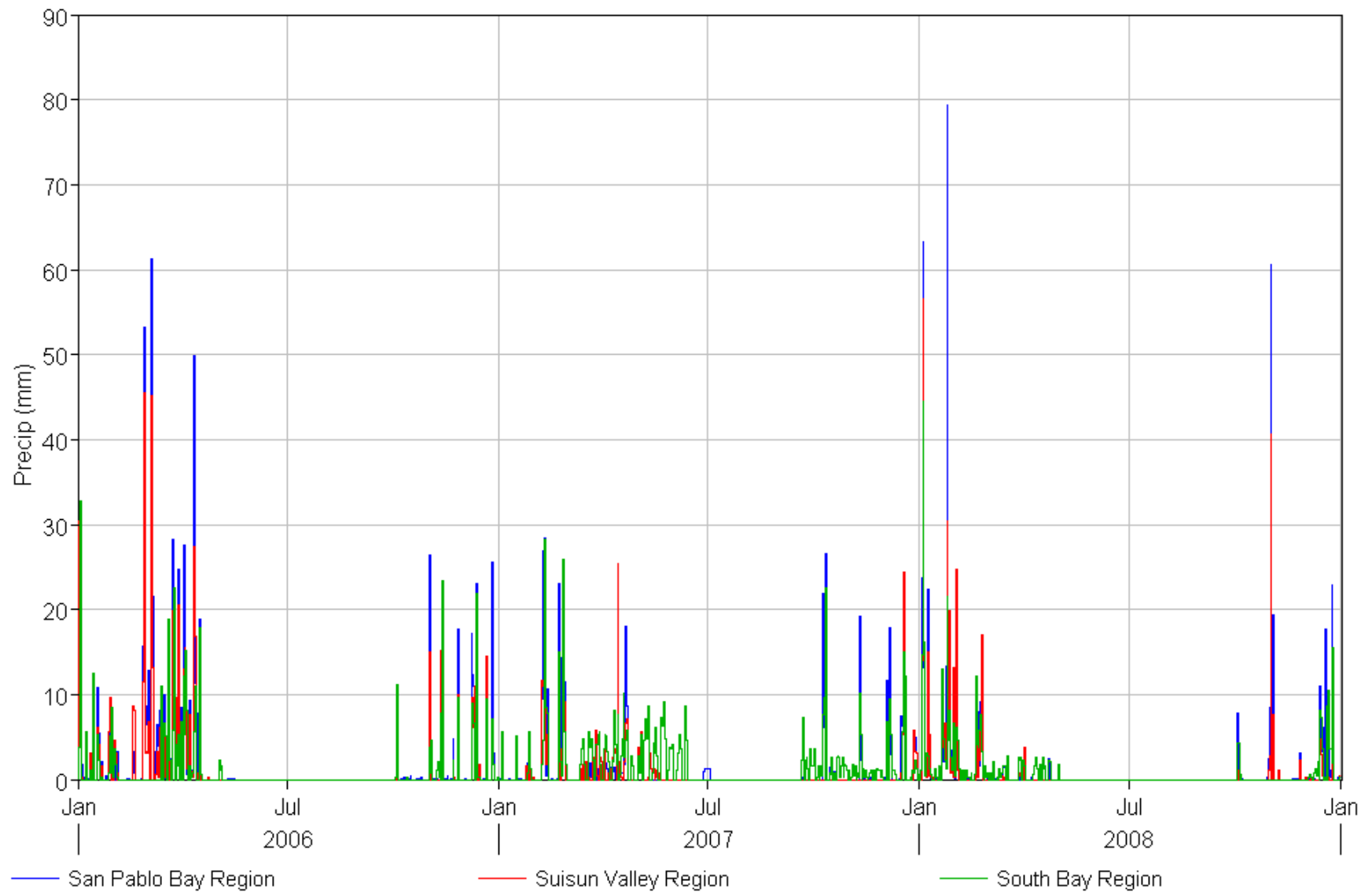


Figure 9 Contemporary model precipitation boundary conditions, 2006–2008.

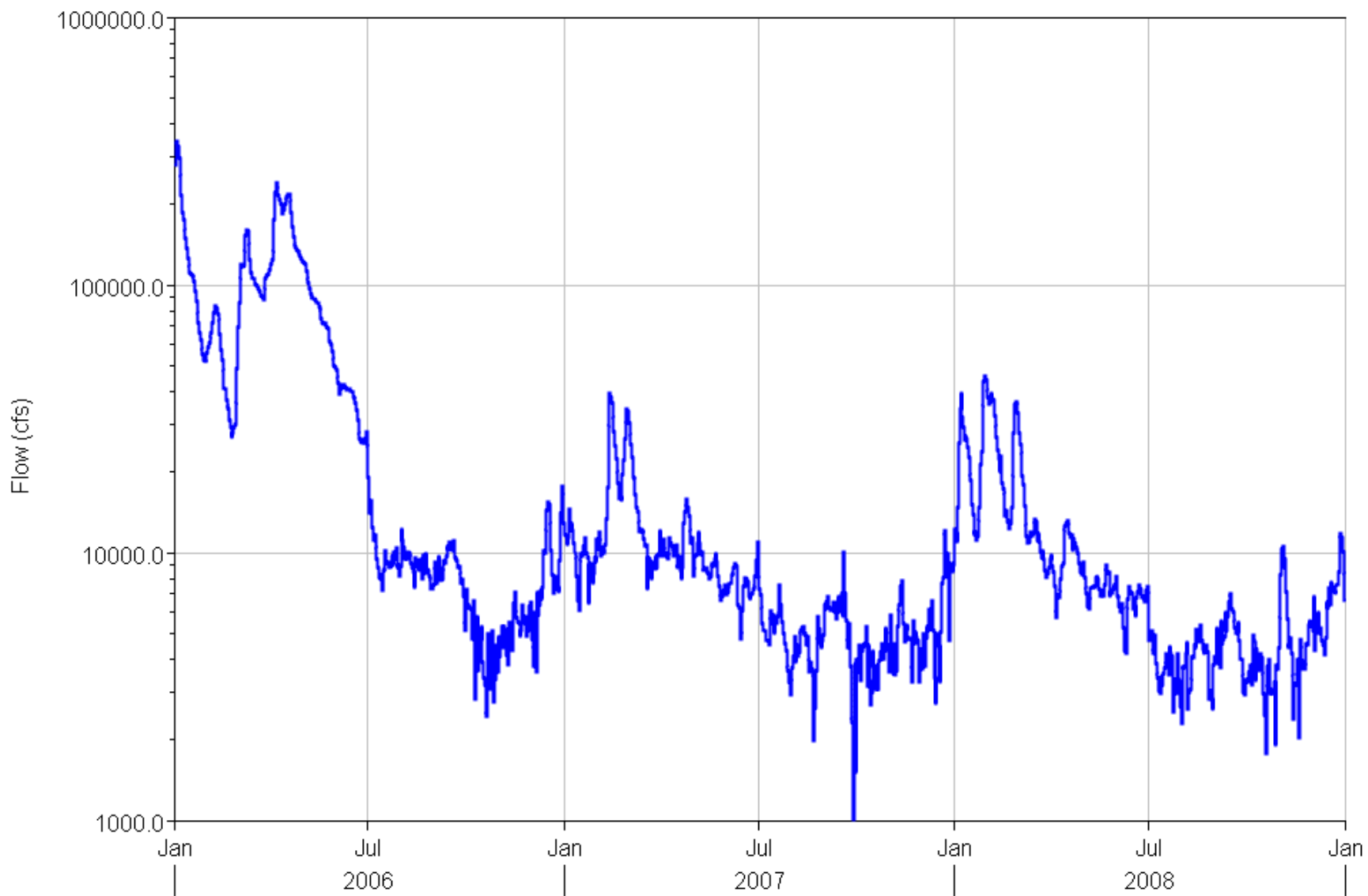


Figure 10 Contemporary model net Delta outflow, 2006–2008.

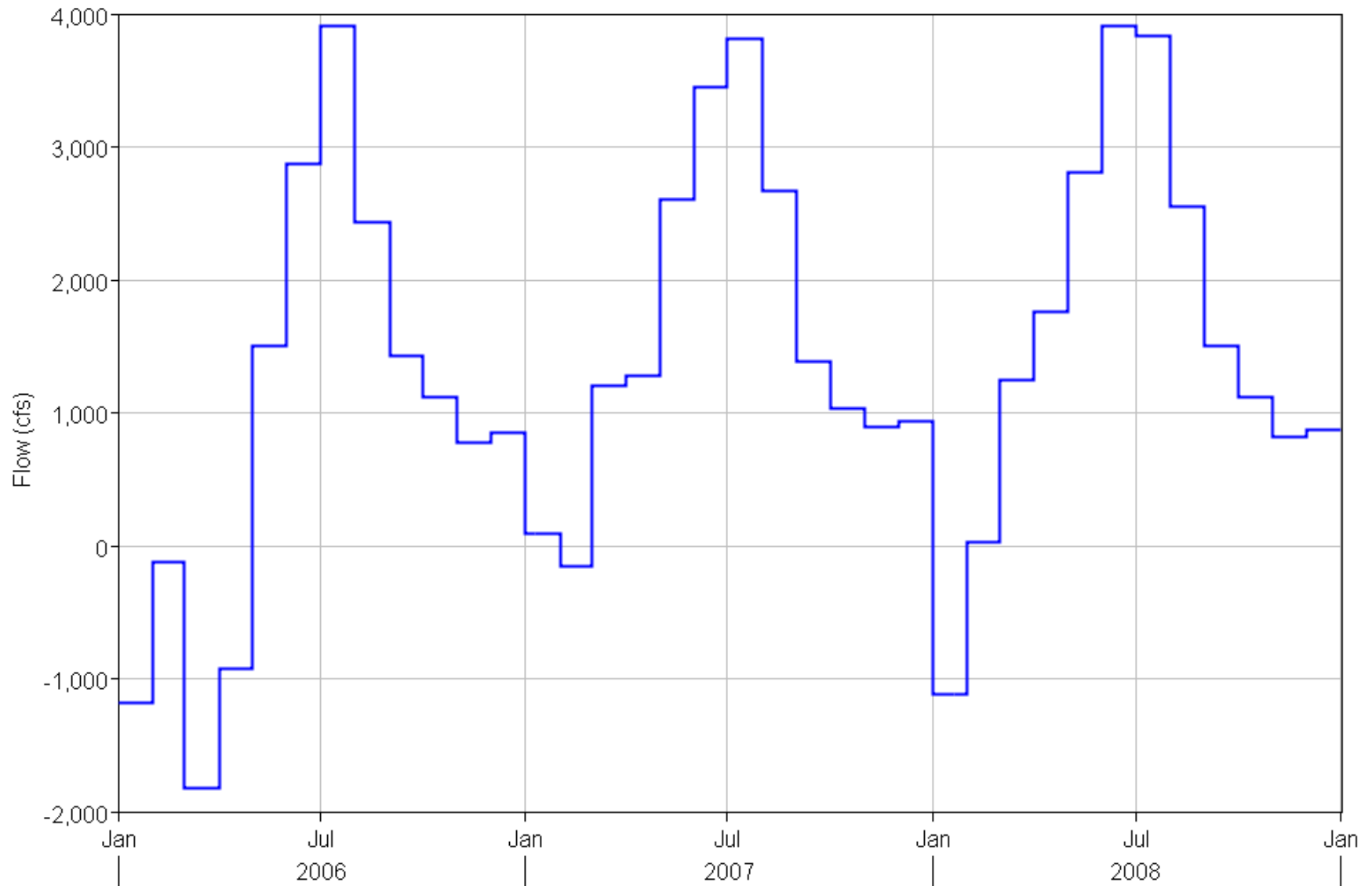


Figure 11 Contemporary model total Delta NCD, 2006–2008.

Observed Data Sources

Model output was compared against observed flow and stage data collected at an array of continuous monitoring stations throughout the estuary. The locations of these calibration stations are shown in Figure 12. Agencies responsible for collecting, performing quality control measures on, and distributing these data include the U.S. Geological Survey (USGS), California Department of Water Resources (CDWR), the U.S. Bureau of Reclamation (USBR), and the U.S. Army Corps of Engineers (USACE). Data were obtained either from the responsible agency's website or a data aggregation site such as the California Data Exchange Center (CDEC) and the Water Data Library.

Modeled salinity data were compared against observed values collected by the USGS Polaris project along a longitudinal transect from the Golden Gate upstream to Rio Vista (Figure 13). Longitudinal transects are taken at approximately monthly intervals in the fall, winter, and spring, and include 38 sampling locations. At each location, vertical salinity profiles are measured at 1 m intervals.

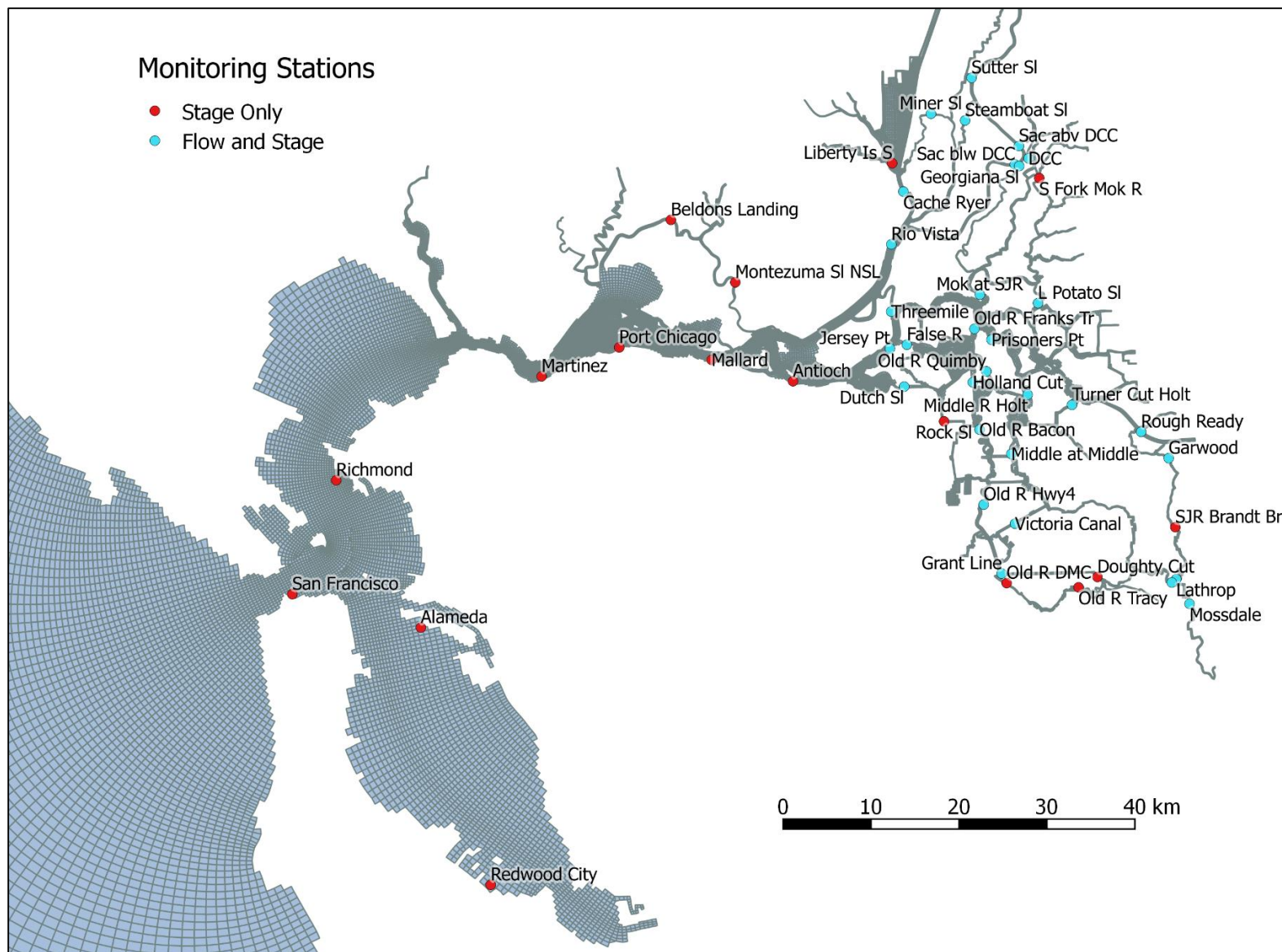


Figure 12 Stations for contemporary Bay–Delta model flow and stage calibration.



Figure 13 USGS Polaris program salinity sampling locations. Map obtained from Polaris project page: <http://sfbay.wr.usgs.gov/access/wqdata/overview/wherewhen/stnmap.html>.

Calibration Results

At each of the continuous monitoring stations, observed flow or stage data were compared against model predicted values on tidal and tidally-averaged time scales. Average computed minus observed values over the simulation time period were calculated to assess tidally-averaged errors. Tidal time scale error metrics included phase error (lag) and amplitude error. The correlation coefficient between modeled and observed was determined after correcting the modeled values for phase error, following the methods described in RMA (2005). Model skill, a metric used for assessing hydrodynamic model accuracy in the San Francisco Estuary (MacWilliams et al. 2015), was also computed.

Model flow and stage error metrics are given in Table 5 and Table 6. Of the 31 flow stations, 22 (71%) had model skill accuracies classified as “accurate” (>0.975). Five stations (16%) had skill accuracies classified as “acceptable” (0.950–0.975), and four stations (13%) were classified as “poor agreement” (<0.950). Of the four stations with poor agreement, two are located in the north Delta and resulted from inaccurate model flow splits through Sacramento River junctions; the other two were located in central Delta areas with complex flow geometries. Of the 48 stage stations, 25 (52%) had model skill accuracies classified as “accurate” (skill value cutoffs were the same as for flow). Eighteen stations were in the “acceptable” range (38%), and five stations (10%) were classified as “poor agreement.” Of the five stations with poor agreement,

four had model skill values just below the “acceptable” classification cutoff (in the range 0.943–0.949). Amplitude ratios were generally above one, indicating slight amplification of the tidal range, and average stage errors were generally negative, indicating computed stages were lower than observed. Individual station plots comparing modeled and observed data are given in Appendix B and Appendix C.

USGS Polaris salinity transect comparisons are shown for 25 cruises in Figure 14 through Figure 16. In each set of images, observed salinities are shown in the left subplot. Model results are shown for the corresponding times and locations on the right. Salinity contours are shown in intervals of 2 psu. The model accurately predicts longitudinal isohaline position and stratification for the majority of the simulation period. A comparison of the modeled and observed X2 position location, determined by linear interpolation between longitudinal stations, is shown in Figure 17. The correlation coefficient and mean absolute error of the model predictions are 0.977 and 3.5 km, respectively. The highest model errors occur during the period of very high flow at the beginning of 2006.

Table 5 Contemporary San Francisco Estuary model flow accuracy metrics.

Station Name	Data Source	Average Observed (m³ s⁻¹)	Average Computed (m³ s⁻¹)	Computed – Observed (m³ s⁻¹)	Lag (min)	Amplitude Ratio	R²	Model Skill	Skill Class
Sacramento River at Rio Vista	USGS	417.6	434.9	17.3	-14	0.979	0.985	0.993	Accurate
Threemile Slough at San Joaquin River	USGS	-39.4	-33.8	5.6	7	1.127	0.981	0.990	Accurate
Cache Slough at Ryer Island	USGS	150.7	134.8	-15.9	-9	0.912	0.985	0.993	Accurate
Sacramento River below Georgiana Slough	USGS	196.6	168.1	-28.5	-7	0.996	0.988	0.992	Accurate
Georgiana Slough at Sacramento River	USGS	106.4	144.6	38.2	-10	1.167	0.989	0.945	Poor agreement
Delta Cross Channel	USGS	56.4	46.0	-10.4	-27	0.826	0.967	0.971	Acceptable
Sacramento River above Delta Cross Channel	USGS	352.4	361.5	9.2	-4	1.119	0.991	0.997	Accurate
Sutter Slough at Courtland	USGS	98.3	78.1	-20.2	-26	1.682	0.881	0.944	Poor agreement
Steamboat Slough between Sacramento R and Sutter Sl	USGS	102.2	95.2	-7.0	-9	1.126	0.982	0.994	Accurate
Miner Slough at Hwy 84 Bridge	USGS	89.9	72.5	-17.4	-13	1.351	0.929	0.968	Acceptable
San Joaquin River at Jersey Point	USGS	173.9	183.5	9.6	-10	0.944	0.980	0.993	Accurate
False River near Oakley	USGS	-27.0	37.4	64.4	0	1.096	0.981	0.992	Accurate

Mokelumne River at San Joaquin River	USGS	94.4	114.1	19.7	-5	1.008	0.978	0.993	Accurate
Little Potato Slough at Terminous Island	USGS	54.6	60.6	6.0	-7	0.915	0.954	0.986	Accurate
San Joaquin River at Prisoners Point	USGS	-106.9	-27.4	79.5	-22	0.875	0.971	0.979	Accurate
Old River at Franks Tract	USGS	-10.6	-61.0	-50.4	29	0.560	0.763	0.853	Poor agreement
Dutch Slough at Jersey Island	USGS	-0.4	-0.7	-0.2	-13	0.997	0.968	0.988	Accurate
Holland Cut near Bethel Island	USGS	-29.9	-30.1	-0.2	-11	0.905	0.973	0.989	Accurate
Old River at Quimby Island	USGS	-36.4	-39.3	-2.9	0	1.018	0.973	0.993	Accurate
Middle River near Holt	USGS	-72.8	-56.4	16.4	-15	0.929	0.965	0.986	Accurate
Turner Cut near Holt	USGS	-29.0	-37.2	-8.1	-7	0.586	0.896	0.913	Poor agreement
Old River at Bacon Island	USGS	-38.8	-33.4	5.4	-18	0.866	0.971	0.982	Accurate
Middle River at Middle River	USGS	-74.5	-83.7	-9.2	-14	0.893	0.963	0.985	Accurate
Old River at Hwy 4	USGS	-79.1	-80.0	-1.0	-8	0.898	0.941	0.984	Accurate
Victoria Canal near Byron	USGS	-44.5	-41.5	3.1	-13	0.705	0.866	0.953	Acceptable
Grant Line Canal near Tracy	USGS	48.9	50.5	1.6	-21	0.847	0.889	0.963	Acceptable
San Joaquin River at Rough & Ready Island	CDWR	27.4	20.0	-7.5	-13	0.766	0.902	0.956	Acceptable
San Joaquin River at Garwood Bridge	USGS	52.0	54.4	2.4	-15	0.861	0.979	0.992	Accurate

San Joaquin River below Old River near Lathrop	CDWR	43.3	50.1	6.8	-1	0.867	0.974	0.989	Accurate
Old River at Head	CDWR	69.5	55.8	-13.7	-12	0.620	0.983	0.976	Accurate
San Joaquin River at Mossdale Bridge	CDWR	112.6	112.8	0.2	-24	0.675	0.994	0.998	Accurate

Table 6 Contemporary San Francisco Estuary model stage accuracy metrics. USGS stations indicated with an asterisk had data measured relative to an arbitrary vertical datum and were shifted by constant values to match average computed values at that location.

Station Name	Data Source	Average Observed (m)	Average Computed (m)	Computed – Observed (m)	Lag (min)	Amplitude Ratio	R ²	Model Skill	Skill Class
San Francisco at Golden Gate	NOAA	0.957	0.939	-0.018	4	1.005	0.995	0.998	Accurate
Alameda	NOAA	0.959	0.973	0.014	13	0.995	0.995	0.997	Accurate
Redwood City	NOAA	1.002	1.002	0.000	20	0.967	0.993	0.992	Accurate
Richmond	NOAA	0.967	0.973	0.005	5	0.995	0.996	0.999	Accurate
Martinez	CDWR	1.126	1.065	-0.061	3	0.991	0.967	0.988	Accurate
Port Chicago	NOAA	1.131	1.111	-0.020	8	0.972	0.982	0.994	Accurate
Sacramento River at Mallard Island	CDWR	1.210	1.169	-0.041	12	0.961	0.973	0.989	Accurate
Montezuma Slough at National Steel	CDWR	1.207	1.129	-0.078	4	1.176	0.969	0.980	Accurate
Montezuma Slough at Beldons Landing	CDWR	1.139	1.130	-0.009	0	0.980	0.949	0.987	Accurate
Sacramento River at Antioch	CDWR	1.306	1.200	-0.106	17	1.008	0.969	0.970	Acceptable
Sacramento River at Rio Vista	USGS	1.278	1.175	-0.103	12	1.078	0.972	0.969	Acceptable

Threemile Slough at San Joaquin River	USGS	1.355	1.205	-0.150	1	1.085	0.970	0.954	Acceptable
Cache Slough at Ryer Island	USGS	1.316	1.211	-0.105	-2	1.096	0.974	0.975	Acceptable
Liberty Island at south end	USGS	1.391	1.228	-0.164	3	1.049	0.910	0.943	Poor agreement
Sacramento River below Georgiana Slough	USGS	1.633	1.516	-0.117	1	1.118	0.987	0.986	Accurate
Georgiana Slough at Sacramento River	USGS	1.617	1.494	-0.123	-1	1.132	0.983	0.983	Accurate
Delta Cross Channel	USGS	1.436	1.322	-0.114	1	1.161	0.935	0.958	Acceptable
South Fork Mokelumne River	USGS	1.414	1.311	-0.103	10	1.119	0.964	0.969	Acceptable
Sacramento River above Delta Cross Channel	USGS	1.683	1.547	-0.136	-4	1.144	0.987	0.984	Accurate
Sutter Slough at Courtland	USGS	1.678	1.455	-0.223	-15	1.224	0.951	0.915	Poor agreement
Steamboat Slough between Sacramento R and Sutter Sl	USGS	1.675	1.519	-0.156	-5	1.163	0.978	0.975	Acceptable
Miner Slough at Hwy 84 Bridge	USGS	1.537	1.365	-0.171	-17	1.224	0.928	0.947	Poor agreement
San Joaquin River at Jersey Point	USGS	1.256	1.181	-0.075	9	1.061	0.967	0.978	Accurate
*False River near Oakley	USGS	1.127	1.129	0.002	34	1.051	0.943	0.973	Acceptable
*Mokelumne River at San Joaquin River	USGS	1.176	1.170	-0.006	1	1.091	0.966	0.990	Accurate
*Little Potato Slough at Terminous	USGS	1.190	1.189	-0.001	1	1.083	0.970	0.991	Accurate

*San Joaquin River at Prisoners Point	USGS	1.158	1.158	0.000	26	1.067	0.937	0.976	Accurate
*Old River at Franks Tract	USGS	1.177	1.177	0.000	1	1.089	0.967	0.990	Accurate
Dutch Slough at Jersey Island	USGS	1.257	1.181	-0.076	-7	1.074	0.943	0.972	Acceptable
*Holland Cut near Bethel Island	USGS	1.162	1.161	0.000	-4	1.092	0.964	0.989	Accurate
Rock Slough	CDWR	1.334	1.192	-0.142	-8	1.062	0.937	0.946	Poor agreement
*Old River at Quimby Island	USGS	1.162	1.160	-0.002	22	1.072	0.936	0.977	Accurate
*Middle River near Holt	USGS	1.170	1.171	0.001	2	1.078	0.966	0.990	Accurate
*Turner Cut near Holt	USGS	1.178	1.176	-0.002	23	1.050	0.936	0.977	Accurate
Old River at Bacon Island	USGS	1.318	1.195	-0.123	4	1.076	0.966	0.960	Acceptable
Middle River at Middle River	USGS	1.336	1.195	-0.141	-5	1.079	0.968	0.952	Acceptable
Old River at Hwy 4	USGS	1.257	1.156	-0.101	-10	1.072	0.960	0.968	Acceptable
Old River at Delta Mendota Canal	USGS	1.254	1.259	0.005	-17	1.025	0.837	0.949	Poor agreement
Old River near Tracy	CDWR	1.339	1.328	-0.011	4	1.037	0.902	0.968	Acceptable
Doughty Cut above Grant Line Canal	CDWR	1.340	1.353	0.013	-6	1.064	0.942	0.983	Accurate
*Victoria Canal near Byron	USGS	1.137	1.138	0.001	-5	1.059	0.960	0.988	Accurate
Grant Line Canal near Tracy	USGS	1.179	1.077	-0.103	-5	1.037	0.920	0.959	Acceptable
San Joaquin River at Rough & Ready Island	CDWR	1.333	1.218	-0.115	6	1.050	0.967	0.968	Acceptable
San Joaquin River at Garwood Bridge	USGS	1.350	1.254	-0.096	-8	1.101	0.961	0.975	Acceptable
San Joaquin River at Brandt Bridge	CDWR	1.577	1.398	-0.179	-13	1.208	0.956	0.961	Acceptable

San Joaquin River below Old River near Lathrop	CDWR	1.751	1.808	0.057	-5	1.062	0.990	0.992	Accurate
Old River at Head	CDWR	1.375	1.403	0.028	-4	-1.000	0.882	0.964	Acceptable
San Joaquin River at Mossdale Bridge	CDWR	1.932	2.038	0.106	7	1.017	0.991	0.991	Accurate

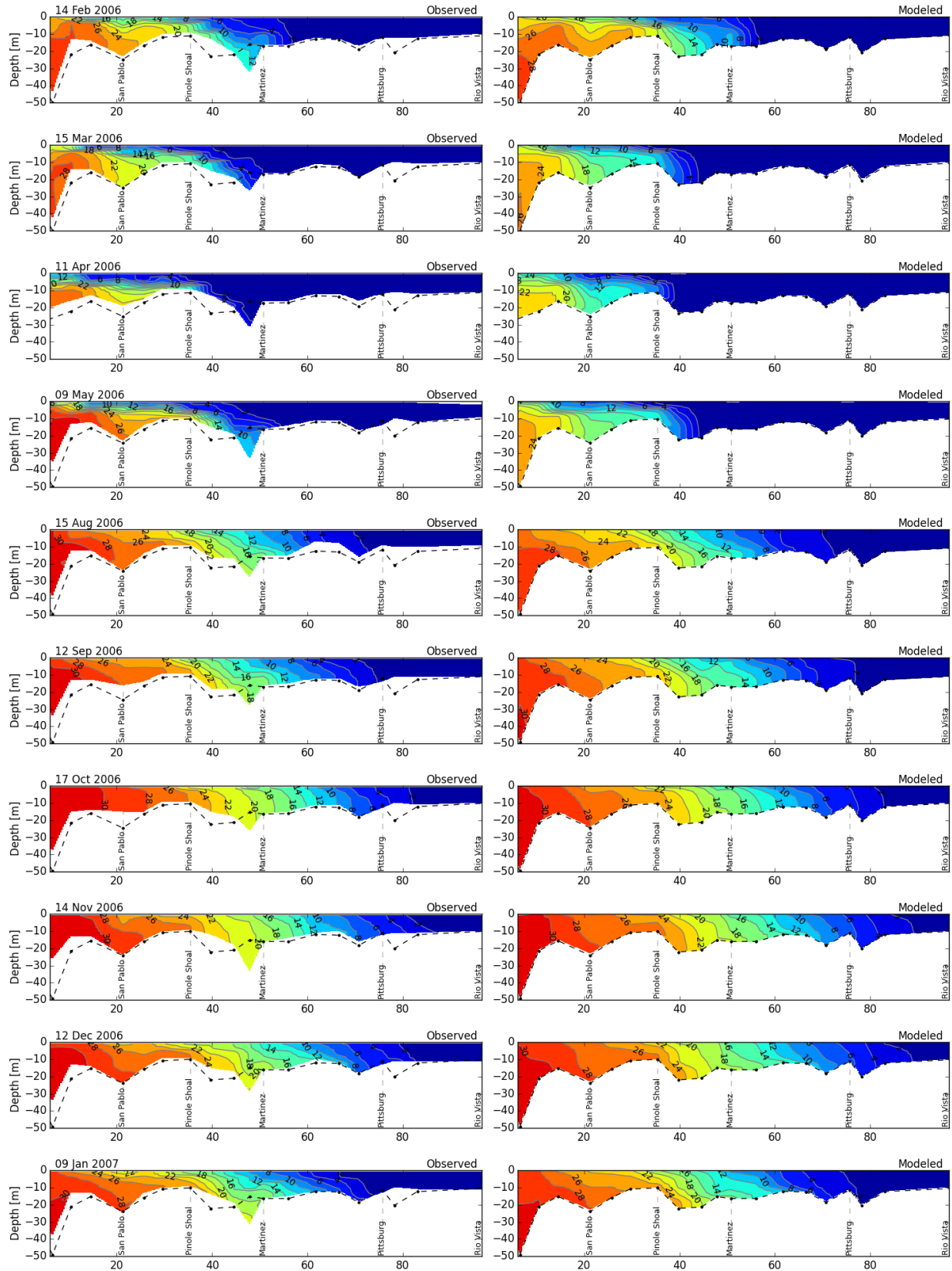


Figure 14 USGS measured (left) and modeled (right) salinity transects for calibration period.

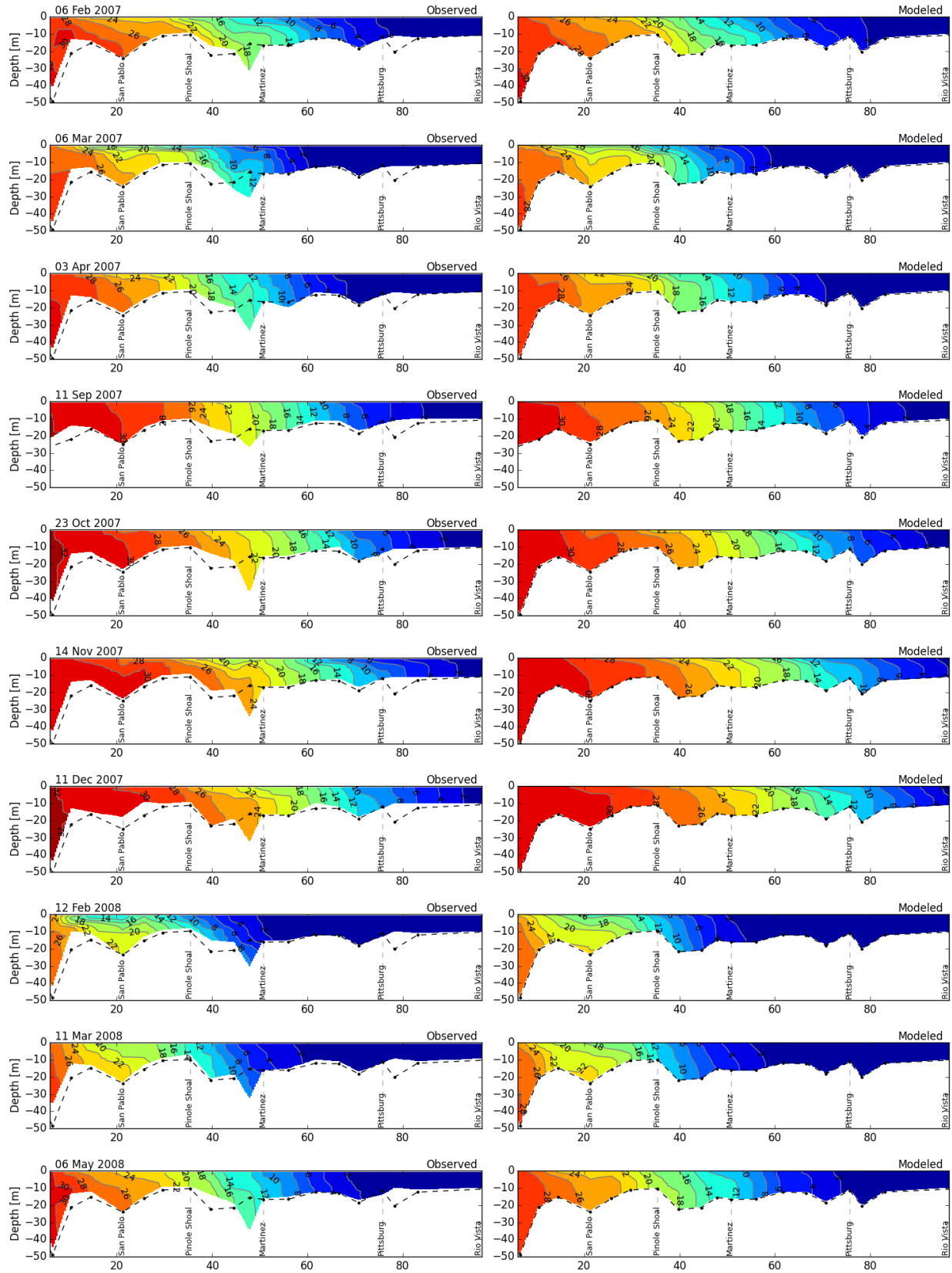


Figure 15 Continuation of Figure 14.

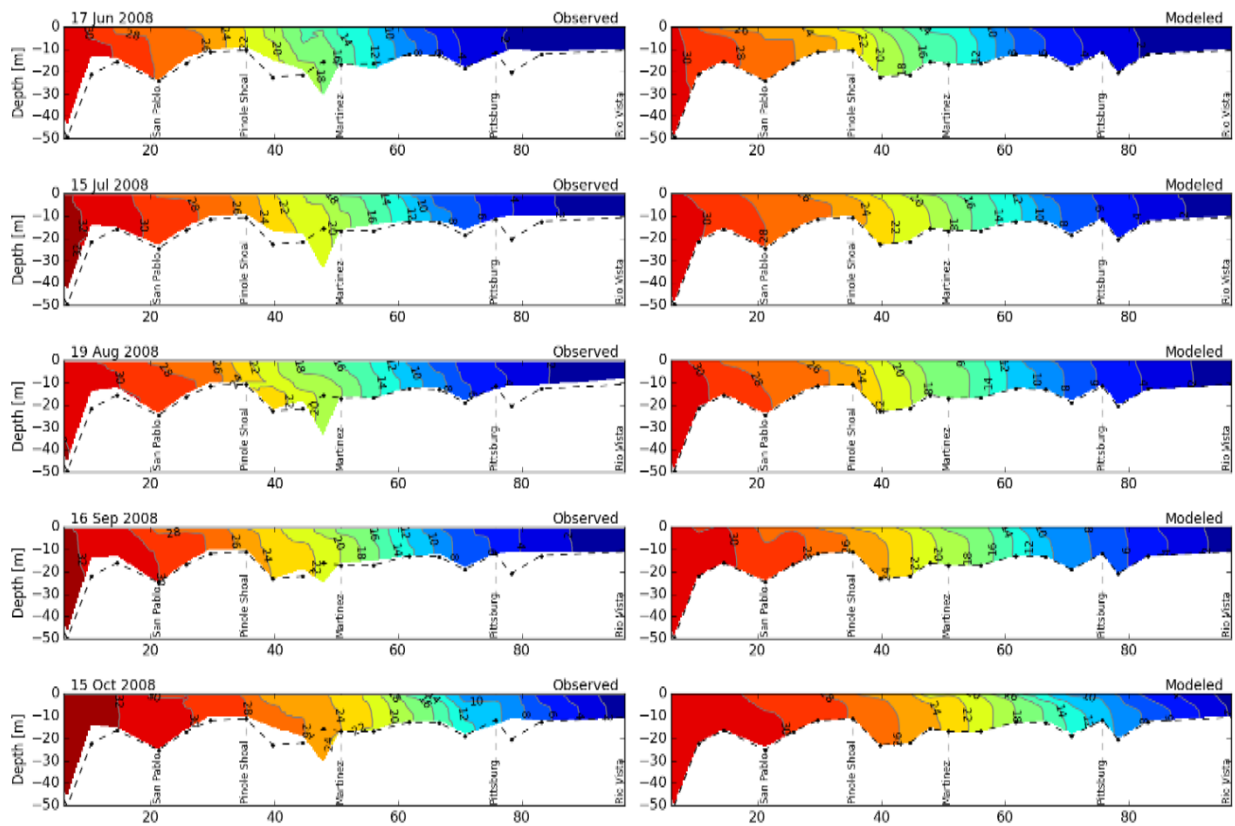


Figure 16 Continuation of Figure 14.

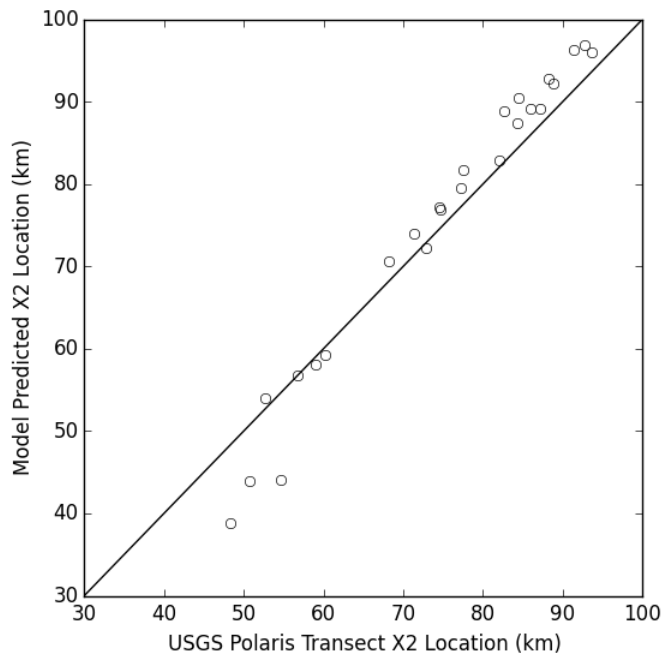


Figure 17 Comparison of observed X2 location based on USGS Polaris cruise data and model-predicted X2 location.

Development and Calibration of the Pre-development San Francisco Estuary Model

This section details the development and calibration of a model of the San Francisco Estuary as it existed in the early 1800's (the "pre-development" system). Construction of the grid relied heavily on work by SFEI and UCD to map pre-development channel configurations and create a digital elevation model of the upper estuary. Model calibration was achieved by varying marsh plain elevations in order to match sparse historical observations of tidal characteristics, including tidal range, marsh plain inundation depth and frequency, and the spatial extents of tidal habitat.

Grid Development

A separate unstructured orthogonal grid was developed for the pre-development model simulations. This grid used the same 2-D horizontal elements as the contemporary Delta grid for San Pablo, Central, and South Bays, as well as the coastal ocean. Landward of Carquinez Strait, the 2-D planform grid was developed based on the pre-development channel configurations (Whipple et al. 2012). Upstream boundaries for all major tributaries were located in approximately the same locations as in the contemporary grid. However because of the greater prevalence of tidally and seasonally inundated land, the total area covered by computational elements is much larger in the pre-development model grid. The lateral boundaries of the grid in the Delta and Suisun Marsh were extended to the present-day 25 ft NAVD88 contour location, corresponding to the extreme upper limit of seasonal inundation and the boundary of land classified as functionally belonging to the Delta by Whipple et al. (2012).

In Phase 2 of this work, the boundaries of the pre-development upper estuary grid were expanded from those used in Phase 1. These expansions were made in order to allow high flow modeling of 2006 and included areas in the Yolo Basin, the east and south periphery of the Delta, and Suisun Marsh (Figure 18).

Planform channel locations and widths for the pre-development Delta were derived from a large number of historical maps, imagery, and other sources and then digitized by Whipple et al. (2012). A similar process was performed for Suisun Bay and Marsh by Manfree (2013). Major channels in the pre-development Delta and Suisun Marsh and main flow paths in Suisun Bay were discretized using flow-aligned quadrilateral elements of comparable resolution to the contemporary model grid. Identical sections of the contemporary grid were used in the pre-development grid in areas where channels had not changed significantly; however, few of these areas existed because of extensive channel straightening, widening, and cross-cutting. Marsh plain and seasonally inundated areas were discretized using triangular elements. Small, low-

order streams were not explicitly considered in the grid development, but were accounted for in the model through subgrid bathymetry.

Detailed images of the pre-development model grid in the Delta and Suisun Bay region are shown in Figure 19 through Figure 23. The channel configuration and bathymetry for the Suisun Bay and Marsh areas, newly added for the Phase 2 work, are shown in Figure 24.

Bathymetry in the pre-development upper estuary is represented using a DEM, the development of which is described in detail by Fleenor et al. (in prep). 2-D historical sounding data, thalweg depth measurements, and natural levee elevations along major channels were digitized and interpolated to create a continuous, smooth DEM of the upper estuary. Where 2-D channel depth data was not available, a parabolic channel cross-section was assumed using measured thalweg depths. Where no channel depth data was available, a width–thalweg depth relationship, developed using limited data from low-order channels, was used to set depths. Marsh plain elevations were set based on tidal inundation characteristics derived from calibration simulations (see Calibration Simulations section).

The resulting 2 m resolution DEM was used to set subgrid bathymetry for the pre-development model grid, using the same subgrid resolution as the contemporary model. The same number and spacing of vertical layers as the contemporary model was also used. The resulting grid contained 203,113 2-D elements, with approximately 520,000 3-D prisms active during a typical simulation.

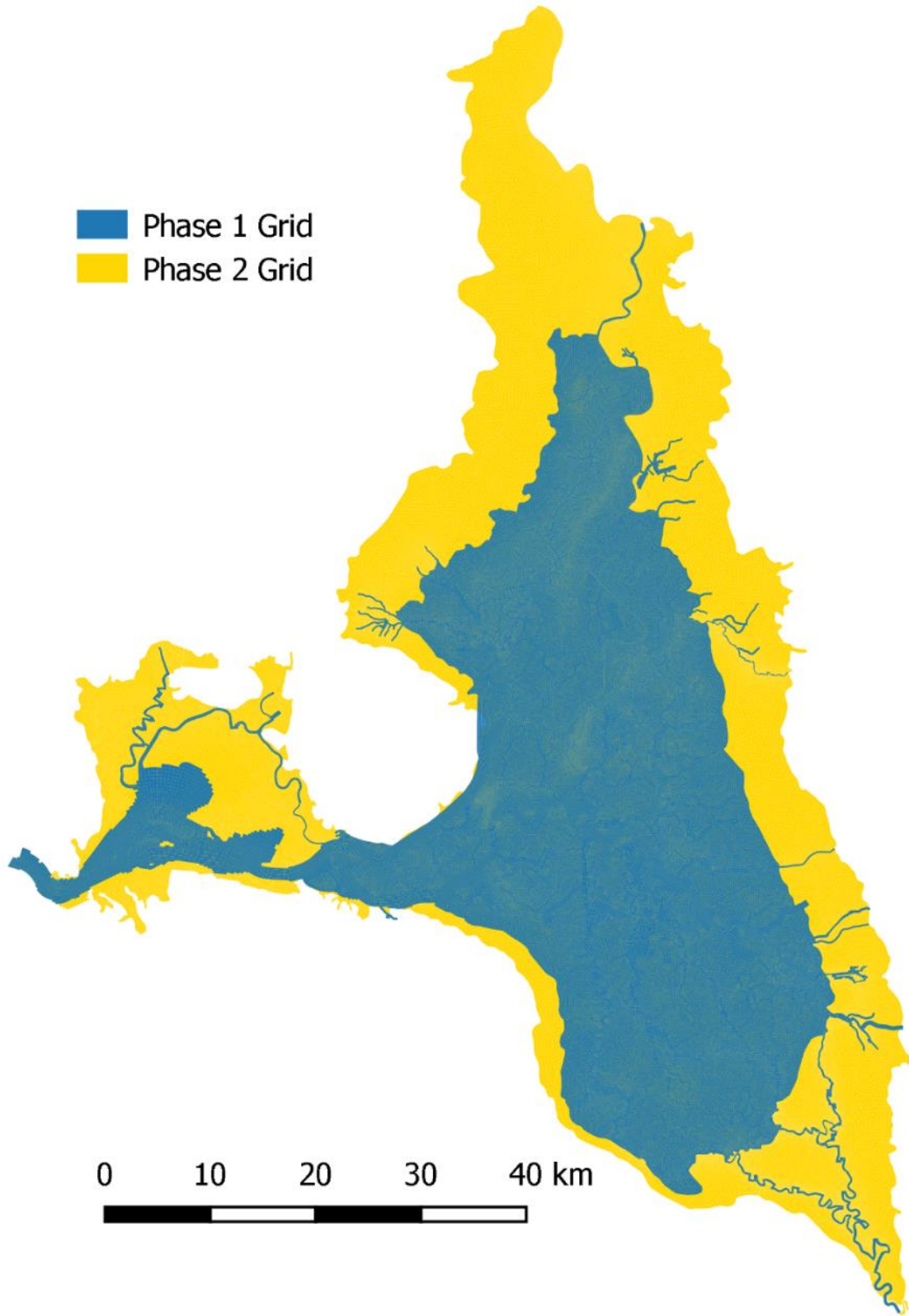


Figure 18 Pre-development model Phase 1 and Phase 2 upper estuary grid extents.

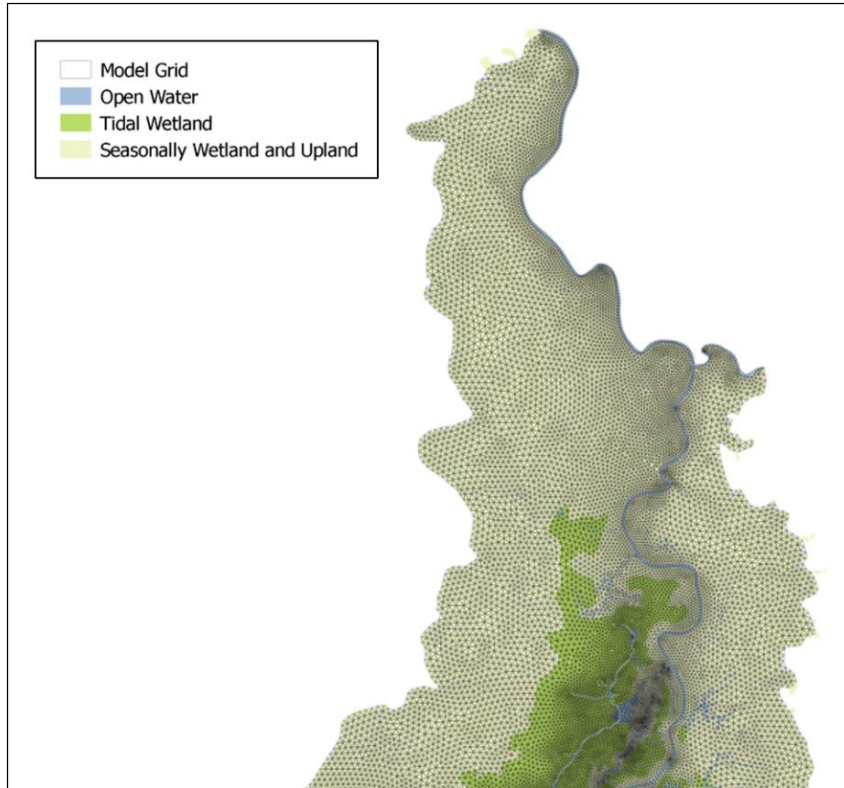


Figure 19 Pre-development model grid detail in north Delta.

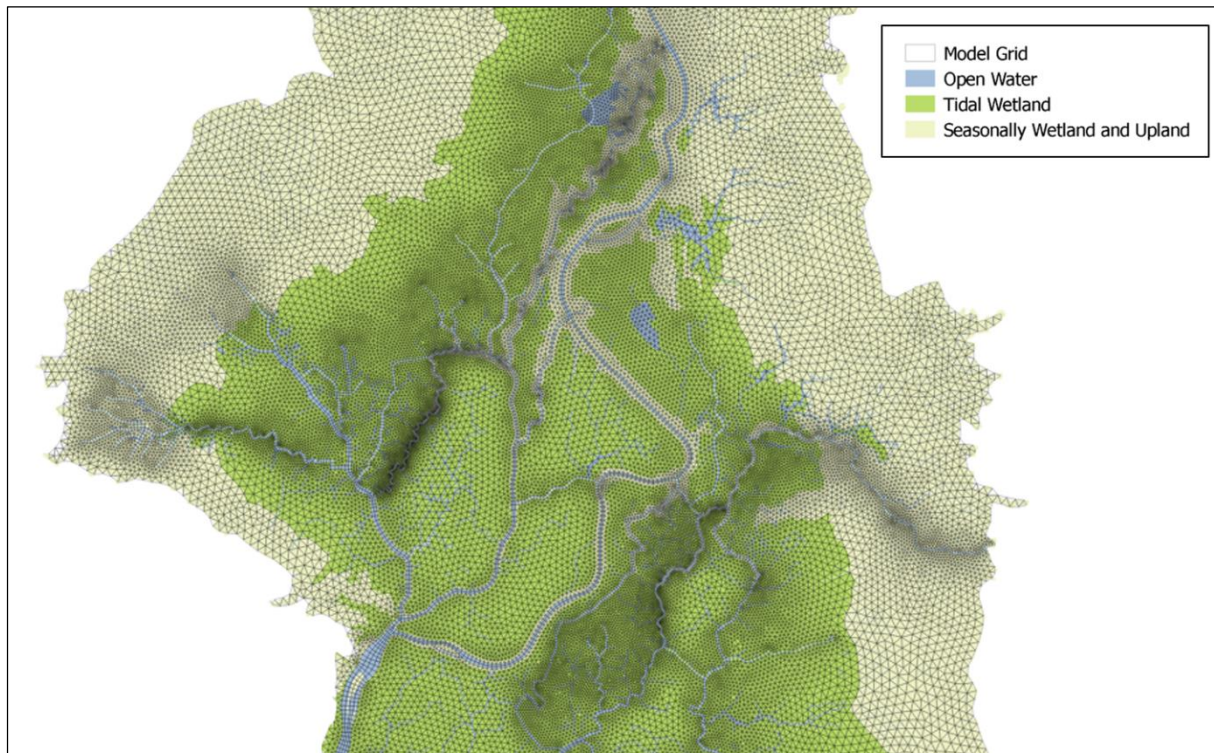


Figure 20 Pre-development model grid detail in lower north Delta.

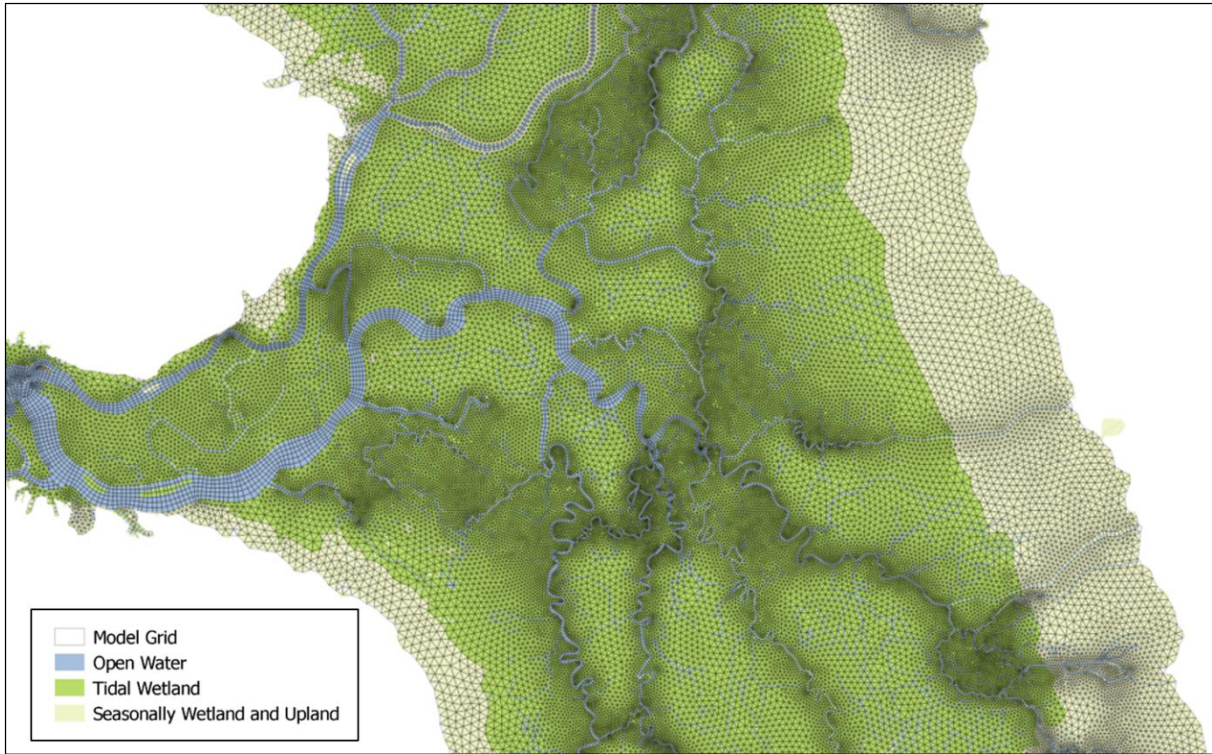


Figure 21 Pre-development model grid detail in the central Delta.

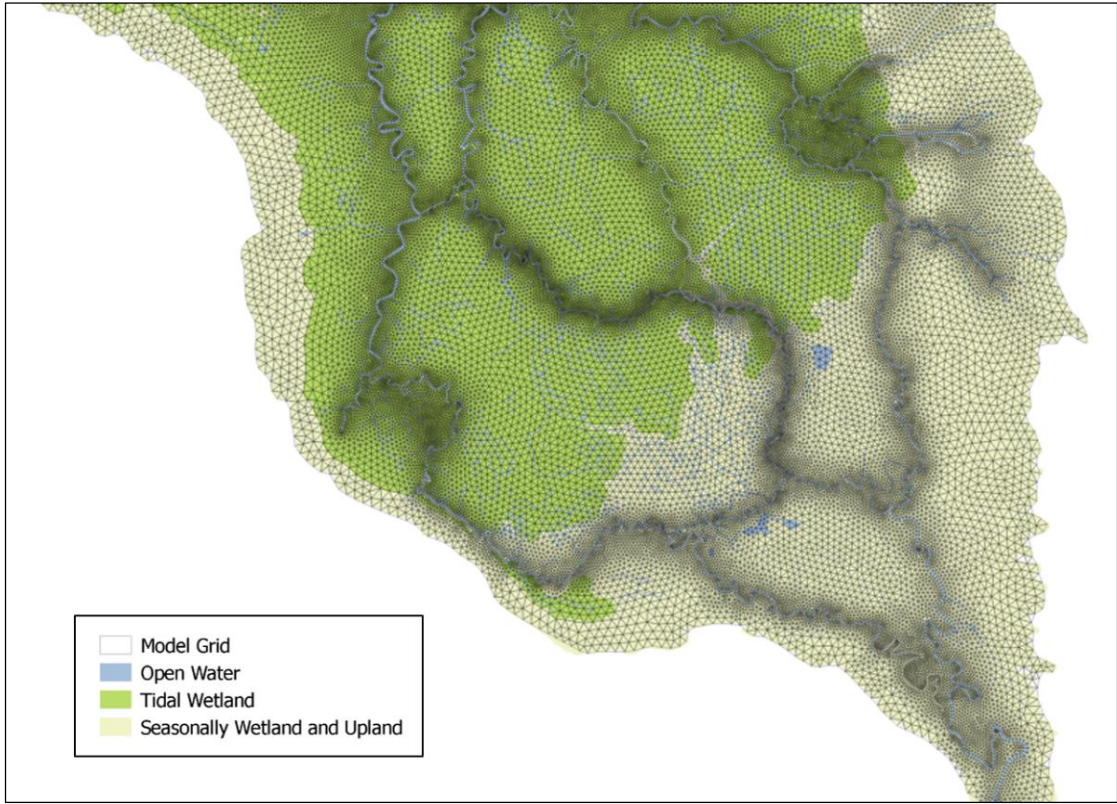


Figure 22 Pre-development model grid detail in the south Delta.

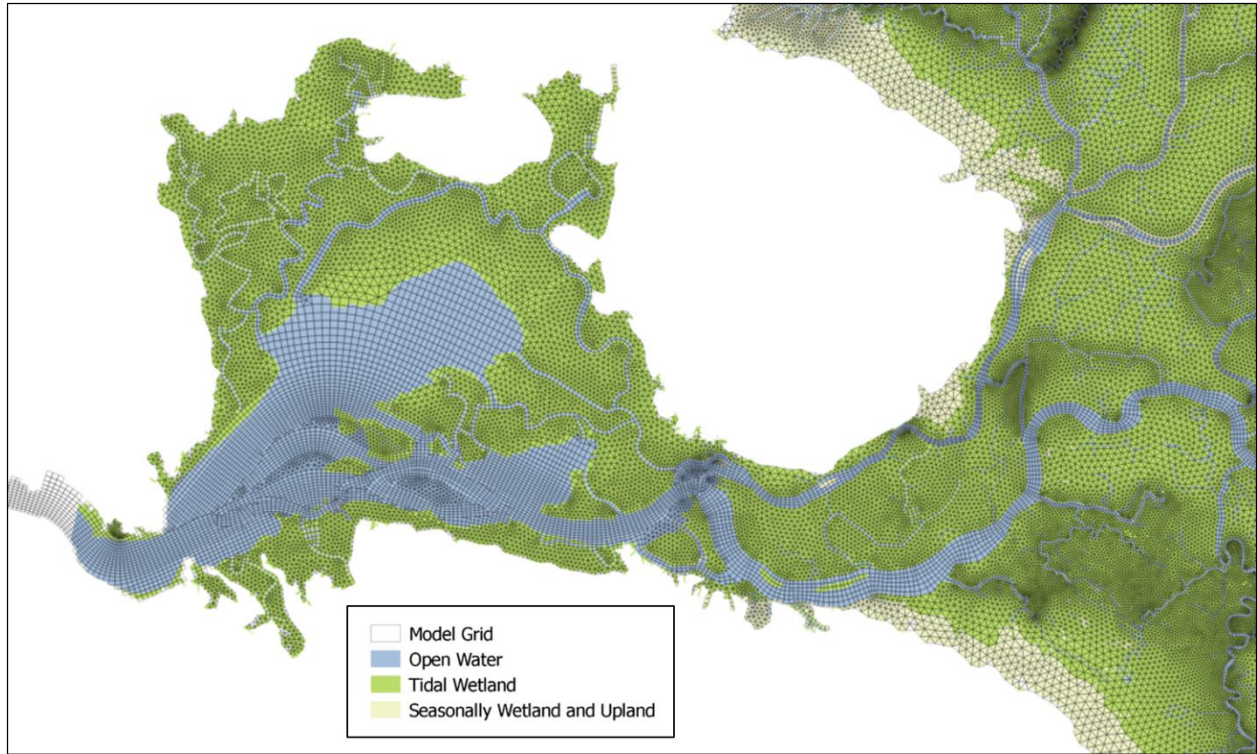


Figure 23 Pre-development model grid detail in Suisun Bay and Suisun Marsh.

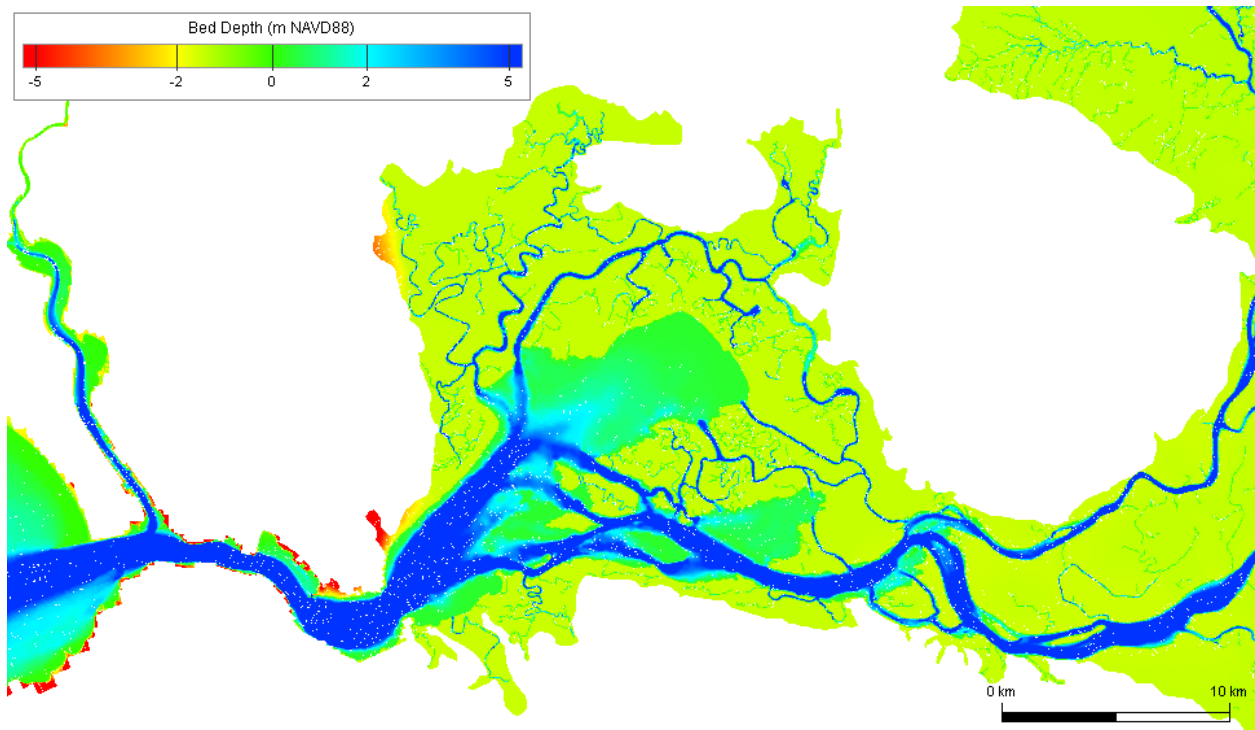


Figure 24 Pre-development model Suisun Bay and Marsh bathymetry.

Model Boundary Conditions

Major riverine boundary locations were the same as those used in the contemporary model, except individual inflows to the Yolo Basin, including Cache and Putah Creeks and Sacramento River spillover near the present day location of Fremont Weir, were prescribed in place of the aggregated Yolo Bypass flow used in contemporary model simulations. River inflows were prescribed a constant freshwater value of 0.07 psu. Boundary flow time series data were extracted from C2VSim “natural flow” hydrologic model simulations at computational nodes corresponding to each boundary inflow location. The hydrologic model simulations were used to route historical (1921–2013) runoff events through the natural landscape of the Central Valley prior to the land use changes of the past 150 years. The development and calibration of this model is described in detail by Kadir et al. (in prep). A description of the calculation of evapotranspiration on the Central Valley floor is given in Fox et al. (2015) and Howes et al. (2015). No major water diversions or hydraulic structures were prescribed for the pre-development model.

Wind speed and direction, and evaporation and precipitation were prescribed as constant within local regions, similar to the contemporary model. In the pre-development model, however, no surface wind stress was applied in the Delta due to the presumed sheltering effects of dense emergent wetland vegetation and the lower incidence of large areas of open water. Net channel depletions as estimated by CDWR were not applied to the pre-development model; rather, the effects of flood storage, evapotranspiration and precipitation within the Delta were estimated in bulk by calculating a time series of net Delta inflow minus net Delta outflow predicted by the C2VSim model. This Delta depletion time series was distributed over 33 elements in main channels throughout the Delta to capture the net effect. The distribution of the channel depletions was spatially variable; the 33 elements were broken into groups of ten, eight, ten, and five elements along the Sacramento River, the Mokelumne River (both north and south forks), the San Joaquin River in the central Delta, and the upper San Joaquin River, respectively. A portion of the total Delta channel depletions at each time step was applied to each group, with the group allocations approximating C2VSim model results of the spatial distribution of depletions. In this way the spatially-coarse C2VSim predictions in the Delta were downscaled and applied to the 3-D model.

The same bed roughness heights as in the contemporary San Francisco Estuary model were prescribed for the pre-development model in the lower estuary and Suisun Bay. In the pre-development Delta and Suisun Marsh a bed roughness height of 0.01 mm was used in the channels and 0.1 mm was used on the marsh plain. During test simulations, these low channel and marsh plain roughness heights were necessary to reproduce tidal ranges and marsh plain flooding/draining speeds consistent with historical observations.

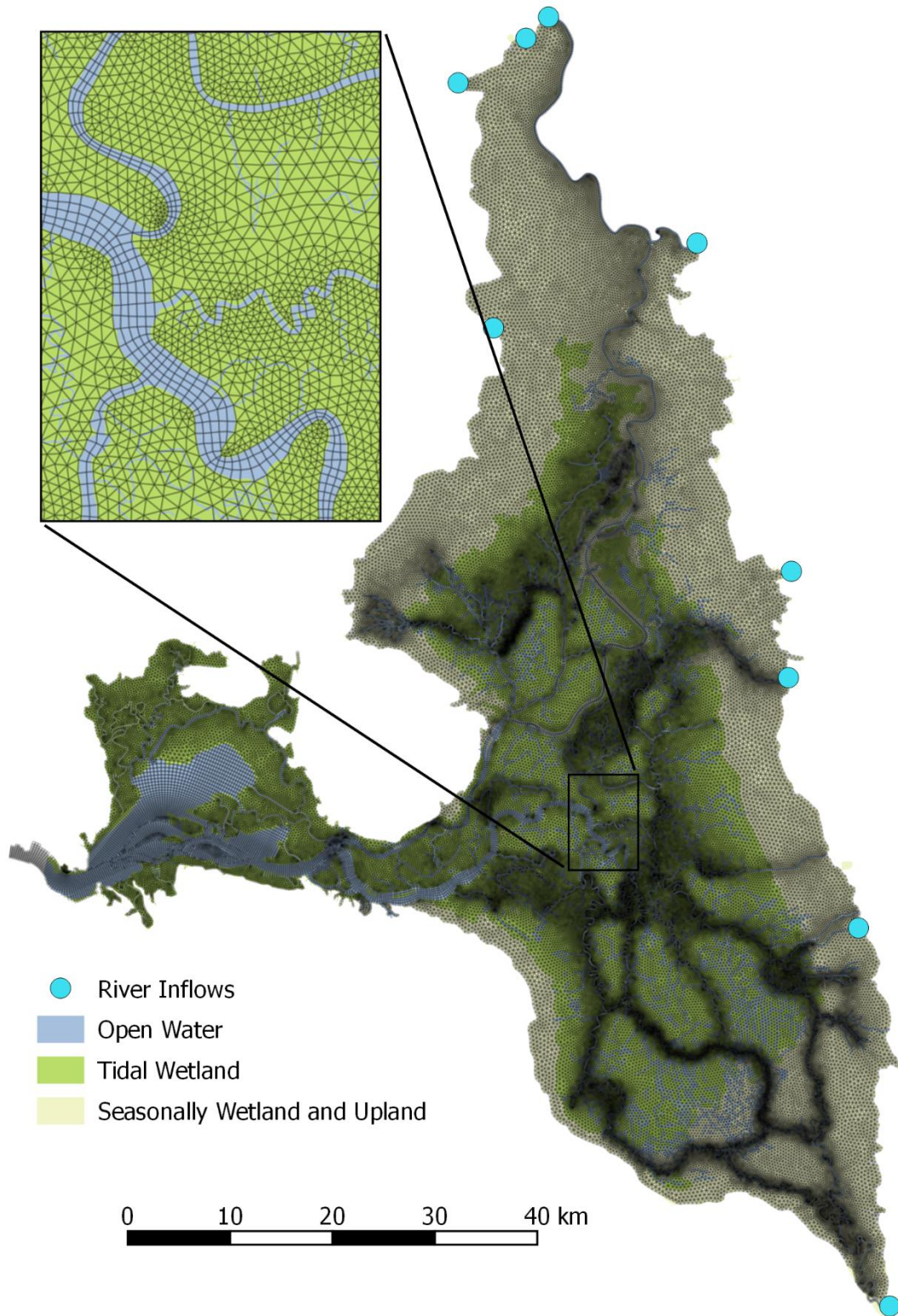


Figure 25 Upper estuary section of the pre-development Delta grid. Boundary inflow locations are shown.

Historical Observed Data Sources

Observed data for comparison with model output were aggregated by SFEI from a wide variety of historical accounts (Table 7). Observations were of three types: tidal range in channels, marsh plain inundation frequency, and depth of marsh plain inundation. For observations of marsh plain inundation depth, specification of whether the observation was made on spring or neap tide was sometimes made. Although the number of historical measurements is few, they cover a wide area, from the Delta mouth to the city of Sacramento in the north, Benson's Ferry to the east, and Stockton to the south.

Data pulled from the historical accounts is generally uncertain as the exact location of the measurement, and observations are typically rough estimates. An example of a very high accuracy observation is an account from a farmer at Horseshoe Bend on the Sacramento River who stated that his two and one half foot high levee was "about one foot above the spring-tide mark," meaning that the pre-leveed marsh was likely overflowed by a foot and a half of water at spring tides (Higley 1860). An example of a less accurate observation was made by a visitor to Stockton, who noted "the tide of the ocean and Bay of San Francisco, sets up here, from one to two feet" (McCollum 1850).

In addition to historical observations of tidal range in channels and marsh plain inundation characteristics, general information about marsh plain inundation flow patterns and the spatial extent of freshwater tidal habitat is known (Whipple et al. 2012) and can be used for calibration.

Table 7 Historical observations of tidal range and marsh plain inundation characteristics.

Observation Type	Value	Location	Source
Tidal range in channel	>0 ft	Sacramento River at Feather River	Sacramento Daily Union (1862)
Tidal range in channel	22 inches	Sacramento River at Sacramento	Sacramento Daily Union (1862)
Tidal range in channel	3.5 ft	Mokelumne River below Benson's Ferry	Thornton (1859)
Tidal range in channel	3 ft	Sacramento River at Isleton	Hall (1879)
Tidal range in channel	6 ft	Cache Slough	Rose et al. (1895)
Tidal range in channel	3-6 ft	Sherman Island	Day (1869)
Tidal range in channel	4-6 ft	Delta mouth	Multiple: see Whipple et al. (2012), p. 129
Tidal range in channel	1-2 ft	San Joaquin River at Stockton	McCollum (1850)
Tidal range in channel	>0 ft	San Joaquin River at head of Old River	Abella and Cook (1960)
Inundation frequency	S ends of islands wetted all tides; N ends only on spring	Tyler and Staten Islands	Thompson (2006)
Inundation frequency	Wetted twice daily	Central Delta	Whipple et al. (2012), p. 130
Inundation frequency	Wetted by spring tides	Eastern margin of Delta	Whipple et al. (2012), p. 131
Depth of marsh plain inundation	1.5 ft (spring tide)	Sacramento River at Horseshoe Bend	Higley (1860)
Depth of marsh plain inundation	6 inches (neap tide)	Sherman Islands	Day (1869)
Depth of marsh plain inundation	6 inches	Bouldin Island	Beaumont (1861)

Calibration Simulations

Because timing of individual historical observations is generally unspecified, a summer low-flow period was simulated in order to remove the influence of high river inflows affecting marsh plain inundation. July of 2008 was chosen as the calibration simulation period. The ocean stage boundary condition was taken as the 6-minute NOAA Point Reyes observed data record, reduced one 1 ft (0.31 m) in order to account for the sea level rise hypothesized to take place over the last 150 years¹. River inflow boundary conditions were taken from the C2VSim model for that period (Figure 26). In-Delta evaporation and other depletions averaged around 500 cfs, and net delta outflow for this period was in the range 2,500–5,000 cfs. Wind and evaporation/precipitation boundary conditions were set as 2008 observed values.

In order to calculate tidal range, the stage time series at each computational cell above a certain depth threshold was analyzed to determine mean higher high water (MHHW) and mean lower low water (MLLW). The difference between those datums was used to represent tidal range in the channels. It was taken in place of the more commonly used tidal range definition of mean high water minus mean low water, where mean high water is defined as the average of the mean higher high water and the mean lower high water (and mean low water is analogously defined). This change in definition was agreed upon by RMA and SFEI as being more likely to reflect the commonly accepted definition of tidal range (daily high water minus daily low water) in the mid-1800s.

Tidal inundation frequency was determined as the number of wetting/drying cycles experienced by each computational cell. A minimum depth cutoff of 2 cm was used as the threshold for declaring cells wet. Many main channel and floodplain cells remained either wet or dry for the duration of the simulation and were therefore excluded from the computations. Depth of spring tide inundation was determined by calculating the maximum depth of inundation for marsh plain cells over the duration of the simulation. Depth of neap tide inundation was determined by calculating the maximum depth of inundation for a subset of the simulation defined by having neap tides. The extent of tidal freshwater habitat was defined by including all cells on the marsh plain that were inundated to at least 2 cm deep within the calibration period.

Calibration of the pre-development model was achieved by modification of the historical DEM in two main ways. First, maps of the modeled tidal range in channels were examined in order to quickly identify artifacts in the DEM. These could be identified by large decreases in modeled tidal range in areas where the DEM contained irregular channel pinch points. This process is detailed in Fleenor et al. (in prep) and mainly occurred near channel junctions where the

¹ NOAA long term sea level trend for the San Francisco station available from: http://tidesandcurrents.noaa.gov/sltrends/sltrends_station.shtml?stnid=9414290

automated channel cross-section generation process encountered problems. The second means of modifying the DEM to achieve calibration was to modify the marsh plain elevation. Lower marsh plain elevations caused a higher frequency and greater maximum depth of marsh plain inundation, but caused a decrease in tidal range at upstream locations because of tidal energy dissipation. Because an infinite number of spatially variable marsh plain elevation data sets could be prescribed, we adopted an approach where a gradual linear increase in elevation was specified moving away from the Sacramento–San Joaquin River confluence. A constant marsh plain elevation equal to the value near the confluence was prescribed for the Suisun Marsh area. In known upland areas, including the farthest upstream areas of the Sacramento, Cosumnes, Mokelumne, and San Joaquin Rivers, the topography was increased locally. Different combinations of base marsh plain elevation and slope increase away from the confluence were set in the DEM and then simulated until a reasonable calibration was achieved.

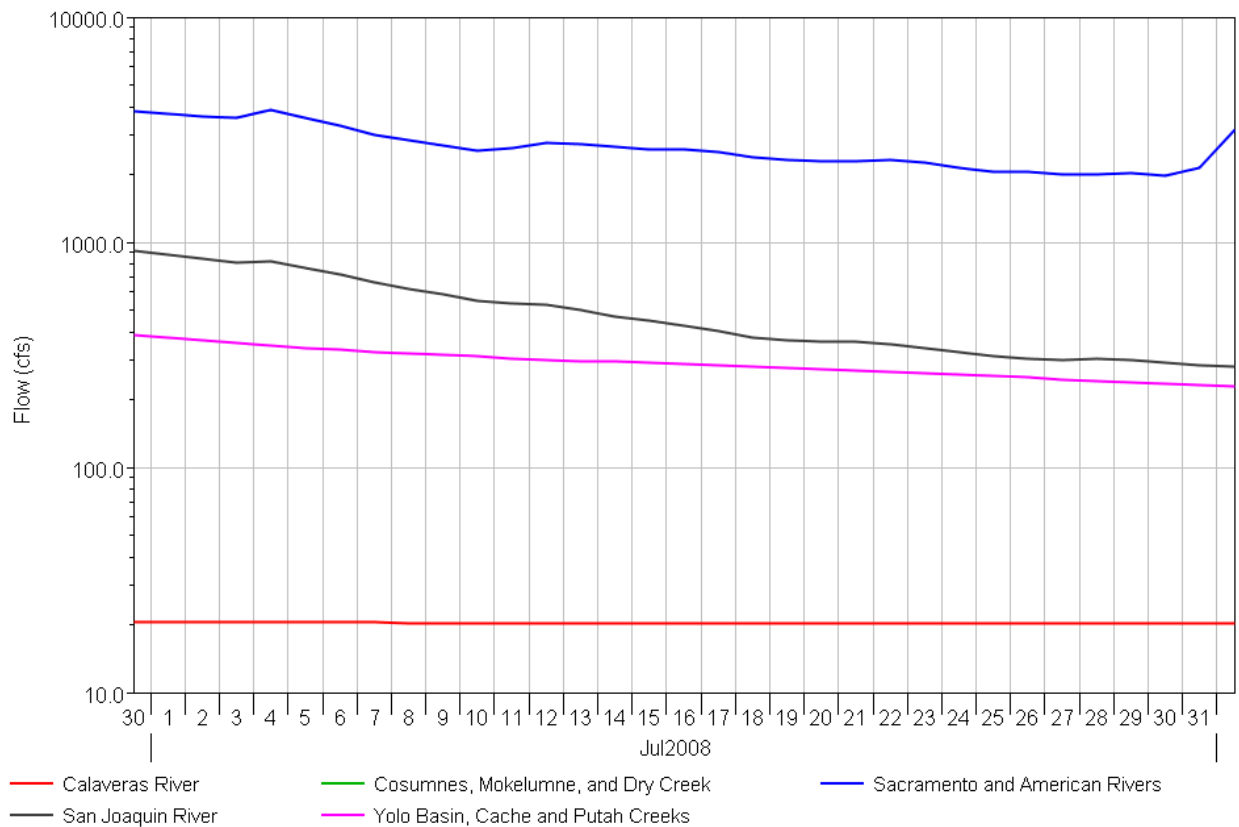


Figure 26 Pre-development model river inflows for calibration period in July 2008.

Calibration Results

Modeled and observed channel tidal ranges are shown in Figure 27. Modeled and observed tidal inundation frequencies are shown in Figure 28, the extent of tidal freshwater habitat is shown in Figure 29, and spring and neap period marsh plain inundation depths are shown in Figure 30.

Modeled tidal ranges in channels generally matched or were slightly below historically observed values at major locations in the Delta, including the Delta mouth, the Sacramento River at Isleton and the city of Sacramento, the Mokelumne River at Benson's Ferry, and the San Joaquin River at Stockton. Although many of the DEM artifacts were identified and removed, it is likely that some may have remained and contributed to the lower modeled tidal range in the channels. The large difference between modeled and observed values at Cache Slough may be the result of an anomalous observed value, or may indicate model inaccuracy in representing the Cache Slough Complex. Although the present day configuration of the complex is responsible for some tidal amplification (RMA 2005), it seems unlikely that the tidal range would be double that observed at the nearby Isleton location.

The model predicted inundation frequency is generally on par with the historical observations. The majority of the Delta is inundated to at least 2 cm depth 15–30 times per month. This corresponds to areas being inundated during higher high tide either every day or only during spring tide periods. Differences in inundation frequency between modeled and observed data may also result from how the definition of marsh plain “wetting” corresponds to the 2 cm cutoff for declaring a computational cell wet.

Modeled tidal inundation depths (Figure 30) were generally lower than observed values. As noted previously, there is a tradeoff between increased tidal inundation depth and frequency and decreased channel tidal ranges. For this calibration, a marsh plain elevation was set to reasonably accurate ranges for both without favoring one metric over the other.

A final aspect of the pre-development Delta hydraulics used for calibration was the flow patterns for marsh plain inundation at higher high tide and lower high tide. At higher high tide, marsh plain is inundated from all directions as water spills over low natural levees (Whipple et al. 2012, Figure 31). At lower high tide, marsh plain inundation occurs from spillover from the heads of blind sloughs that enter the plain from off the main channels (Whipple et al. 2012, Figure 32).

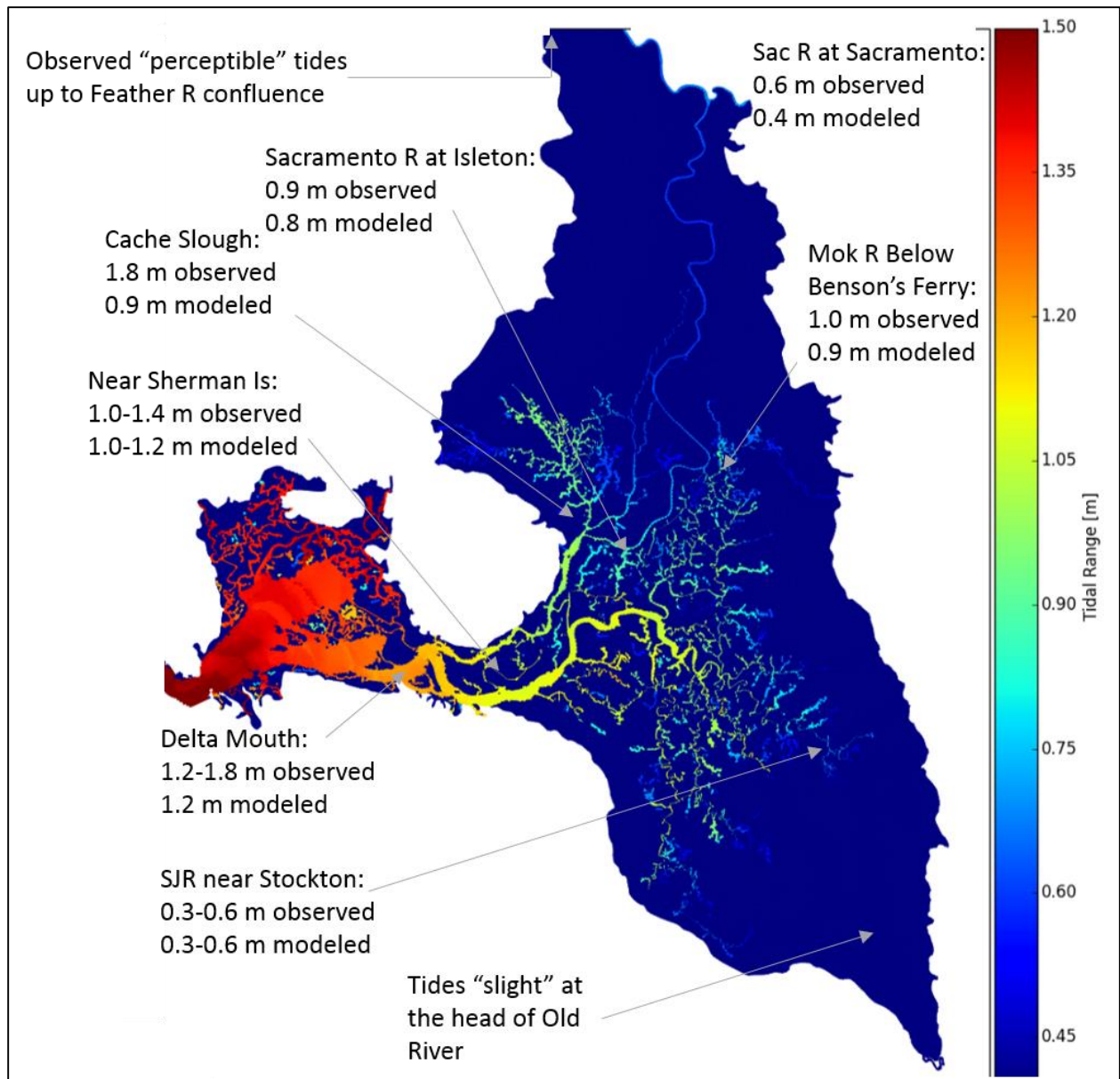


Figure 27 Modeled pre-development Delta tidal range and point locations of historical observed data. Historical observed data sources are given in Table 7.

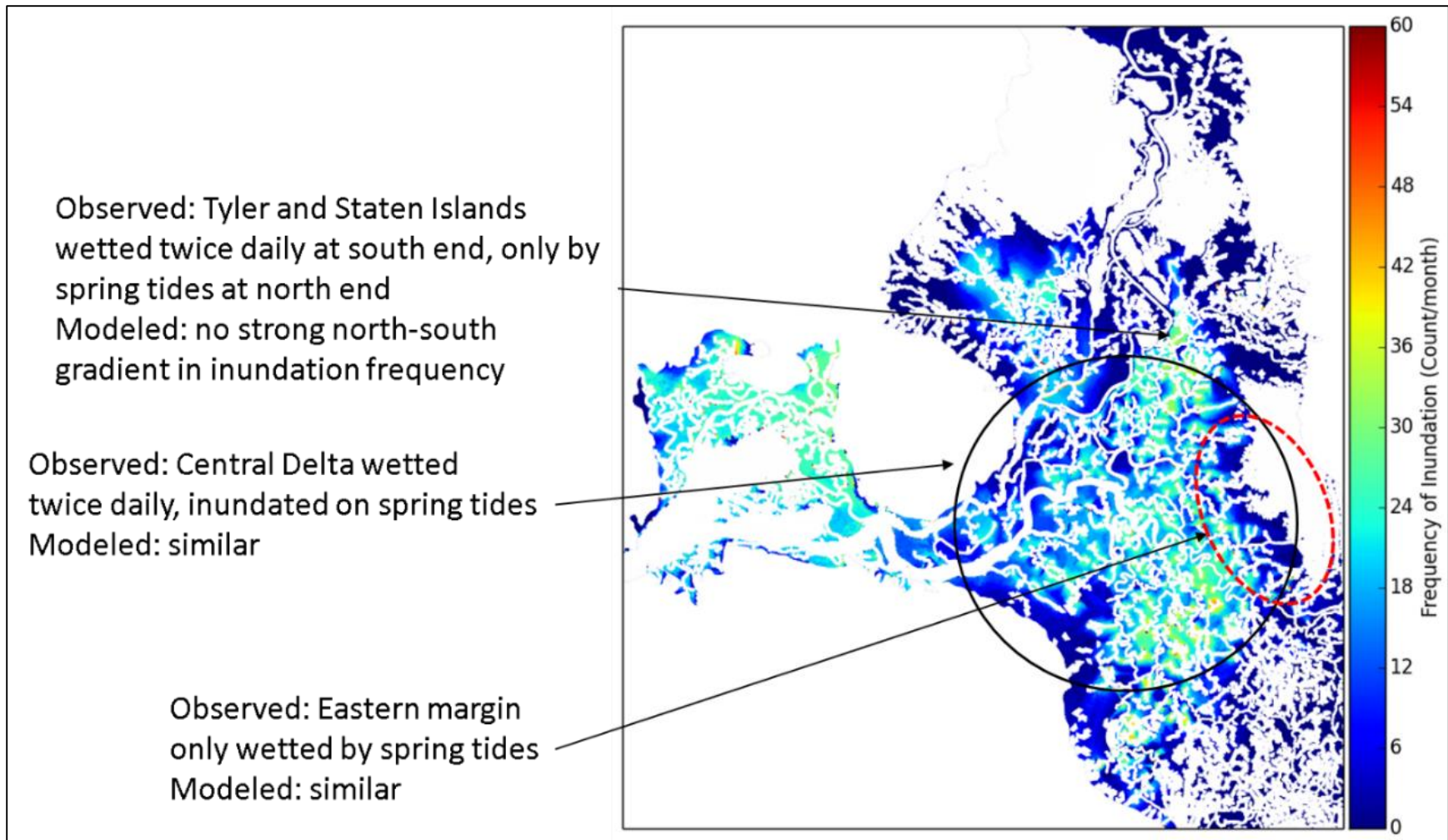


Figure 28 Modeled pre-development Delta tidal inundation frequency and point locations of historical observed data. Historical observed data sources are given in Table 7.

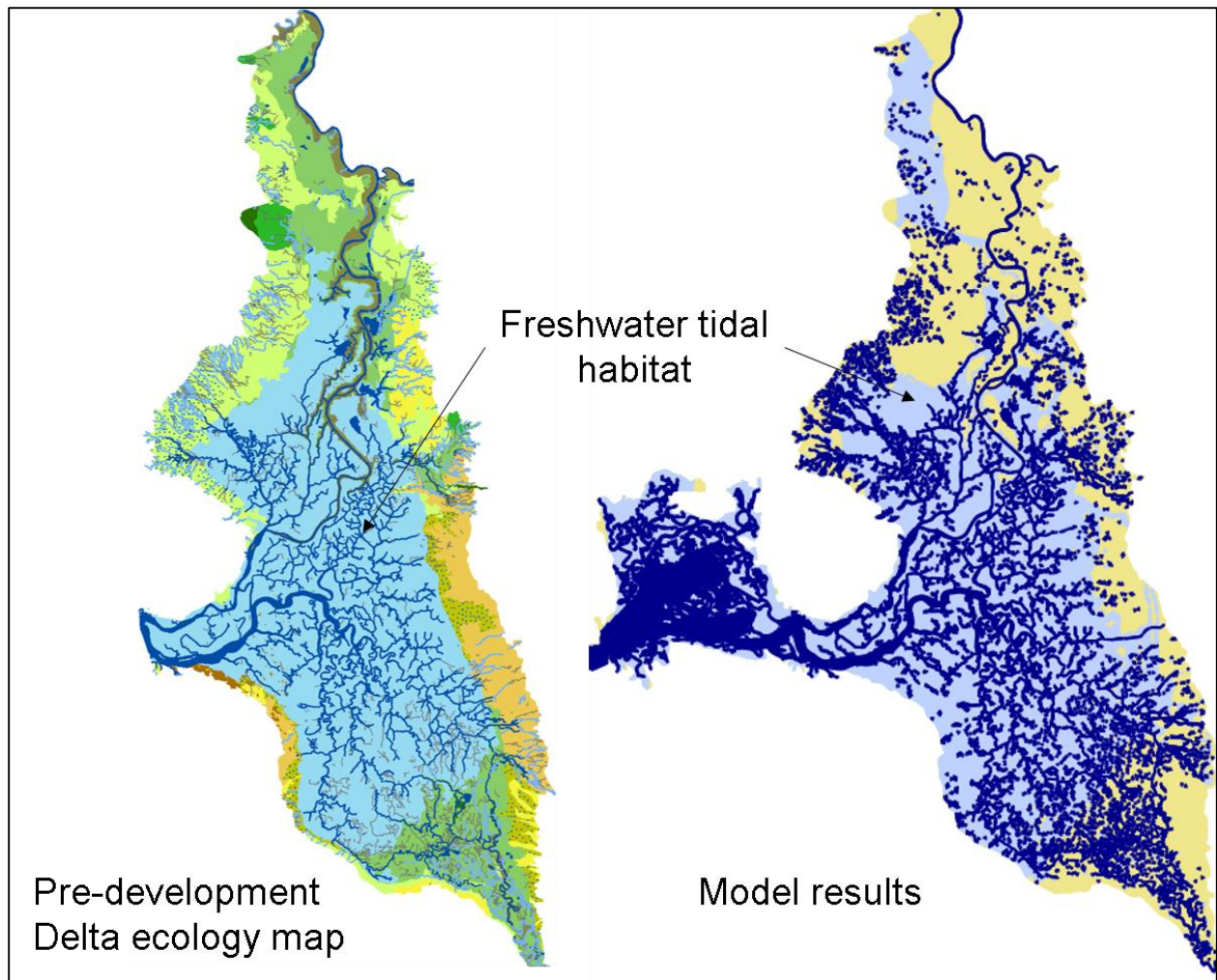


Figure 29 Spatial extent of modeled pre-development Delta tidal freshwater habitat (right) and historical habitat delineation map (left) from Whipple et al. (2012).

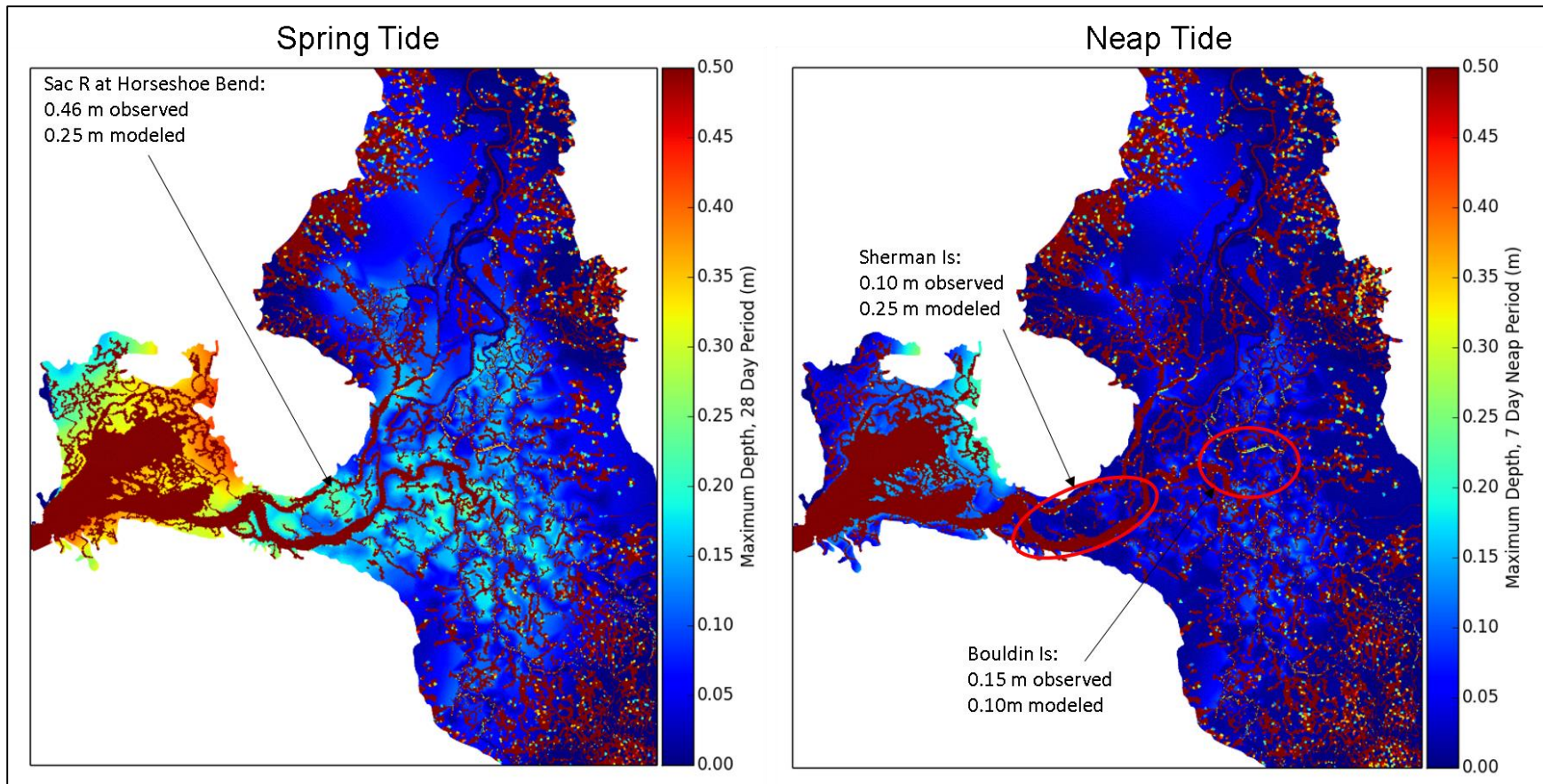


Figure 30 Modeled pre-development Delta marsh plain inundation depths and locations of historical observed data. Maximum modeled depths of water are shown for a spring tide period on the left and for a neap tide period on the right. Historical observed data sources are given in Table 7.

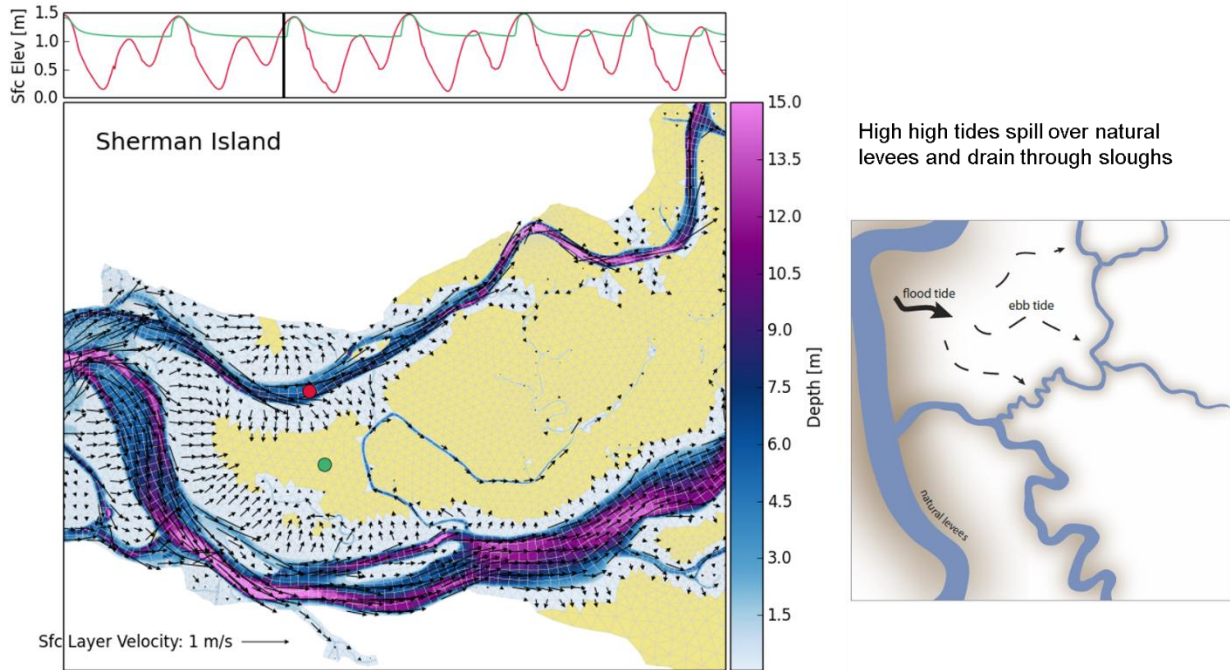


Figure 31 Modeled higher high tide flooding patterns in the pre-development Delta (left) and conceptual representation from Whipple et al. (2012) (right).

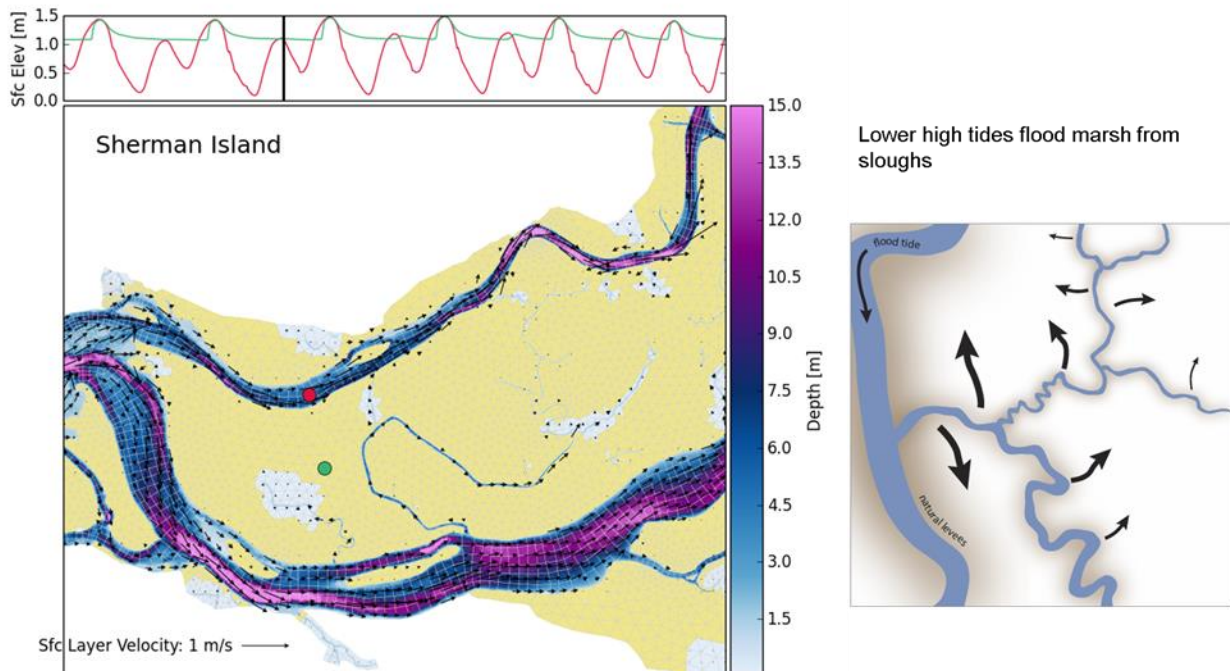


Figure 32 Modeled lower high tide flooding patterns in the pre-development Delta (left) and conceptual representation from Whipple et al. (2012) (right).

Simulation Runs for Analysis

A recent three year period was chosen for analysis: 2006–2008. This period was chosen to include both a relatively high flow year (2006) and a relatively low flow year (2008) in order to span the range of hydrologic conditions experienced in the estuary. A continuous period is a requirement for the statistical isohaline analysis. A relatively recent time period was chosen so that the contemporary system simulation could easily be compared to observed data from continuous monitoring stations. The specific time period for the simulations was February 2006–October 2008. The start date was chosen to coincide with a USGS Polaris transect date, so an accurate depiction of the initial salinity field could be prescribed in the model. The end of the simulation was chosen around when the fall low-flow period was ending. CDWR Water Year Hydrologic Classification Indices for the Sacramento Valley are listed as *wet*, *dry*, and *critical* for water years 2006, 2007, and 2008, respectively. San Joaquin Valley Classification Indices are *wet*, *critical*, and *critical* for the same years.

Boundary conditions for the contemporary simulation are the same as those presented for the contemporary calibration run and are presented in Figure 3 through Figure 9 and Table 4. Contemporary simulation river inflows and diversions are shown in Figure 3 through Figure 5. Pre-development simulation river inflows are shown in Figure 33 and Figure 34; no diversions were specified for that simulation. The contemporary simulation ocean stage boundary condition is shown in Figure 7. The same time series, but shifted -1 ft to account for sea level rise, was used for the pre-development simulation. River inflow salinity boundary conditions are shown in Figure 6 for the contemporary simulation. River salinities were set at a constant freshwater level of 0.067 psu for the pre-development simulation. Evaporation and precipitation boundary conditions for South Bay, San Pablo Bay, and Suisun Bay were the same for both simulations and are shown in Figure 8 and Figure 9. Total net channel depletions for the contemporary and pre-development Deltas are compared in Figure 35. NCD estimates provided by CDWR are given on a monthly timescale. The NCD calculated by the C2VSim model is given on a daily time scale and reflects the influence of precipitation events within the Delta, temporary storage of water, and return flows.

A comparison of net Delta outflow is shown in Figure 36 and Figure 37. In general, the pre-development system has higher peak flows in the winter and spring and higher sustained flows in the late spring and early summer. The contemporary system has higher outflows in the late summer and fall period. During 2006, net Delta outflows are similar for the two systems. In 2007 and 2008, net Delta outflows for the two systems differ appreciably. In spring, pre-development Delta outflows are two to three times higher than in the contemporary simulation. During the late summer and early fall period, however, contemporary system flows are approximately double the pre-development outflows.

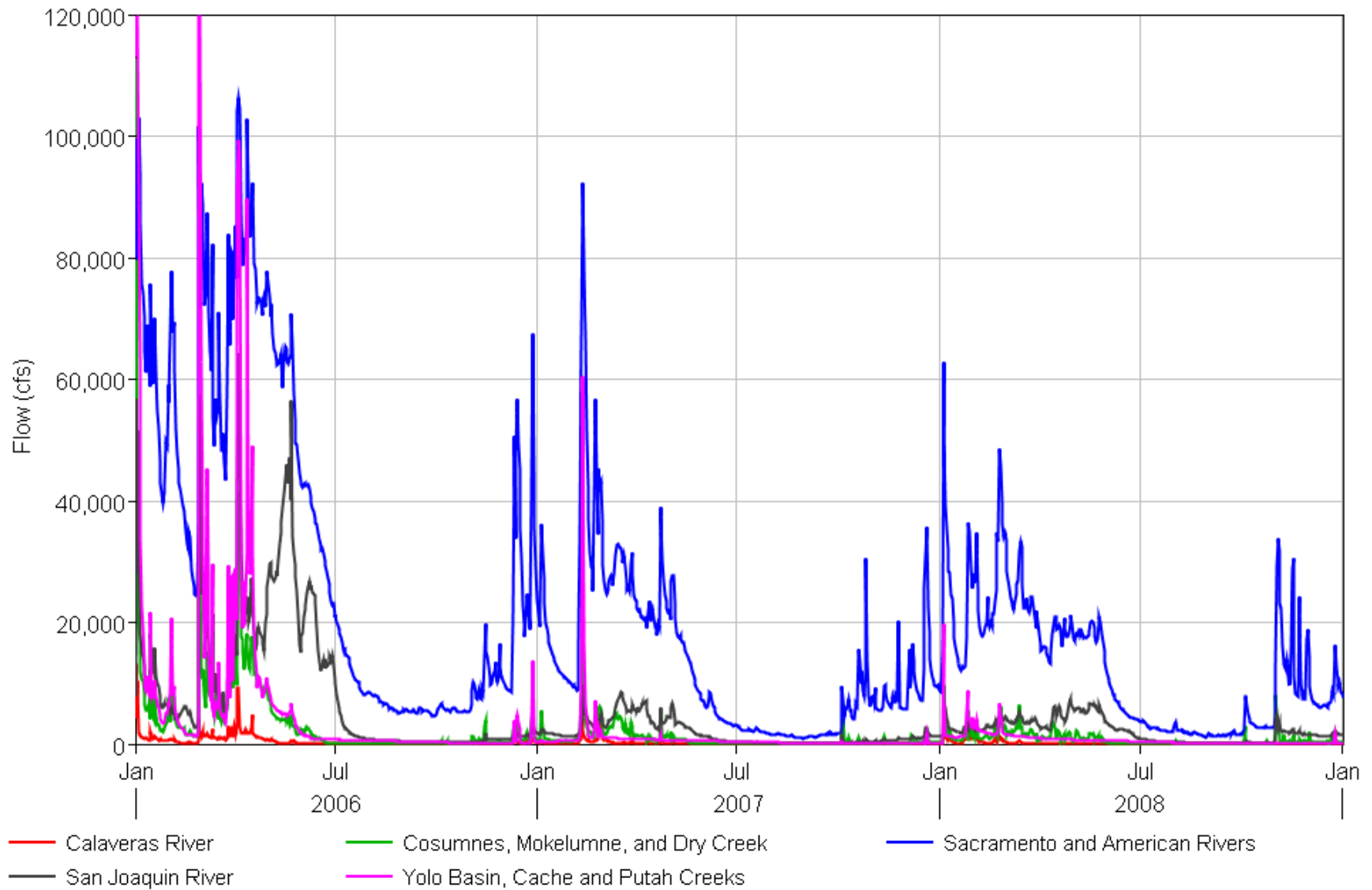


Figure 33 Pre-development model river inflow boundary conditions, 2006–2008.

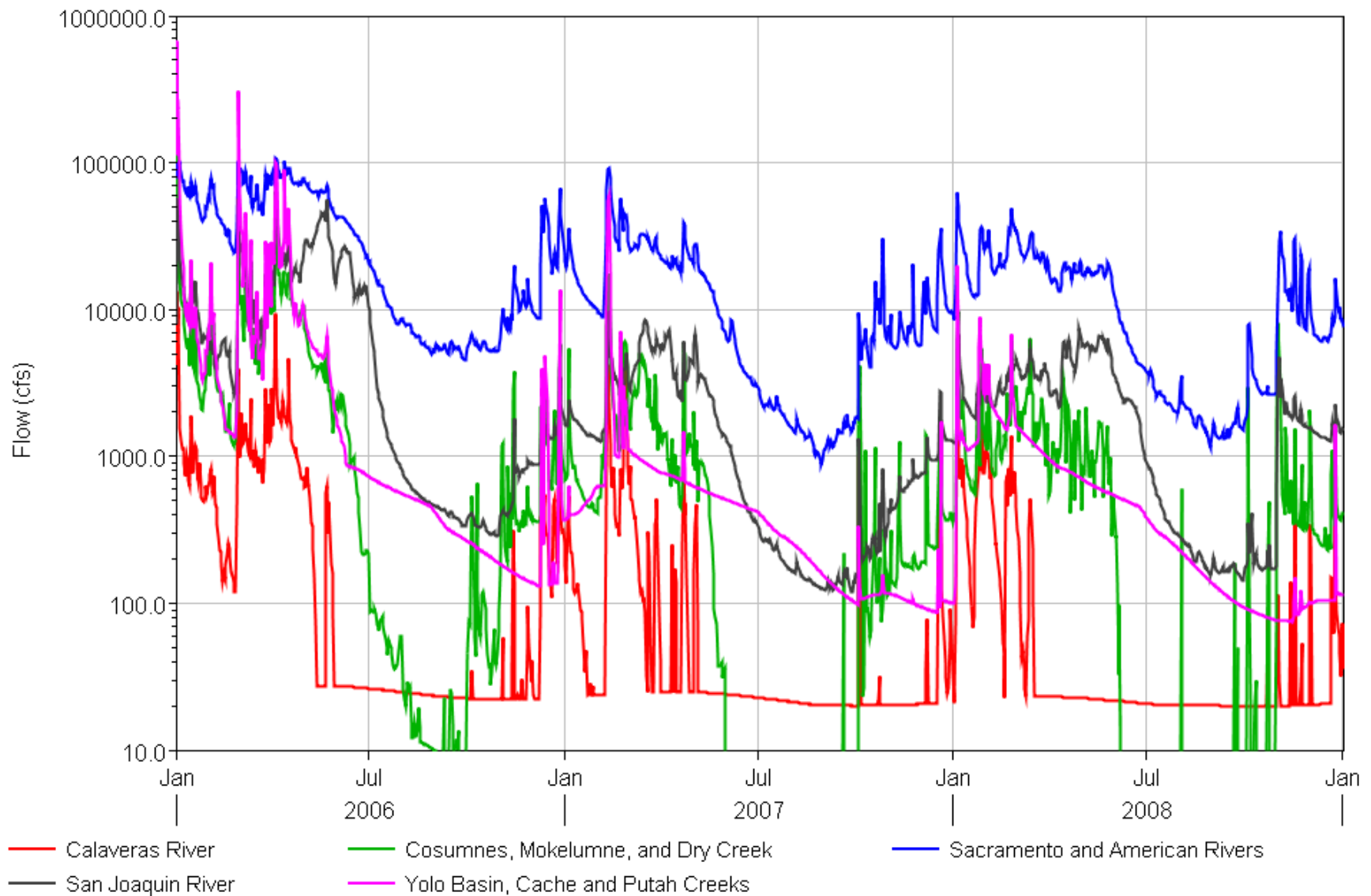


Figure 34 Pre-development model river inflow boundary conditions, 2006–2008, log scale.

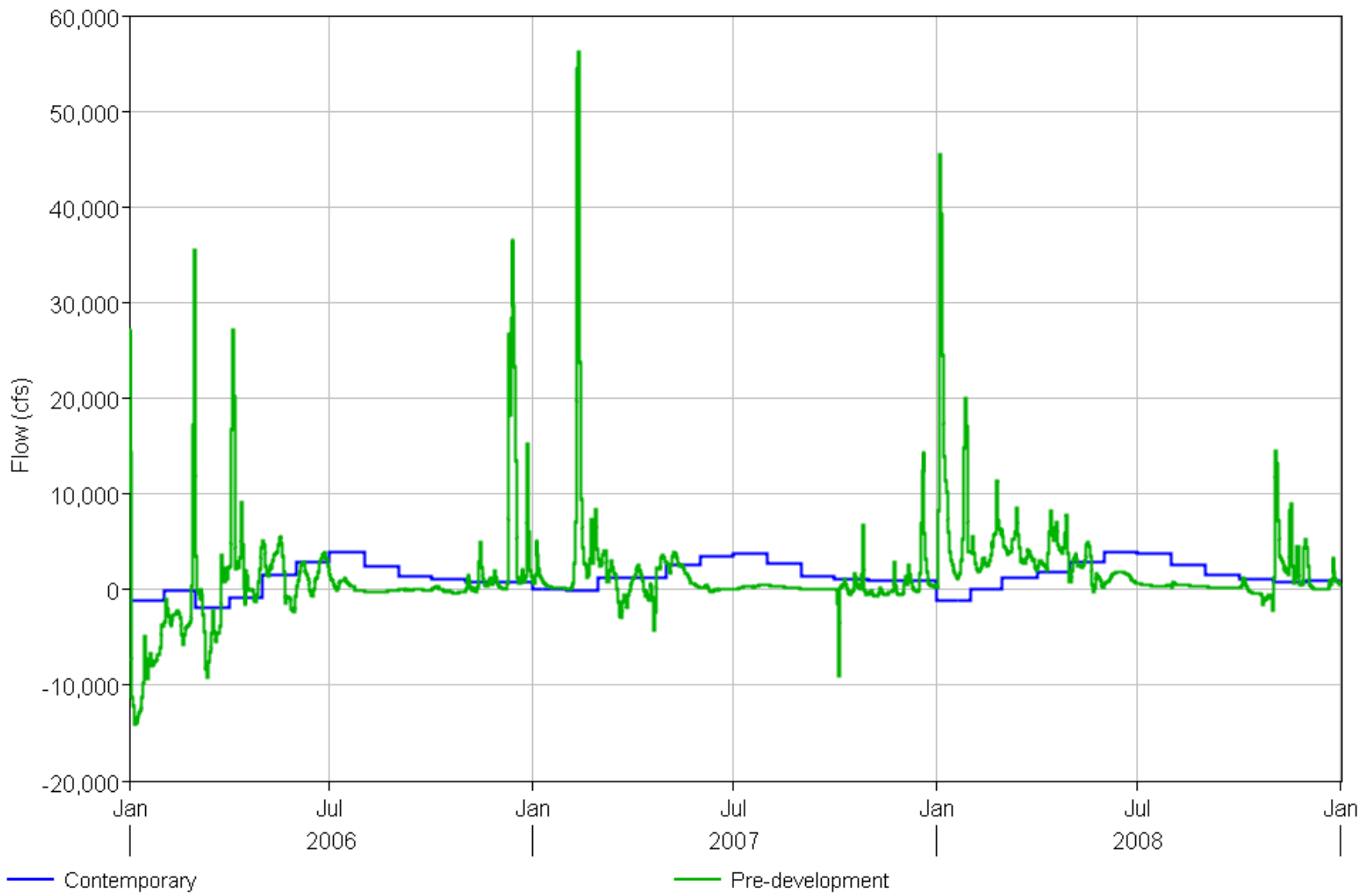


Figure 35 Comparison of pre-development and contemporary Delta total net channel depletions, 2006–2008.

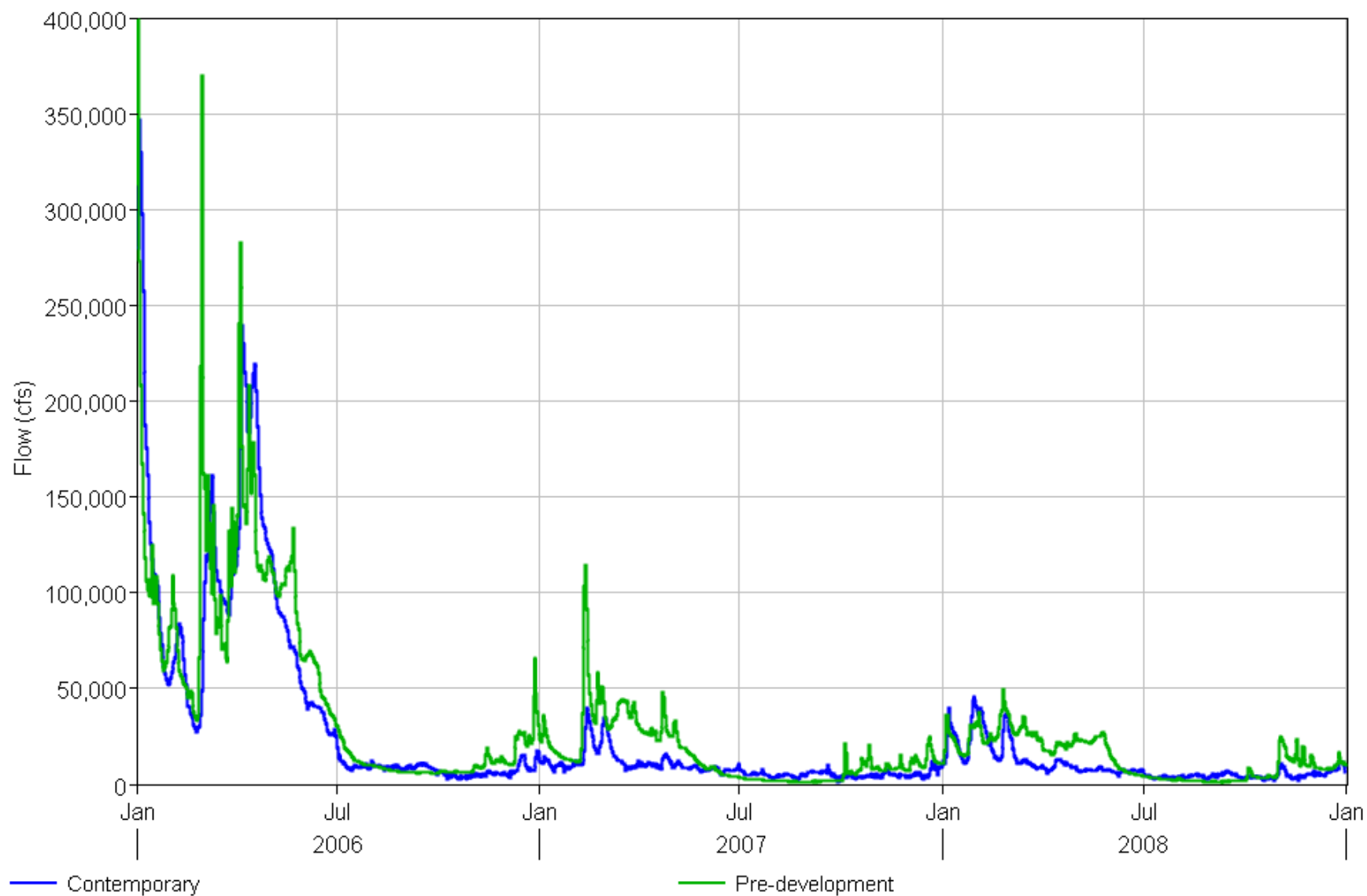


Figure 36 Comparison of pre-development and contemporary simulation net Delta outflow, 2006–2008.

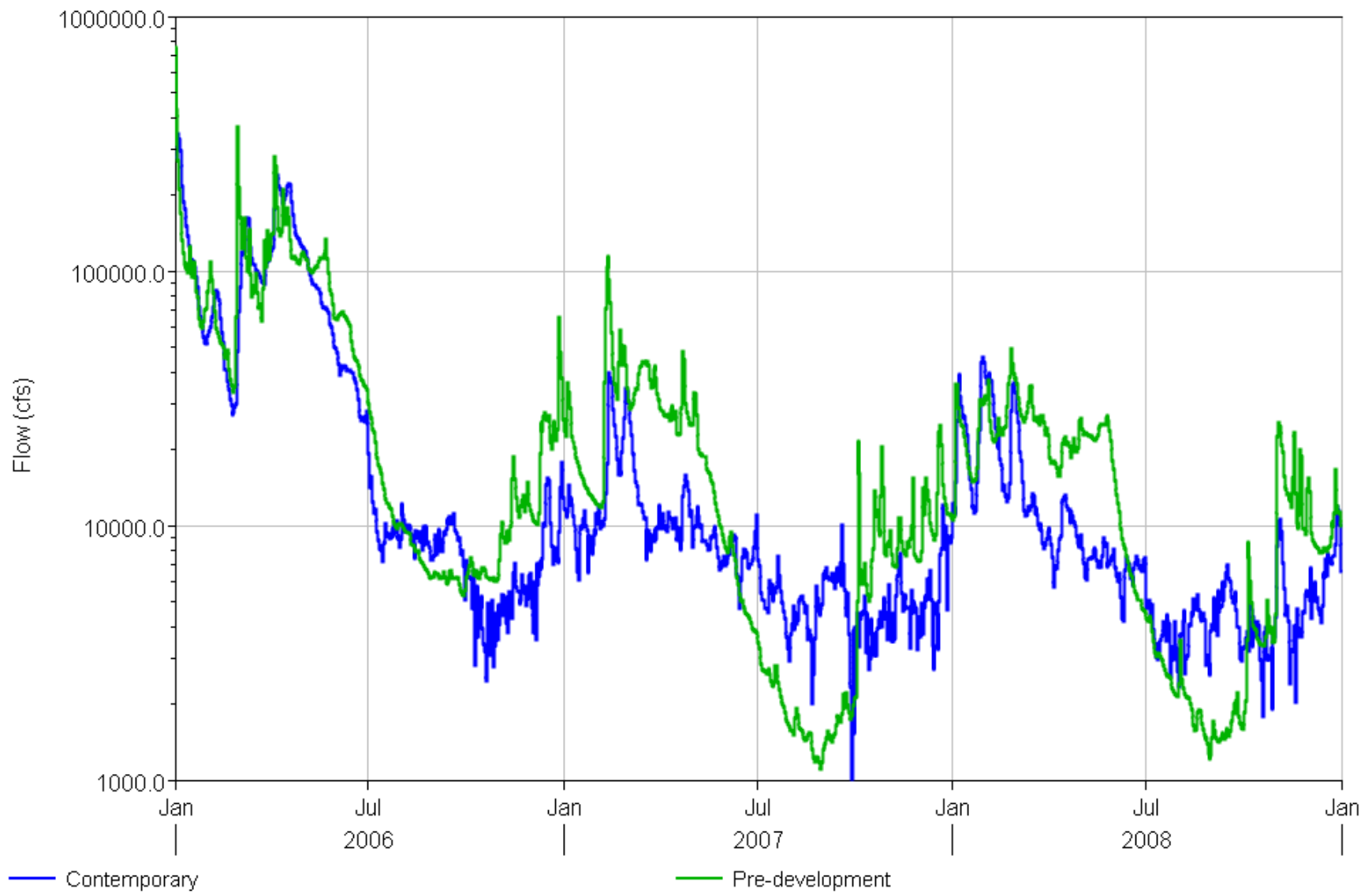


Figure 37 Comparison of pre-development and contemporary simulation net Delta outflow, 2006–2008, log scale.

Isohaline Analysis

The method used to characterize differences in the salinity regimes of the pre-development and contemporary systems was a statistical analysis of isohaline positions. Regressions were developed to relate isohaline position to net Delta outflow for each system; the responses of the two systems could then be compared in a way that was independent of net Delta outflow, which has a large effect on isohaline position and significantly differs in the two simulations. The focus of the isohaline analysis is on the 2 psu bottom salinity isohaline, known as X2. The value of X2 is of interest to managers due to observed correlations with abundance of many aquatic organisms (Jassby et al. 1995, Kimmerer 2002). Recent declines in some of these organisms have resulted in regulations stipulating target X2 values during specified periods of ecological importance.

Literature Review

Salt intrusion length scales in estuaries have been widely studied by analytical approaches and mechanistic modeling (e.g. Hansen and Rattray 1965, Lerczak et al. 2009, Hetland and Geyer 2004, MacWilliams et al. 2015). The length scale of salt intrusion is typically defined as the axial distance from the inlet to a specific isopycnal location. In the San Francisco Estuary, the length scale of most interest is X2, the axial distance from the Golden Gate to the location of 2 psu salinity at the bed of the channel (Jassby et al. 1995). When 2 psu salinity extends landward of the confluence, X2 is defined as the average of the axial distances up the Sacramento and San Joaquin Rivers (Gross et al. 2009).

The initial fitting of X2 to Delta outflow (Jassby et al. 1995) used an autoregressive equation of the form

$$X2(t) = \theta_0 + \theta_1 X2(t - 1) + \gamma_f \log Q(t) \quad (1)$$

where t is time (days), Q ($\text{m}^3 \text{s}^{-1}$) is the net Delta outflow, and θ_0 , θ_1 , and γ_f are fitting parameters. In Jassby et al. (1995) and subsequent X2 analyses, the Delta outflow was estimated by the DAYFLOW program, a water balance based method for estimating outflow that does not account for temporal variation in water volume storage in the Delta. In addition, it should be noted that this fitting approach and subsequent approaches described here do not account for variation in the strength of salt intrusion processes over the spring-neap cycle which has been found to be large in some settings (e.g., Lerczak et al. 2009).

Monismith et al. (2002) proposed an autoregressive relationship between $X2$ and Q consistent with the Hansen and Rattray analysis:

$$X2(t) = \alpha X2(t - 1) + (1 - \alpha)\beta Q(t)^\gamma \quad (2)$$

where α , β , and γ are the fitting parameters. γ describes the responsiveness of the salt intrusion length to flow, α is the weight applied to the autoregressive term, and β is a scaling coefficient. Monismith et al. (2002) show that the expected value of γ is $-1/3$ when the assumptions of Hansen and Rattray (1965) are applied. Most notably, these assumptions include a single vertical eddy diffusivity which is constant in time and space. When using a least squares procedure to fit Equation 2 to observed $X2$ values, however, Monismith et al. (2002) found a γ value of $-1/7$, suggesting a strong inertia of salinity with changes in Delta outflow.

The autoregressive form of Equation 2 was also adopted by MacWilliams et al. (2015) with an additional parameter used to account for changes in the time scale of salinity response to changes in Delta outflow.

$$X2(t) = \alpha(t)X2(t - 1) + (1 - \alpha(t))\beta Q(t)^\gamma \quad (3)$$

where α is bounded between zero and one:

$$\alpha(t) = \min[1, \max[0, mQ(t) + b]] \quad (4)$$

and m and b are fitting parameters. This variable α form of the autoregressive relationship allows $X2$ to respond to flow changes more rapidly at high Delta outflow.

This and other $X2$ relationships have associated definitions of antecedent flow. Antecedent flow for a given time step is the steady-state flow analogue which results in the same $X2$ as predicted by Equation 3.

$$X2(t) = \beta Q_{ant}(t)^\gamma \quad (5)$$

Antecedent flow can be determined by substituting Equation 5 into Equation 3 and solving for Q_{ant} . In the MacWilliams et al. (2015) formulation, recursive substitution for $X2(t)$ for M days into the past yields:

$$Q_{ant}(t) = \left[(1 - \alpha(t))Q(t)^\gamma + \sum_{t'=t-M}^{t-1} \left(\prod_{t''=t'+1}^t \alpha(t'') \right) \times (1 - \alpha(t'))Q(t')^\gamma \right]^{1/\gamma} \quad (6)$$

A similar fitting approach was adopted by Hutton et al. (2015) in the Delta Salinity Gradient (DSG) Model. In that case Equation 5 was used but the antecedent flow was estimated by a G-model approach (Denton 1993)

$$\frac{dQ_{ant}(t)}{dt} = \frac{(Q(t) - Q_{ant}(t))Q_{ant}(t)}{\beta_G} \quad (7)$$

where β_G is a fitting parameter ($\text{m}^3 \text{s}^{-1} \text{ days}$) and β_G/Q_{ant} provides a time scale for the rate of change of salinity. In the terminology of Denton (1993) Q_{ant} is referred to using the variable $G(t)$. A closed form solution to Equation 7 is provided by Denton and Sullivan (1993)

$$Q_{ant}(t) = \frac{\bar{Q}(t)Q_{ant}(t-1)}{Q_{ant}(t-1) + (\bar{Q}(t) - Q_{ant}(t-1))e^{-\bar{Q}(t)/\beta}} \quad (8)$$

where $\bar{Q}(t)$ is the average flow during the daily interval over which the antecedent flow is updated. A major advantage of the Hutton et al. (2015) DSG approach over the MacWilliams et al. (2015) approach is that negative daily Delta outflow can be accommodated.

Closely associated with the isohaline analysis approaches is the concept of self-similarity of the salinity field. This is the idea that the salinity field, at least within the central region of the estuary, responds in a coordinated way to changes in outflow. A consequence is that the analysis of a specific isohaline (i.e., X2) can be assumed to be indicative of the response of the entire estuarine salt field to outflow, and additional isohaline locations can be predicted based on the X2 position.

In the DSG approach, Hutton et al. (2015) assumed the 2 psu bottom salinity (X2) to correspond to a surface specific conductivity of 2.64 mS/cm (equal to 1.36 psu using the UNESCO conversion equations). Assuming self-similarity, they could then predict the position of a surface isohaline anywhere in the estuary relative to the reference X2 bottom isohaline position:

$$X = X2 * \left[\frac{\log\left(\frac{S - S_b}{S_0 - S_b}\right)}{\tau} \right]^{-\gamma} \quad (9)$$

$$\tau = \log\left(\frac{1.36 - S_b}{S_0 - S_b}\right) \quad (10)$$

S_0 and S_b are the downstream and upstream boundary condition salinities, respectively, and S is the target surface salinity. In order to take into account deviations from the assumption of self-similarity, which primarily occur at high outflow conditions, they assumed that S_0 varies with X2 according to:

$$S_0(t) = \hat{S} + (1.36 - \hat{S}) * e^{(-\gamma_S * X2(t)^\delta)} \quad (11)$$

where \hat{S} is the ocean salinity. By calculating S_0 at several locations throughout the estuary, the optimal fit for parameters γ_S and δ can be determined.

Analysis Methods

A dataset of hydrodynamic model predicted X2 was estimated for each system based on simulation results by daily-averaging salinity at the bed along the transects shown in Figure 38. The location of the 2 psu isohaline on each transect was estimated by linear interpolation between the two output locations on the transect that bound 2 psu. When X2 was located landward of the Sacramento–San Joaquin confluence, the X2 distances up the Sacramento River and San Joaquin River were tracked separately. The average of the two X2 values was also calculated.

Because of differences in channel configuration, the pre-development and contemporary system transects diverge in certain locations. This can be seen through Suisun Bay, at Horseshoe Bend on the lower Sacramento River, and through the many bends along the middle San Joaquin River. To facilitate salinity isohaline comparisons between the two systems, the isohaline distances of the pre-development system were mapped to contemporary distances so that an isohaline at the same geographical locations (e.g., Rio Vista, Jersey Point) in both systems has the same value.

The three-parameters of the Hutton et al. (2015) approach (β , γ , and β_G) were fit to the hydrodynamic model predicted daily X2 using a nonlinear least-squares fitting method implemented in the Python Scipy numerical library². The resulting statistical model predicted X2 is compared with the hydrodynamic model predicted X2 in the following section.

In addition to the 2 psu bottom salinity isohaline, the previously described analysis was also performed for 1 psu surface salinity, 6 psu surface salinity, and 2.64 mS/cm surface specific conductivity isohalines. The 1 psu and 6 psu locations may be used to characterize the low-salinity zone (LSZ) habitat in the upper estuary. The 2.64 mS/cm surface conductivity is used in regulatory contexts and is often assumed to correspond to the 2 psu bed salinity (X2). In addition to the individual isohaline fits, model time series for X2 and the 1 and 6 psu surface isohaline distances were fit concurrently using Equation 9 in order to obtain β , γ , and β_G parameter estimations representative of the entire low salinity zone.

Two estimations of net Delta outflow, Q , were used in the analysis. The first was the tidally averaged, 3-D hydrodynamic model predicted outflow at Martinez. The second was the Net Delta Outflow Index (NDOI), the sum of the daily Delta inflows minus net channel depletions. The model predicted outflow at Martinez takes into account outflow variations due to spring-neap filling and draining of the estuary and is a more accurate predictor of weekly changes in isohaline location. However, the NDOI is more easily calculated and isohaline relationships

² Documentation available at: http://docs.scipy.org/doc/scipy/reference/generated/scipy.optimize.curve_fit.html

derived from it are of greater use to long-term salinity analyses.

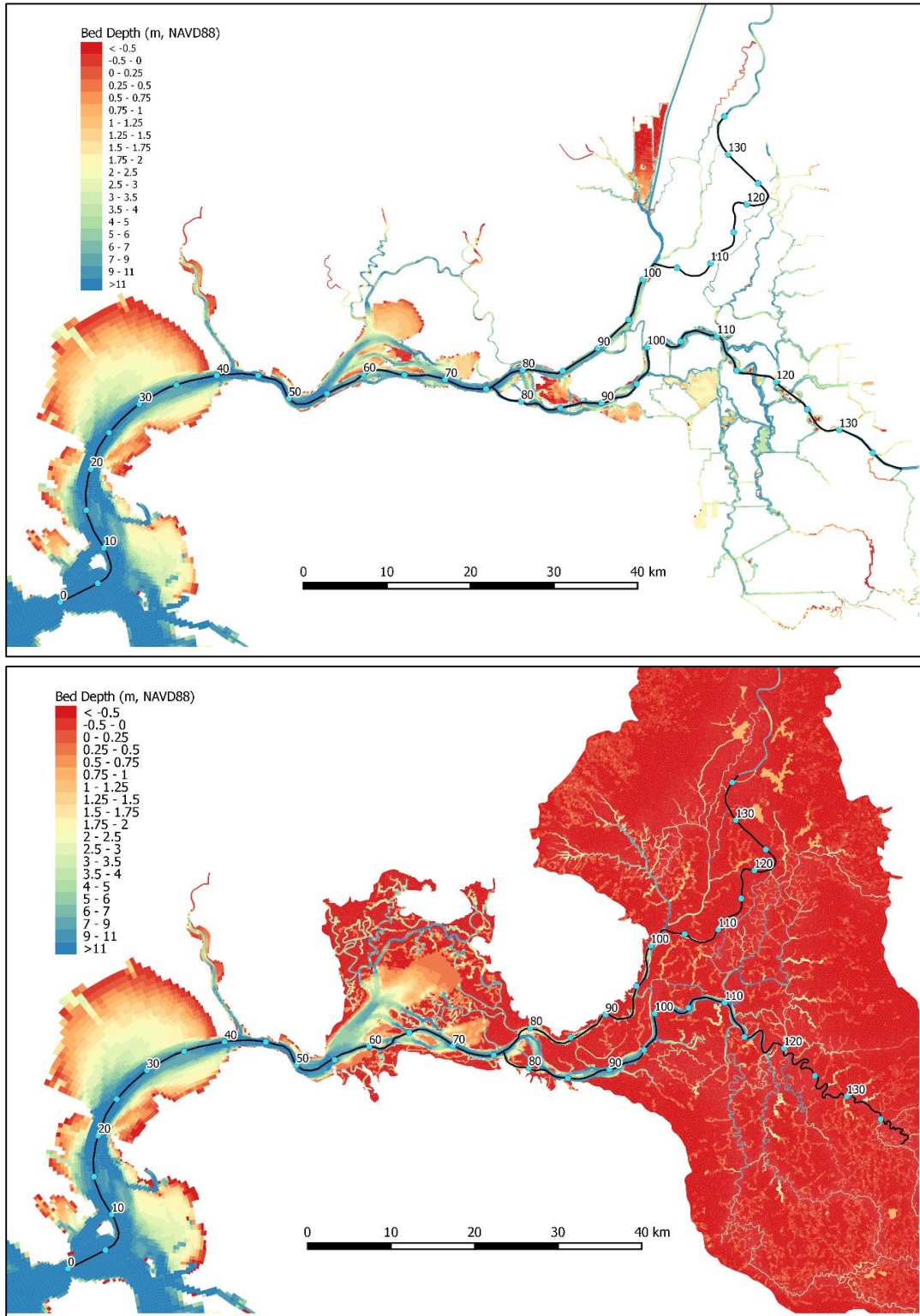


Figure 38 Contemporary (top) and pre-development (bottom) isohaline transect locations. Transect distances are given in km.

Results

Isohaline Regression Analysis

The longitudinal location of X2 for the contemporary and pre-development system simulations is shown in Figure 39. When X2 is located landward of the confluence (approximately 76 km), the average of the Sacramento and San Joaquin River X2 positions is shown. Results were highly dependent on the differing net Delta outflows for the two systems (see Figure 36 and Figure 37). Similar outflows through much of 2006 led to similar X2 isohaline locations. Much larger differences were seen in late 2006 through 2008, where larger pre-development system outflows in winter and spring resulted in X2 locations 10–20 km seaward of the contemporary system. The lower pre-development system outflows in summer and fall led to greater salinity intrusion into the Delta. Trends are similar for the other isohalines analyzed (Figure 40 through Figure 42), although differences in isohaline position between the two systems were generally greater for the lower salinity isohalines.

The isohaline regression analysis approach provides a convenient way to analyze the response of each estuarine system in a way that is independent of outflow. In particular, the parameter γ quantifies the sensitivity of the isohaline position to changes in outflow. The parameter β_G quantifies the time response of the system to changes in outflow. The regression fit for the river-averaged X2 in the contemporary system simulation is shown in Figure 43. Model-calculated outflow at Martinez was used for the independent outflow variable, Q . The fit is accurate, with a standard error of 1.70 km and a correlation coefficient of 0.986. The calculated exponential fitting parameter γ is -0.230, which is identical to the value of -0.230 reported by MacWilliams et al. (2015) for simulations spanning 1994–1997.

The regression fit for the river-averaged X2 for the pre-development system simulation is shown in Figure 44. Fits for the remainder of the isohalines are given in Appendix D. Table 8 lists the fit parameters and regression error metrics for each of the isohalines for each system type.

The exponential fitting parameter γ quantifies the sensitivity of the isohaline response to changes in net Delta outflow. Higher absolute values of the exponent indicate an isohaline that responds by moving greater distances in response to flow changes than an exponent with a lower absolute value. In the 2006–2008 contemporary system simulations, X2 is located most of the time between Martinez and the confluence. In this wider area, its location is less responsive to changes in outflow. The 1 psu surface isohaline and the 6 psu surface isohaline spend more of the simulation around narrower regions in the Delta and Carquinez Strait, respectively. Regression fits reflect this with higher γ values for these isohalines. The 2.64 mS/cm line responds similarly to the 1 psu line.

γ values for the pre-development system were very similar to the contemporary system values. For X2, the calculated γ value was slightly more negative, indicating its location in the pre-

development upper estuary was slightly more sensitive to changes in outflow. For the 6 psu surface isohaline, the γ value was slightly less negative, indicating a less sensitive isohaline than in the contemporary system. The γ values for the 1 psu and 2.64 mS/cm isohalines were approximately equal in the two systems.

For X2 and the 1 psu and 2.64 isohalines, the parameter β_G , which quantifies the time response of the system to changes in outflow, was lower in the pre-development system. As this parameter is in the denominator in Equation 7, this indicates the pre-development system generally responded faster to changes in net Delta outflow. For the 6 psu isohaline, β_G is higher in the pre-development system, indicating a slower response to outflow changes.

It can be difficult to understand the salinity regimes of the two systems based only on abstract statistical model fit parameters. For this reason, the fitting parameters for X2 listed in Table 8 were used to generate X2 time series for each system using identical input net Delta outflow time series. The results are shown for contemporary system outflows in Figure 45 and pre-development system outflows in Figure 46. The X2 locations in each system were seen to behave very similarly, given the same outflows. The mean absolute difference in X2 location over all of the simulations was 3.23 km, and 90% of the differences are within 4.68 km.

Table 8 Individual isohaline regression fit statistics. Average Sacramento and San Joaquin isohaline position and hydrodynamic model calculated outflow at Martinez were used as inputs for the analysis.

Isohaline	Parameter	Pre-development	Contemporary
2 psu Bottom Salinity	β	277	281
	γ	-0.237	-0.230
	β_G ($\text{m}^3 \text{s}^{-1} \text{ day}$)	4458	5739
	Standard Error (km)	2.26	1.70
	R^2	0.985	0.986
1 psu Surface Salinity	β	365	387
	γ	-0.281	-0.282
	β_G ($\text{m}^3 \text{s}^{-1} \text{ day}$)	5042	5983
	Standard Error (km)	2.49	2.61
	R^2	0.987	0.979
6 psu Surface Salinity	β	351	426
	γ	-0.319	-0.345
	β_G ($\text{m}^3 \text{s}^{-1} \text{ day}$)	6328	5906
	Standard Error (km)	3.57	2.81
	R^2	0.965	0.971
2.64 mS/cm Surface Specific Conductance	β	356	384
	γ	-0.282	-0.286
	β_G ($\text{m}^3 \text{s}^{-1} \text{ day}$)	5017	5908
	Standard Error (km)	2.56	2.58
	R^2	0.986	0.978

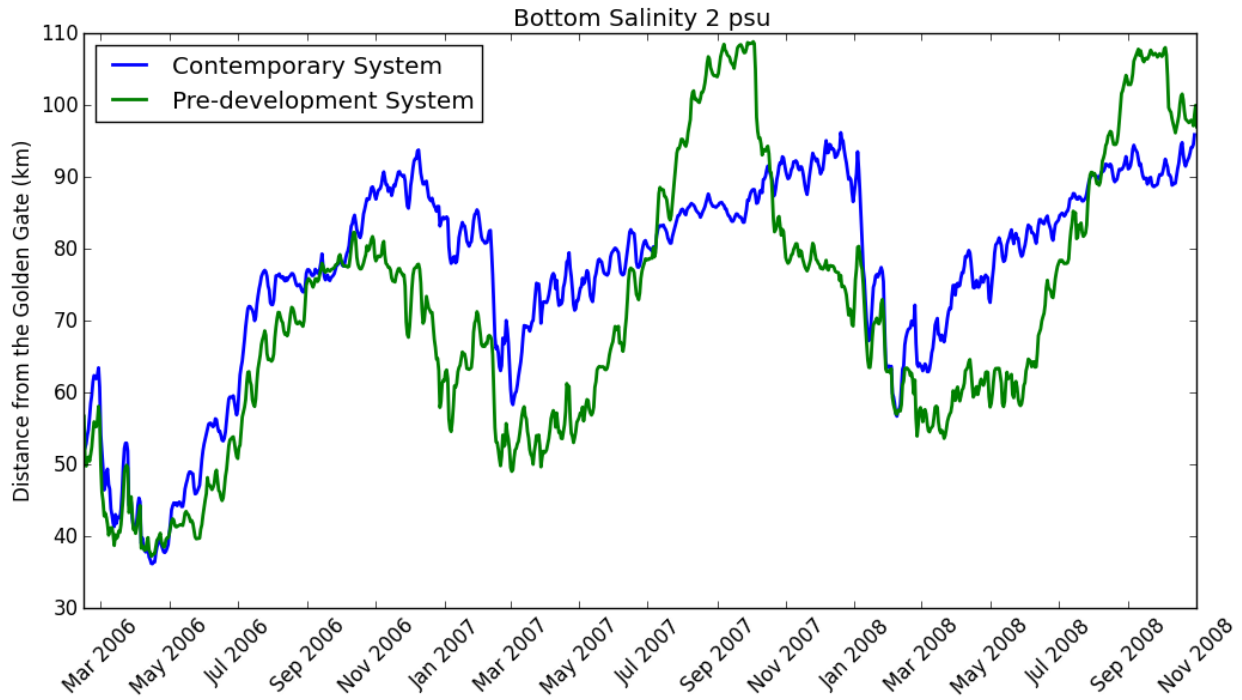


Figure 39 Contemporary and pre-development simulation results of 2 psu daily-averaged bottom salinity. Average Sacramento and San Joaquin isohaline position is shown.

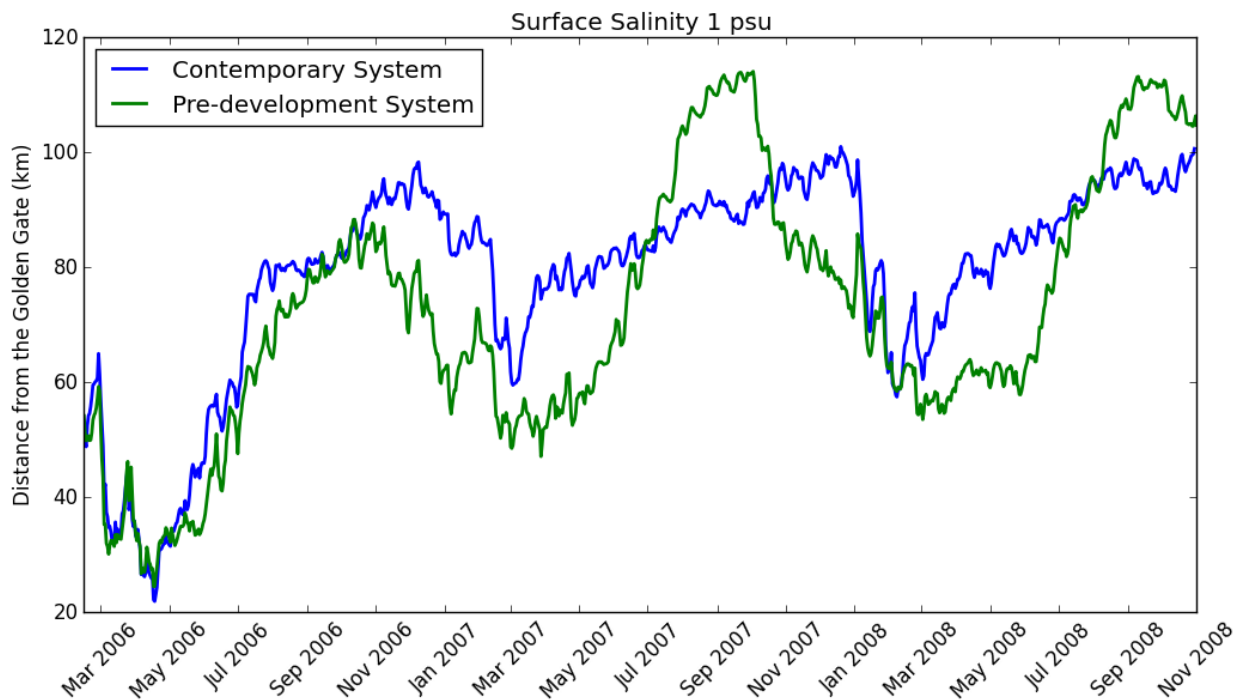


Figure 40 Contemporary and pre-development simulation results of 1 psu daily-averaged surface salinity. Average Sacramento and San Joaquin isohaline position is shown.

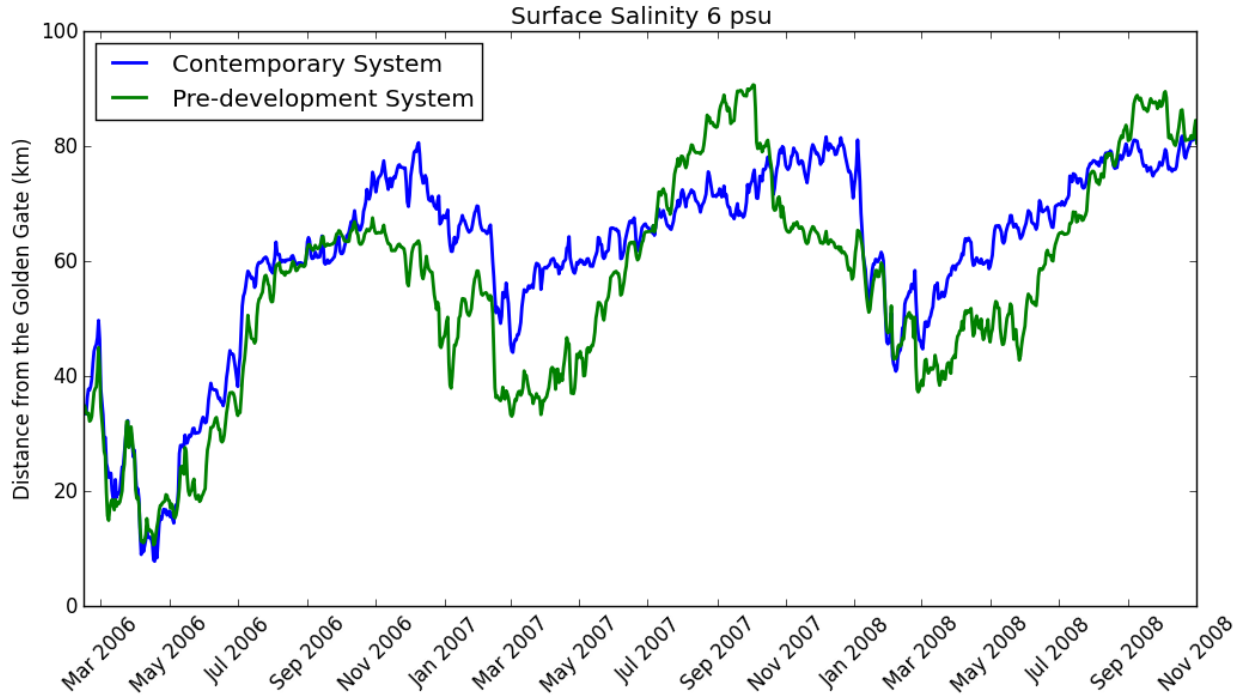


Figure 41 Contemporary and pre-development simulation results of 6 psu daily-averaged surface salinity. Average Sacramento and San Joaquin isohaline position is shown.

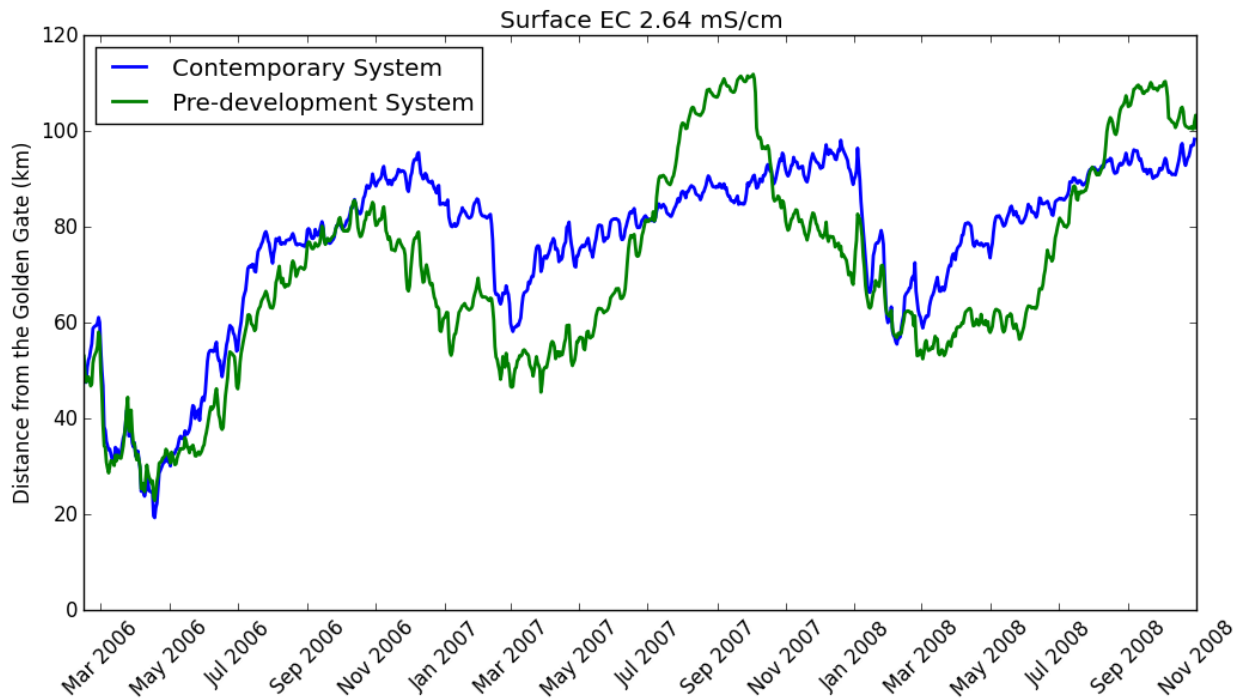


Figure 42 Contemporary and pre-development simulation results of 2.64 mS/cm daily-averaged surface conductance. Average Sacramento and San Joaquin isohaline position is shown.

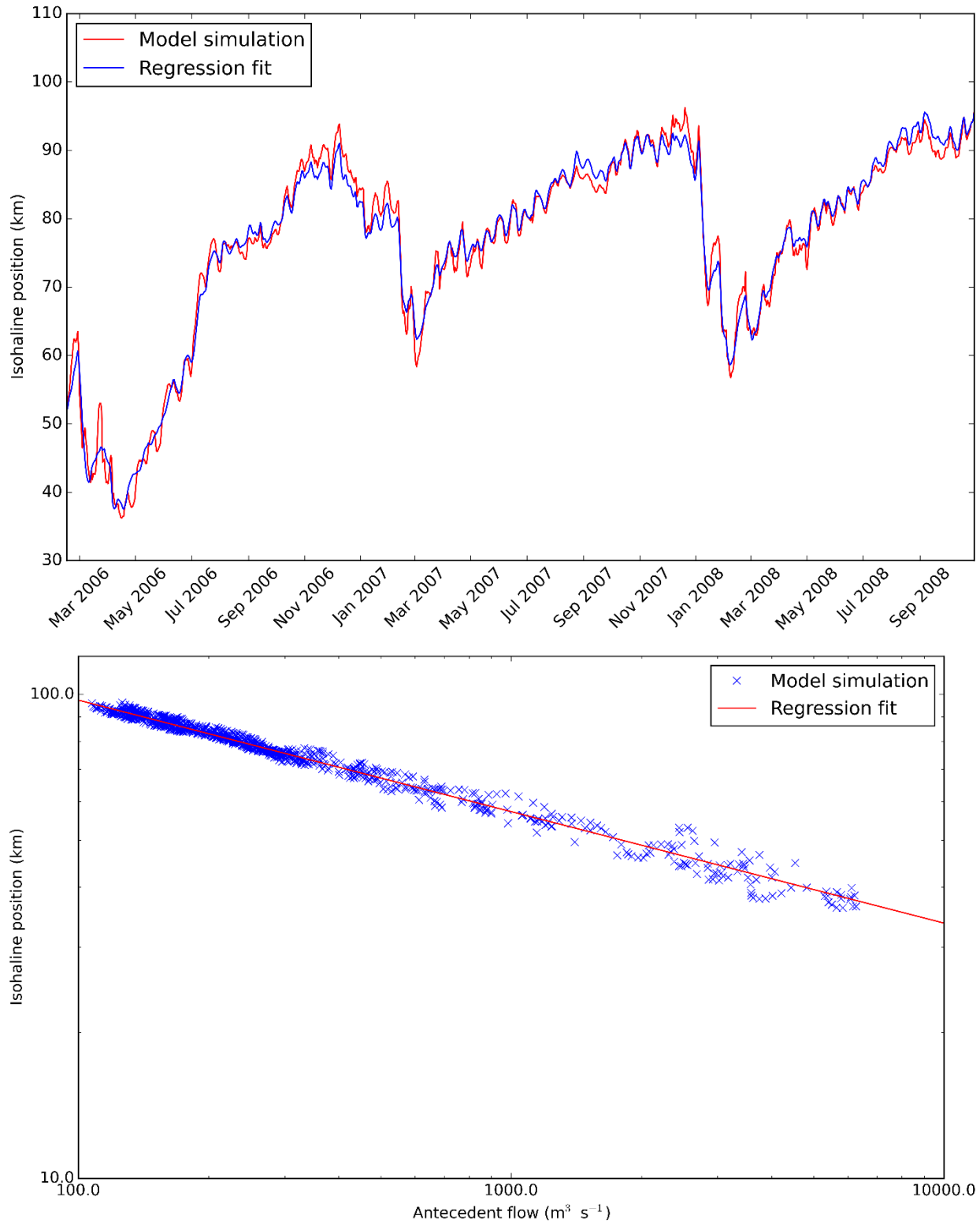


Figure 43 Contemporary system simulation 2 psu bottom salinity regression and hydrodynamic model time series comparison (top) and regression fit (bottom). Model-calculated outflow at Martinez is used for the independent outflow variable, Q .

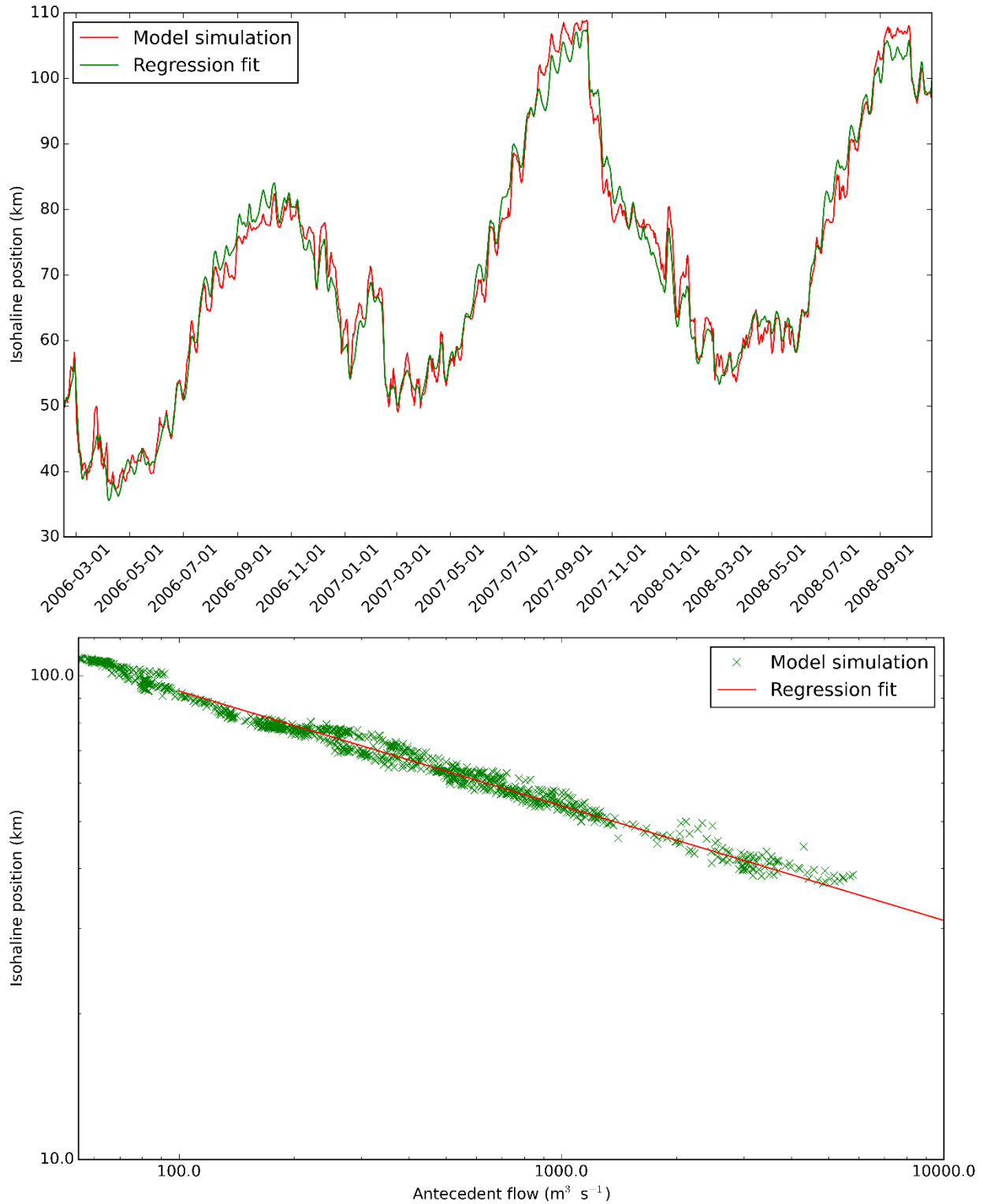


Figure 44 Pre-development system simulation 2 psu bottom salinity regression and hydrodynamic model time series comparison (top) and regression fit (bottom). Model-calculated outflow at Martinez is used for the independent outflow variable, Q .

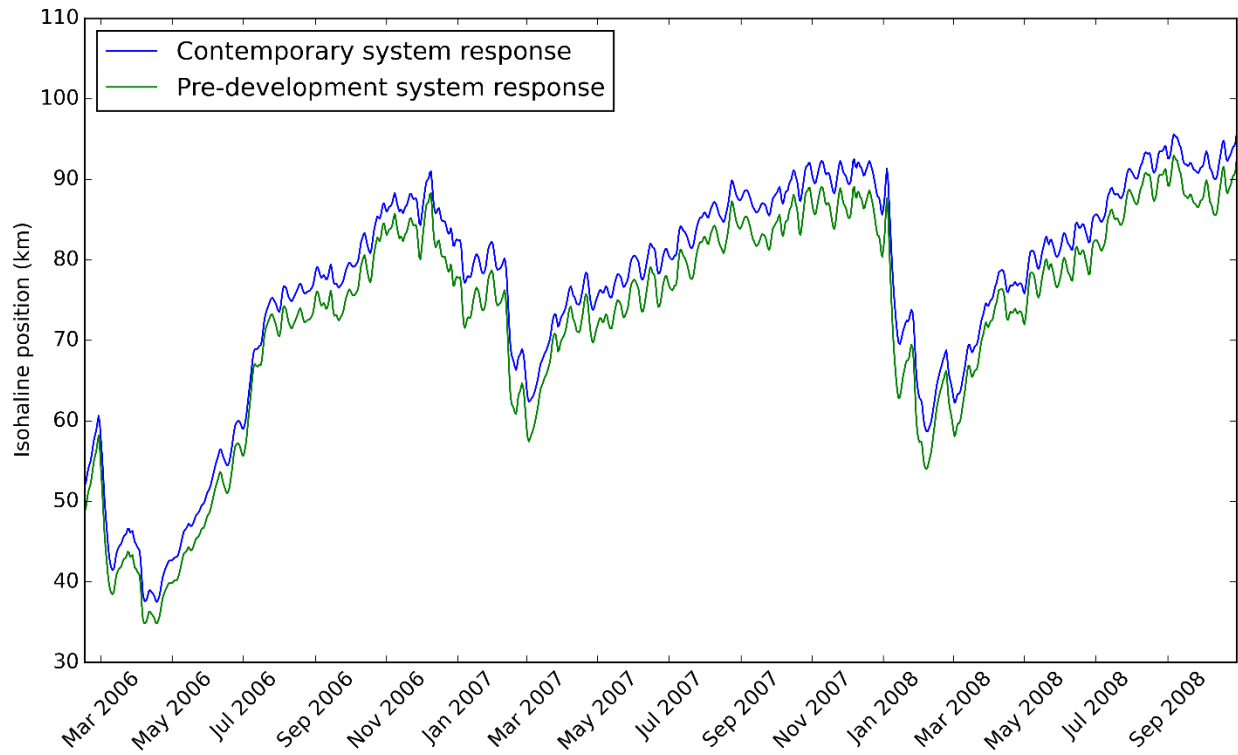


Figure 45 X2 isohaline response to contemporary simulation net Delta outflows.

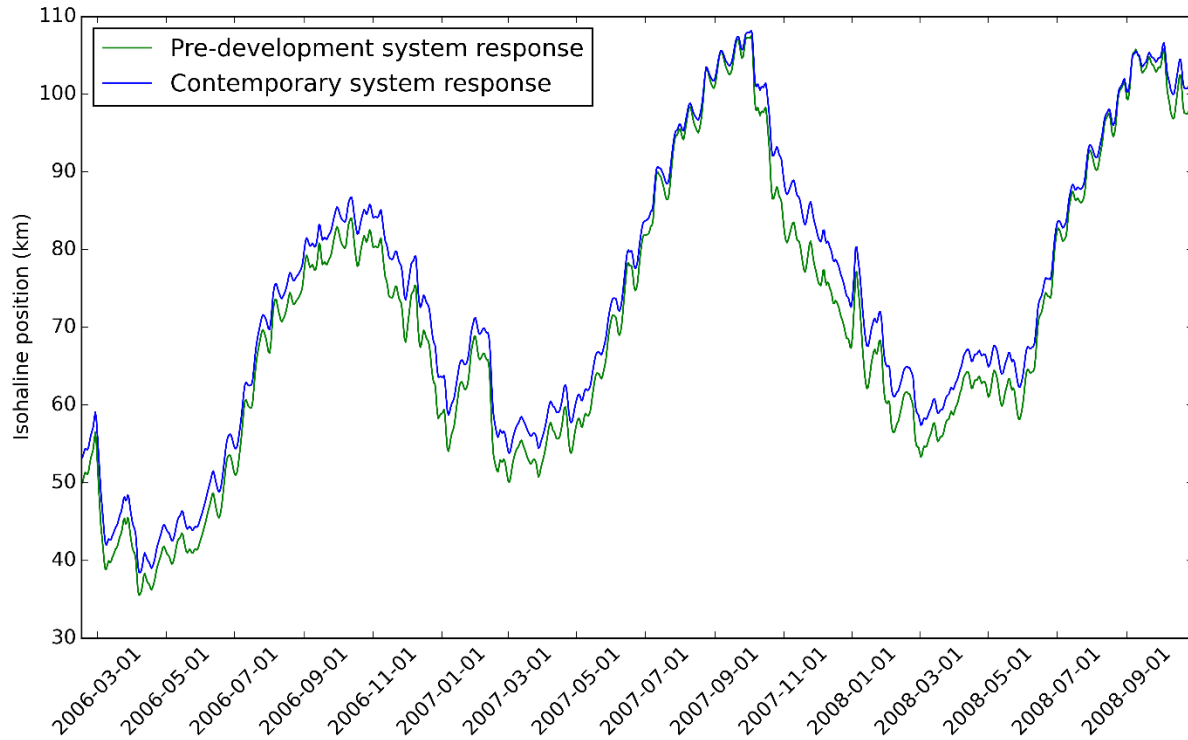


Figure 46 X2 isohaline response to pre-development simulation net Delta outflows.

Sacramento River and San Joaquin River X2 Regressions

In order to examine differences between the salinity-outflow responses of the Sacramento River and San Joaquin River, separate X2 isohaline fits for each transect were calculated, based on their individual time series records and model-calculated outflow at Martinez. The resulting best-fit parameters are shown in Table 9 in comparison with the river-averaged values presented in the previous section.

In the contemporary system, the isohaline response parameter, γ , indicated a slightly lower sensitivity to outflow along the San Joaquin River, but Sacramento and San Joaquin values were similar (difference = 0.006). In the pre-development system, the San Joaquin River value indicated a higher sensitivity to outflow and there was a greater difference between rivers (0.019). In the river-averaged case, γ differed by 0.007 between the pre-development and contemporary systems. In the split river case, the differences were 0.005 and 0.020 for the Sacramento River and San Joaquin River, respectively. Individual river regression fits were found to have similar or slightly worse accuracy.

In the pre-development simulation, salinity intrudes significantly further (approximately 10 km) up the San Joaquin River than the Sacramento River during very low flows. This happens very quickly after X2 passes upstream of Jersey Point and is due to the bathymetry and geometry of that reach. The fast salinity intrusion during these times leads to a more negative γ than in the contemporary simulation, where summer and fall low flows remain higher and X2 is never located far upriver. The San Joaquin River regression fits are shown in Figure 47 and Figure 48. It should be noted that the assumption of X2 dependence on net Delta outflow is questionable for positions very far inland; during these times, Sacramento River flow is typically ten times greater than San Joaquin River flow.

Differences between the two systems along the Sacramento River were not great and are not shown. Results for the 1 psu, 6 psu, and 2.64 mS/cm surface isohalines showed similar trends and are also not presented.

Table 9 Individual X2 regression fit statistics for the Sacramento River, San Joaquin River, and the averaged position. Estuary outflow is estimated as model-predicted outflow at Martinez.

Parameter	Simulation Type					
	Contemporary			Pre-development		
	Sacramento	San Joaquin	Average	Sacramento	San Joaquin	Average
β	288	275	281	262	294	277
γ	-0.233	-0.227	-0.230	-0.228	-0.247	-0.237
β_G ($m^3 s^{-1} day$)	5619	5865	5739	4360	4543	4458
Standard error (km)	1.71	1.82	1.70	2.33	3.10	2.26
R^2	0.986	0.983	0.986	0.983	0.974	0.985

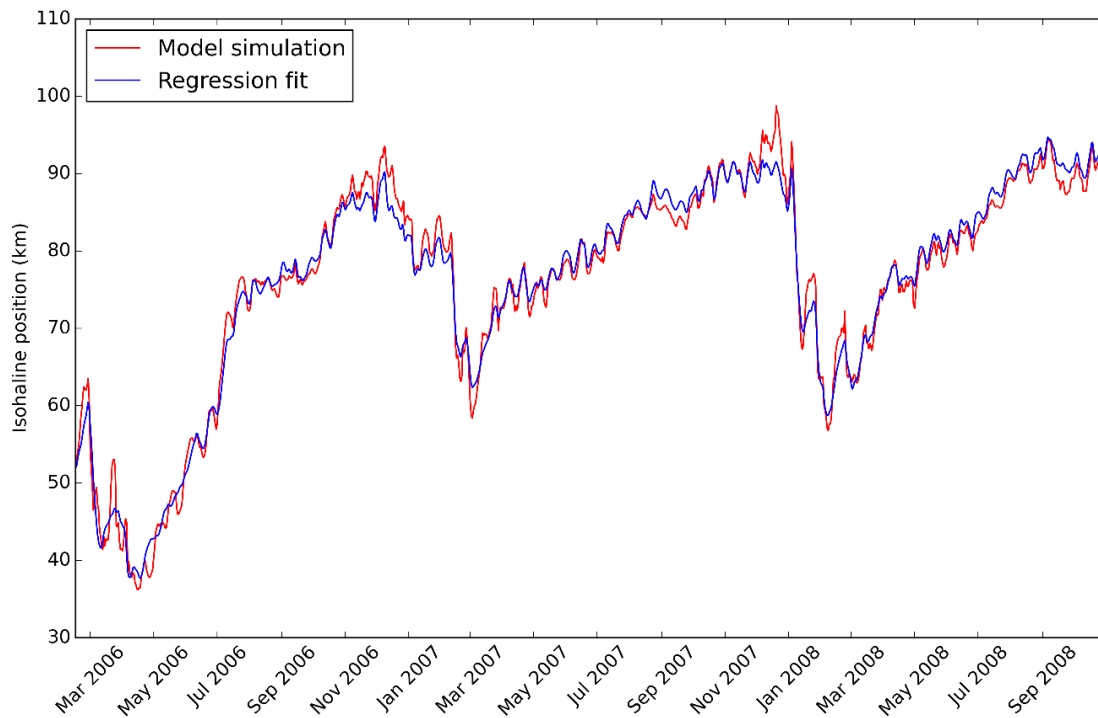


Figure 47 Contemporary system simulation San Joaquin River X2 regression and hydrodynamic model time series comparison. Model-calculated outflow at Martinez is used for the independent outflow variable, Q .

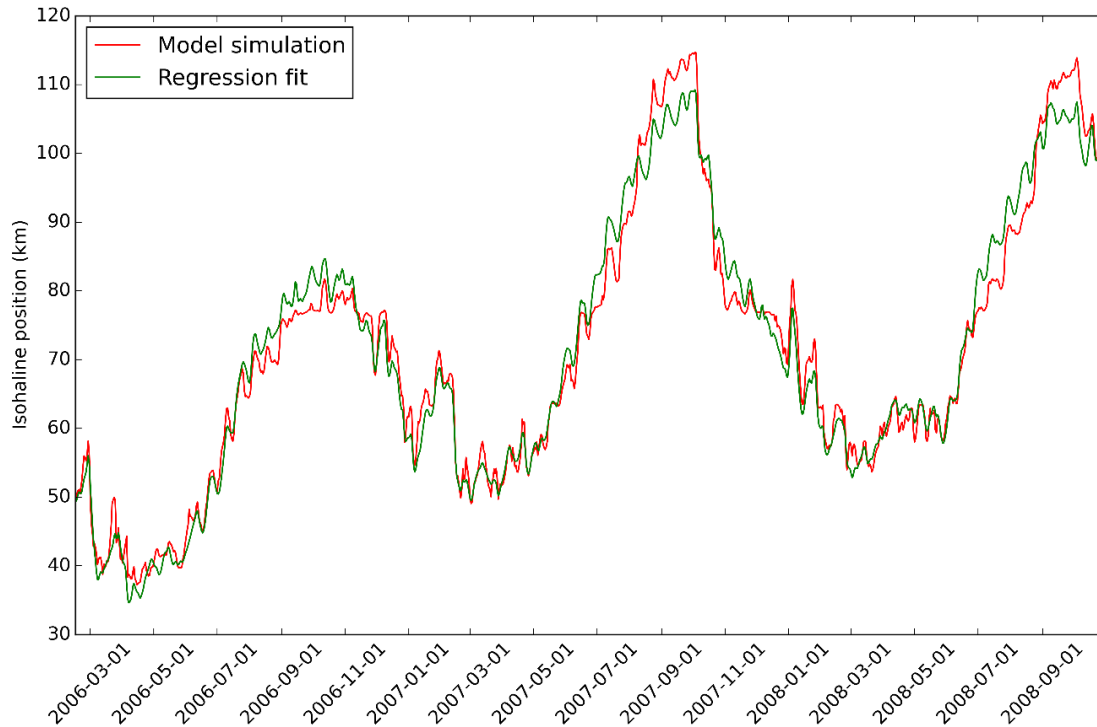


Figure 48 Pre-development system simulation San Joaquin River X2 regression and hydrodynamic model time series comparison. Model-calculated outflow at Martinez is used for the independent outflow variable, Q .

X2 Regressions Using Net Delta Outflow Index

Because of the utility in using the Net Delta Outflow Index (NDOI) in long time period analyses of estuary salinity, the X2 fitting parameters were re-calculated using NDOI as the outflow time series, instead of the previously reported model calculated outflow at Martinez. NDOI was calculated as the daily sum of the Delta riverine inflows minus net channel depletions. A comparison between NDOI and model calculated outflow at Martinez are shown for the contemporary and pre-development simulations in Figure 49 and Figure 50, respectively. Fit parameters are given in Table 10. River-averaged X2 positions and regression results are shown in Figure 51 and Figure 52.

In comparison to the results calculated using model calculated outflow at Martinez, there is little difference in the contemporary system fit parameters β and γ . The parameter β_G , which quantifies the response of the system to changes in outflow, is significantly different because the spring-neap filling and draining signal is absent in the NDOI outflow time series. This removes the ability of the regression to capture the spring-neap cycle movements in X2, resulting in poorer fit metrics.

The pre-development system fit parameters are significantly different from those calculated using model predicted outflow at Martinez. One reason why this might be the case is that the NDOI outflow time series is even less able to capture the rapid salinity intrusion on the San Joaquin River (as noted in the previous section) during low-flow than the model-calculated Delta outflow. Much of this rapid intrusion occurs during neap tides and isn't captured by the dependence on NDOI. As a result, model fit parameters are poorer (Table 10) and the fit is visually worse during low-flow conditions (Figure 52).

Table 10 Individual X2 regression fit statistics for the Sacramento River, San Joaquin River, and the averaged position. Estuary outflow is estimated using NDOI.

Parameter	Simulation Type					
	Contemporary			Pre-development		
	Sacramento	San Joaquin	Average	Sacramento	San Joaquin	Average
β	287	275	281	286	318	301
γ	-0.231	-0.225	-0.228	-0.238	-0.256	-0.247
β_G ($\text{m}^3 \text{s}^{-1} \text{ day}$)	6823	7235	7025	5080	4923	4987
Standard error (km)	2.31	2.34	2.28	3.69	4.24	3.65
R^2	0.974	0.972	0.974	0.958	0.951	0.961

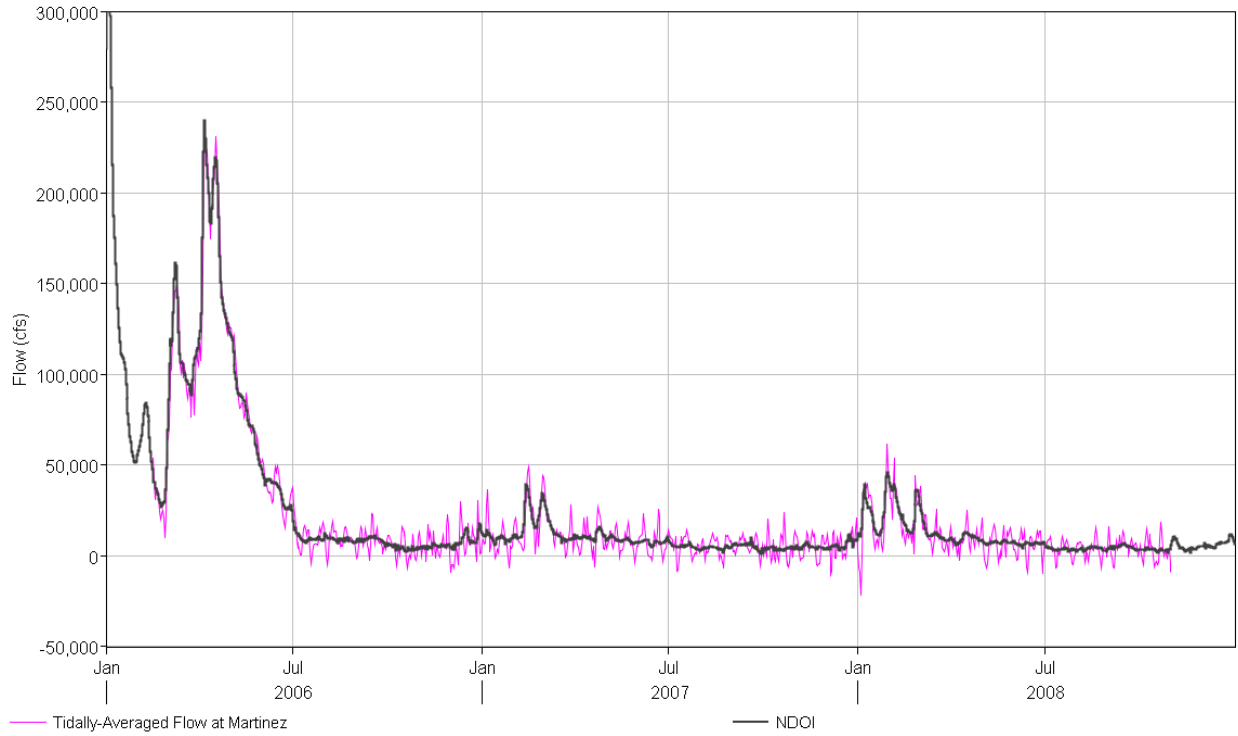


Figure 49 Comparison of contemporary simulation NDOI (black line) and model-predicted outflow at Martinez (magenta line).

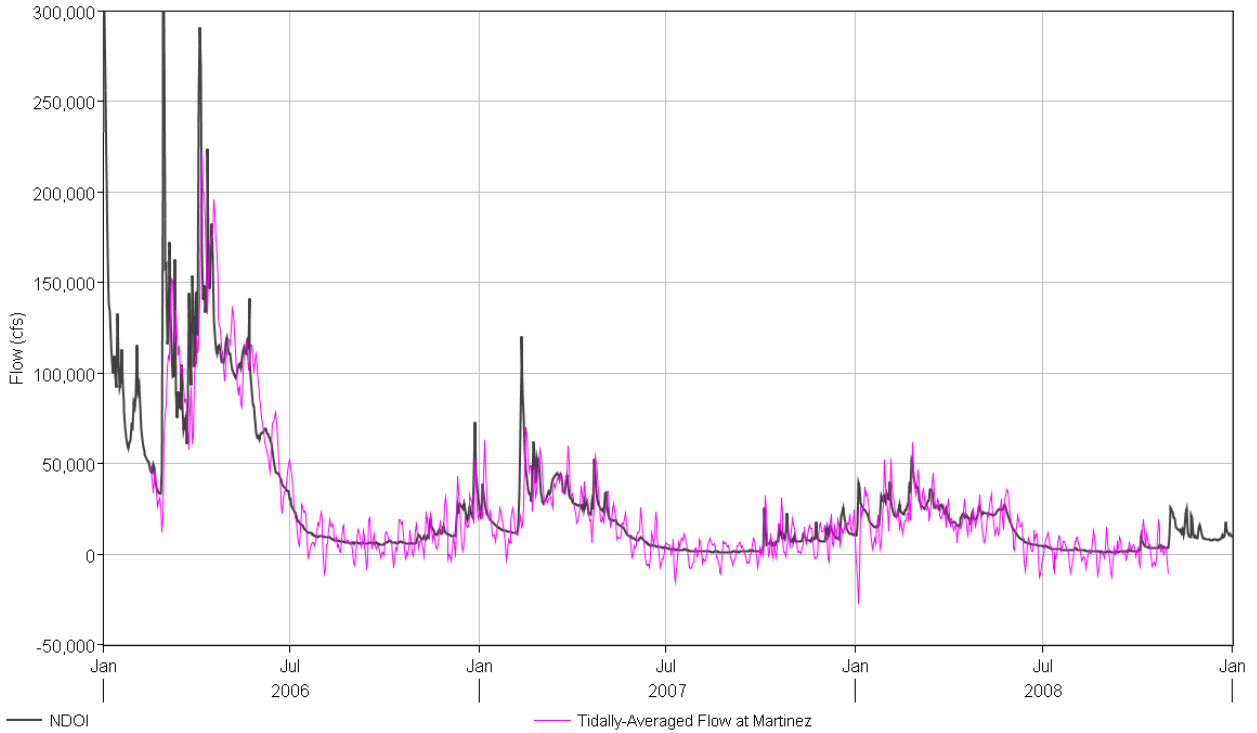


Figure 50 Comparison of pre-development simulation NDOI (black line) and model-predicted outflow at Martinez (magenta line).

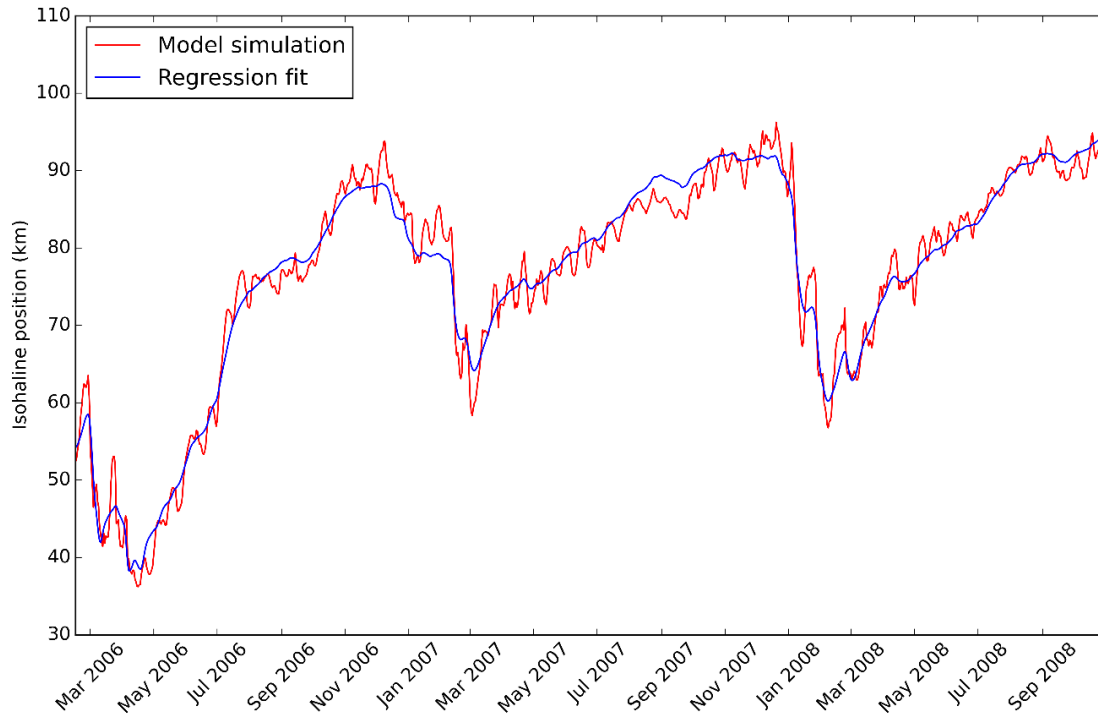


Figure 51 Contemporary system simulation X2 regression and hydrodynamic model time series comparison. NDOI is used for the independent outflow variable, Q .

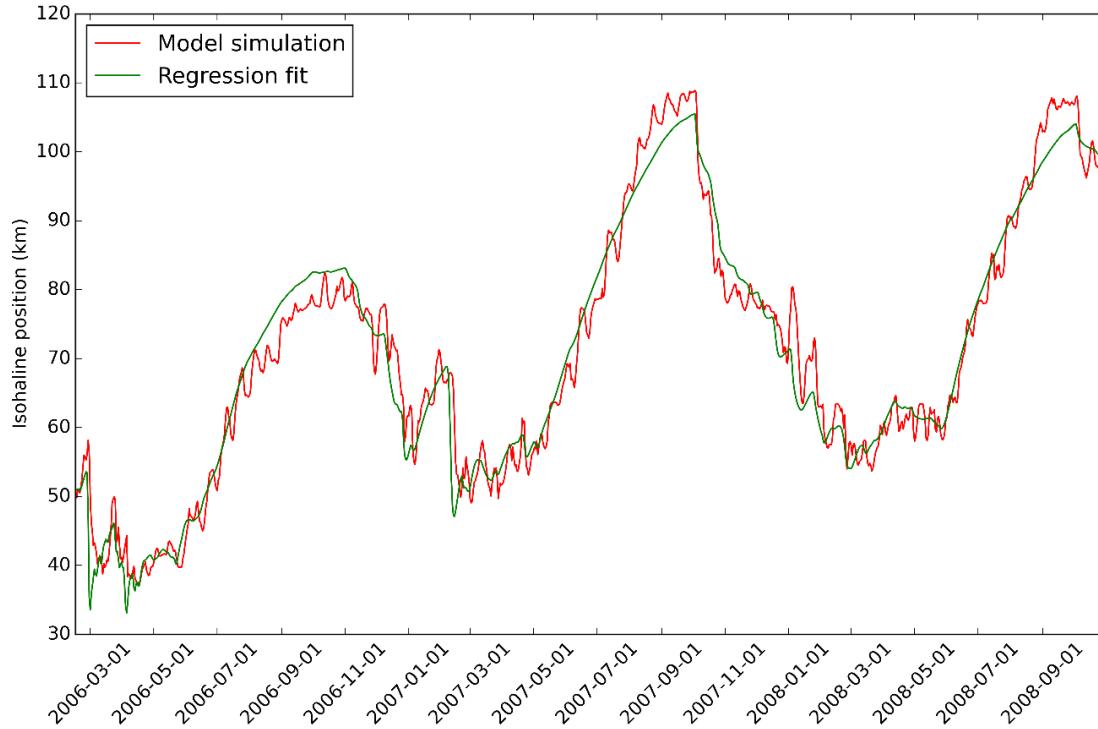


Figure 52 Pre-development system simulation X2 regression and hydrodynamic model time series comparison. NDOI is used for the independent outflow variable, Q .

Delta Salinity Gradient Model: Regression Fit to Multiple Isohalines

For a final aspect of the isohaline analysis, the self-similarity properties of the DSG model (given in Equation 9) were used to fit model time series for X2 and the 1 and 6 psu surface isohaline distances concurrently in order to obtain β , γ , and β_G parameter estimations representative of the entire low salinity zone. In order to accomplish this, the parameters γ_S and δ in Equation 11 first needed to be determined.

To calculate the fitting parameters γ_S and δ , Equations 9–11 were rearranged and combined to obtain: (Hutton 2014)

$$S_0 = e^{\left[\frac{\left(\frac{X}{X2}\right)^{\frac{-1}{\gamma}} * \log(1.36 - S_b) - \log(S - S_b)}{\left(\frac{X}{X2}\right)^{\frac{-1}{\gamma}} - 1} \right]} + S_b \quad (12)$$

S_0 was then calculated at several stations throughout the estuary based on 3-D model results, and a best fit for the parameters was determined based on the aggregate data from all stations. To avoid situations where S_0 is undefined, time series points when the salinity at the station, S , was less than S_b or when the ratio $\left(\frac{X}{X2}\right)$ was greater than 0.9 were removed from the data set. Following Hutton et al. (2015), \hat{S} was assumed to equal 34.9 psu (corresponding to a specific conductivity of 53 mS/cm) and S_b was assumed to equal 0.09 psu (corresponding to 200 μ S/cm). Stations upstream of 70 km in the contemporary simulation and 55 km in the pre-development simulation were omitted because of: (1) limited data availability after the constraints were taken into account, and (2) optimization fitting parameters which were inconsistent with downstream values (e.g., $\gamma_S > 1$ and $\delta < 0$).

S_0 fitting parameters are shown for individual stations spaced at 5 km intervals along the longitudinal transect in Table 11 (contemporary simulation results) and Table 12 (pre-development simulation results). The aggregate fitting parameters calculated for the contemporary simulation ($\gamma_S = 2.01E-5$, $\delta = 2.38$) were similar to those reported in the DSG Model Documentation report (Hutton 2014) calculated using DSM2 model outputs ($\gamma_S = 3.98E-5$, $\delta = 2.22$). Values calculated for the pre-development simulation were showed a higher γ_S ($=4.73E-4$) parameter and a lower δ parameter ($=1.72$).

Using Equations 9 and 10, X2, the 1 psu surface isohaline, and the 6 psu surface isohaline were simultaneously fit using an optimization routine. The 2.64 mS/cm surface EC isohaline was assumed to correspond to X2 and is redundant. Simultaneous fitting of these three isohalines yielded results shown in Table 13 and Figure 55–Figure 56 and for the model-calculated outflow case and Table 14 and Figure 57–Figure 58 for the NDOI case. The fitting parameters γ_S and δ sometimes yielded S_0 values less than 6 psu. Since these values invalidate the calculation of the 6 psu surface isohaline, they were omitted from the optimization. This procedure only removes

approximately 6% of the 6 psu isohaline time series from the calculations in the contemporary system simulation, and no values in the pre-development simulation.

Because the DSG approach fits three isohaline positions simultaneously, the accuracy of fit metrics are necessarily worse than individual isohaline fit values, with standard errors of 2.61 km and 2.98 km for the contemporary and pre-development simulations, respectively, compared to 1.70 and 2.26 km in the individual X2 fit case. The sensitivity of isohaline positions to outflow (the γ parameter) is higher in all cases than the individual X2 results, because of the incorporation of 1 psu and 6 psu isohalines, which individual fitting results showed to have higher γ values.

The DSG results showed similar relative differences between the contemporary and pre-development systems as in the individual fit of X2 results.

To examine the effectiveness of the variable S_0 procedure, fit parameters were calculated for the DSG model for the contemporary system using the average Sacramento and San Joaquin River X2 positions, model calculated outflow at Martinez, and a constant $S_0 = \hat{S}$ downstream salinity. (This can be compared to the corresponding variable- S_0 results, shown in the third column of Table 13.) While the fit parameters were similar ($\beta=306$, $\gamma=-0.248$, $\beta_G=5315$), the fit was significantly worse (standard error=3.25 km, $R^2=0.970$). Visually, most of the difference in standard error came from a poorer fit of the 6 psu surface isohaline in high outflow conditions for the constant S_0 case.

Finally, it should be noted that from the derivation procedure laid out in Section 2 of the DSG User Manual (Hutton 2014), it is possible to re-derive the equations describing the self-similarity of the system to use the modeled X2-equivalent surface isohaline as a reference, rather than X2. In the DSG approach, this would remove the assumption that 2.64 mS/cm surface EC corresponds to X2 and may result in more accurate regression model fits to the data. This, however, is beyond the scope of the current work.

Table 11 Contemporary system simulation S_0 model fitting parameters. Aggregate fit parameters were calculated using stations 40–70.

Station Distance (km)	γ_s	δ	Median S_0 position (km)
40	2.25E-06	2.91	20.26
45	7.33E-06	2.63	19.84
50	1.48E-05	2.46	19.21
55	9.22E-05	2.04	19.36
60	1.63E-05	2.41	18.48
65	2.92E-05	2.28	18.91
70	2.16E-05	2.34	19.00
75	4.10E+04	-2.31	25.46
40–70	2.01E-05	2.38	19.21

Table 12 Pre-development system simulation S_0 model fitting parameters. Aggregate fit parameters were calculated using stations 40–55.

Station Distance (km)	γ_s	δ	Median S_0 position (km)
40	4.54E-05	2.25	19.58
45	1.79E-04	1.94	20.03
50	3.25E-03	1.29	22.14
55	6.63E-02	0.62	23.11
60	6.36E+00	-0.40	22.91
65	1.07E+00	-0.04	21.17
70	1.43E+05	-2.62	21.09
40–55	4.73E-04	1.72	21.21

Table 13 Delta Salinity Gradient model regression fit statistics for the Sacramento River, San Joaquin River, and the averaged position. Estuary outflow is estimated using model calculated outflow at Martinez.

Parameter	Simulation Type					
	Contemporary			Pre-development		
	Sacramento	San Joaquin	Average	Sacramento	San Joaquin	Average
β	300	298	303	273	299	304
γ	-0.244	-0.244	-0.247	-0.240	-0.255	-0.258
β_G ($m^3 s^{-1}$ day)	5134	5324	5158	4401	4963	4560
Standard error (km)	2.56	2.97	2.61	3.41	4.16	2.98
R^2	0.975	0.967	0.975	0.977	0.972	0.981

Table 14 Delta Salinity Gradient model regression fit statistics for the Sacramento River, San Joaquin River, and the averaged position. Estuary outflow is estimated using NDOI.

Parameter	Simulation Type					
	Contemporary			Pre-development		
	Sacramento	San Joaquin	Average	Sacramento	San Joaquin	Average
β	293	305	310	300	327	328
γ	-0.240	-0.247	-0.249	-0.255	-0.269	-0.269
β_G ($m^3 s^{-1}$ day)	5436	6401	6446	4865	5001	4659
Standard error (km)	3.18	3.39	3.15	4.45	4.99	4.27
R^2	0.962	0.958	0.963	0.956	0.954	0.961

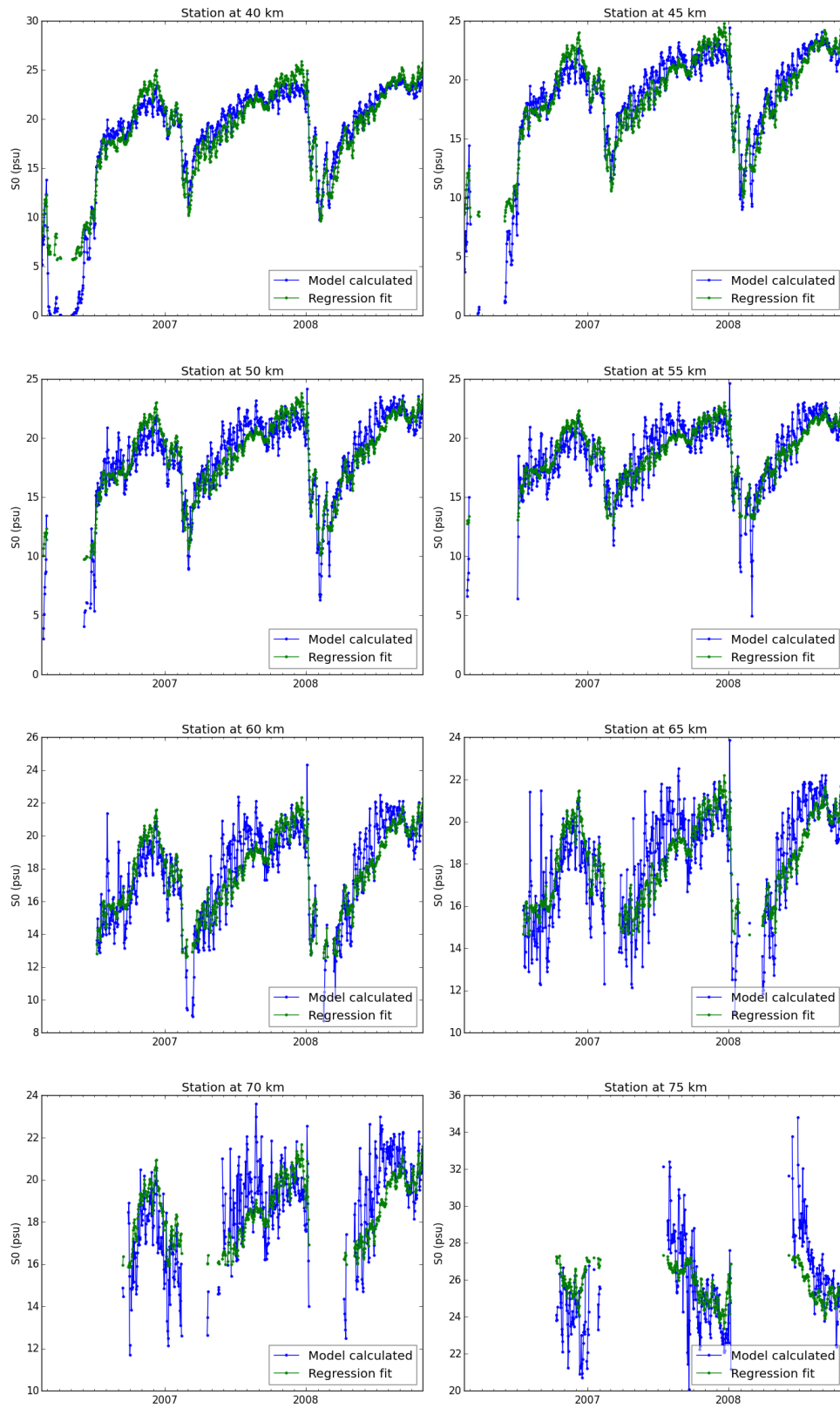


Figure 53 Contemporary simulation S_0 calculated values and regression model fits for stations at 5 km intervals along the salinity transect.

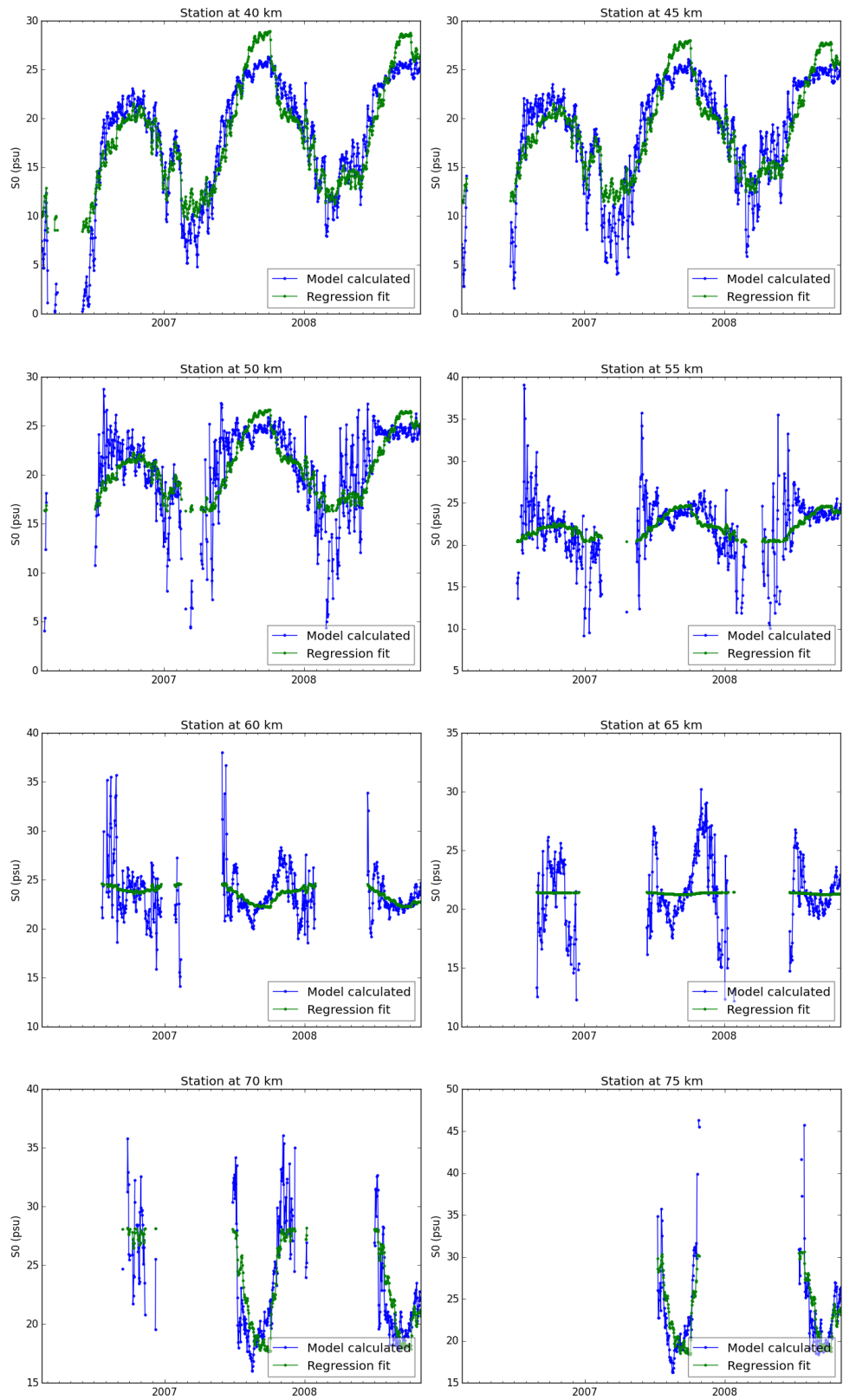


Figure 54 Pre-development simulation S_0 calculated values and regression model fits for stations at 5 km intervals along the salinity transect.

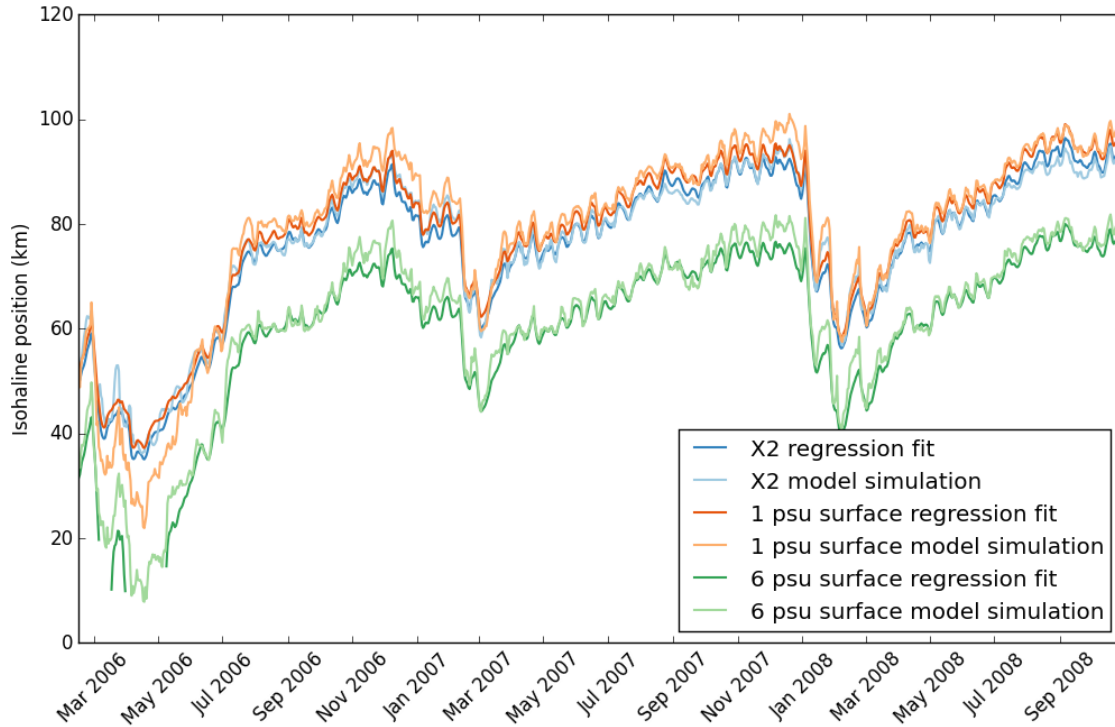


Figure 55 Contemporary system simulation DSG regression and hydrodynamic model time series comparison. Model calculated flow at Martinez is used for the outflow variable, Q .

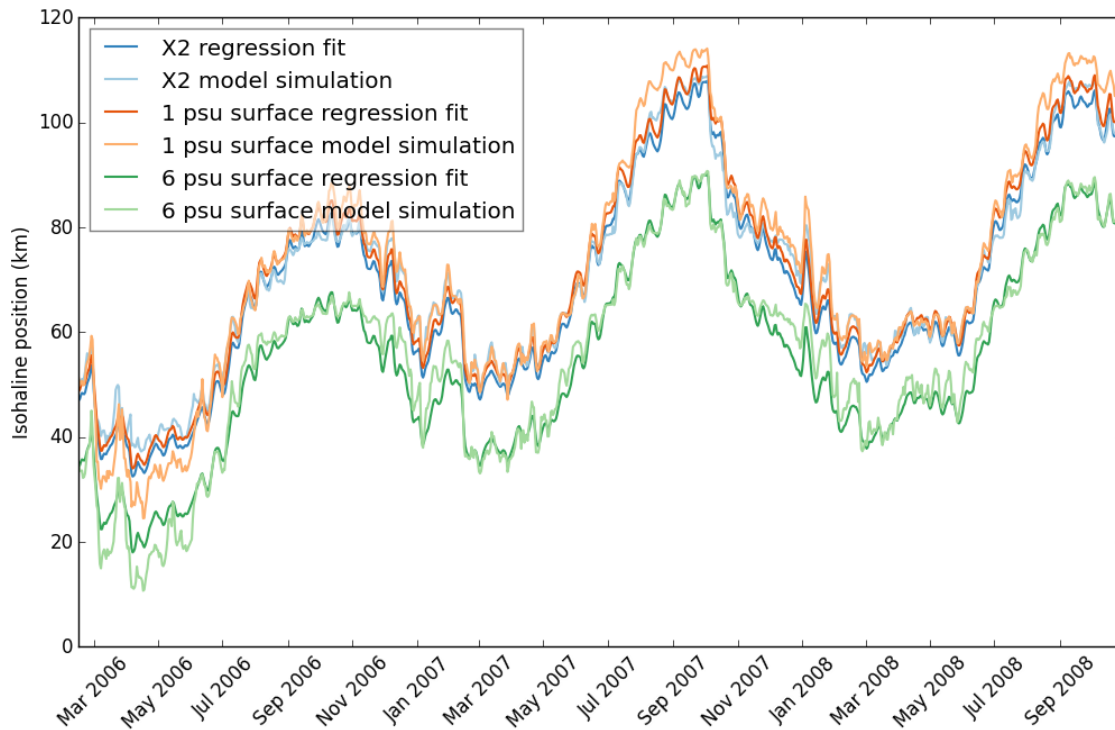


Figure 56 Pre-development system simulation DSG regression and hydrodynamic model time series comparison. Model calculated flow at Martinez is used for the outflow variable, Q .

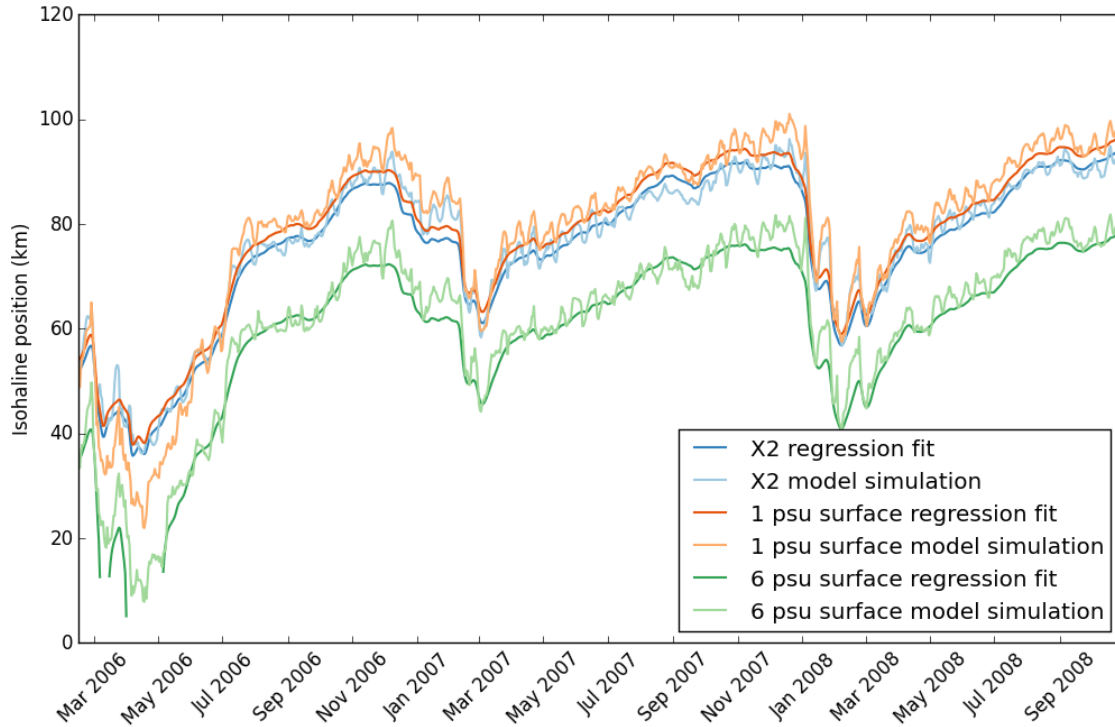


Figure 57 Contemporary system simulation DSG regression and hydrodynamic model time series comparison. NDOI is used for the outflow variable, Q .

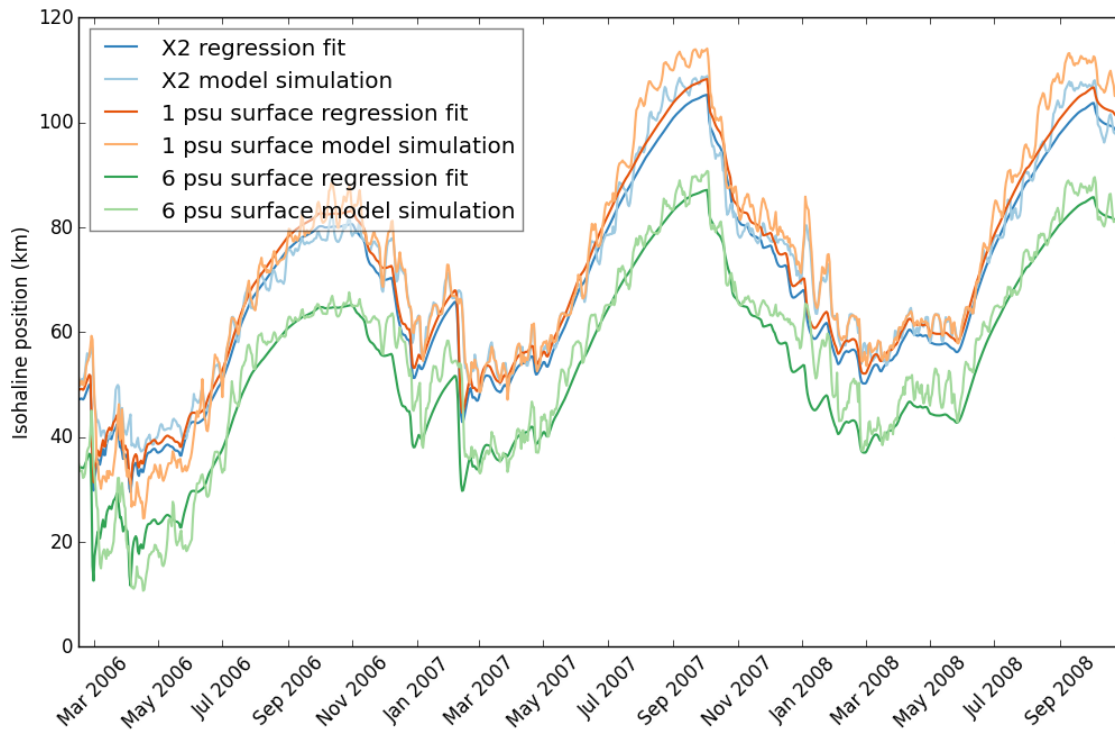


Figure 58 Pre-development system simulation DSG regression and hydrodynamic model time series comparison. NDOI is used for the outflow variable, Q .

Summary

Salinity regimes of the contemporary and pre-development estuary were modeled using a 3-D hydrodynamic model and river inflow and boundary conditions specific to each system.

Because of differences in the hydrological regimes between the two systems (pre-development peak flows are typically higher in the winter and spring and base flows are lower in summer), a direct comparison of modeled salinity is not useful. Salinity is significantly more variable in the pre-development system. In order to compare the salinity response of each system in a way that is independent of estuary outflow, an isohaline position regression was performed, utilizing the concept of antecedent flow. Of the parameters that are fit in the regression, the exponential fit parameter γ reflects the sensitivity of salinity in the modeled estuary system to outflow, and can be used to draw conclusions about differences in the contemporary and pre-development salinity regimes.

Regression fits using the model predicted X2 isohaline location and model predicted outflow for each simulation yielded accurate results. For the contemporary simulation, the calculated γ value matched previously reported values closely. Differences in gamma between the contemporary and predevelopment systems were small and indicated that, despite large changes in marsh plain area and channel connectivity and geometry, given similar outflow, the pre-development Delta X2 location would be within 5 km of the contemporary system X2 90% of the time. Subsequent analyses of additional isohalines as well as an aggregate analysis incorporating multiple isohalines, yielded similar relative differences in γ . An analysis using the NDOI, the sum of net Delta inflows minus net channel depletions, yielded poorer regression fits because the estuary spring-neap filling-draining cycles were not accounted for; however, similar relative differences in salinity sensitivity to outflow were still found. An analysis of the isohaline positions along the Sacramento River and San Joaquin River transects separately, instead of their averaged position, showed a reach of the San Joaquin River in the central Delta in the pre-development system to be particularly sensitive to salinity intrusion during low-flow periods.

Low-Salinity Zone Habitat Characteristics

The low salinity zone (LSZ) is defined as the area in the estuary where depth averaged salinity is within the range 0.5-6 psu (Kimmerer 2013). This zone is associated with large observed accumulations of suspended particulate matter and aquatic organisms (Bureau 1998). The accumulation is associated with a number of hydrodynamic mechanisms, including the interaction of gravitational circulation with river outflow creating a residual current null zone (Bureau 1998). The LSZ is therefore important for its unique physical, chemical, and ecological properties. In this section, we analyze the spatial and time-varying LSZ characteristics of total volume, total area, and average depth, and compare results between the contemporary and pre-development simulations.

Analysis Methods

To analyze the characteristics of the LSZ, detailed model output was given for every computational prism in the grid at two hour intervals. Because of the computational resources required for the analysis, a representative subset of the full simulation period (Feb 2008 through Oct 2008) was chosen for analysis. Depth averaged salinity was calculated by dividing the total salt mass in a vertical stack of computational prisms and by the total volume in that stack. That volume of water is counted towards the volume of the LSZ if the depth averaged salinity is within the range 0.5–6 psu. If depth averaged salinity is in that range, the wetted surface area of the computational cell is counted towards the LSZ area. Average depth was computed as the total LSZ water volume divided by the total LSZ area. In the pre-development simulation, cells having maximum water depths less than 5 cm were excluded from the analysis, as these depths were considered too shallow to be ecologically important for aquatic organisms.

The LSZ analysis of Kimmerer (2013) depth averaged model results for salinities and then daily averaged them to calculate a metric which would reflect what a stationary pelagic fish would be exposed to over the course of a day. In the pre-development estuary, however, large areas of tidal marsh become inundated and then dry out over a tidal cycle. The daily-averaged salinities of areas that are sometimes dry are less straightforward of a metric. In this analysis, we calculated depth-average salinities at each two hour time step and summed these areas to get instantaneous LSZ area. These areas are reported; we also apply a tidal filter in order to get daily averaged values that can then be related to X2. This approach gives us a metric that is more relatable to fish species that move on and off the marsh plain throughout the day rather than remaining stationary. Relating the LSZ characteristics to X2 allowed us to compare the two systems at similar antecedent flows.

Results

Figure 59 shows LSZ characteristics for each of the two simulations. Differences in net Delta outflow and bathymetry between the two simulations result in very different time series for LSZ volume and area. In the spring months, higher outflow in the pre-development simulation pushes the low salinity zone out toward Martinez. The volume and surface area of the LSZ are lower there because of the estuary geometry at this location. The LSZ average depth, however, is higher than in the contemporary simulation because the area of the LSZ which is located at the western edge of Suisun Bay is exposed to shallow depths. During the summer months, the volume and surface area of the LSZ is higher in the pre-development simulation, as the LSZ is located predominantly in Suisun Bay and Marsh. There are large tidal variations in LSZ area and average depth as the marsh plain is inundated on tidal time scales (Figure 60). In the fall, the LSZ moves up into the Delta in both simulations. In the contemporary system, wider and deeper main channels account for a greater volume of the LSZ. The prevalence of small blind sloughs and marsh plain in the pre-development system gives the LSZ greater spatial area and shallower average depths. On average, there is higher variation in LSZ volume, area, and average depths in the pre-development simulation.

Comparing the LSZ characteristics on the basis of X2 location (Figure 61) allows the effects of net Delta outflow to be minimized in the analysis. The volume of the LSZ is found to be similar for both systems for much of the range of X2. Only when salinity intrudes far enough into the Delta (such that X2 is located at or landward of Decker Island on the Sacramento River and Blind Point on the San Joaquin), are large differences in LSZ volume found. There, the wider and deeper main channels of the contemporary system yield higher LSZ volumes. For X2 locations landward of Martinez, the pre-development Delta has larger LSZ areas and shallower average depths than the contemporary system. Tidal variation in these characteristics is also much higher in the pre-development system. The only exception is the area around the Sacramento–San Joaquin River confluence, where topographical constraints produce similar LSZ areas and average depths.

The lower average depths of LSZ in the pre-development system mean that more of this habitat is in the photic zone, resulting in the potential for higher autochthonous primary productivity.

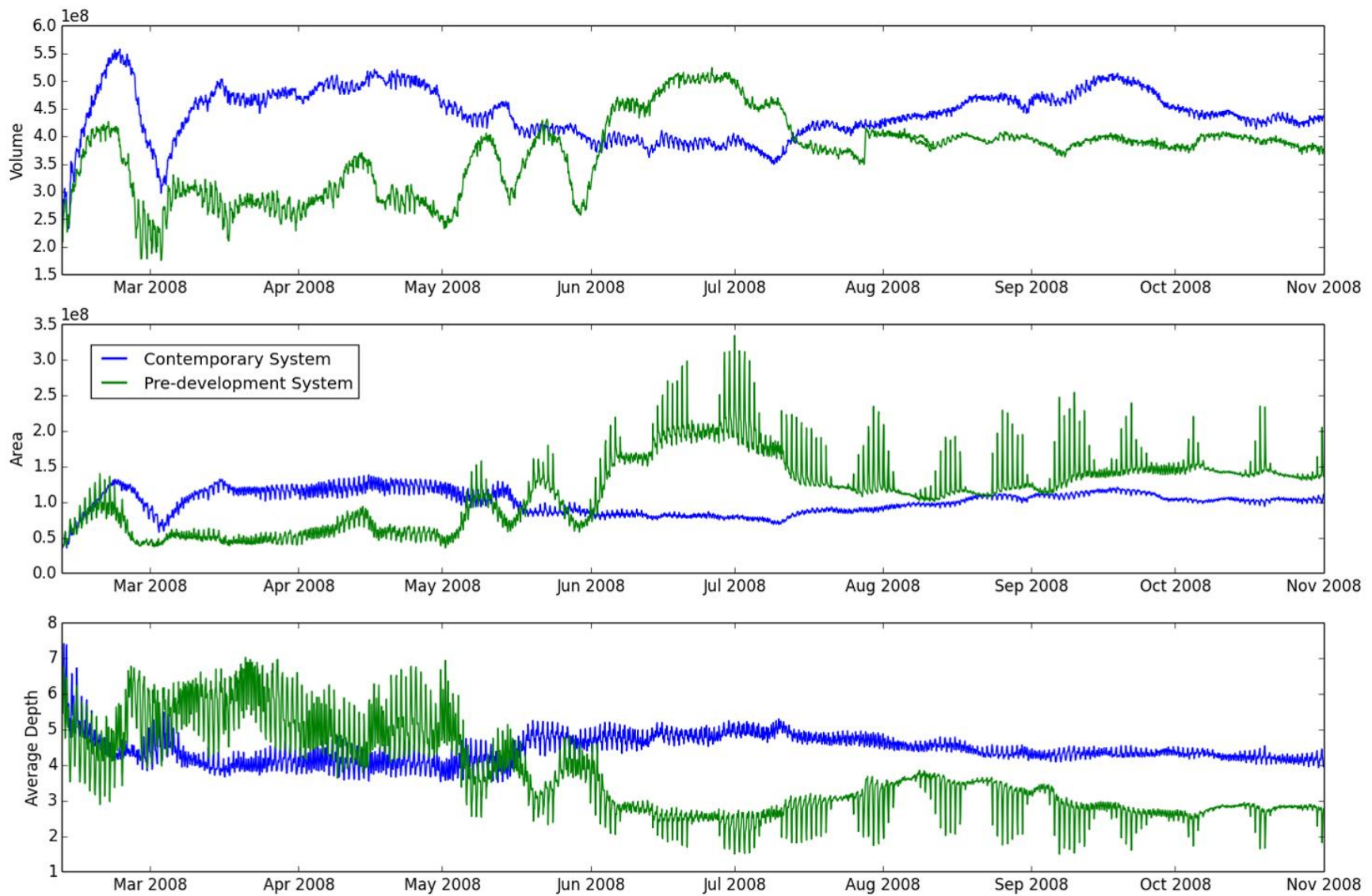


Figure 59 Volume, area, and average depth of the low-salinity zone for the pre-development and contemporary model simulations in 2008.

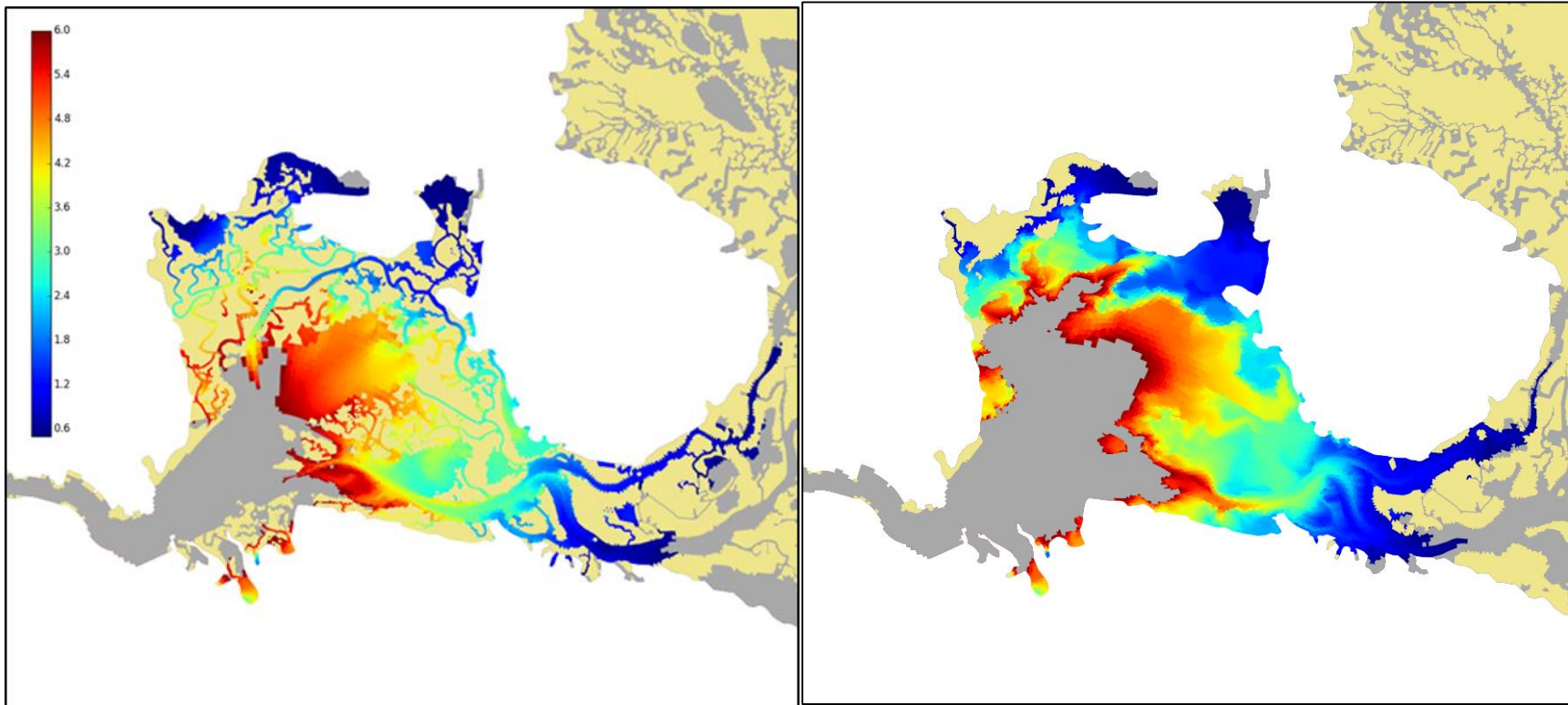


Figure 60 Low tide (left) and high tide (right) low salinity zone variation in the pre-development estuary. Gray areas indicate water with depth average salinity outside of the 0.5–6 psu zone. Beige areas indicate dry cells.

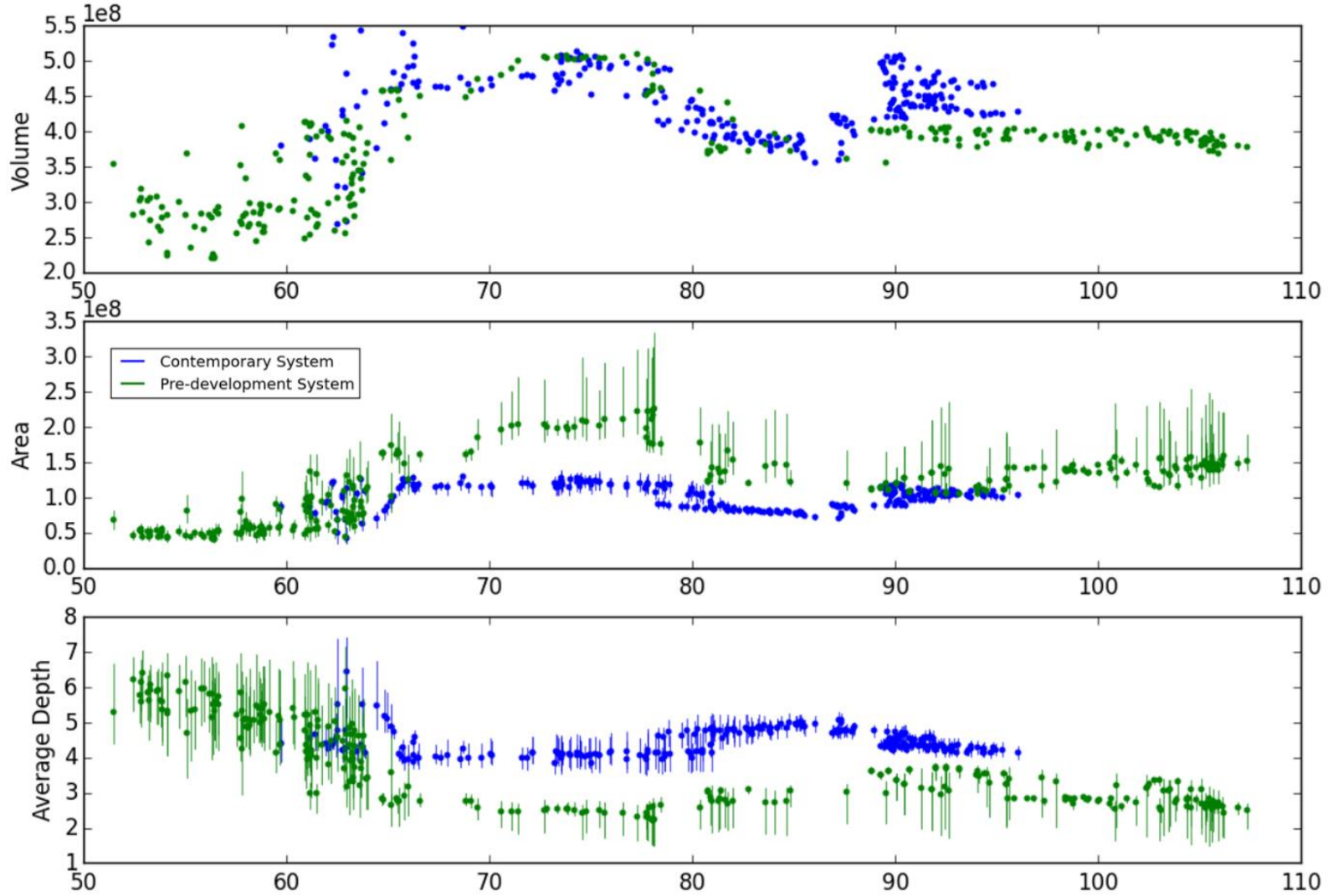


Figure 61 Volume, area, and average depth of the low-salinity zone for the pre-development and contemporary model simulations as a function of X2 location. Analysis period is 2008. In the lower two plots, points indicate daily average values; the daily range for each variable is shown as a line.

Upper Estuary Tidal Prism

Tidal prism is defined as the volume of water entering and exiting an estuary between mean high and low tides. It is an important metric for an estuary, as it relates to the amount of energy available for raising and lowering water levels within the estuary. Higher tidal prisms mean that a greater amount of water is pushed into and out of the estuary by tidal action, which is then available to increase the amount of intertidal habitat within an estuary. In the pre-development system, the large amount of functional marsh was hypothesized to increase the available storage space for water, resulting in an increase in tidal prism for the pre-development system in comparison to the contemporary system.

Gilbert (1917) calculated the tidal prism in the San Francisco Estuary in both its pre-development condition and its condition at the time of the writing (which was heavily impacted by sedimentation from hydraulic mining debris). He estimated a decrease in tidal prism of 3.5–4.5% between the pre-development system and 1917, with hydraulic mining sedimentation responsible for 2–3% of the reduction and marsh reclamation responsible for 1.5%. The contemporary system estimate of Gilbert (1917), however, came at a time of high hydraulic mining sediment impacts in the estuary and before the Sacramento and San Joaquin deep water shipping channels were dredged or the permanently flooded islands of today had been breached. Also, the pre-development tidal prism calculation of Gilbert only implicitly accounted for the hydrodynamic effects of shallow water flows. The pre-development system has large areas of densely vegetated marsh, a large number of shallow, sinuous channels, and more sinuous and shallower main channels as compared to the contemporary upper estuary. All of these attributes act to dissipate energy, decreasing the volume of water capable of being exchanged into the system from what is theoretically possible based on a volume analysis. The advantage of modeling the two systems and calculating tidal prism is that these hydrodynamic effects are explicitly taken into account in order to provide a more realistic estimation of tidal prism.

In this section we analyze and compare the tidal prism of the estuary upstream of Martinez in the contemporary and pre-development systems.

Analysis Methods

Tidal prism was calculated for the contemporary and pre-development system simulation for the same time period used in the LSZ analysis (Feb–Oct 2008). Cross-sectional flow was output at a cross-section at Martinez at fifteen minute intervals during each simulation. Tidally-averaged flow was calculated using a Godin filter; this flow record was subtracted from the original flow record to obtain tidal flow at the cross-section. Tidal flow was then integrated over each flood and ebb cycle in order to obtain the total volume of water moving past the cross-

section during each tide. Tidal prism was calculated as the average over all of the flood and ebb tidal volumes.

Results

The upper estuary tidal prism was calculated as $200 \times 10^6 \text{ m}^3$ for the contemporary simulation and $205 \times 10^6 \text{ m}^3$ for the pre-development simulation. This represents a 2.5% decrease in prism from the pre-development estuary to the system of today. The decrease is less than that reported by Gilbert, but it should be considered that: 1) Gilbert's calculations were made for the entire estuary from the Golden Gate, and 2) there have most likely been increases in tidal prism between 1917 and today due to shipping channel construction, island breaches, and the transport of hydraulic mining sediment out of the estuary.

Table 15 shows the monthly comparison of tidal prism for the two systems. In the summer months when astronomical forcing of high tide water levels is greater, the tidal prism increase in the pre-development system is larger ($10 \times 10^6 \text{ m}^3$) than the period average. In the spring and fall months where high tide water level forcing is lower, the difference between the tidal prisms in the two systems is small.

Figure 62 shows a time series plot of the tidal flows at Martinez for the two systems for a low-flow period in July. Ebb tide is defined as the positive direction. As peak flood tide enters the upper estuary, greater flows are seen in the pre-development system because of the marsh area available for flooding. On peak ebb, flows in the contemporary system are greater. One explanation for this is that the inundated marsh plain area takes longer to drain than the water in the channels. The flood tide flows associated with lower high water are comparable in the two systems, but the ebb tide flows associated with higher low water are much larger in the pre-development estuary. This may be the result of the water that previously inundated large areas of marsh finally getting a chance to drain. Figure 63 provides support for this mechanism. The volume of water in areas of shallow depth is seen to increase with a time lag from deeper water volume increases and also drains more slowly. The greater total volume in the contemporary upper estuary is attributable to wider, deeper channels, and flooded islands.

Table 15 Tidal prism comparison by month.

Time Period	Pre-development Upper Estuary Tidal Prism (10⁶ m³)	Contemporary Upper Estuary Tidal Prism (10⁶ m³)
Full Simulation Period	205.3	200.0
March 2008	206.0	203.6
April 2008	202.7	200.0
May 2008	205.5	194.7
June 2008	206.1	195.8
July 2008	208.0	199.6
August 2008	206.7	201.8
September 2008	204.7	200.5
October 2008	199.9	195.5

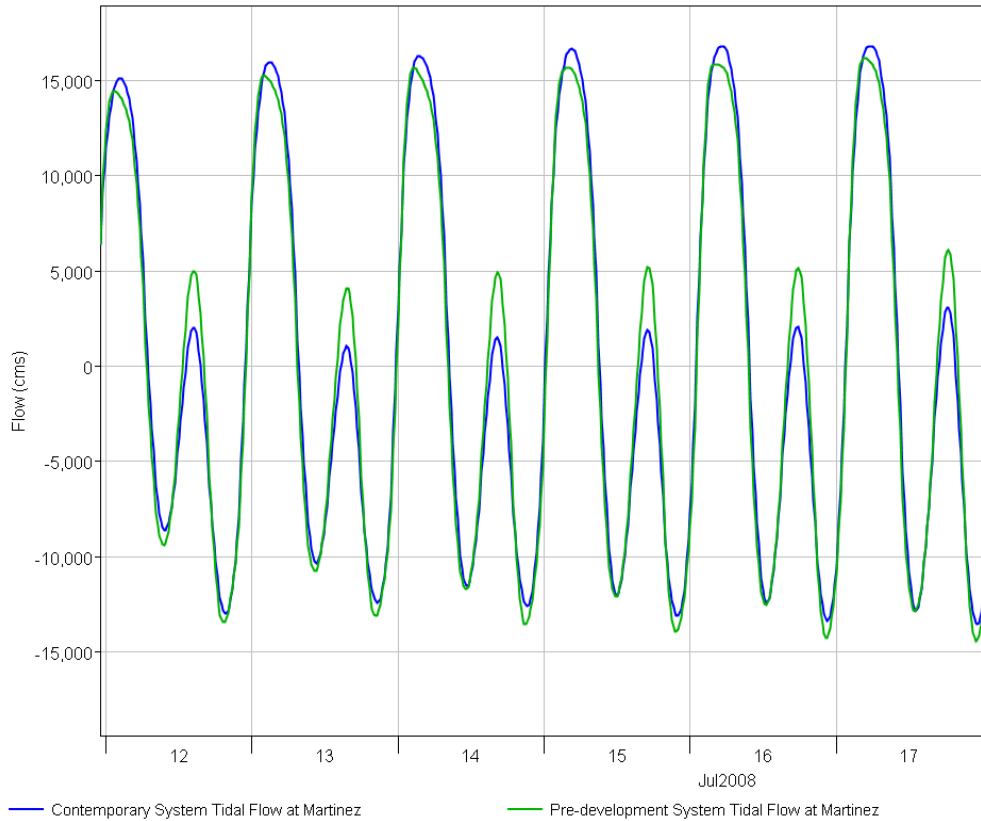


Figure 62 Tidal flow at Martinez. Positive flows are defined as the ebb direction.

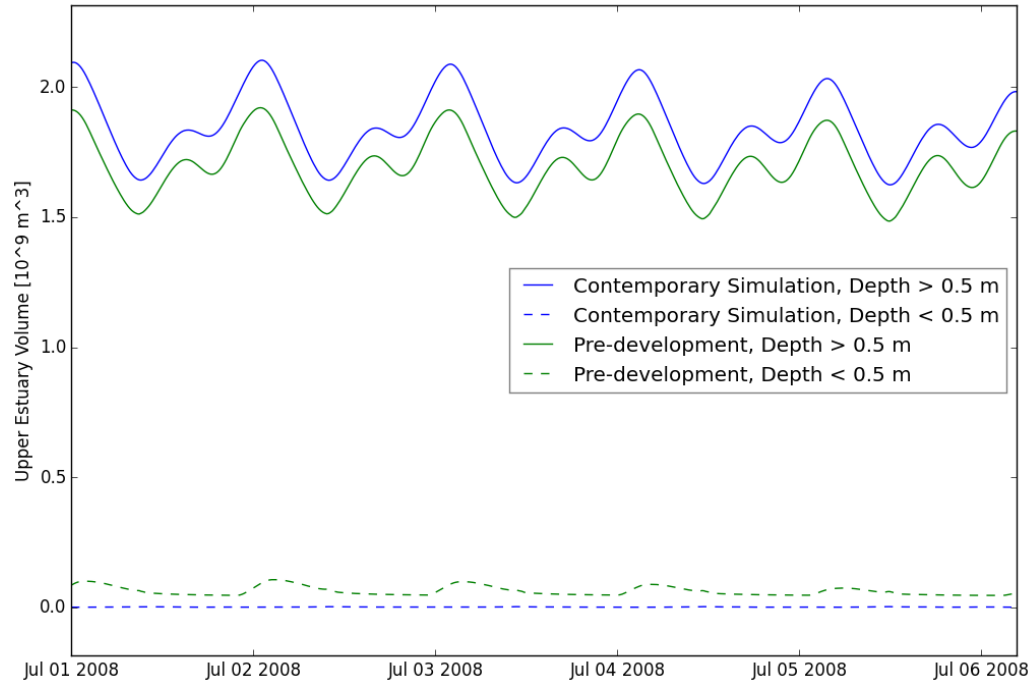


Figure 63 Water volume upstream of Martinez. Solid lines show water volume in areas with a maximum depth greater than 0.5 m. Dashed lines show shallow water volume.

Channel Velocity Analysis

The magnitude of velocities in channels is important to fish, aquatic vegetation, and has implications for water quality and sediment transport to or from marsh areas. Velocities in estuaries are typically asymmetric, resulting from the hydrodynamic, bottom friction, and estuarine geometry effects that distort a symmetric incoming tide from the coastal ocean. Progressive wave theory suggests that the incoming high water portion of the tidal wave will move faster than the low water portion (Friedrichs and Aubrey 1988). This is a consequence of waves moving faster in deeper water (wave celerity = $\sqrt{\text{gravity} * \text{water depth}}$) and the fact that bottom friction has a greater influence in shallow water. As a result, the high water peak tends to “catch up” with the low water trough as it moves through the system and, at a given location in the estuary, the flood period becomes shorter than the ebb period. Ignoring net outflows caused by riverine inputs, a shorter flood period results in higher velocities. The ebb tide will necessarily have a relatively longer period and lower velocities. This type of system is known as “flood dominant.” The case where the ebb tide has a shorter period and a higher velocity is called “ebb dominant.”

The above explanation of progressive wave theory predicting flood dominant behavior assumes a channelized estuary. When there are significant overbank flows, progressive wave theory predicts that high tide will experience shallow water and a greater influence of bottom friction. The incoming high water portion of tidal wave slows down relative to the low tide trough, and higher velocities are expected on ebb tide (ebb dominance).

The San Francisco estuary is different from a typical system because it has mixed tides and water levels progress from higher high water to lower low about 80% of the time (Malamud-Roam 2000). This characteristic has led to an overall ebb dominance in the contemporary, channelized system, counter to the flood dominance predicted by theory (Malamud-Roam 2000). Also counter to the theory, work by Enright et al. (2013) in Suisun Marsh found ebb dominance within a channelized reach and a switch to significant flood dominance for a natural channel with overbank flow.

An analysis of maximum modeled channel velocities is presented in this section to rectify differences in wave theory and field observations of channel velocity. Flood versus ebb dominance was classified for several cross-sections throughout the upper estuary and compared between the pre-development and contemporary systems.

Analysis Methods

Cross-sectionally averaged velocities were output every 15 minutes at the locations shown in Figure 64. Locations were chosen to cover a wide area of the Delta and were located at present day continuous monitoring sites where the channel geometry has not changed significantly between the two systems. Tidally averaged velocities were calculated with a Godin filter and then subtracted from the velocity time series to obtain tidal velocities.

A time series analysis of tidal velocities was performed to calculate tidal periods, average tidal velocities, maximum tidal velocities, and tidal excursions. To this end, the velocity time series was analyzed sequentially; for each tidal period (flood vs ebb), we calculated mean velocity and tidal excursion (as the sum of velocity times 15 minutes for each step in tidal period). Mean velocities and tidal excursions are reported as averages over all flood or ebb cycles. Maximum velocities were calculated as the 95th percentile using a distribution of all flood or ebb velocities. Positive flow direction was defined as seaward or ebb.

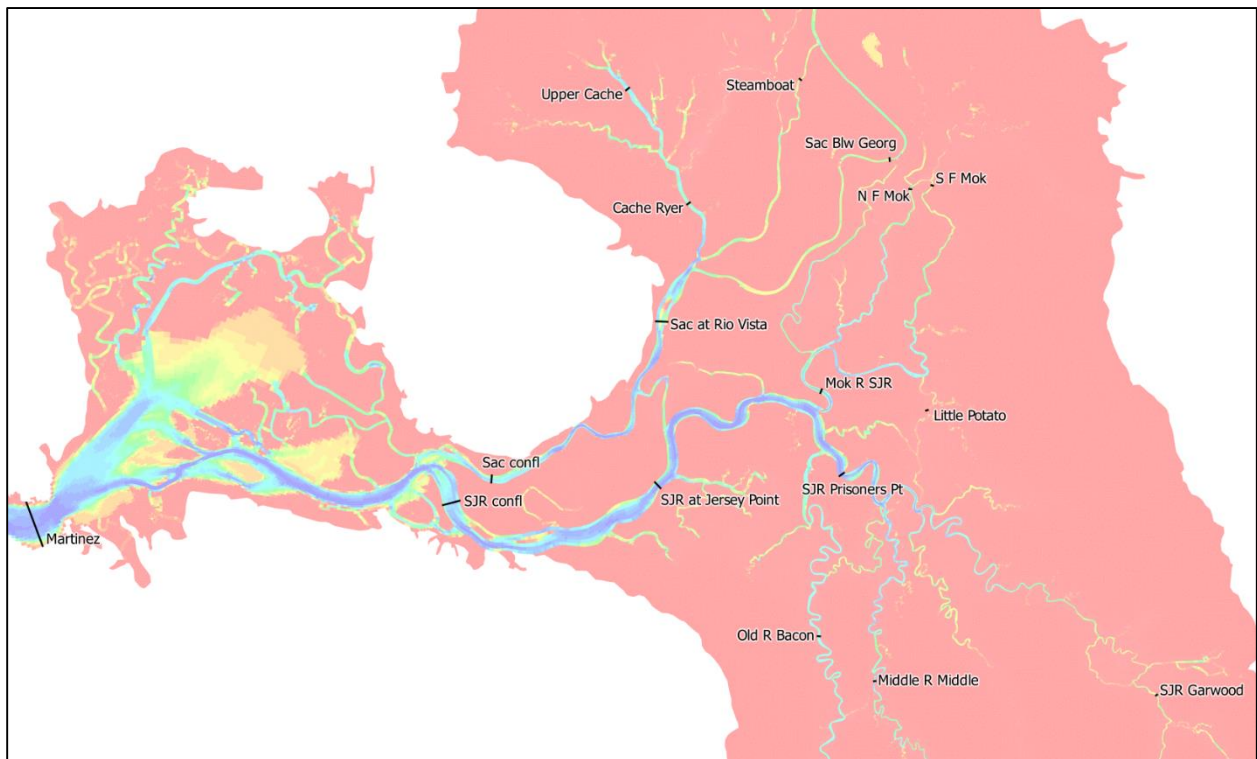


Figure 64 Locations of cross-sections for channel velocity analysis.

Results

The results of the channel velocity analysis are presented in Table 16. Cross-section locations in the western Delta at Martinez and near the confluence show ebb dominance in both the contemporary and pre-development systems. Many of the other cross-sections analyzed, however, show higher maximum velocities and shorter periods on ebb (ebb dominance) occurring in the pre-development system, and flood dominance occurring in the contemporary system. Figure 65 shows a time series of one such location, Cache Slough at Ryer Island. Maximum ebb velocities decrease from the pre-development system to the contemporary system, and maximum flood velocities increase. The trend in average tidal velocities was harder to interpret, with the highest average velocities typically occurring on flood tide in both systems.

The result of the channel analysis is consistent with the progressive wave theory prediction of ebb dominance in a system with overbank flows. The later arrival of peak ebb velocities in the pre-development system relative to the contemporary system (Figure 65) also supports this. Since sediment transport roughly scales with velocity cubed (Morgan-King and Schoellhamer 2013), more sediment may have been transported into the Delta in the pre-development system.

Table 16 Tidal velocity, period, and excursion statistics. Shorter periods and higher absolute maximum velocities associated with ebb tide are highlighted yellow to indicate ebb dominance. Shorter periods and higher absolute maximum velocities associated with flood tide are highlighted blue to indicate flood tide dominance.

Location	System	Flood tide excursion	Ebb tide excursion	Flood period	Ebb period	Flood mean velocity	Ebb mean velocity	Flood 95th percentile velocity	Ebb 95th percentile velocity
		(km)	(km)	(hr)	(hr)	(cm/s)	(cm/s)	(cm/s)	(cm/s)
Martinez	Contemporary	10.0	10.0	6.51	5.91	-42.2	38.0	-73.7	86.8
	Pre-development	9.5	9.5	6.38	6.04	-41.3	38.7	-68.7	77.4
Sacramento River near confluence	Contemporary	8.5	8.5	6.27	6.15	-37.5	33.4	-62.6	64.1
	Pre-development	9.5	9.5	6.35	6.04	-41.2	38.4	-69.1	75.7
San Joaquin River near confluence	Contemporary	5.6	5.5	6.85	5.96	-22.6	20.8	-38.0	44.9
	Pre-development	6.6	6.6	6.38	6.02	-28.4	26.7	-49.2	55.0
San Joaquin River at Jersey Pt	Contemporary	10.0	10.0	6.18	6.22	-44.8	38.9	-69.7	68.7
	Pre-development	9.6	9.6	6.25	6.15	-42.0	39.2	-70.7	73.5
Sacramento River at Rio Vista	Contemporary	7.8	7.8	6.13	6.28	-35.2	31.1	-56.1	54.4
	Pre-development	3.4	3.4	6.18	6.22	-15.1	13.8	-24.6	25.1
Upper Cache Slough	Contemporary	1.0	1.0	6.00	6.40	-4.6	4.0	-8.3	6.7
	Pre-development	1.4	1.4	6.34	6.05	-6.1	6.2	-9.7	10.8
Cache Slough at Ryer Is	Contemporary	10.7	10.7	5.99	6.42	-49.6	42.5	-78.1	73.2
	Pre-development	11.0	11.0	6.27	6.12	-48.3	46.2	-73.6	77.4
San Joaquin River at Prisoners Pt	Contemporary	5.3	5.3	6.12	6.28	-24.1	20.8	-37.1	34.4
	Pre-development	4.6	4.6	6.24	6.15	-20.3	19.3	-32.6	34.0
Old River at Bacon Is	Contemporary	4.3	4.3	6.25	6.15	-19.1	17.5	-27.5	29.5
	Pre-development	6.4	6.4	6.24	6.15	-28.3	27.8	-41.3	41.6
Middle River at Middle River	Contemporary	4.7	4.6	6.44	5.96	-20.2	19.0	-31.9	36.4
	Pre-development	3.5	3.5	6.33	6.05	-15.0	15.4	-22.4	23.4
Mokelumne River at San Joaquin River	Contemporary	6.3	6.3	5.99	6.41	-29.0	23.7	-44.1	40.8
	Pre-development	13.9	13.8	6.27	6.12	-60.4	57.1	-92.3	103.3
San Joaquin River at Garwood	Contemporary	4.0	4.0	6.21	6.19	-17.4	15.8	-28.6	27.5
	Pre-development	3.4	3.4	6.00	6.38	-14.7	14.0	-24.2	23.8
Sacramento River below Georgiana Sl	Contemporary	5.5	5.4	5.68	6.73	-26.3	19.9	-42.8	34.1
	Pre-development	4.5	4.5	6.15	6.02	-19.4	16.7	-34.5	36.4
Little Potato Sl	Contemporary	2.9	2.9	5.75	6.65	-13.9	10.4	-21.8	19.1
	Pre-development	2.3	2.3	5.74	6.64	-11.2	8.6	-17.4	17.5
South Fork Mokelumne River	Contemporary	1.8	1.8	5.52	6.87	-9.1	6.7	-19.3	15.8
	Pre-development	4.7	4.7	6.81	5.56	-19.3	22.4	-29.1	38.6
North Fork Mokelumne River	Contemporary	2.2	2.2	5.69	6.71	-10.6	7.6	-19.2	14.5
	Pre-development	5.5	5.5	6.51	5.87	-23.3	24.6	-34.2	40.1
Steamboat Slough	Contemporary	7.3	7.3	5.46	6.94	-36.6	26.1	-57.2	43.8
	Pre-development	5.3	5.3	6.43	6.15	-23.0	20.0	-38.2	39.9

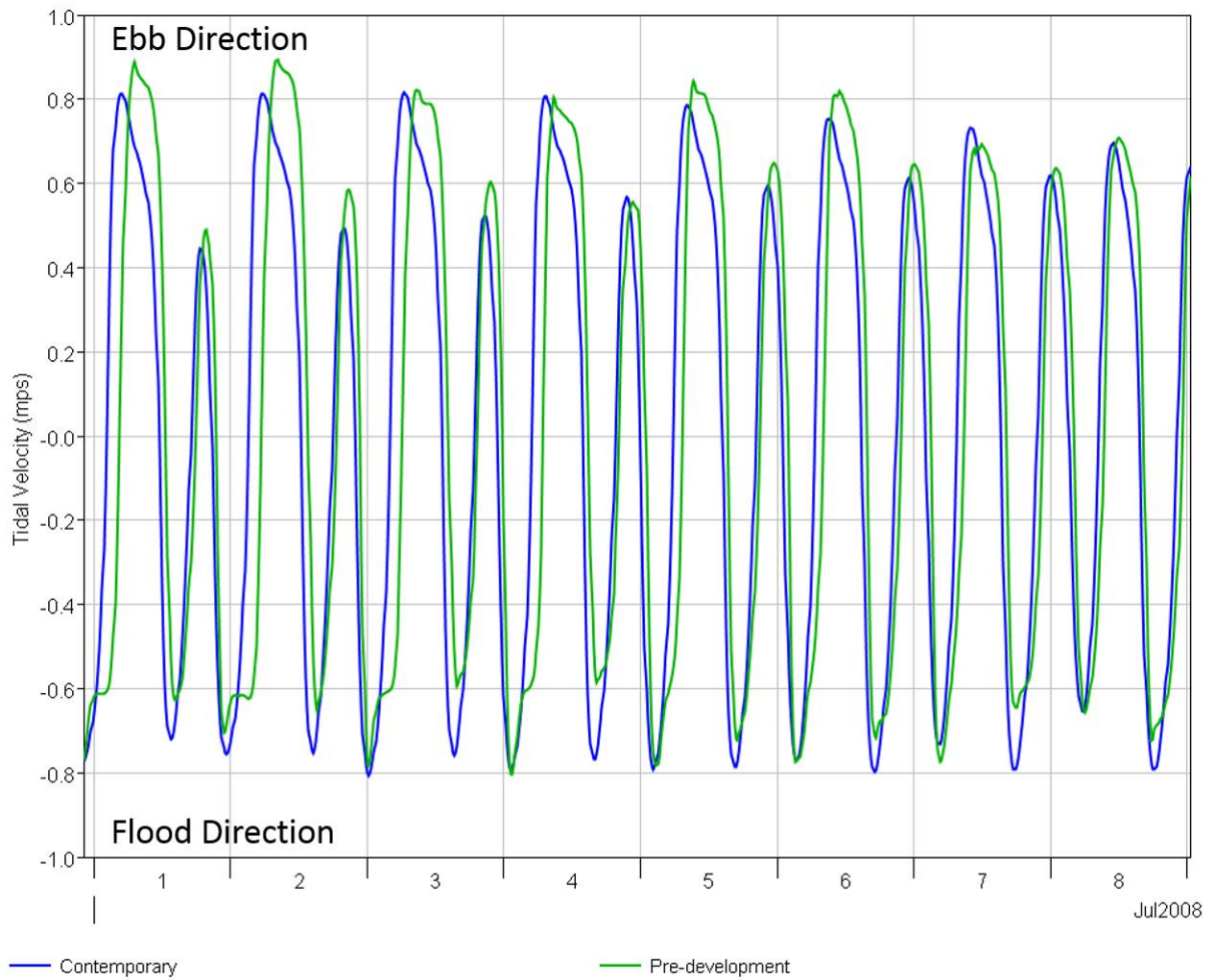


Figure 65 Cross-sectionally averaged velocity time series at Cache Slough at Ryer Island.

Source Water Fingerprinting

Source water fingerprinting runs are useful in visualizing general flow patterns through the upper estuary. Major riverine inflows are tagged with specific tracers to indicate their source, and model results are analyzed to determine the majority source of water at any point in the estuary. Plots of individual river tracer concentrations can also show how the influence of a source is distributed over the Delta. When different river inflows have different water chemistries or water qualities, source water fingerprinting can be an effective means of understanding water quality distributions in the Delta or predicting upstream migration of fish.

Analysis Methods

A source water fingerprinting analysis was conducted for the same Feb–Oct 2008 subset of the full three year simulations used in the previous analyses. For both the contemporary and pre-development models, an initial concentration of zero was set for all river inflow tracers. Inflows were tagged according to the groupings shown in Table 17. Each river inflow was tagged with 100 mg/L of its respective tracer. Two types of source water visualization maps were created. The first shows each individual computational cell colored according to its dominant water source. The second shows relative concentrations of each individual inflow group. Relative concentrations are given as a percentage of the total mass of tracer in each cell. Cells that are below the 5% cutoff are colored gray. Cells having depths less than 0.5 m are colored beige to indicate they are dry or have shallow water.

The source water visualizations were performed for three snapshots during 2008, chosen to represent a range of inflow conditions. These dates were chosen as 1 March, 1 May, and 1 July. Figure 36 and Figure 37 show inflow conditions for this period.

Table 17 Source waters for inflows groups for fingerprinting analysis.

Tracer Number	Contemporary Simulation River Inflows	Pre-development Simulation River Inflows
1	Sacramento River, American River	Sacramento River, American River
2	San Joaquin River, Calaveras Rivers	San Joaquin River, Calaveras Rivers
3	Cosumnes River, Mokelumne River	Cosumnes River, Mokelumne River, Dry Creek
4	Yolo Bypass, Toe Drain	Yolo Basin inflows, Cache Creek, Putah Creek

Results

Figure 66 through Figure 68 compare the dominant source water distributions for three dates during the 2008 simulation period. In the contemporary system, Sacramento River water dominates the northern, central, and western areas of the estuary due to its higher magnitude flows. The San Joaquin River is important in the south Delta, but reverse flows down Old and Middle River corridor pull Sacramento River water into the region as well. The influence of the Yolo Bypass and Cosumnes/Mokelumne sources decreases appreciably with lower flows in the summer. The dominant source water distributions in the pre-development system are similar. The San Joaquin River influences a wider area in the south Delta because of the lack of export pumping. The Cosumnes/Mokelumne source influences more area to the south than the contemporary system. Sacramento River water is the dominant source throughout the majority of the estuary, but the influences of other sources do not lessen in the summer low-flow period to the extent seen in the contemporary system. Seasonal high water and tidal inundation of the marsh plain results in broad regions of source water zones for the pre-development system plots.

Figure 69 through Figure 74 show individual source water relative concentrations. These display similar trends as the dominant source water maps. An additional important aspect seen in these plots, however, is the prevalence of non-Sacramento source water in the western and central Delta. On all three dates examined, Sacramento River water dominates Suisun Bay and the western Delta, with only trace amounts of other source waters present, in the contemporary system. By the low-flow fall date, the Sacramento River also dominates the central Delta. However in the pre-development system, appreciable portions (10–20%) of water in Suisun Bay came from San Joaquin or Cosumnes/Mokelumne sources for most of the simulation. The central Delta is also more equitably distributed between sources.

It should be noted that the mechanism of applying net channel depletions in the model may have an effect on the source water distributions, especially during low-flow periods. While an attempt was made to spatially distribute net channel depletions according to C2VSim predictions, which account for regional differences in meteorology and hydrogeology, the approach of applying depletions to the main channels, rather than marsh plain areas where the bulk of them are assumed to occur, may influence the model predicted source water distributions.

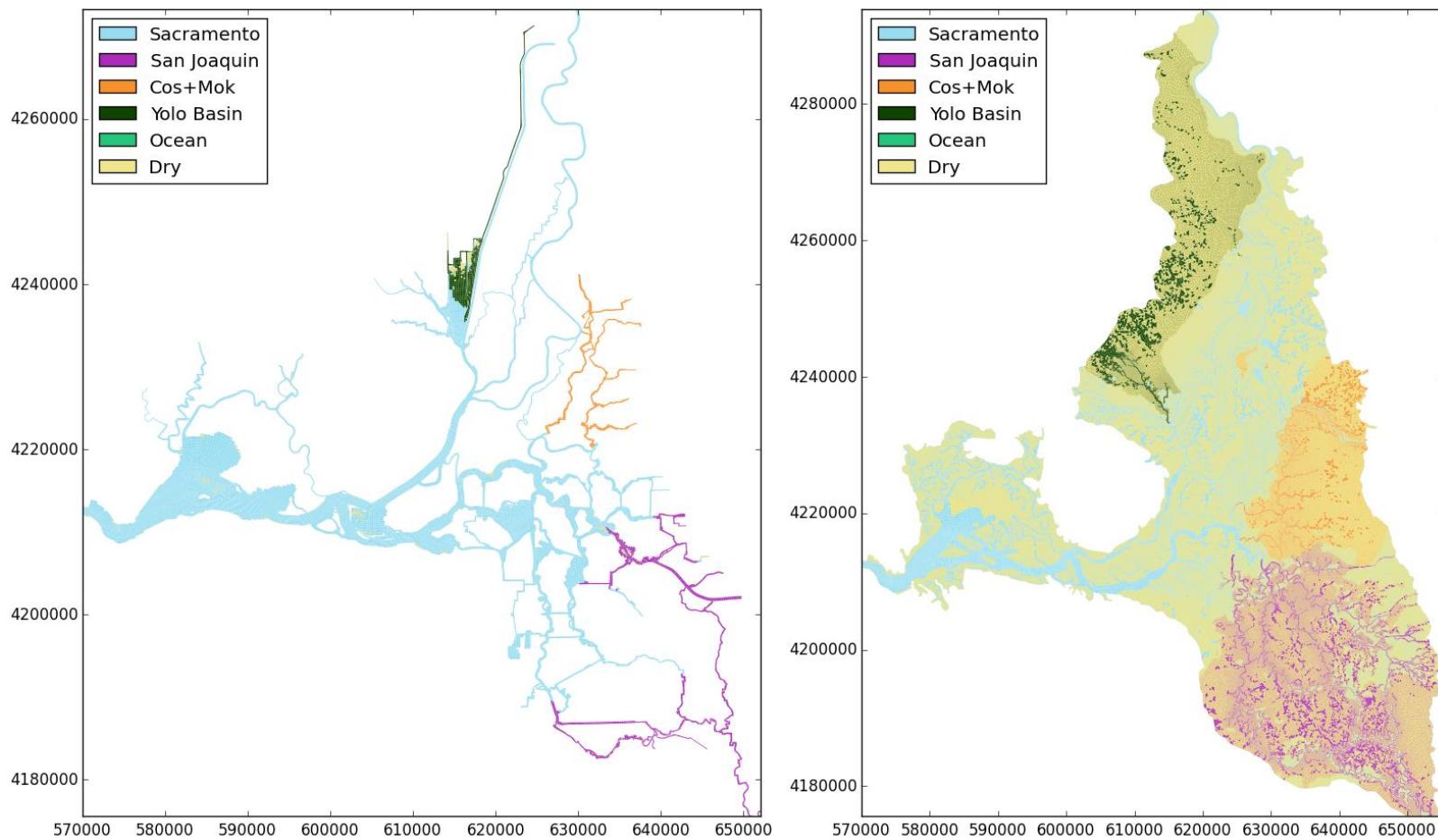


Figure 66 Simulated majority water source distributions on 1 March 2008 for contemporary system (left) and pre-development system. Dry cells are colored beige. Cells having shallow water are lightly colored.

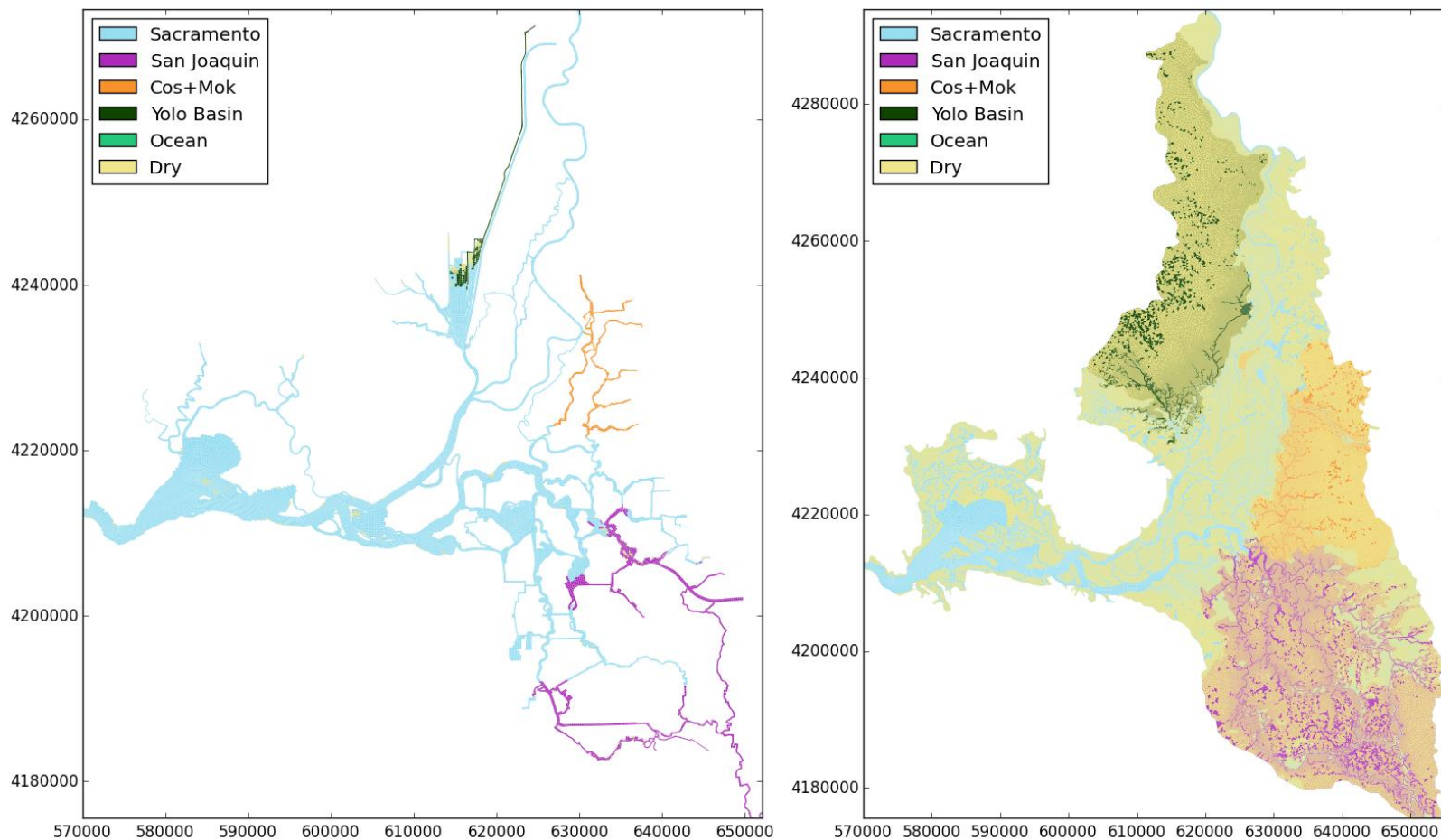


Figure 67 Simulated majority water source distributions on 1 May 2008 for contemporary system (left) and pre-development system. Dry cells are colored beige. Cells having shallow water are lightly colored.

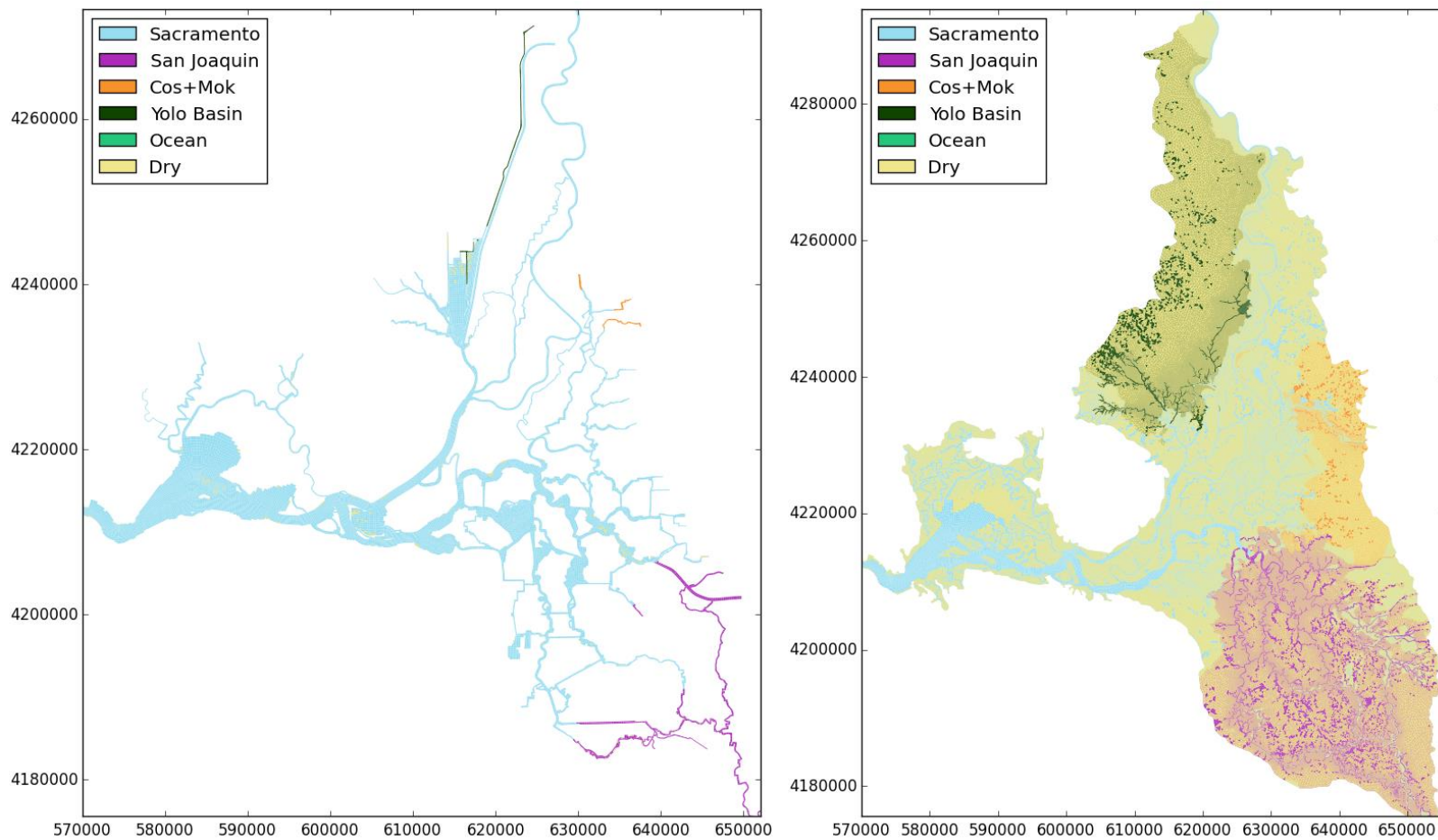


Figure 68 Simulated majority water source distributions on 1 July 2008 for contemporary system (left) and pre-development system. Dry cells are colored beige. Cells having shallow water are lightly colored.

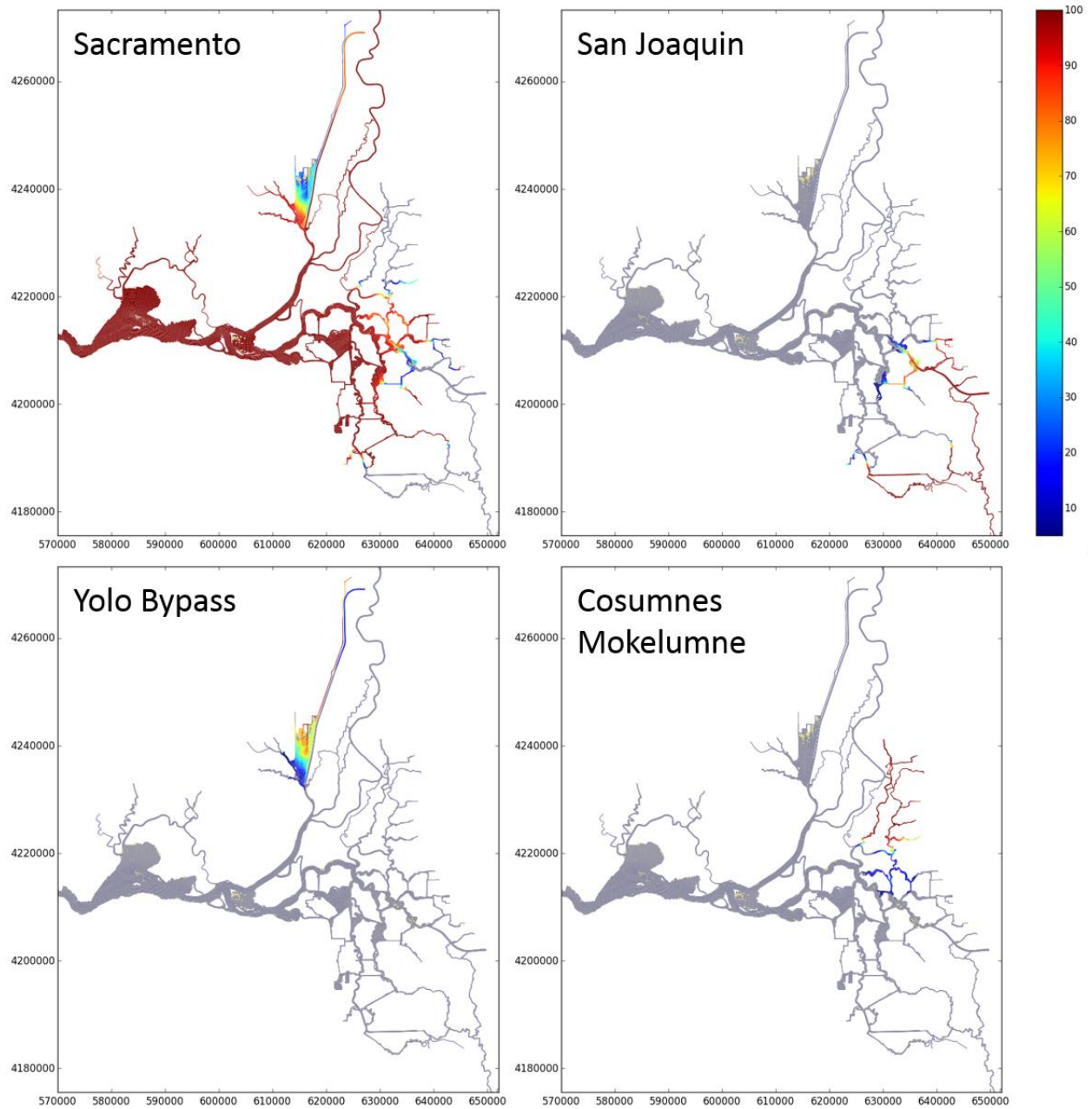


Figure 69 Individual water source relative concentrations for the contemporary model simulation, 1 March 2008. Cells with less than 5% of a given source water are colored gray.

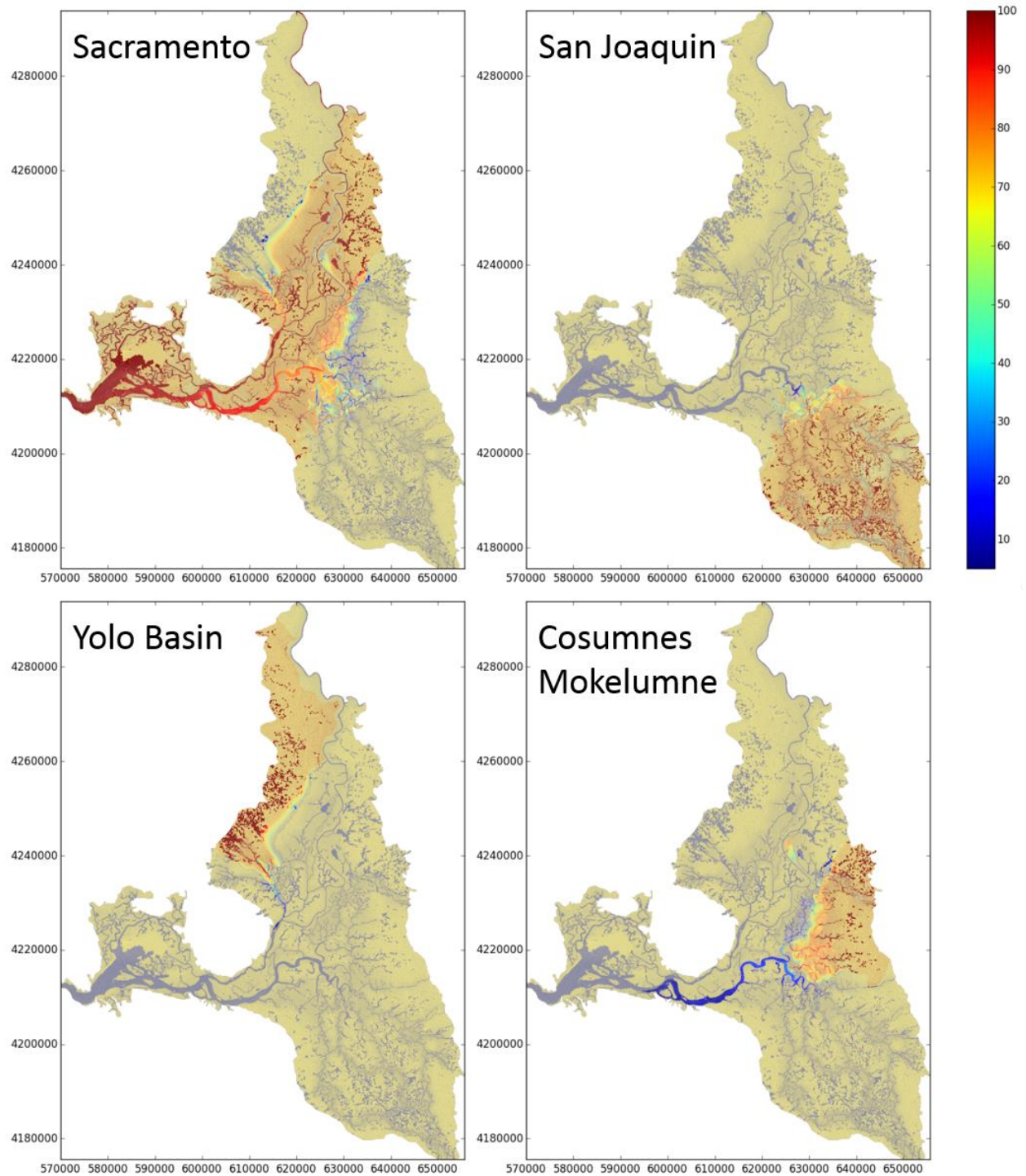


Figure 70 Individual water source relative concentrations for the pre-development model simulation, 1 March 2008. Dry cells are colored beige. Cells having shallow water are lightly colored. Cells with less than 5% of a given source water are colored gray.

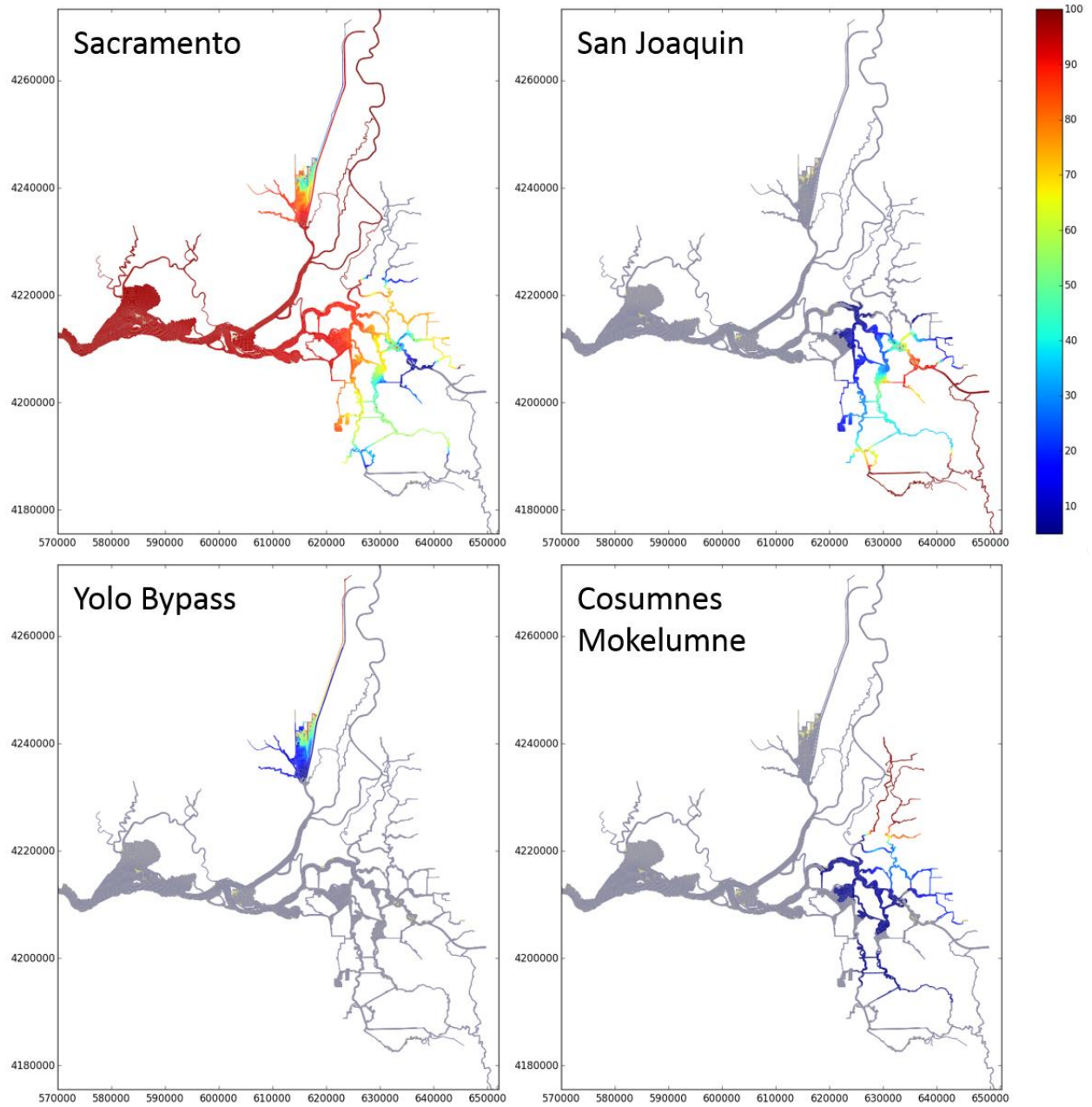


Figure 71 Individual water source relative concentrations for the contemporary model simulation, 1 May 2008. Cells with less than 5% of a given source water are colored gray.

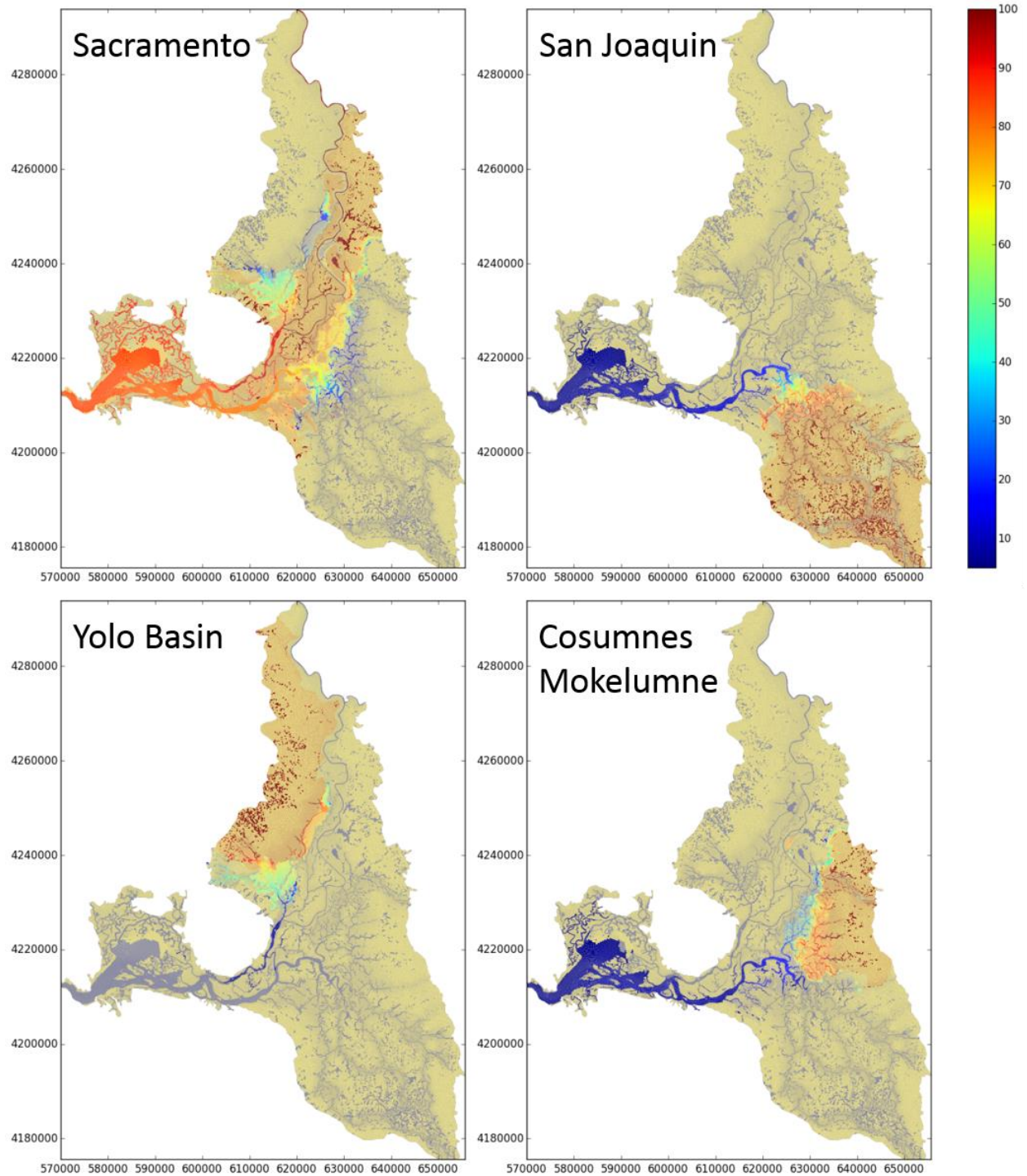


Figure 72 Individual water source relative concentrations for the pre-development model simulation, 1 May 2008. Dry cells are colored beige. Cells having shallow water are lightly colored. Cells with less than 5% of a given source water are colored gray.

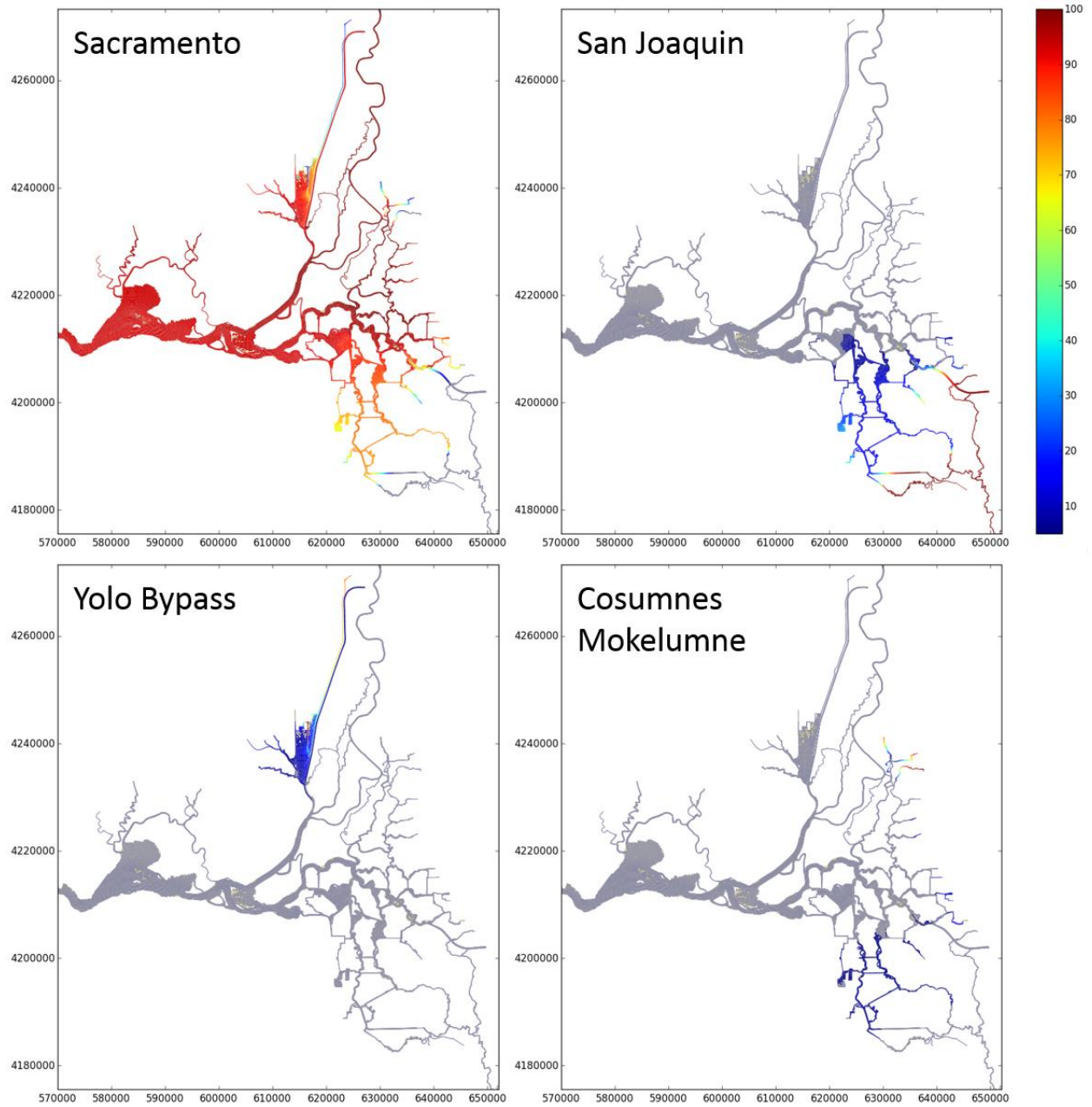


Figure 73 Individual water source relative concentrations for the contemporary model simulation, 1 July 2008. Cells with less than 5% of a given source water are colored gray.

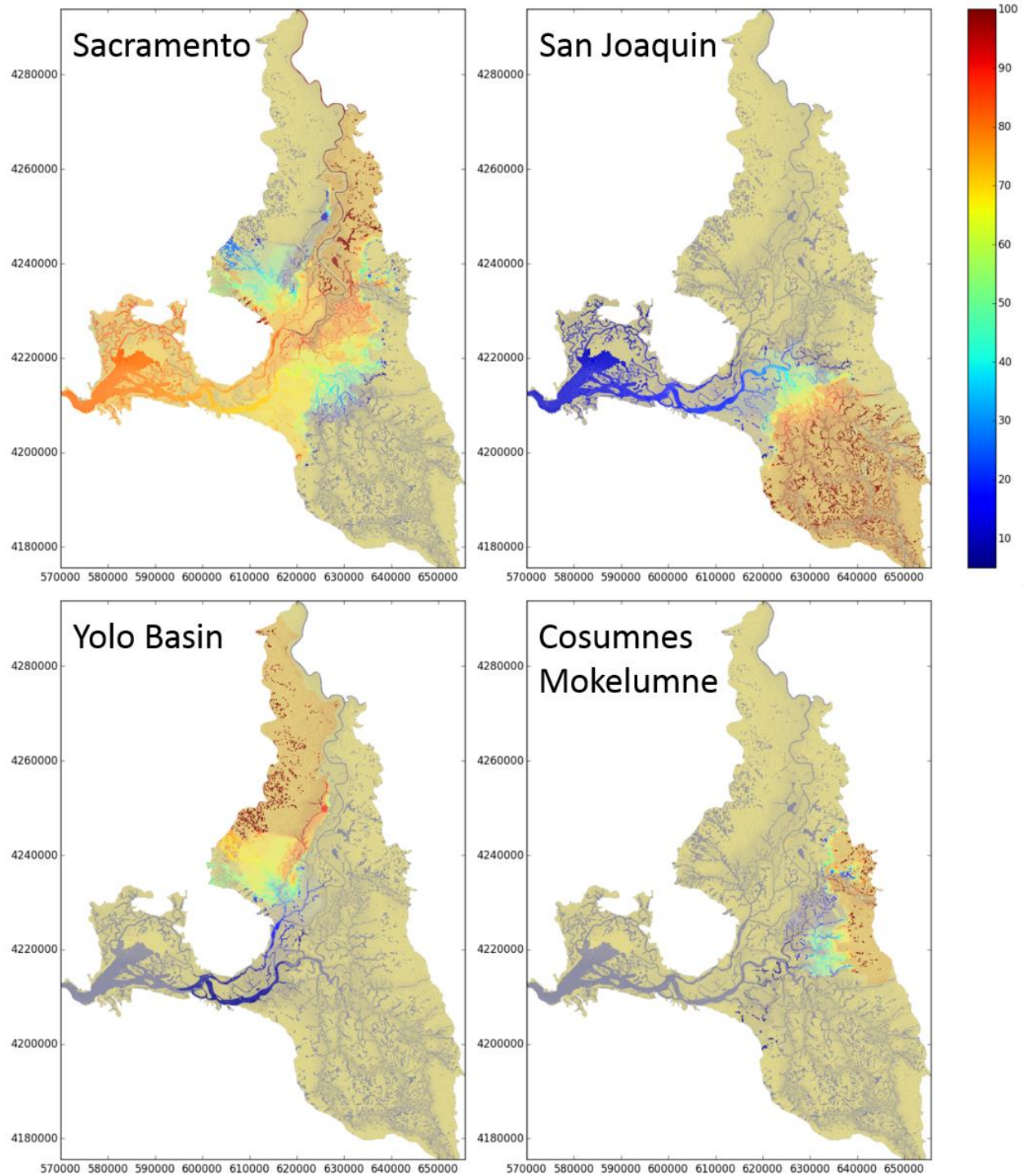


Figure 74 Individual water source relative concentrations for the pre-development model simulation, 1 July 2008. Dry cells are colored beige. Cells having shallow water are lightly colored. Cells with less than 5% of a given source water are colored gray.

References

- Abella R, Cook SF. 1960. *Colonial expeditions to the interior of California Central Valley, 1800-1820*. Berkeley, CA: University of California Press.
- Beaumont D. California State Land Office, 1861. *Swamp and Overflowed Lands Reports and Correspondence*. Box 44. *Courtesy of California State Archives, Sacramento*.
- Bureau JR. 1998. Results from the hydrodynamic element of the 1994 entrapment zone study in Suisun Bay. Sacramento (CA): Interagency Ecological Program for the San Francisco Bay-Delta Estuary. Technical Report 56. p 13-62.
- [CDWR] California Department of Water Resources. 1986. Memorandum to Peter Lee, Dick Kretsinger, and James McDaniel. Subject: Salinity Unit Conversion Equations. June 24, 1986. Available from: <http://www.water.ca.gov/suisun/facts/salin/memo.cfm>
- [CDWR] California Department of Water Resources. 1993. Sacramento-San Joaquin Delta atlas.
- Casulli V. 1990. Semi-implicit finite difference methods for the two-dimensional shallow water equations. *J Comput Phys* 86:56–74.
- Casulli V. 2009. A high-resolution wetting and drying algorithm for free-surface hydrodynamics. *Int J Numer Methods Fluids* 60:391–408.
- Casulli V, Cattani E. 1994. Stability, accuracy and efficiency of a semi-implicit method for three-dimensional shallow water flow. *Comput Math Appl* 27:99–112.
- Casulli V, Cheng RT. 1992. Semi-implicit finite difference methods for three-dimensional shallow water flow. *Int J Numer Methods Fluids* 15:629–648.
- Casulli V, Stelling GS. 2011. Semi-implicit subgrid modelling of three-dimensional free-surface flows. *Int J Numer Methods Fluids* 67:441–449.
- Casulli V, Walters RA. 2000. An unstructured grid, three-dimensional model based on the shallow water equations. *Int J Numer Methods Fluids* 32:331–348.
- Casulli V, Zanolli P. 2005. High resolution methods for multidimensional advection-diffusion problems in free-surface hydrodynamics. *Ocean Model* 10:137–151.
- Cheng RT, Casulli V, Gartner JW. 1993. Tidal, residual, intertidal mudflat (TRIM) model and its application to San Francisco Bay, California. *Estuarine, Coastal and Shelf Science*. 36:235–280.
- Day S. 1869. Report of Sherman Day, Surveyor-General. In *Fresh water tide lands of California*, ed. M. D. Carr & Co.

- Denton RA. 1993. Accounting for antecedent conditions in seawater intrusion modeling— applications for the San Francisco Bay–Delta. Hydraulic Engineering '93, Shen HW, Su ST, Wen F, Editors. American Society of Civil Engineers, 448–453.
- Denton RA, Sullivan GD. 1993. Antecedent flow-salinity relations: application to Delta planning models. Contra Costa Water District Report.
- Enright C, Culberson SD, Burau JR. 2013. Broad timescale forcing and geomorphic mediation of tidal marsh flow and temperature dynamics. *Estuaries and Coasts* 36:1319–1339.
- Fagherazzi S, Gabet EJ, Furbish DJ. 2004. The effect of bidirectional flow on tidal channel planforms. *Earth Surface Processes and Landforms* 29:295–309.
- Fleenor WE, Bell A, Safran S. 2015. Development of a digital elevation model for the historical SacramentoSan Joaquin Delta. *San Francisco Estuary and Watershed Sciences* In prep.
- Fofonoff NP, Millard Jr. RC. 1983. Algorithms for computation of fundamental properties of seawater. UNESCO technical papers in marine science 44. 58 p.
- Fox P, Hutton PH, Howes DJ, Draper AJ, Sears L. 2015. Reconstructing the natural hydrology of the San Francisco Bay-Delta watershed. *Hydrology and Earth System Sciences* 19:4257–4274.
- Friedrichs CT, Aubrey DG. 1988. Non-linear tidal distortion in shallow well-mixed estuaries: a synthesis. *Estuarine, Coastal, and Shelf Science* 27:521–545.
- Gilbert GK. 1917. *Hydraulic-mining debris in the Sierra Nevada*. U.S. Geological Survey. Washington, DC: U.S. Government Printing Office.
- Gross ES, Koseff JR, Monismith SG. 1999. Evaluation of advective transport schemes for simulation of salinity in a shallow estuary. *J Hydraul Eng* 125(1):32–46.
- Gross ES, MacWilliams ML, Kimmerer WJ. 2009. Three-dimensional modeling of tidal hydrodynamics in the San Francisco Estuary. *San Franc Estuary Watershed Sci* 7(2).
- Hall WH. 1879. William Hammond Hall Collection, Field Books, Box 3, Book 45, 8-32. Courtesy of California State Archives, Sacramento.
- Hansen DV, Rattray Jr. M. 1965. Gravitational circulation in straits and estuaries. *J Mar Res* 23: 104–122.
- Hetland RD, and Geyer WR. 2004: An idealized study of the structure of long, partially mixed estuaries. *J Phys Ocean* 34:2677–2691.
- Higley HA. 1860. *Annual report of the Surveyor-General for the year 1860*. State Land Office.

- Howes DJ, Fox P, Hutton PH. 2015. Evapotranspiration from natural vegetation in the Central Valley of California: monthly grass reference-based vegetation coefficients and the dual crop coefficient approach. *J Hydrol Eng, ASCE* 20(10):04015004.
- Hutton PH. 2014. Delta Salinity Gradient (DSG) Model: Version 1.0 Model Documentation. Report prepared for Metropolitan Water District of Southern California. July 1, 2014.
- Hutton PH, Rath JS, Chen L, Ungs MJ and Roy SB. 2015. Nine Decades of Salinity Observations in the San Francisco Bay and Delta: Modeling and Trend Evaluations, *J of Water Res Planning and Management, ASCE*. In press.
- Jassby AD, Kimmerer WJ, Monismith SG, Armor C, Cloern JE, Powell TM, Schubel JR, Vendlinski TJ. 1995. Isohaline position as a habitat indicator for estuarine populations. *Ecol Appl* 5:272–289.
- Kadir T, Huang G, Chung F. 2015. Estimating 1922-2013 daily inflows to the Sacramento–San Joaquin Delta under natural vegetative conditions using SWAT and C2VSIM models. *San Francisco Estuary and Watershed Sciences*. In prep.
- Kantha LH, Clayson CA. 1994. An improved mixed layer model for geophysical applications. *J Geophys Res* 99: 25235–25266.
- Kimmerer WJ. 2002. Effects of freshwater flow on abundance of estuarine organisms: physical effects or trophic linkages? *Mar Ecol Prog Ser* 243:39–55.
- Kimmerer WJ. 2004. Open water processes of the San Francisco Estuary: from physical forcing to biological responses. *San Francisco Estuary and Watershed Science* [Internet]. Available from: <http://escholarship.org/uc/item/9bp499mv>.
- Kimmerer WJ, MacWilliams ML, Gross ES. 2013. Variations of fish habitat and extent of the low-salinity zone with freshwater flow in the San Francisco Estuary. *San Francisco Estuary and Watershed Science* 11(4).
- Leopold LB, Collins JN, Collins LM. 1993. Hydrology of some tidal channels in estuarine marshland near San Francisco. *Catena* 20(5):469–493.
- Lerczak HA, Geyer WR, Ralston DK. 2009. The temporal response of the length of a partially stratified estuary to changes in river flow and tidal amplitude. *J Phys Ocean* 39(4): 915–933.
- MacWilliams ML, Bever AJ, Gross ES, Ketefian GS, Kimmerer WJ. 2015. Three-dimensional modeling of hydrodynamics and salinity in the San Francisco Estuary: An evaluation of model accuracy, X2, and the low salinity zone. *San Franc Estuary Watershed Sci* 13(1).

McCollum WS. 1850. California as I saw it; pencillings by the way of its gold and gold diggers, and incidents of travel by land and water. Los Gatos, CA: Talisman Press. Courtesy of Library of Congress.

Malamud-Roam KP. 2000. Tidal regimes and tide marsh hydroperiod in the San Francisco Estuary: theory and implications for ecological restoration. Dissertation, University of California, Berkeley.

Manfree A. 2014. Historical Ecology. Ch 2 in Suisun Marsh, Moyle PB, Manfree AD, Fiedler PL Eds. University of California Press.

Mars, 23rd Annual Progress Report to the State Water Resources Control Board. California Department of Water Resources, Bay-Delta Office, Delta Modeling Section.

Monismith SG, Kimmerer WJ, Burau JR, Stacey MT. 2002. Structure and flow-induced variability of the subtidal salinity field in northern San Francisco Bay. *J Phys Ocean* 32:3003–3019.

Morgan-King TL, Schoellhamer DH. 2013. Suspended-sediment flux and retention in a backwater tidal slough complex near the landward boundary of an estuary. *Estuaries and Coasts* 36:300–318.

[MWH] MWH Global. 2014. Natural Flow Routing Model. Report Prepared for State Water Contractors, San Luis Delta-Mendota Water Authority, and Metropolitan Water District of Southern California. April 2014.

[RMA] Resource Management Associates. 2005. Flooded islands pre-feasibility study: RMA Delta Model calibration report. Prepared for the California Department of Water Resources for submittal to the California Bay–Delta Authority. 158 p.

[RMA] Resource Management Associates. 2014. Hydrodynamic and salinity transport modeling of the historical Bay–Delta system. Technical memorandum prepared for Metropolitan Water District of Southern California. April 2014. 101 p.

Rodi W. 1987. Examples of calculation methods for flow and mixing in stratified flows. *J Geophys Res* 92:5305–5328.

Rose AH, Manson M, Grunsky CE. State Printing Office, Sacramento, 1895. *Report of the Commissioner of Public Works to the Governor of California*.

Sacramento Daily Union, Is the Sacramento Valley Inhabitable?, 24 March 1862. Courtesy of California Digital Newspaper Collection.

[SFEI] San Francisco Estuary Institute-Aquatic Science Center. 2014. A Delta Transformed: Ecological Functions, Spatial Metrics, and Landscape Change in the Sacramento-San Joaquin

Delta. Prepared for the California Department of Fish and Wildlife and Ecosystem Restoration Program. A Report of SFEI-ASC's Resilient Landscapes Program, Publication #729, San Francisco Estuary Institute-Aquatic Science Center, Richmond, CA.

Smith SD, Banke EG. 1975. Variation of the sea surface drag coefficient with wind speed. *Quart J R Meteorol Soc* 101:655–673.

Thompson J. 2006. Early reclamation and abandonment of the central Sacramento-San Joaquin Delta. *Sacramento History Journal* 6(1-4):41-72.

Thornton SR. 1859. U.S. v. Anastasio Chaboya, Land Case No. 406 ND, Sanjon de los Miquelemes, U.S. District Court, Northern District. 200. Courtesy of The Bancroft Library, UC Berkeley.

[USACE] U.S. Army Corps of Engineers, Hydrological Engineering Center. 2010. HEC-RAS River Analysis System: User's Manual, Version 4.1, Davis, CA: HEC, US Army Corps of Engineers.

Umlauf L, Burchard H. 2003. A generic length-scale equation for geophysical turbulence models. *J Mar Res* 61:235–265.

Van Leer B. 1974. Towards the ultimate conservative difference scheme, II: monotonicity and conservation combined in a second order scheme. *J Comput Phys* 14:361–370.

Wang R, Ateljevich E. 2012. A Continuous Surface Elevation Map for Modeling (Chapter 6). In *Methodology for Flow and Salinity Estimates in the Sacramento-San Joaquin Delta and Suisun*

Warner JC, Sherwood CS, Arango HG, Signell RP. 2005. Performance of four turbulence closure models implemented using a generic length scale method. *Ocean Model* 8:81–113.

Whipple AA, Grossinger RM, Rankin D, Stanford B, Askevold RA. 2012. Sacramento-San Joaquin Delta Historical Ecology Investigation: Exploring Pattern and Process. Prepared for the California Department of Fish and Game and Ecosystem Restoration Program. A Report of SFEI-ASC's Historical Ecology Program, Publication #672, San Francisco Estuary Institute-Aquatic Science Center, Richmond, CA.

Appendix A: Specific Conductivity to Salinity Conversion Methods

The electrical conductance (EC) of estuarine water is easily measured in the field using a conductivity sensor. However, since EC is not strictly a conserved quantity, it must be converted to salinity for use in model simulations. Because of different ionic strengths of dissolved salts and different ionic compositions of source water, a universal equation to convert EC to salinity does not exist. A standardized equation is available from UNESCO (Fofonoff and Millard Jr. 1983), but this assumes the water contains a canonical ionic composition based on pure seawater samples. For water where the majority of the salinity is ocean-derived, the UNESCO conversion provides a good approximation. For locations where the water is dominated by land-derived salts, the approximation may not be accurate. For this reason, a brief analysis was performed to examine differences in salinity predicted using the UNESCO equation to those predicted using site-specific EC-salinity regressions, which take into account the ionic composition of the predominant source water at a given location. The site specific regressions used were those reported in CDWR (1986). The comparison focused on locations in the typical range of the low salinity zone and conductivity values in the low salinity zone range, because of their relevance to this study.

Salinity conversion results are shown in Table 18. In general, the site-specific salinity regressions tended to predict higher salinities than the UNESCO equations by 7–10%. The largest differences were found at the furthest downstream sites at the highest salinities and were in the range 15–19%. Because of the relatively small differences in salinities predicted using the equation sets, the UNESCO equations were retained for the conversions made in this study because of their simplicity. A pseudo-code subroutine for conversion using the UNESCO equations is given below.

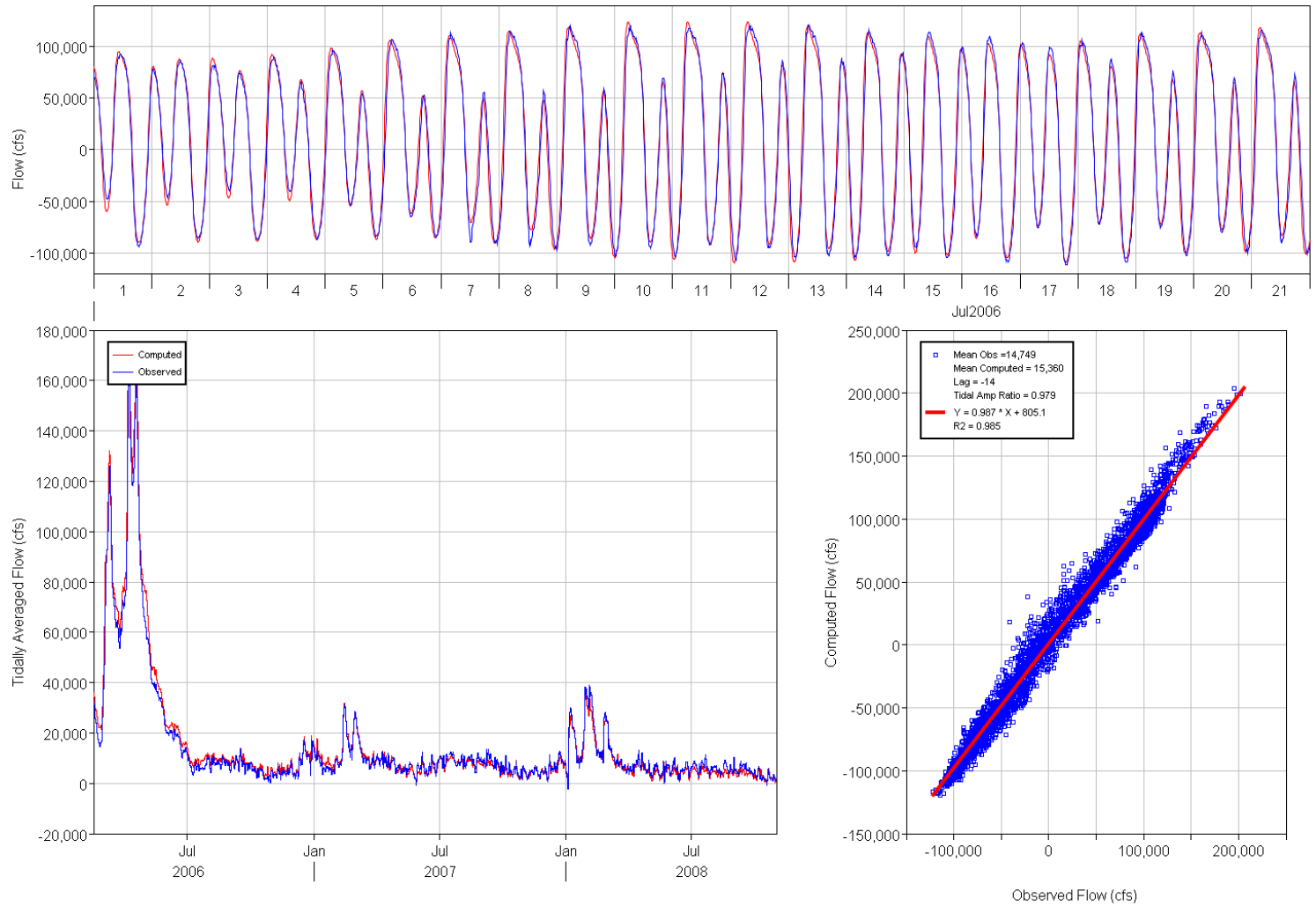
```
def convert_EC_to_salinity(datain):
    # datain is EC in uS/cm
    # dataout is salinity in psu
    a = [ 0.0080, -0.1692, 25.3851, 14.0941, -7.0261, 2.7081 ]
    b = [ 0.0005, -0.0056, -0.0066, -0.0375, 0.0636, -0.0144 ]
    Rt = datain/53087.
    x = 400.*Rt
    y = 100.*Rt
    sum1 = 0.0
    for k in range(len(a)):
        sum1 += (a[k] + 8.606*b[k]) * Rt**(k/2.)
    dataout = sum1 - (a[0]/(1.+1.5*x*x) + 8.606*b[0]/(1.+y**0.5+y**1.5))
    return dataout
```

Table 18 Salinity conversion method sensitivity analysis.

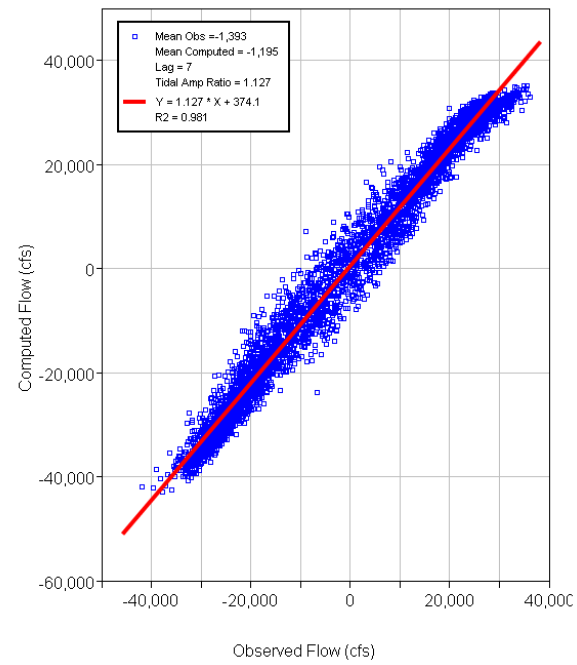
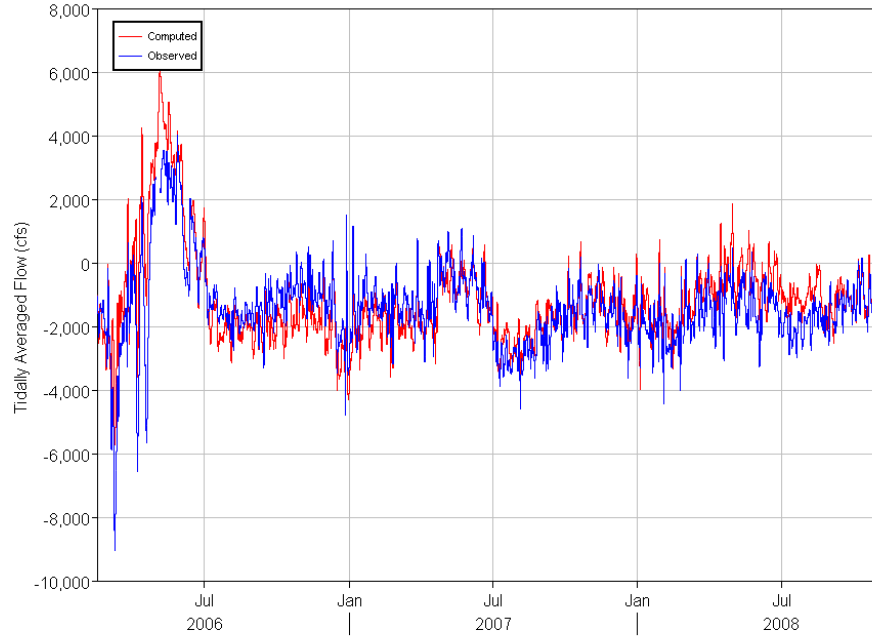
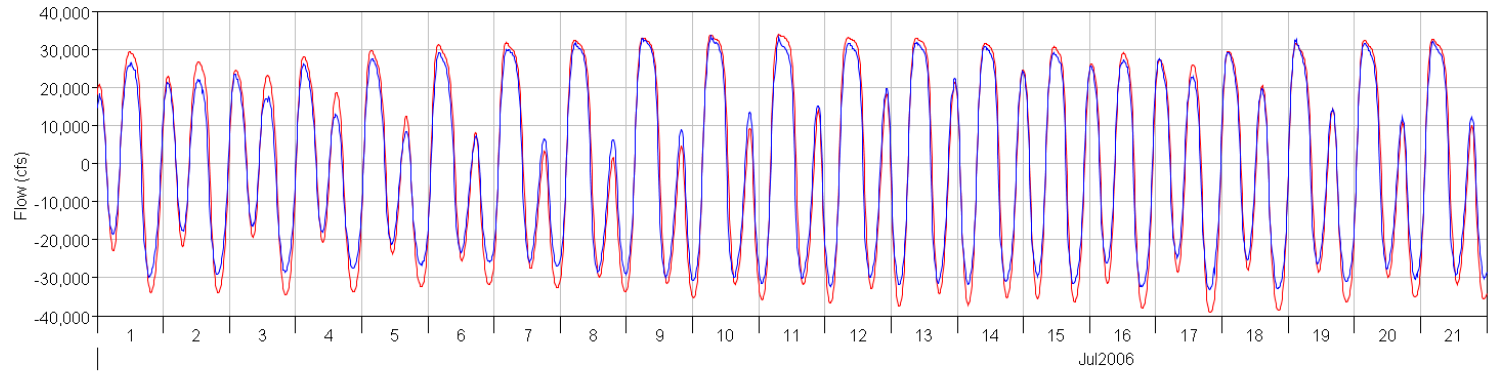
	EC = 1000 uS/cm		EC = 2000 uS/cm		EC = 3000 uS/cm		EC = 4000 uS/cm		EC = 5000 uS/cm		EC = 6000 uS/cm	
	Unesco Salinity (psu) = 0.492		Unesco Salinity (psu) = 1.016		Unesco Salinity (psu) = 1.558		Unesco Salinity (psu) = 2.113		Unesco Salinity (psu) = 2.679		Unesco Salinity (psu) = 3.253	
Site	Site Eqn Predicted Salinity (psu)	% Difference from Unesco										
Martinez	0.511	3.8	1.186	15.4	1.861	17.7	2.536	18.2	3.211	18.1	3.886	17.7
Port Chicago	0.493	0.3	1.156	12.8	1.818	15.4	2.480	16.0	3.142	15.9	3.804	15.6
Sacramento R at Middle Ground Is	0.424	14.9	1.046	2.9	1.669	6.9	2.291	8.1	2.913	8.4	3.536	8.3
Sacramento R at Chipps Is	0.552	11.4	1.163	13.5	1.774	13.0	2.386	12.1	2.997	11.2	3.608	10.3
Sac R 1.5 km E of Pt Sacramento	0.574	15.4	1.159	13.2	1.745	11.3	2.330	9.8	2.915	8.4	3.500	7.3
Sacramento R at Emmaton	0.555	12.1	1.112	9.0	1.669	6.9	2.226	5.2	2.783	3.8	3.341	2.6
Sacramento R at Rio Vista	0.539	9.0	1.065	4.7	1.592	2.1	2.118	0.2	2.645	1.3	3.171	2.6
San Joaquin R at Antioch	0.555	12.1	1.122	9.9	1.688	8.0	2.255	6.5	2.822	5.2	3.388	4.1
San Joaquin R at Jersey Pt	0.536	8.6	1.059	4.1	1.581	1.4	2.103	0.5	2.625	2.0	3.147	3.3
San Joaquin R at Twitchell Is	0.541	9.5	1.074	5.6	1.607	3.1	2.141	1.3	2.674	0.2	3.207	1.4
Average	0.528	9.7	1.114	9.1	1.700	8.6	2.286	7.8	2.873	7.5	3.459	7.3

Appendix B: Contemporary San Francisco Estuary Model Individual Flow Station Plots

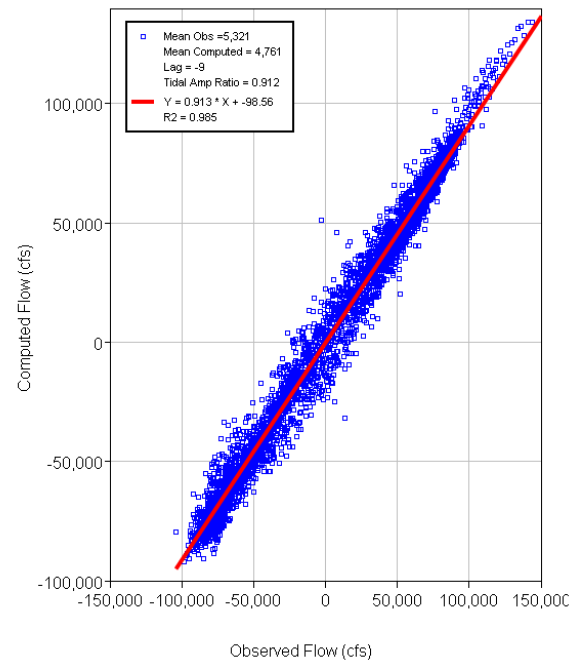
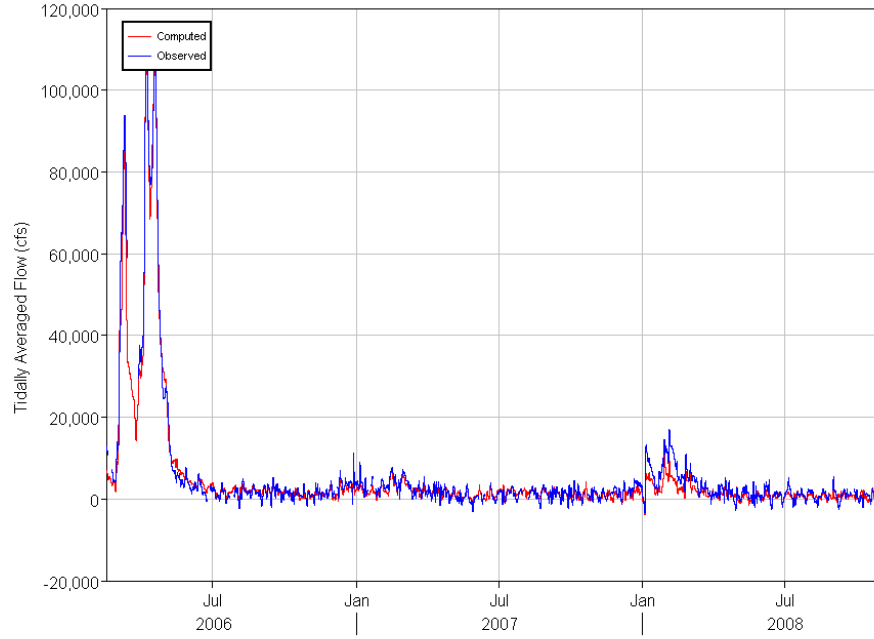
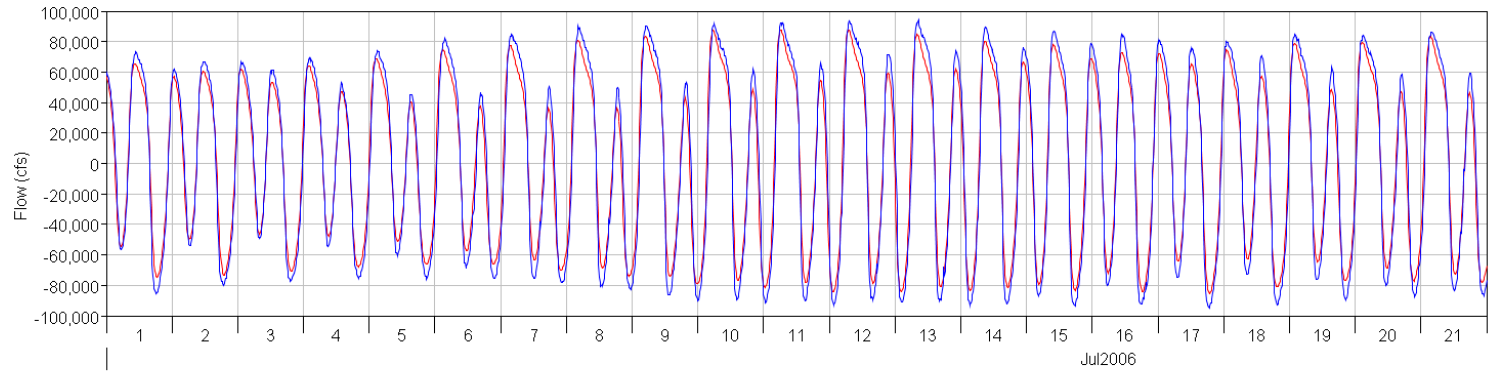
SRV - Sac River at Rio Vista



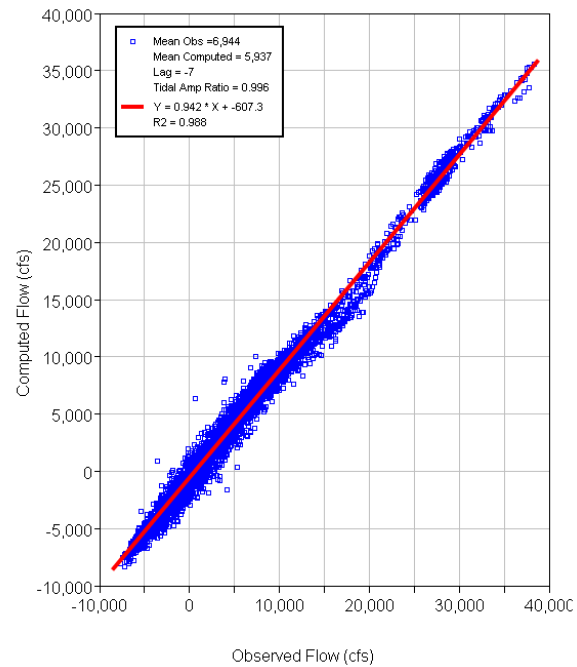
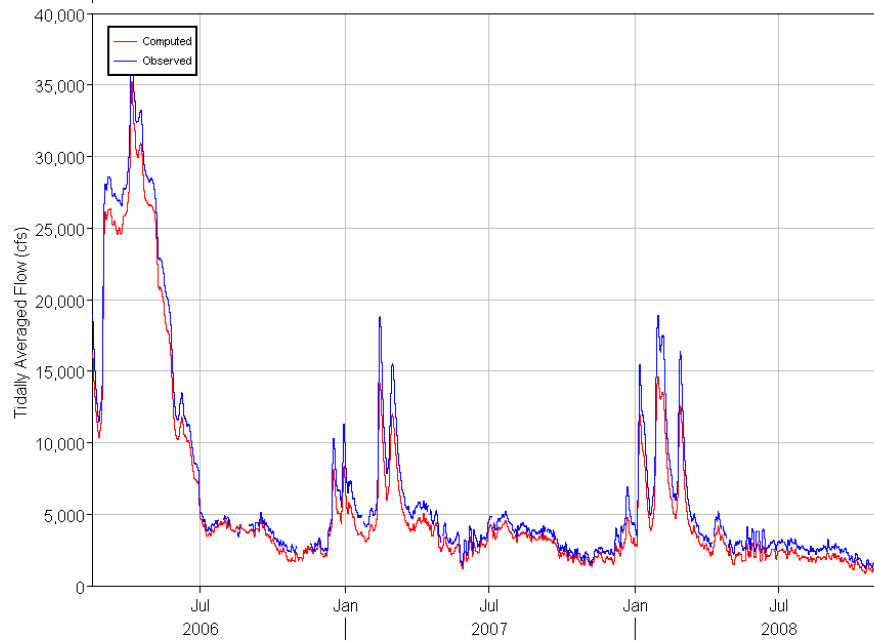
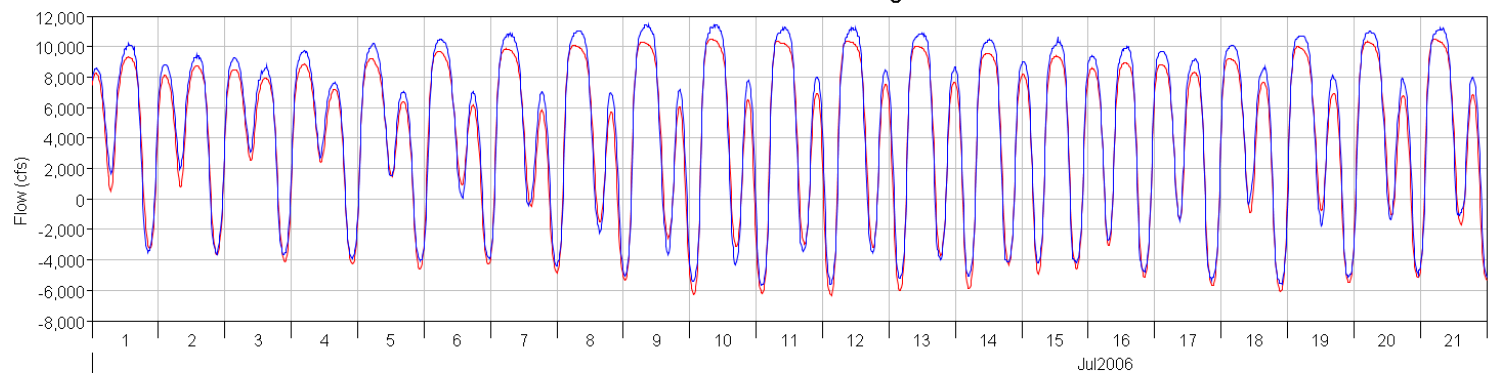
TSL - Threemile Slough



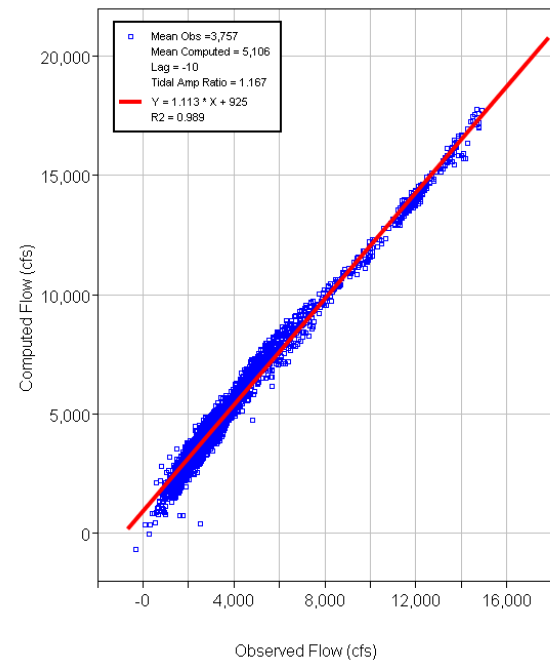
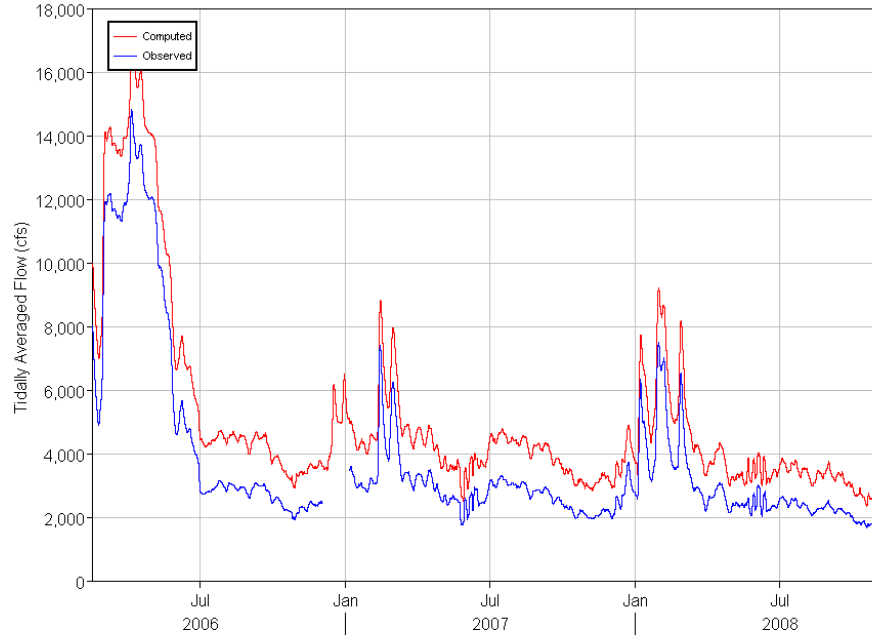
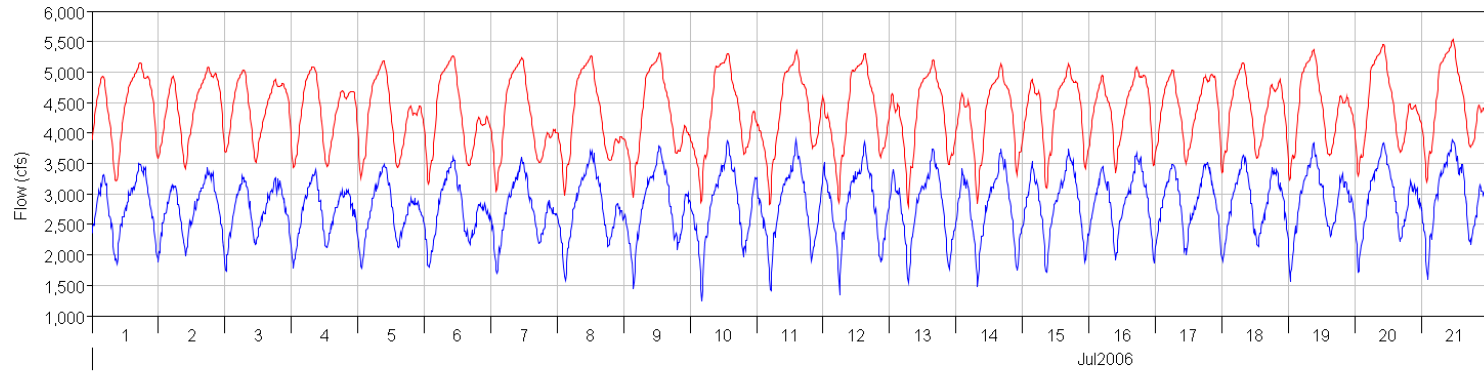
RYI - Cache SI at Ryer Island



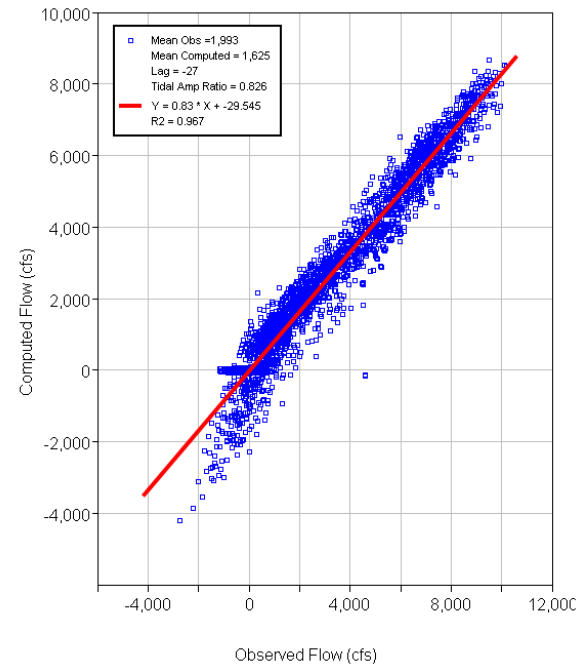
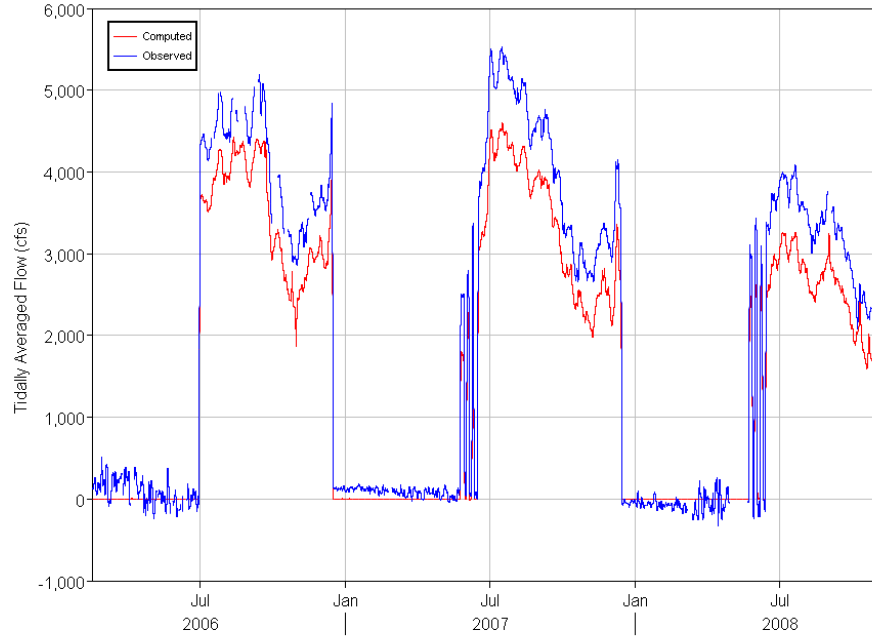
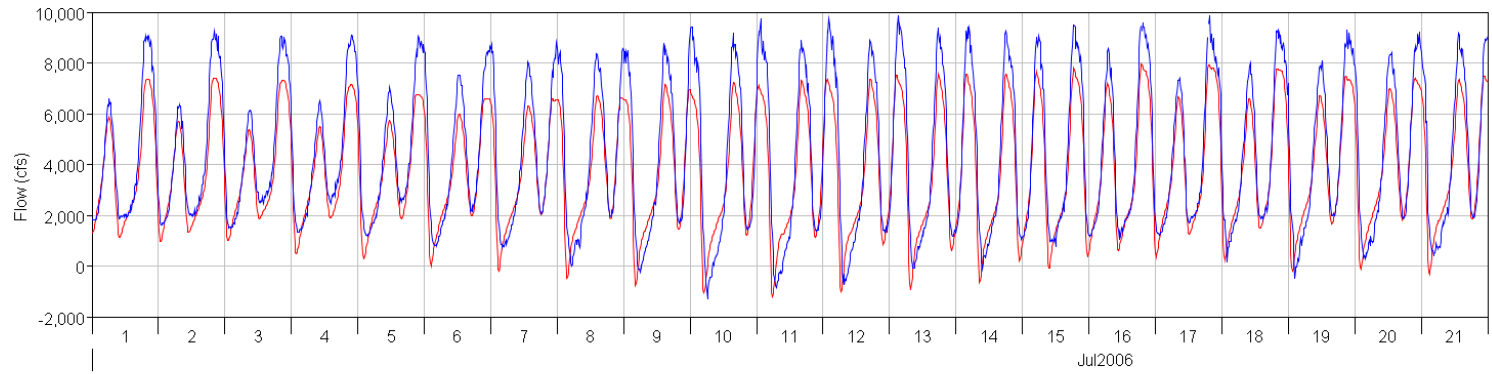
GES - Sacramento R below Georgiana SI



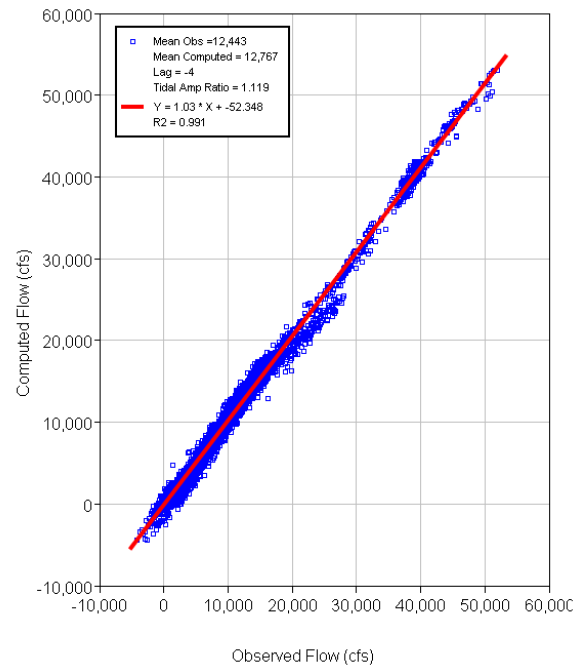
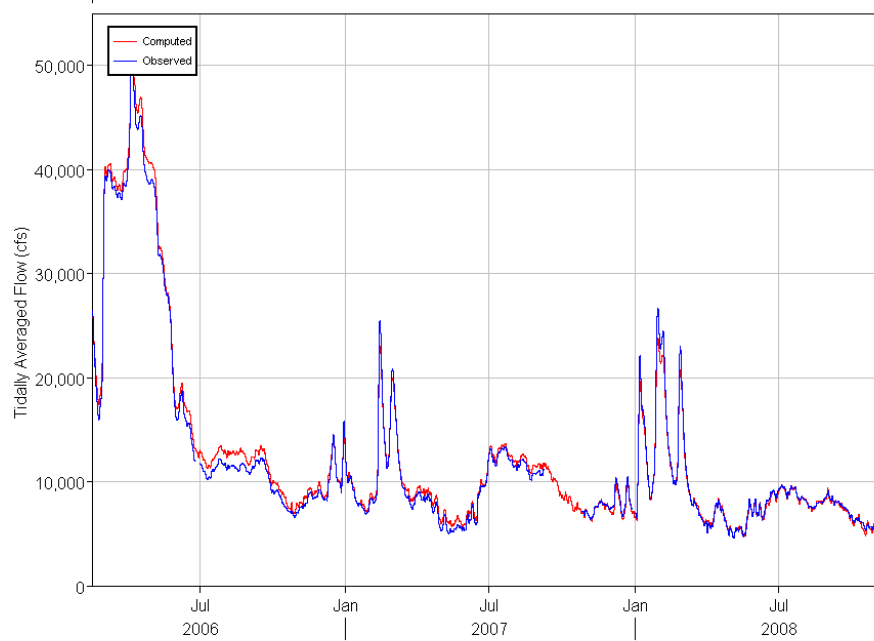
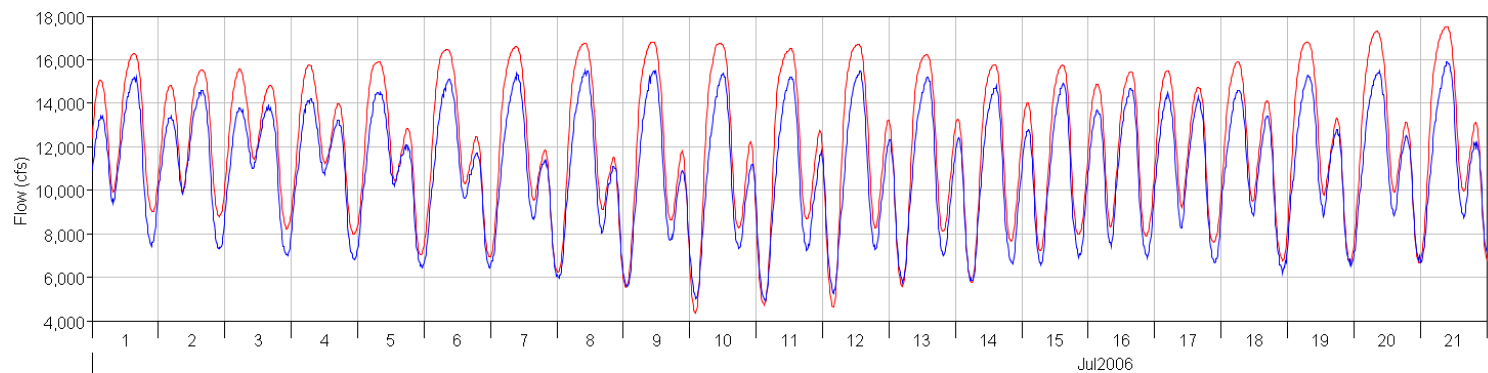
GSS - Georgiana Slough



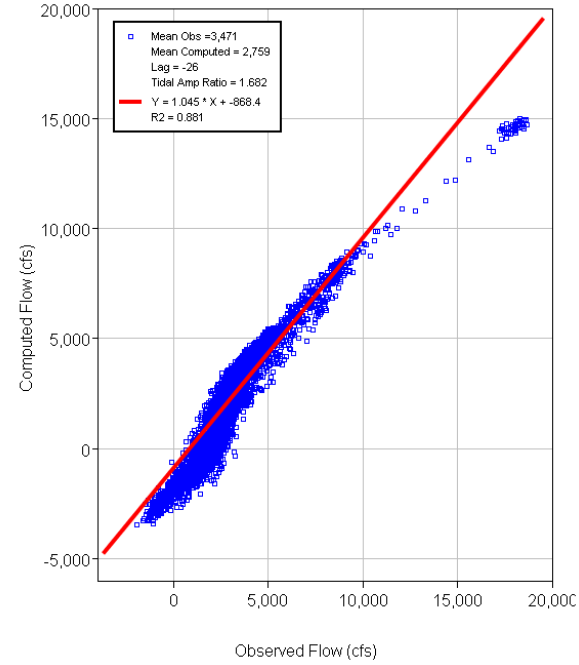
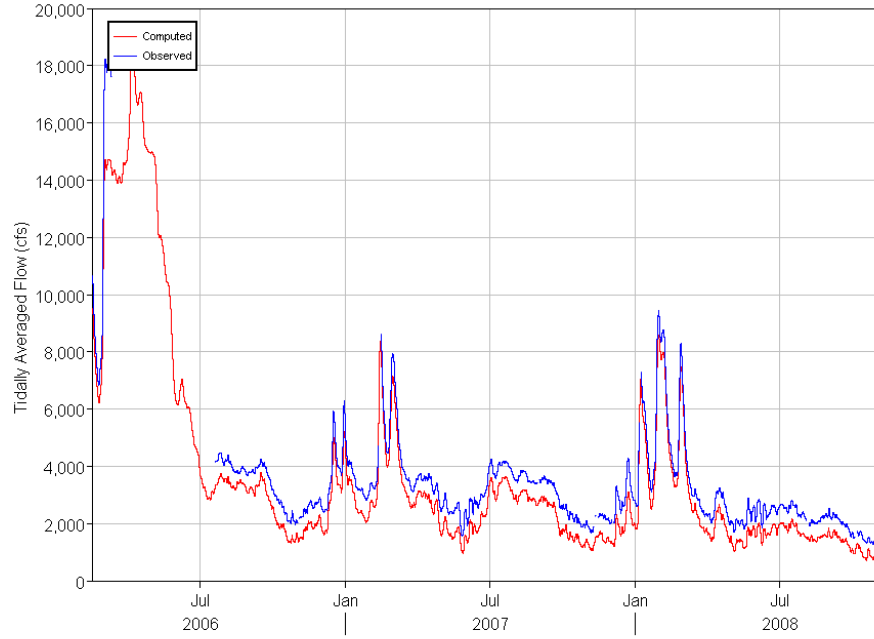
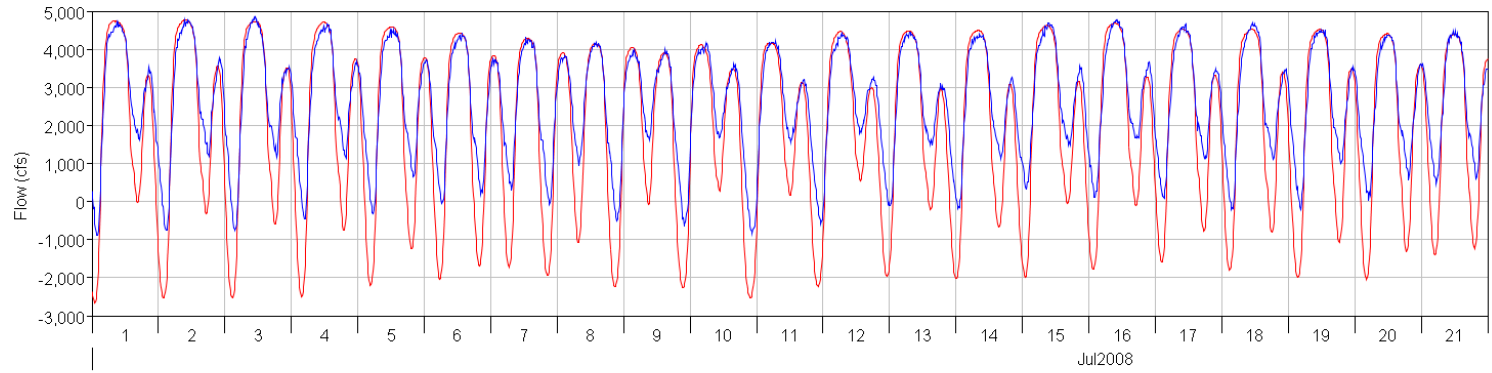
DCC - Delta Cross Channel



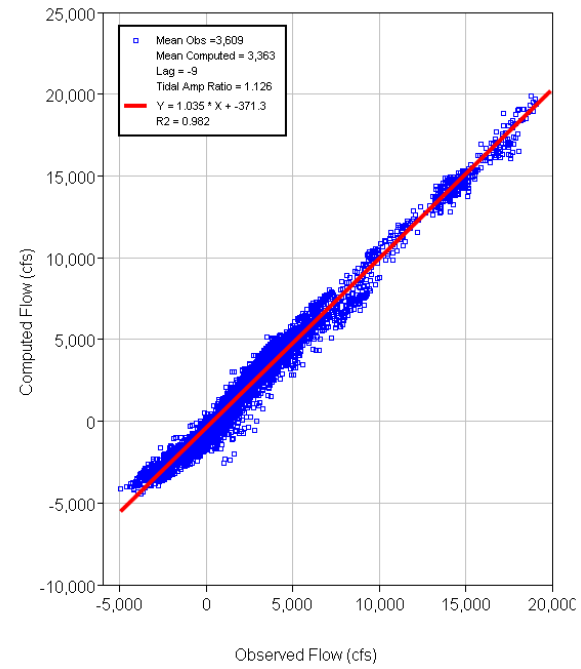
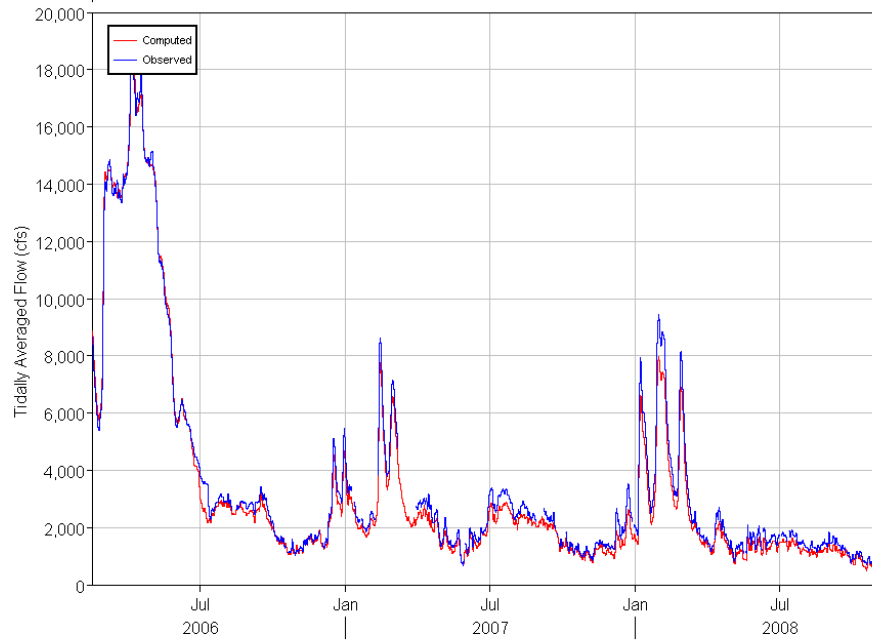
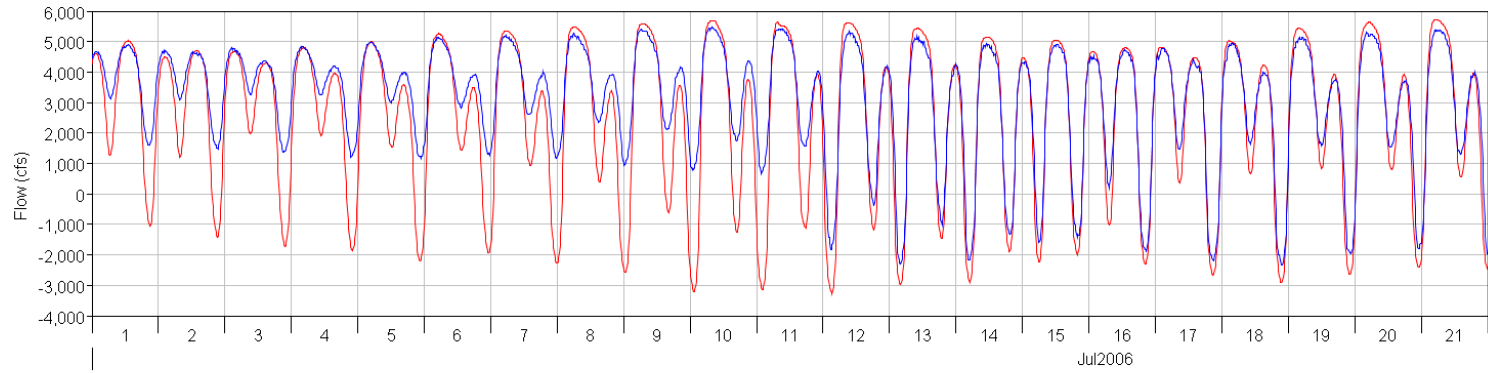
SDC - Sacramento R above DCC



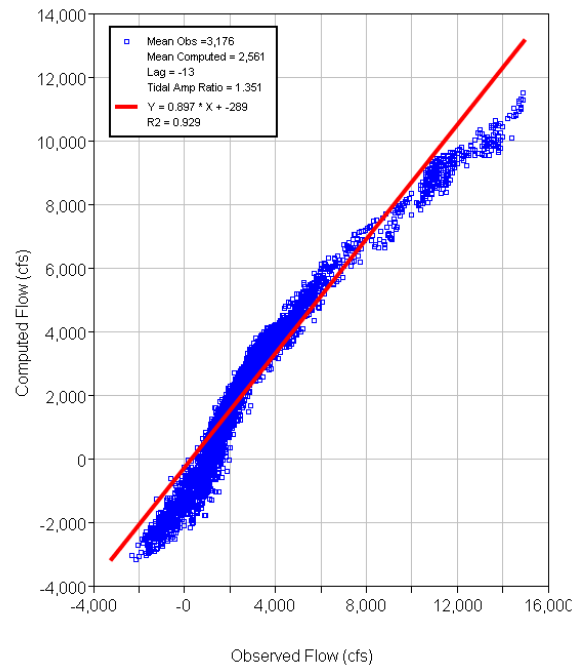
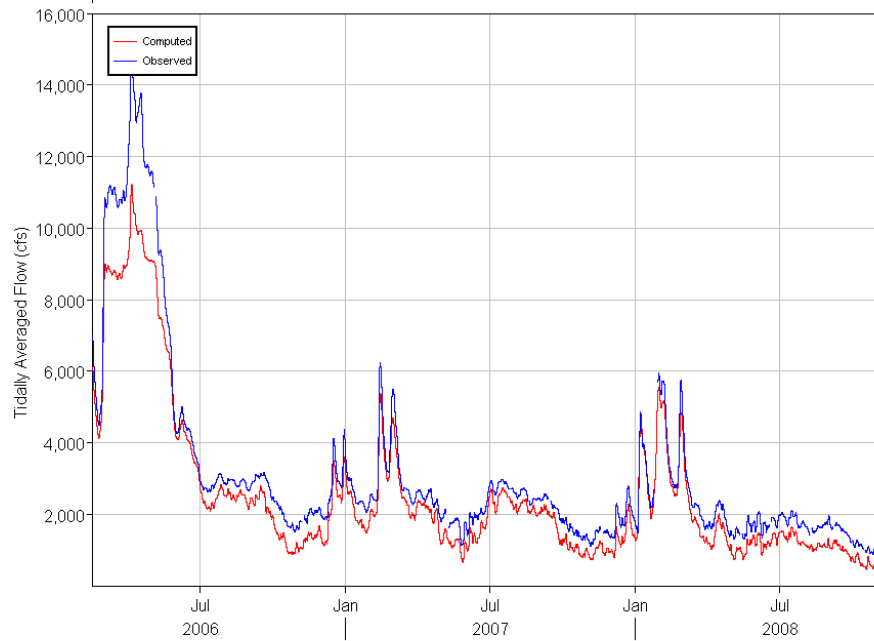
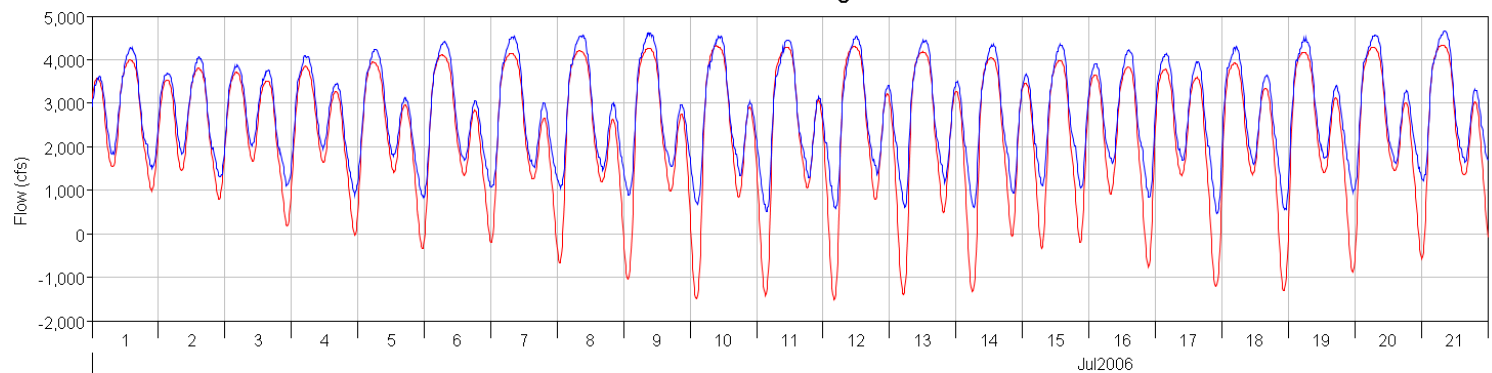
SUT - Sutter Slough



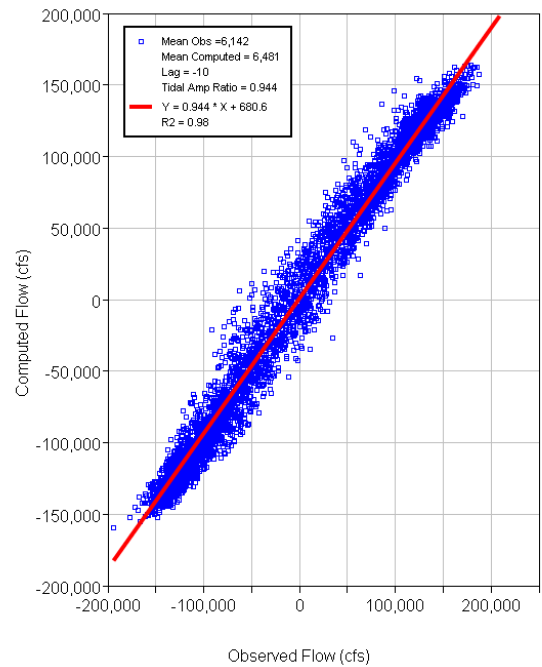
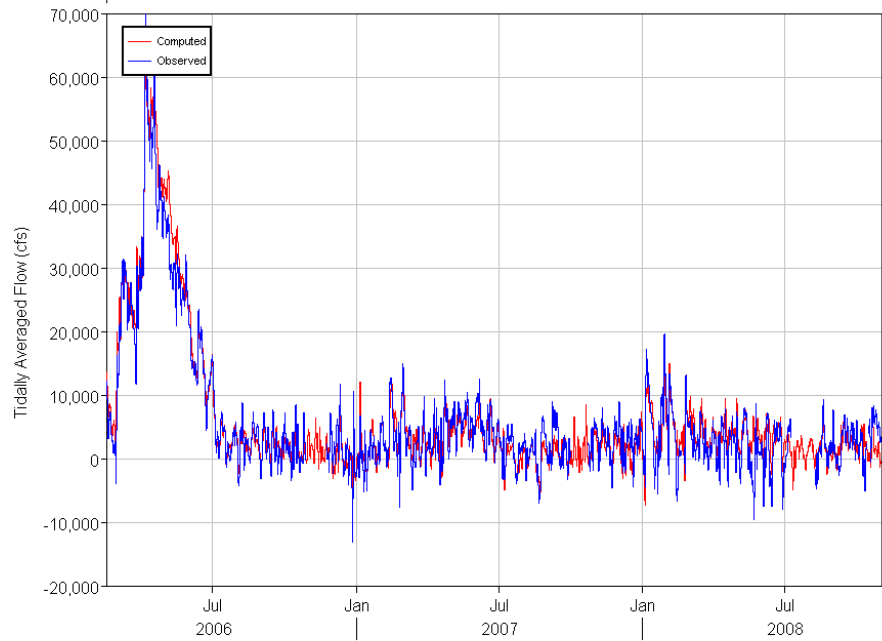
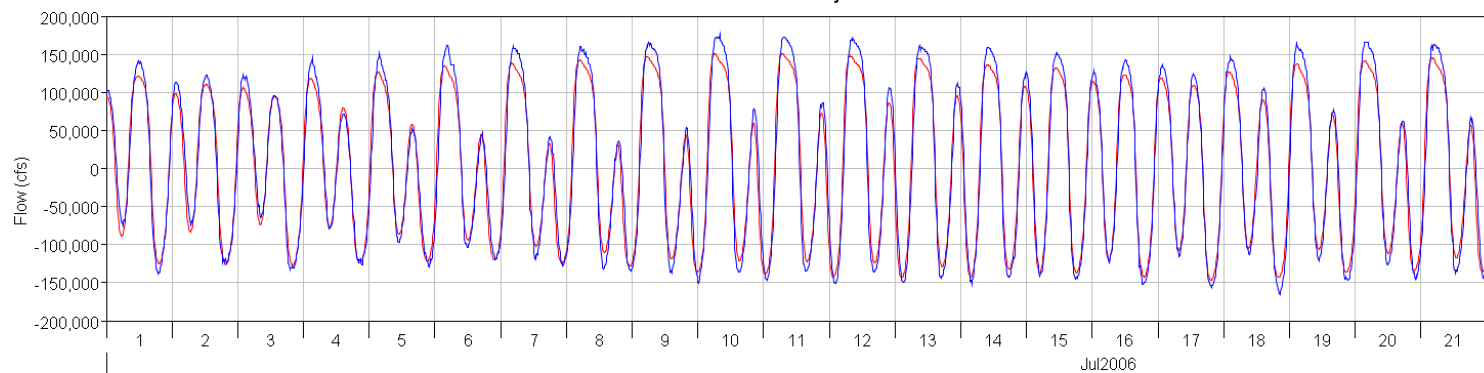
SSS - Steamboat Slough



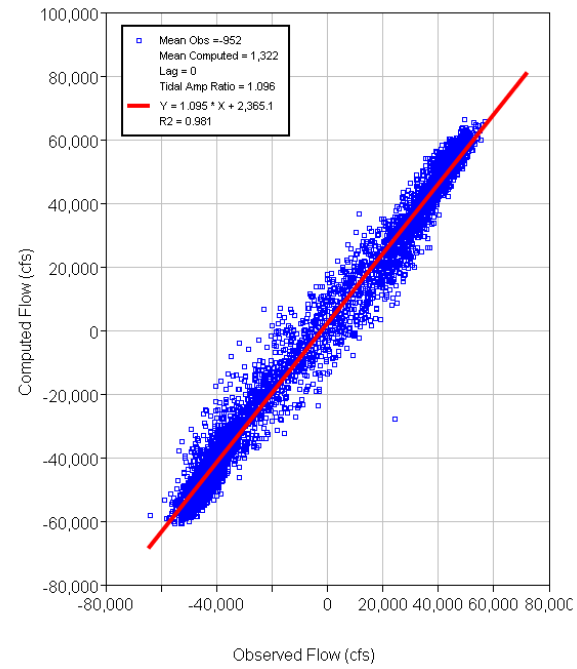
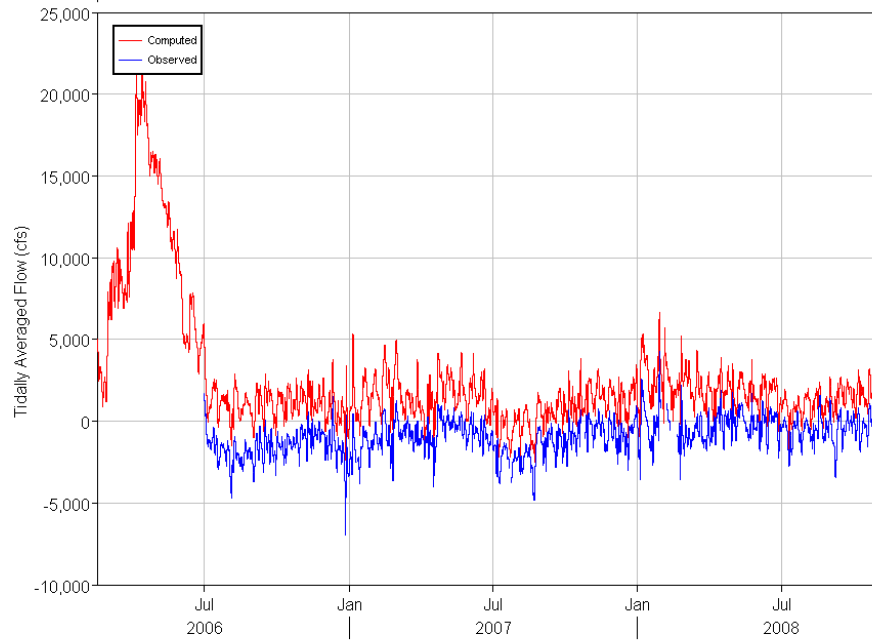
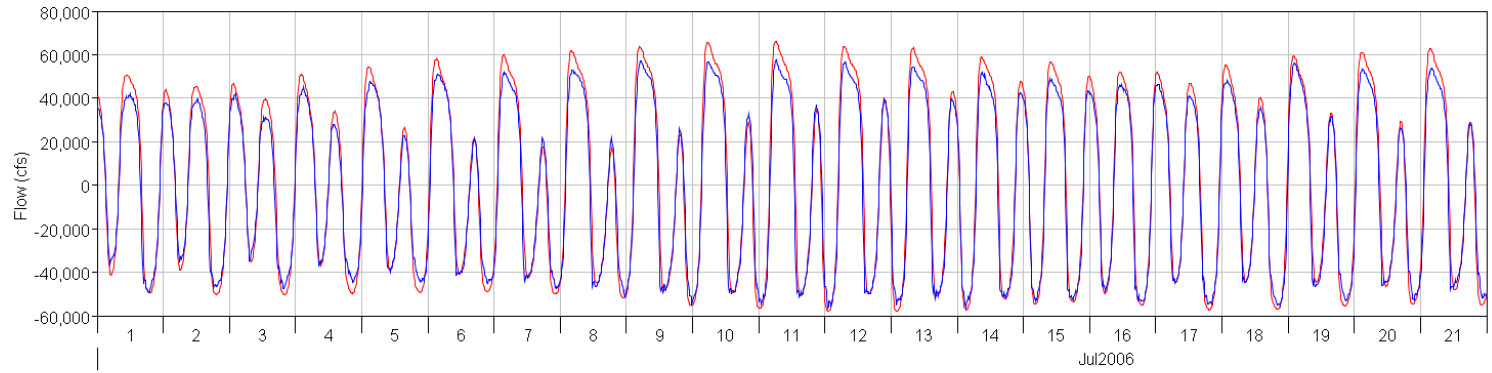
HWB - Miner Slough



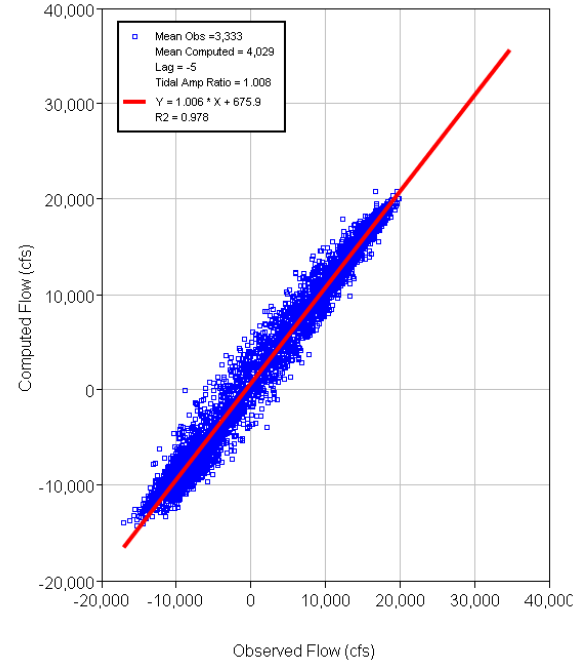
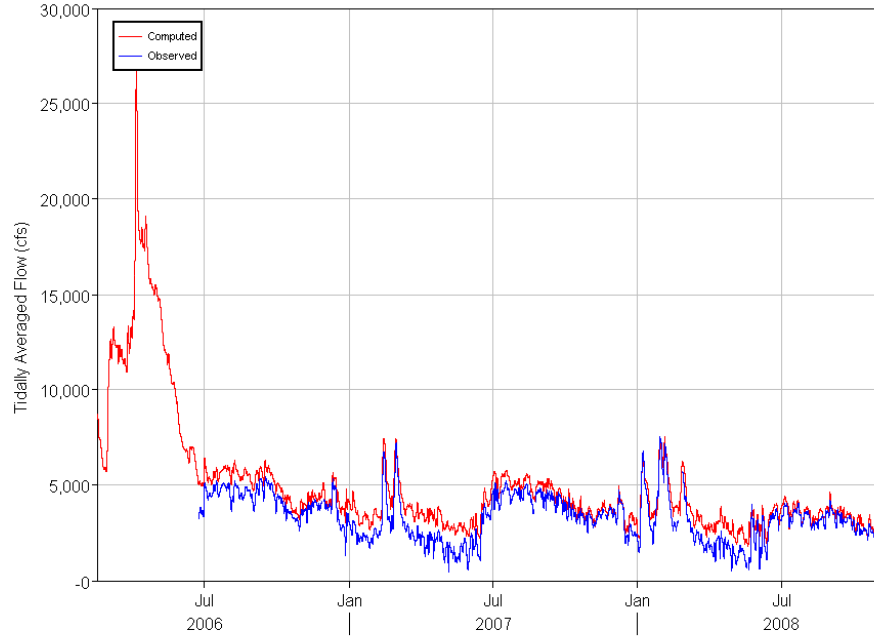
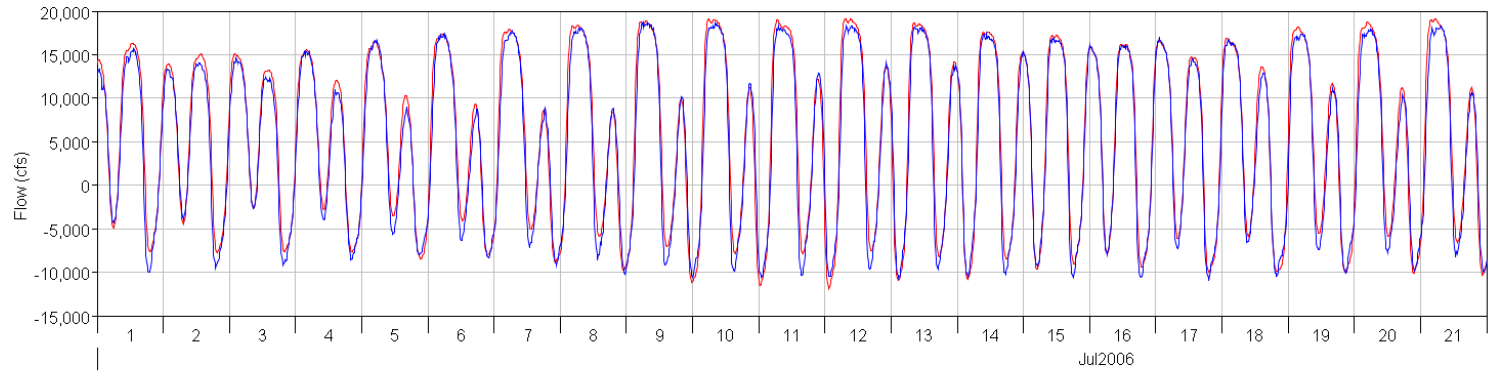
SJJ - SJR at Jersey Pt



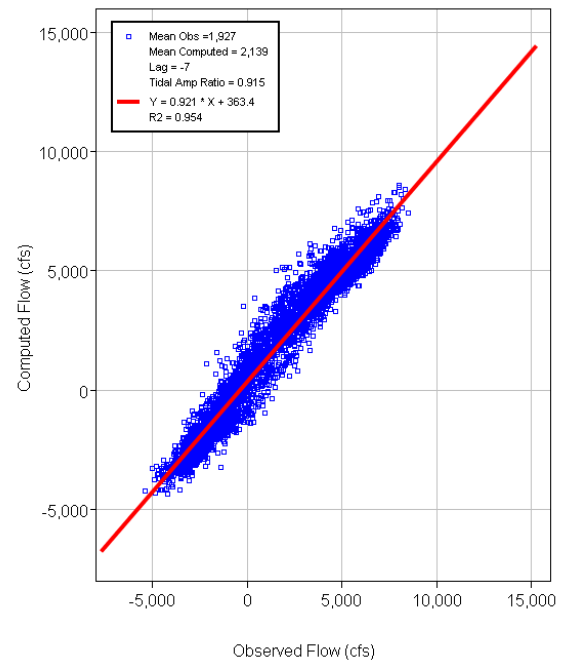
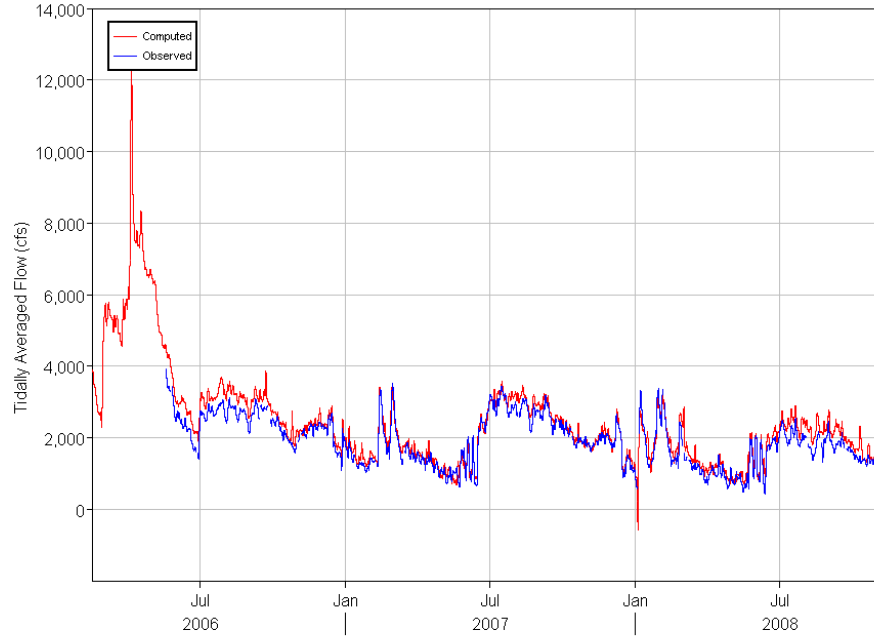
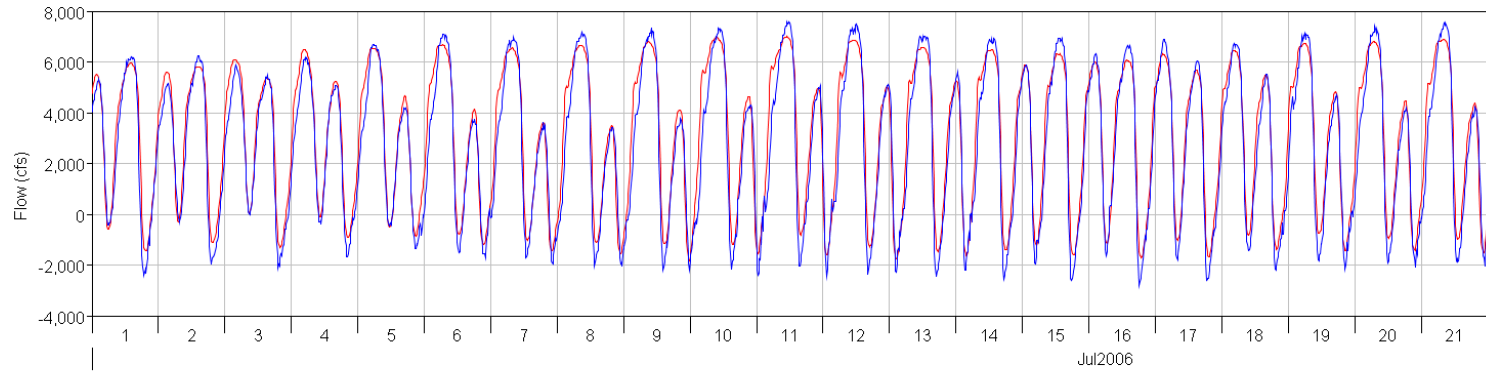
FAL - False River



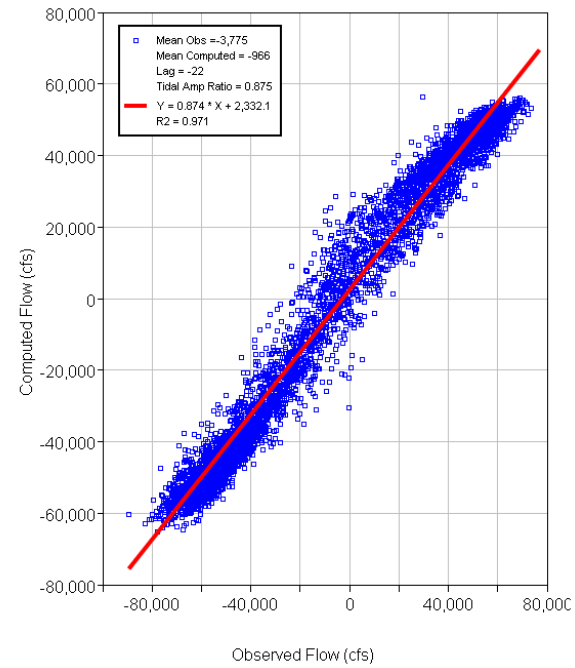
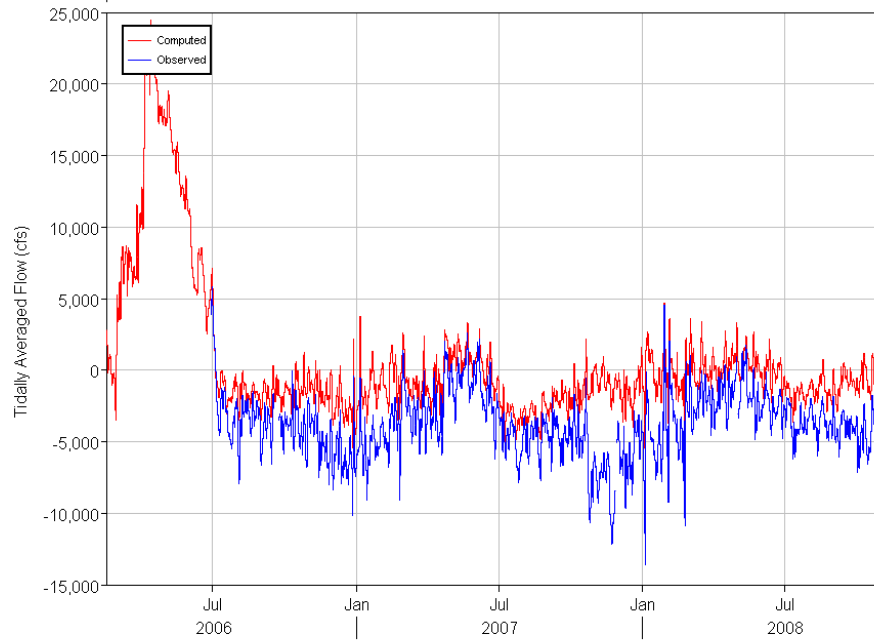
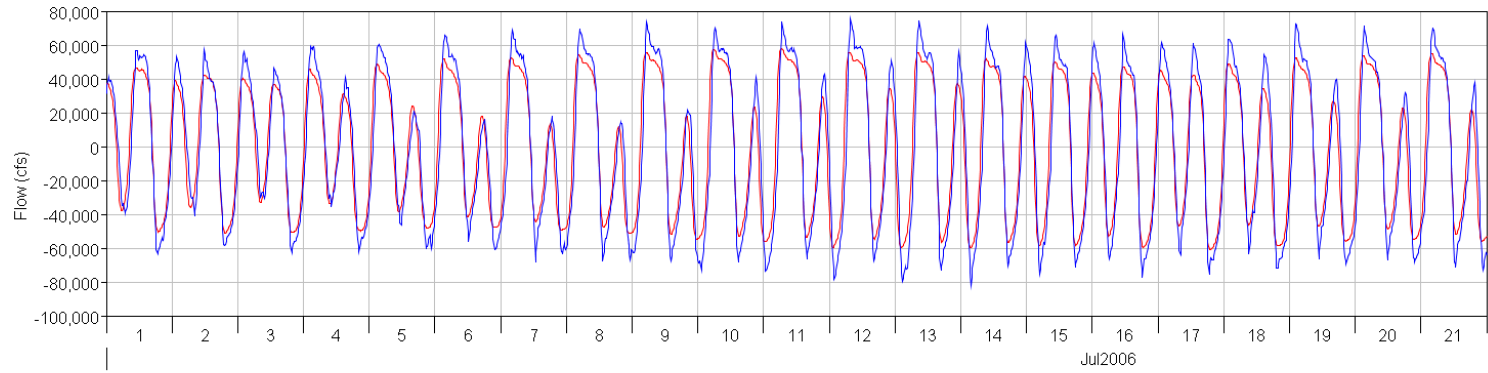
MOK - Mokelumne R at SJR



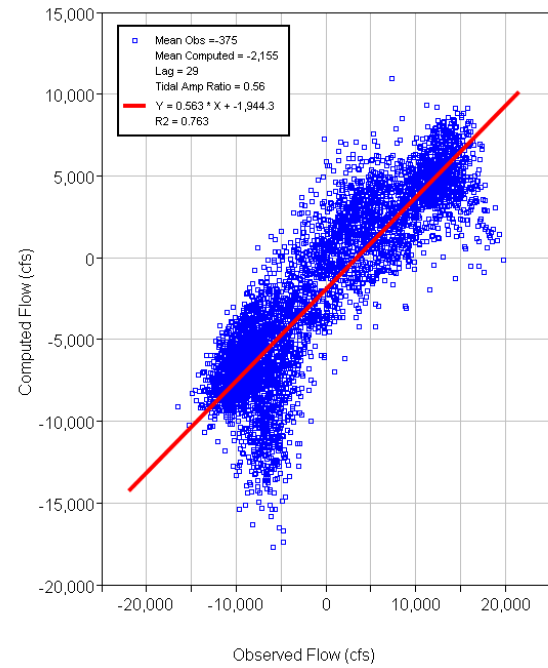
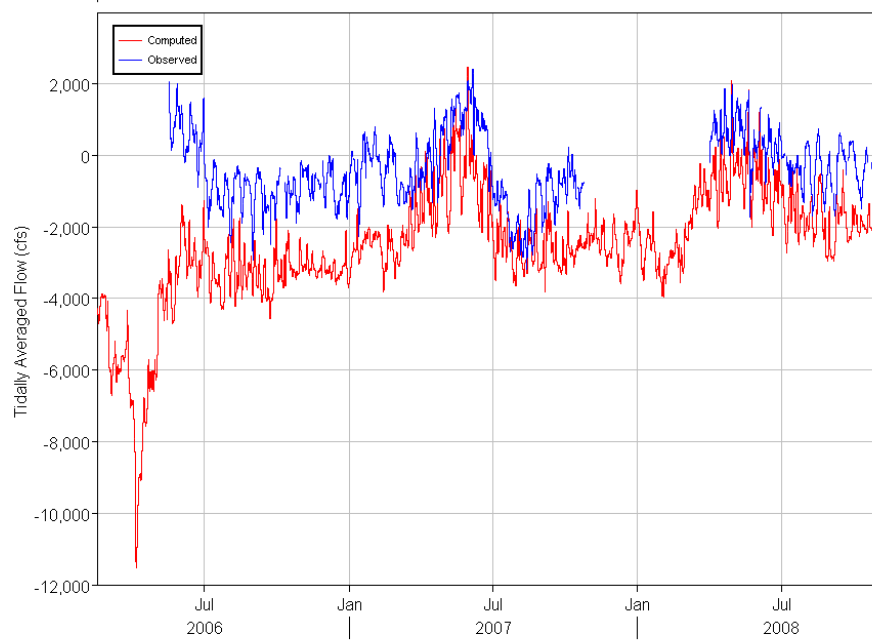
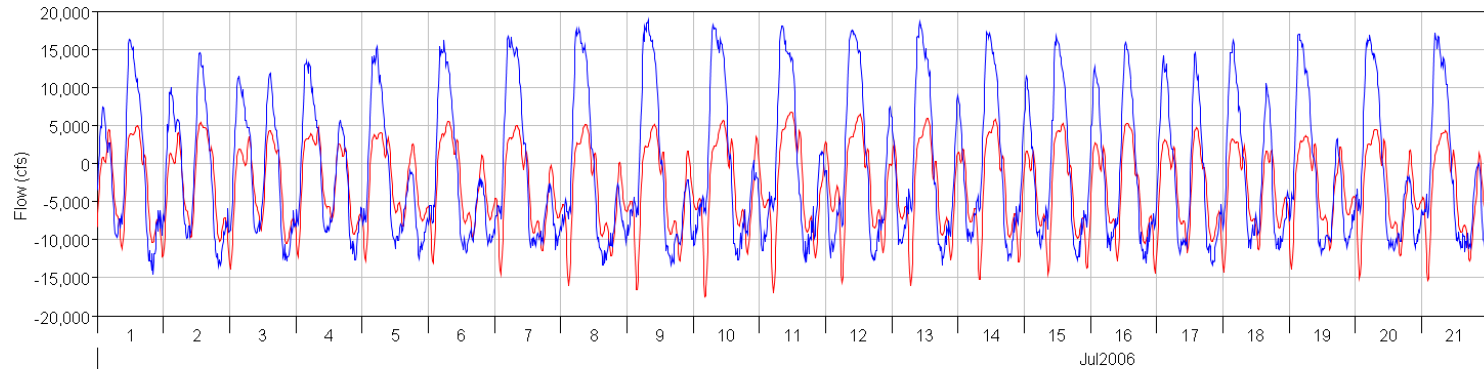
LPS - Little Potato Slough



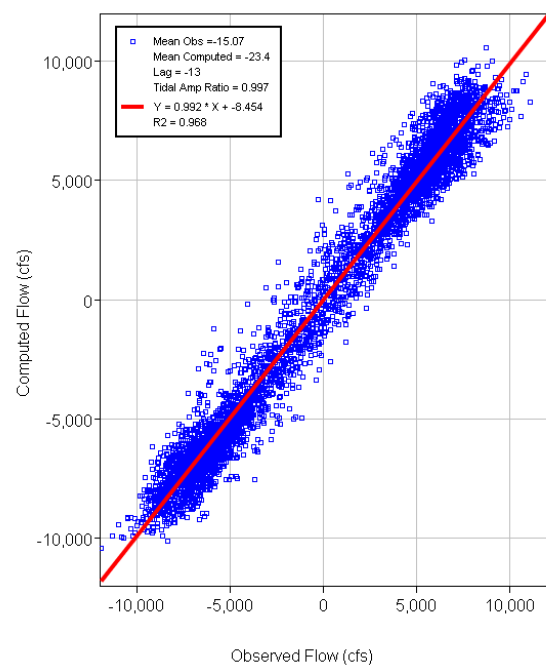
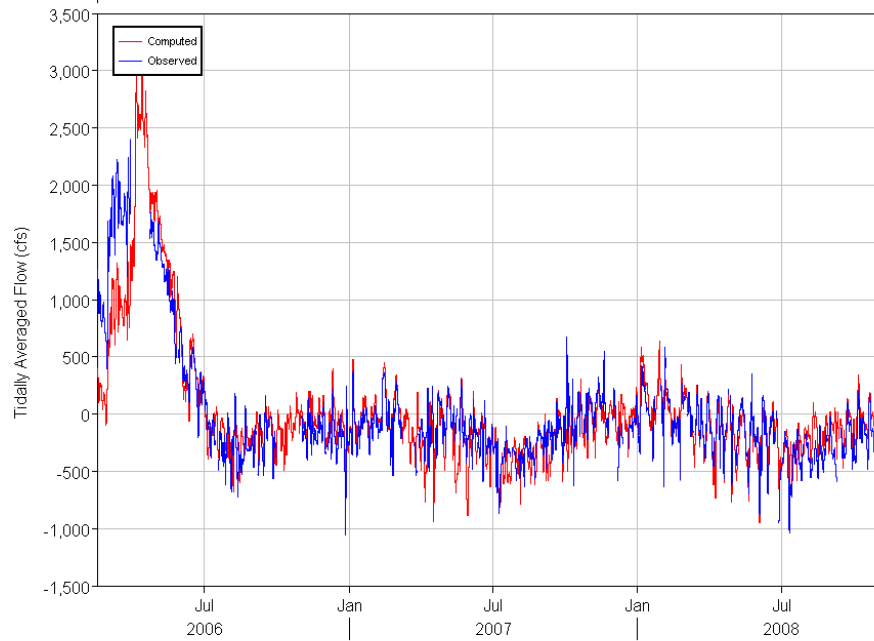
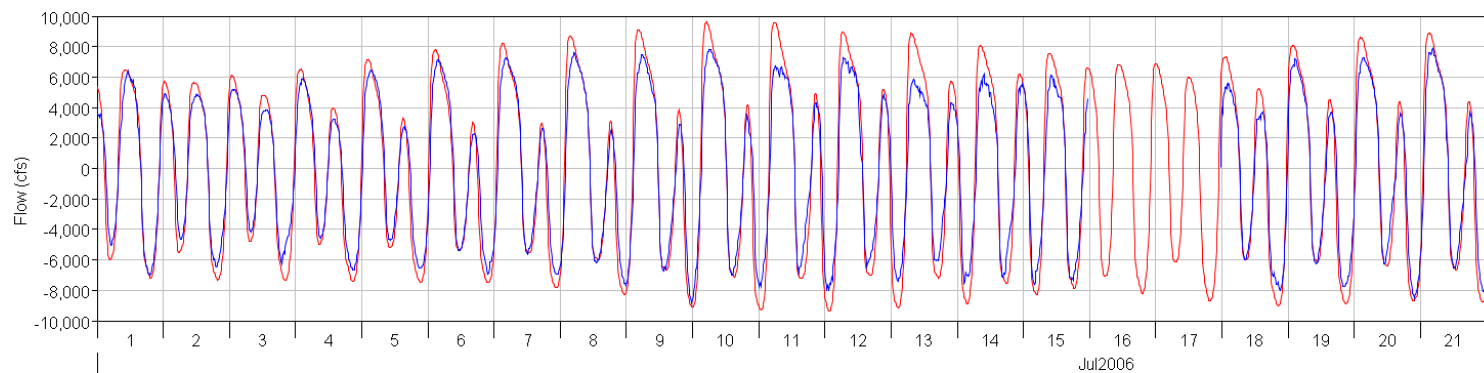
PRI - SJR at Prisoners Pt



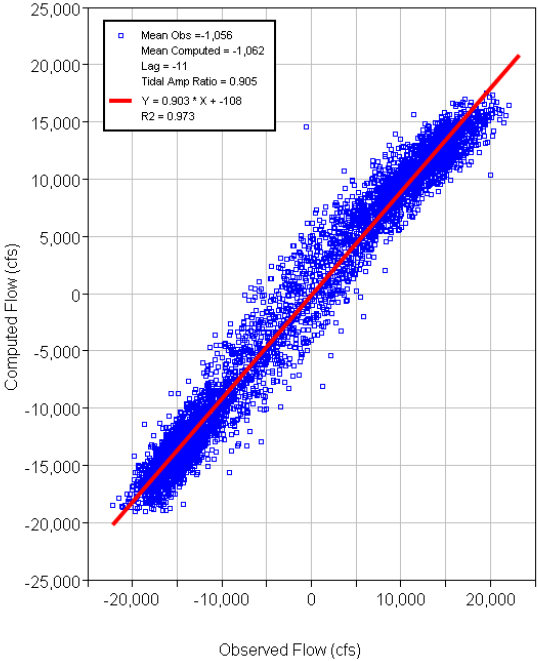
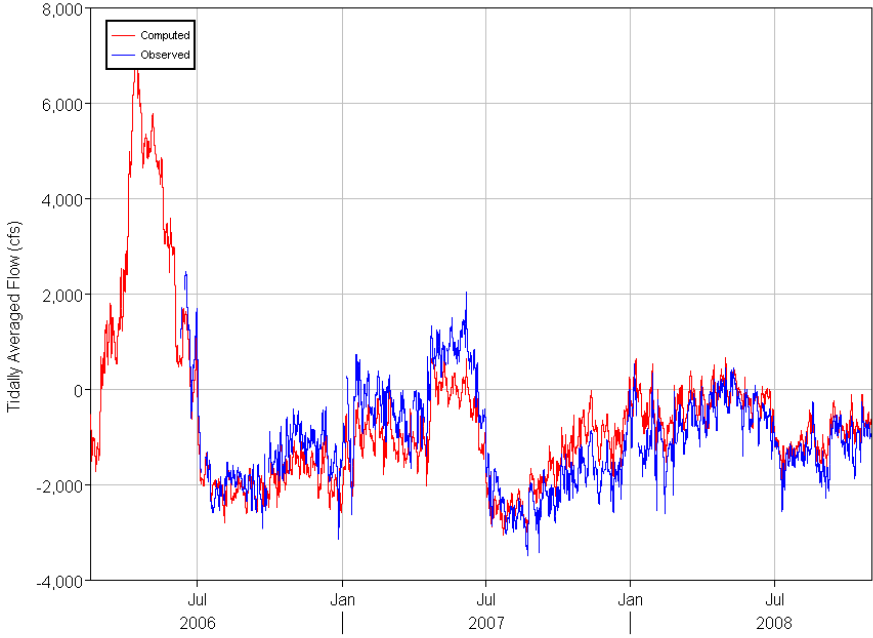
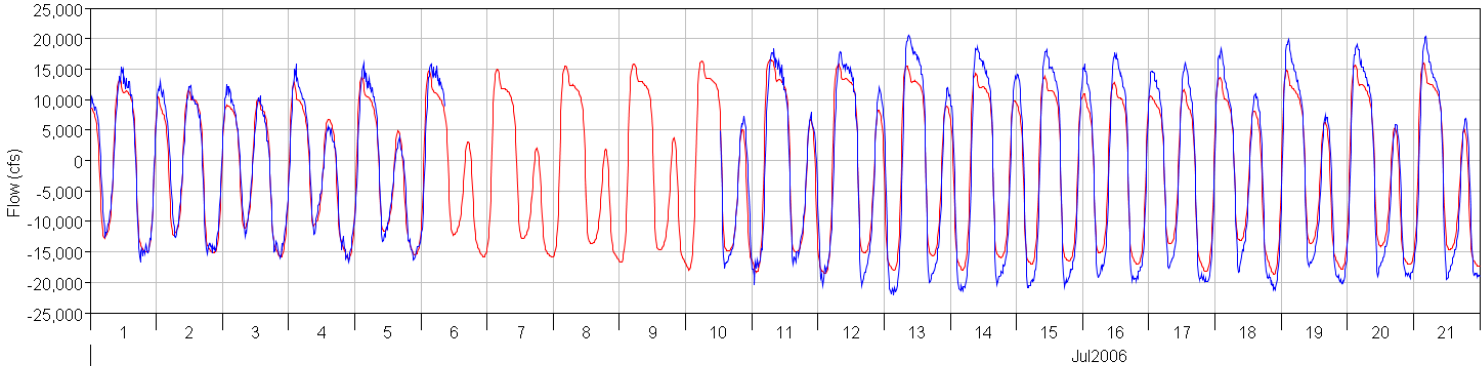
OSJ - Old River at Franks Tract



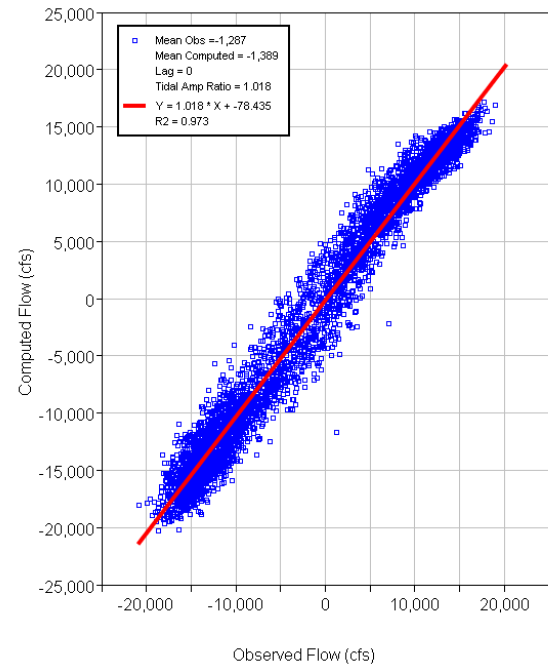
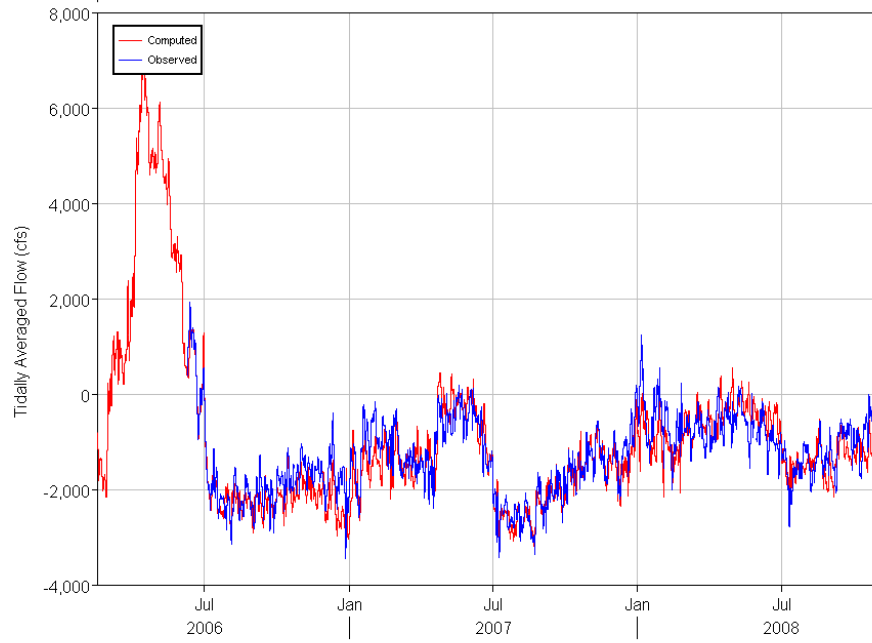
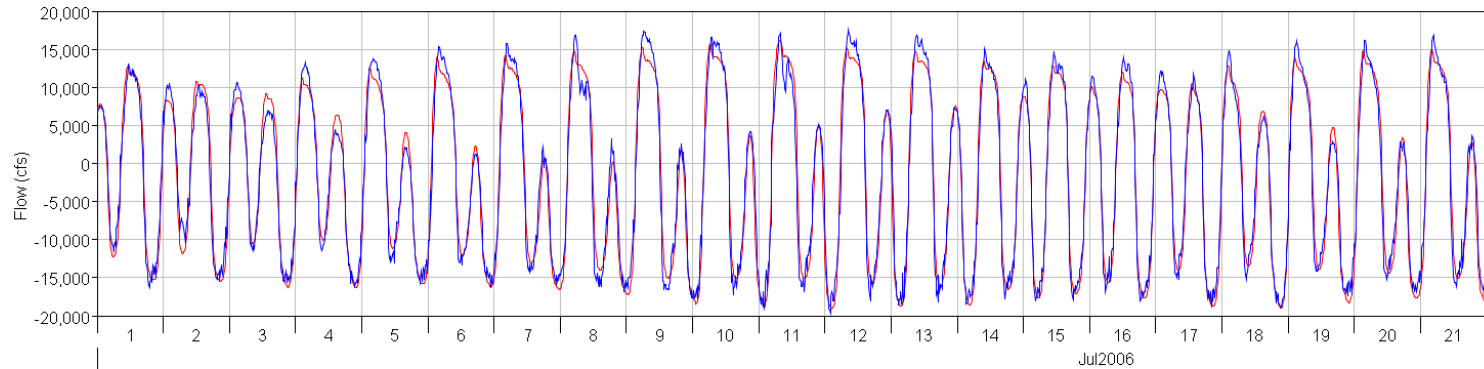
DSJ - Dutch SI



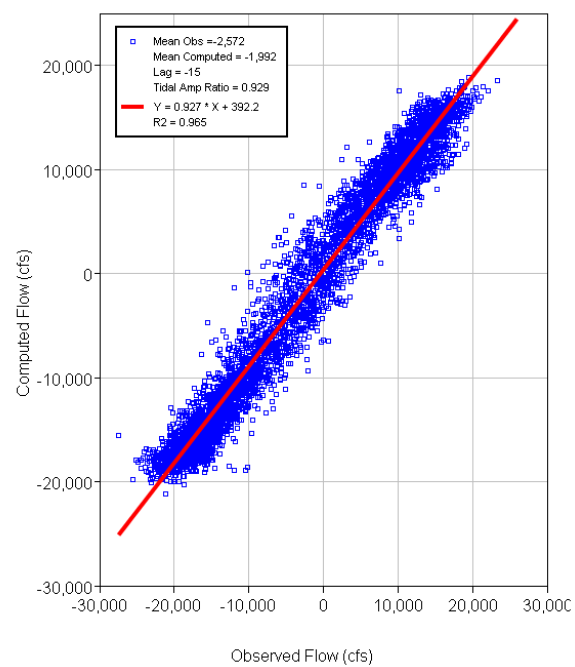
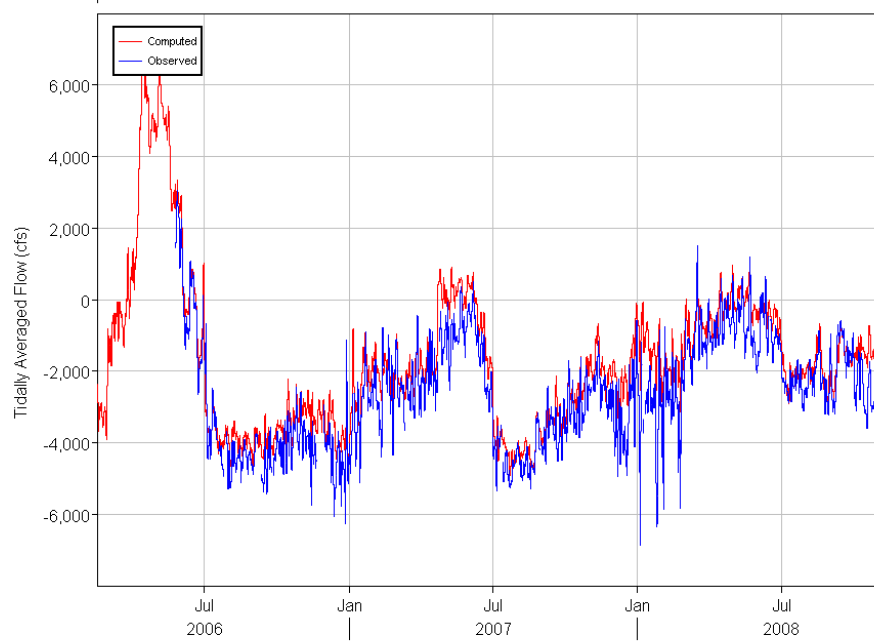
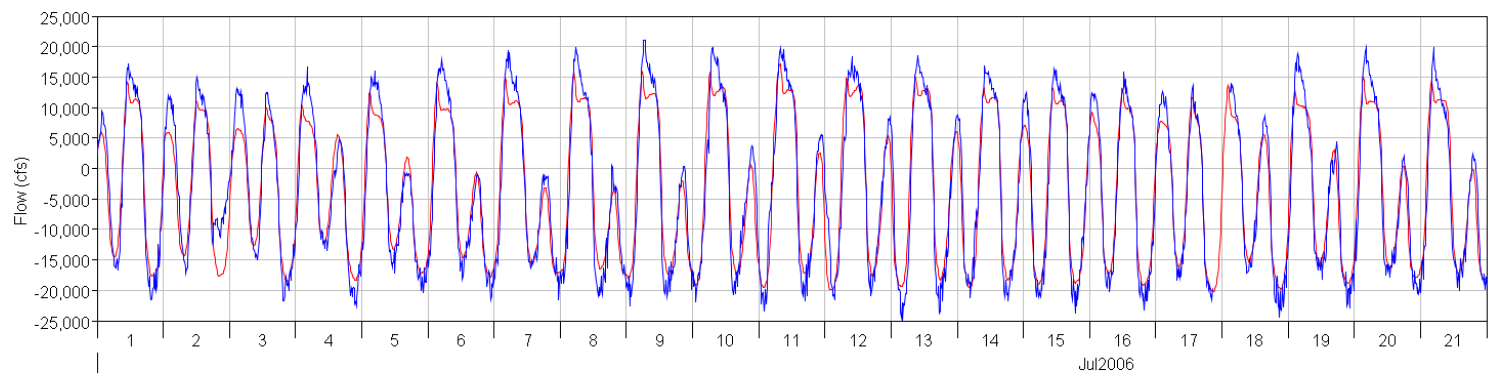
HOL - Holland Cut



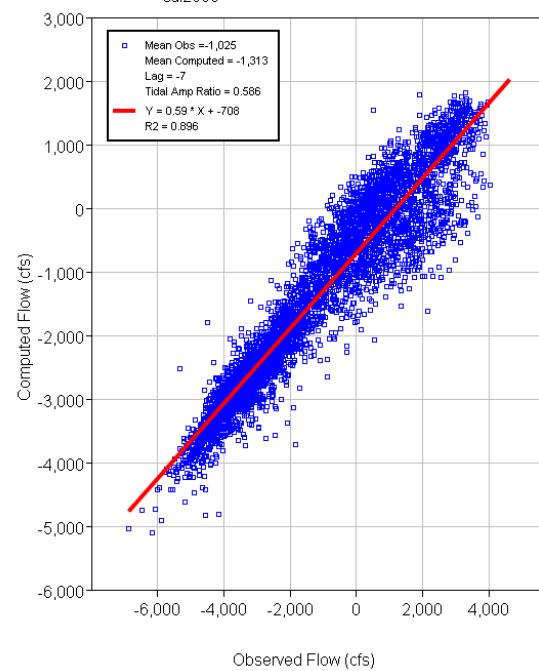
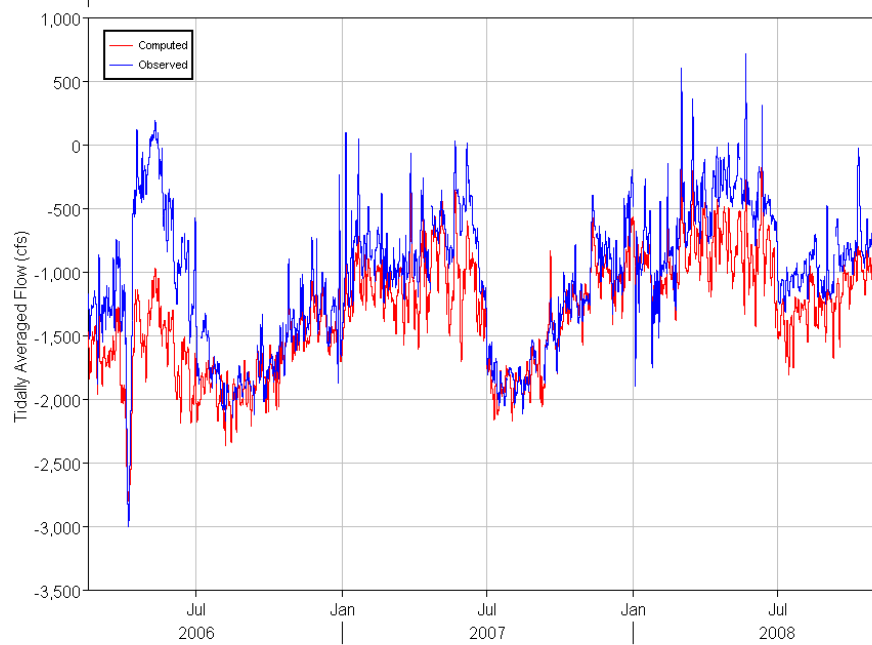
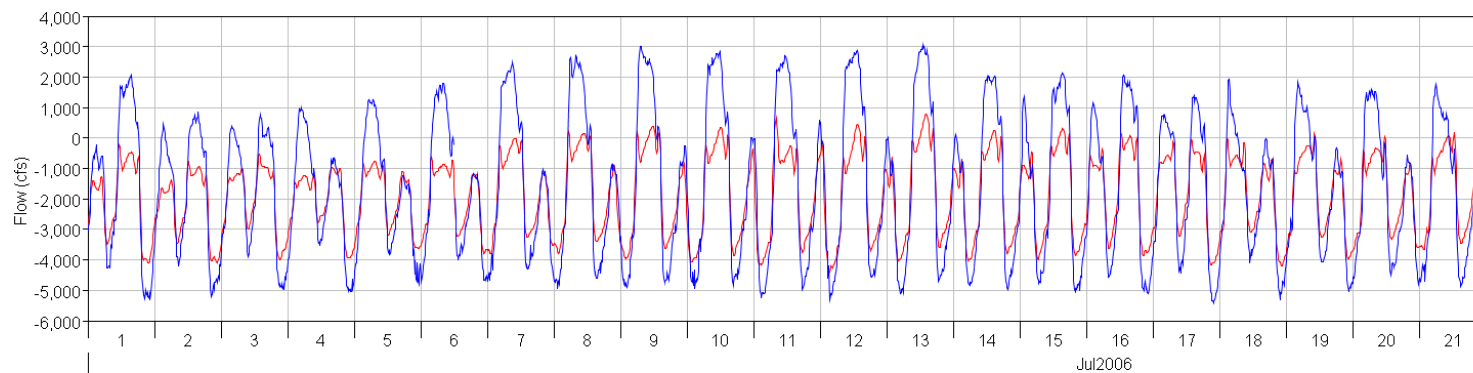
ORQ - Old River at Quimby



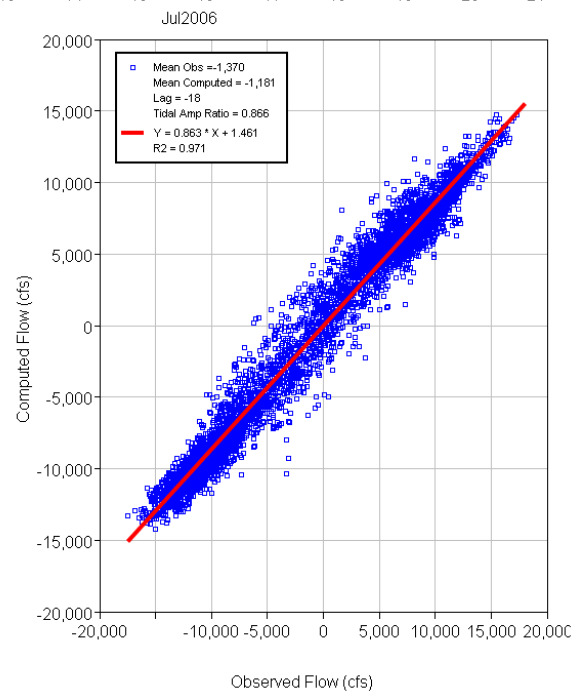
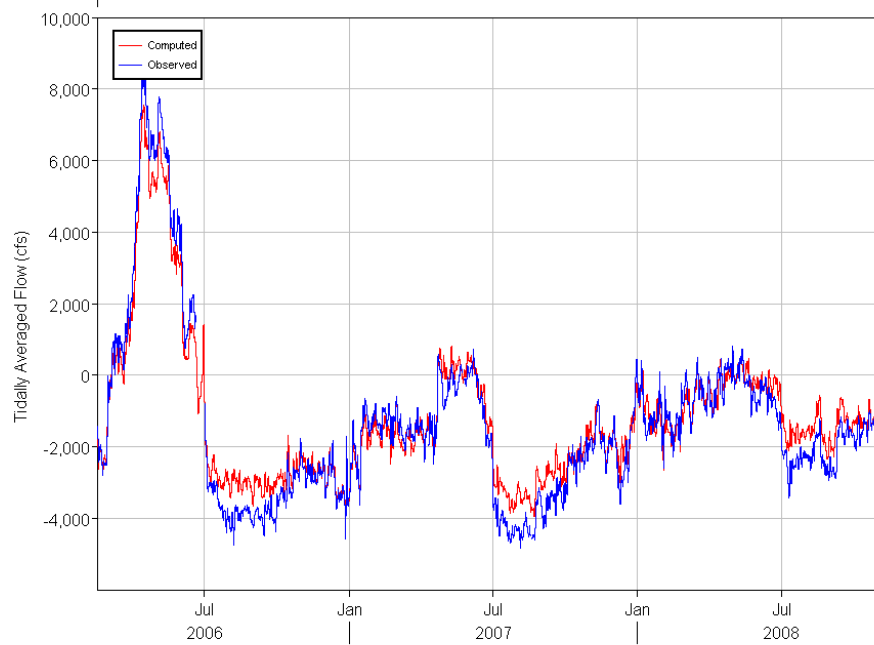
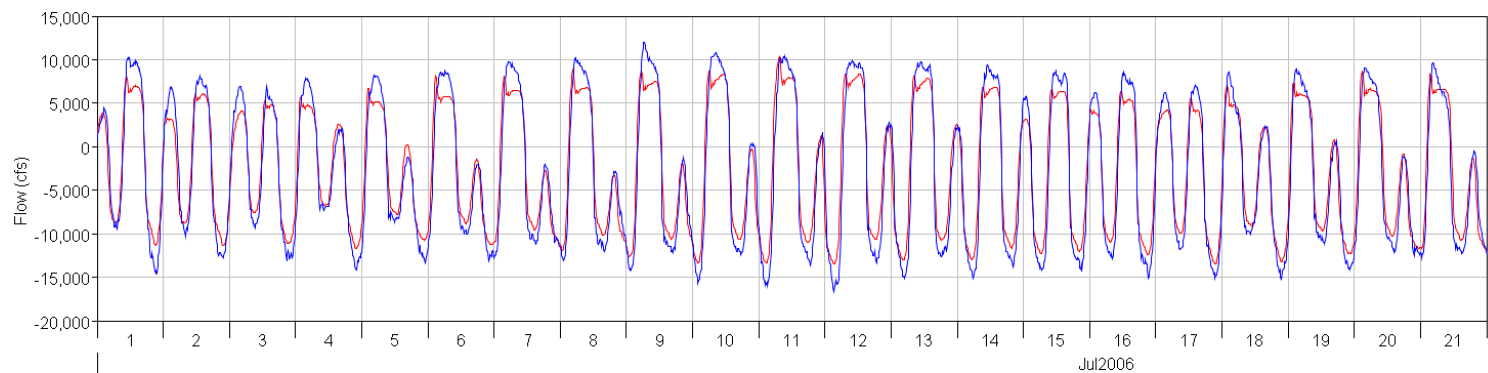
HLT - Middle River at Holt



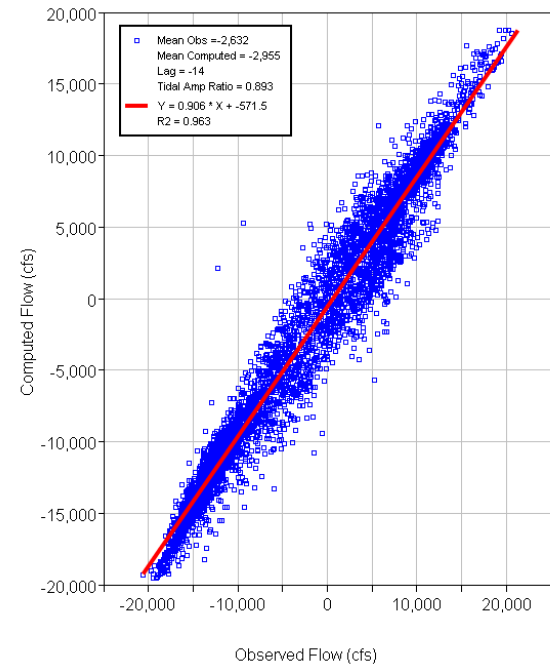
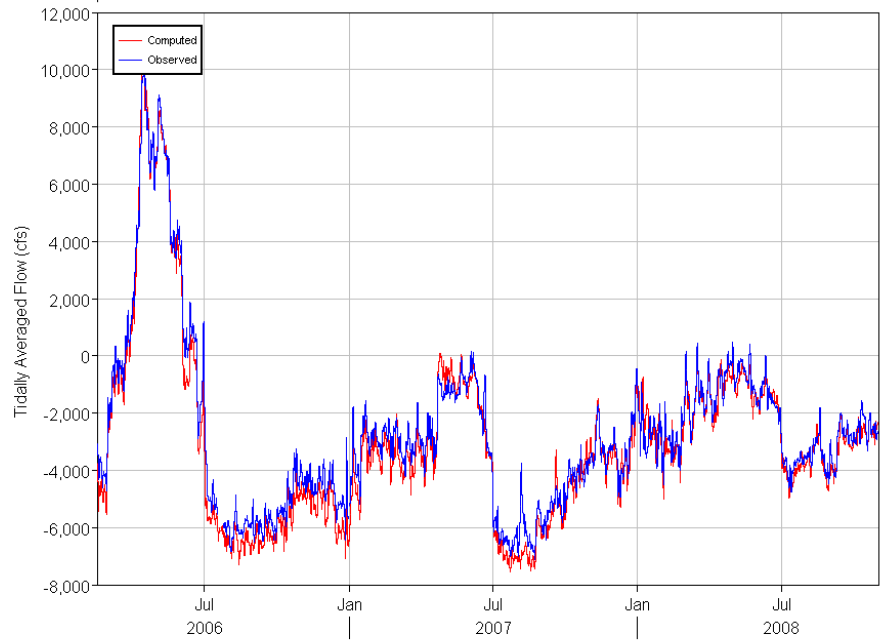
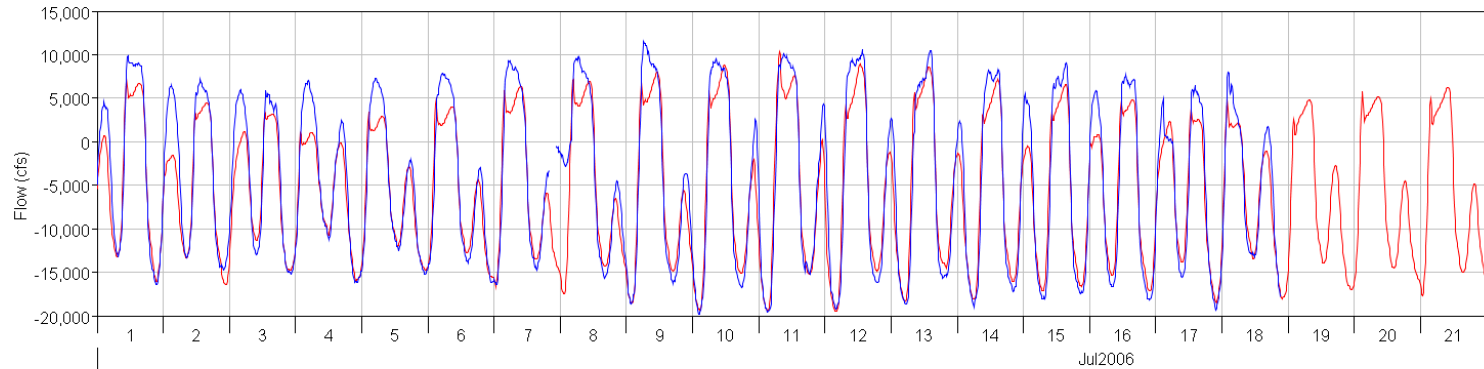
TRN - Turner Cut at Holt



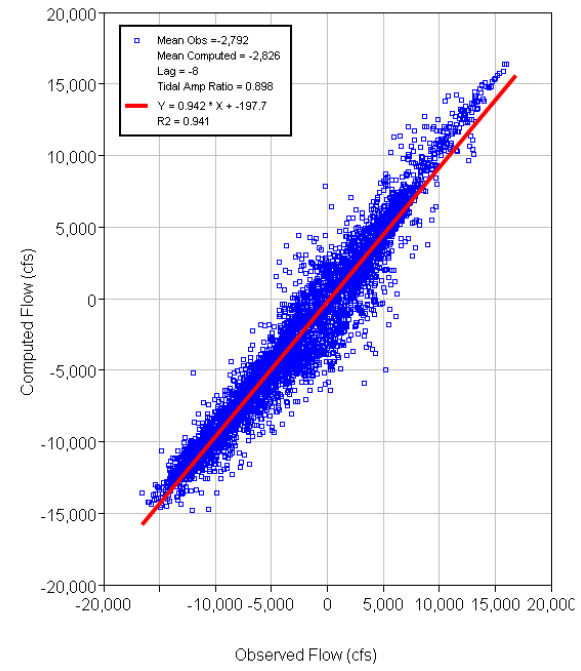
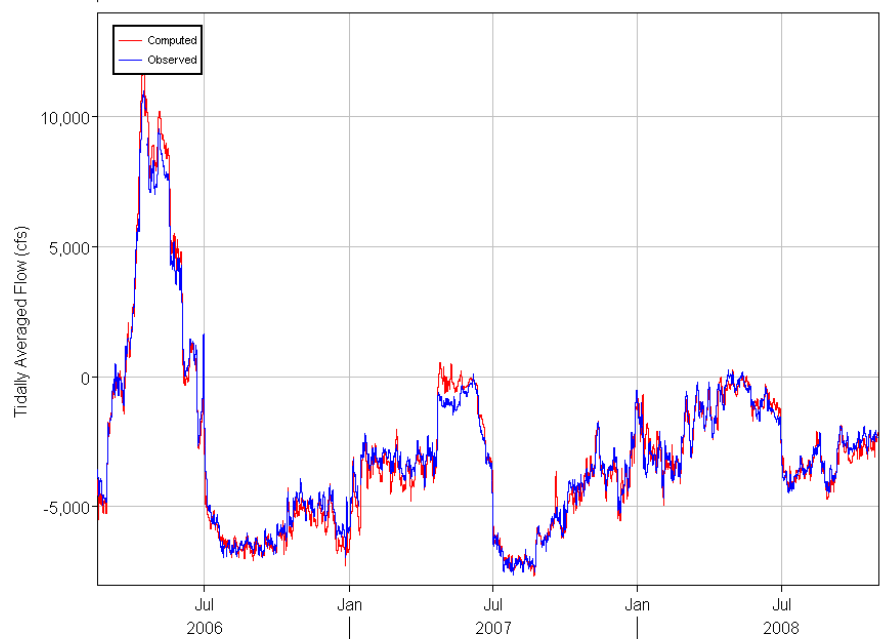
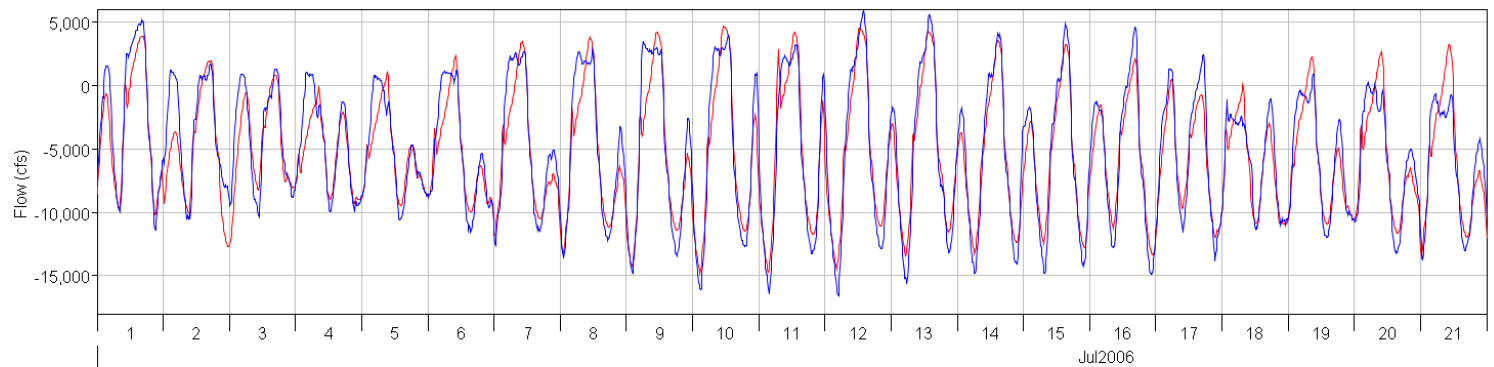
OBI - Old River at Bacon



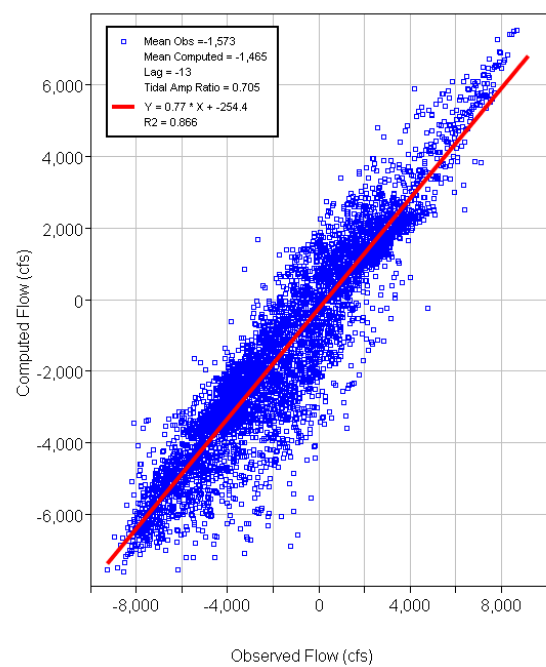
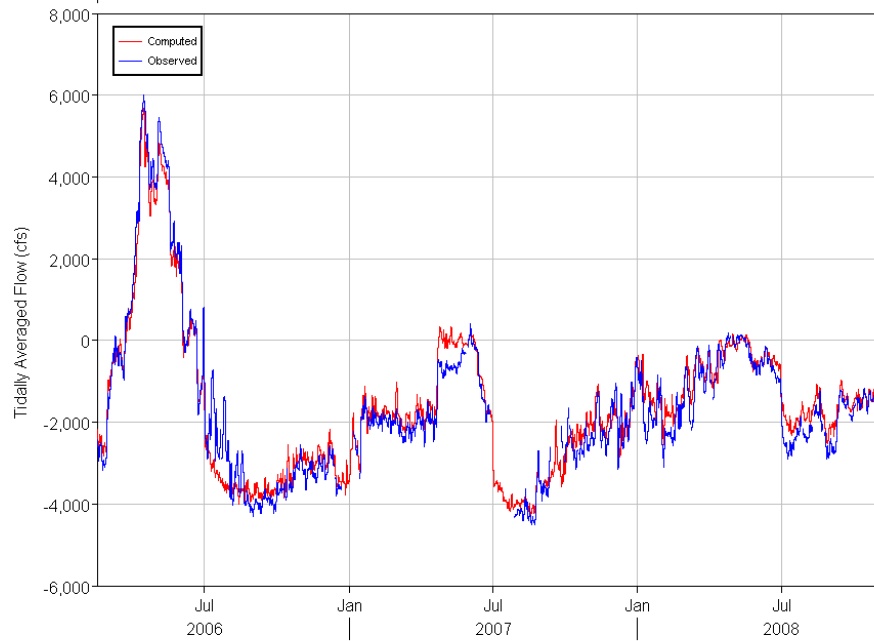
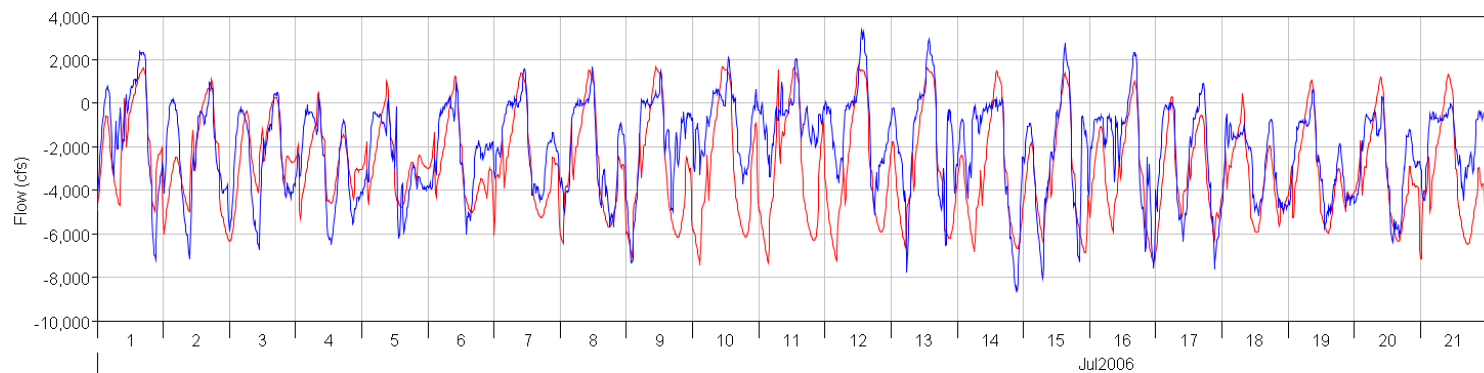
MDM - Middle River at Middle



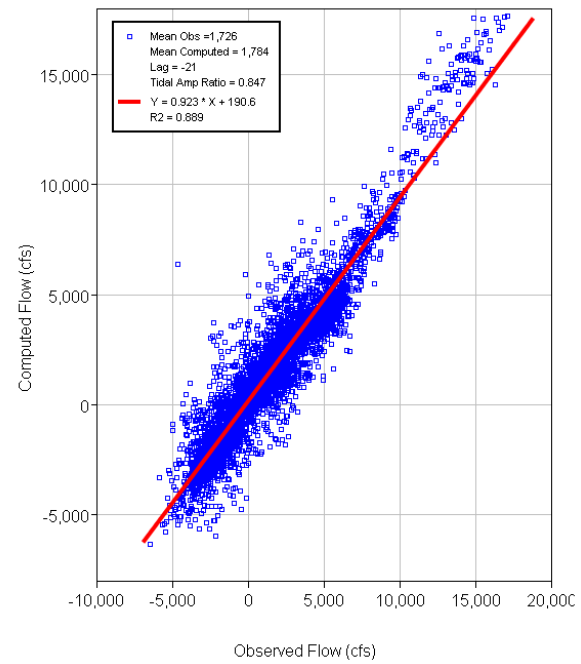
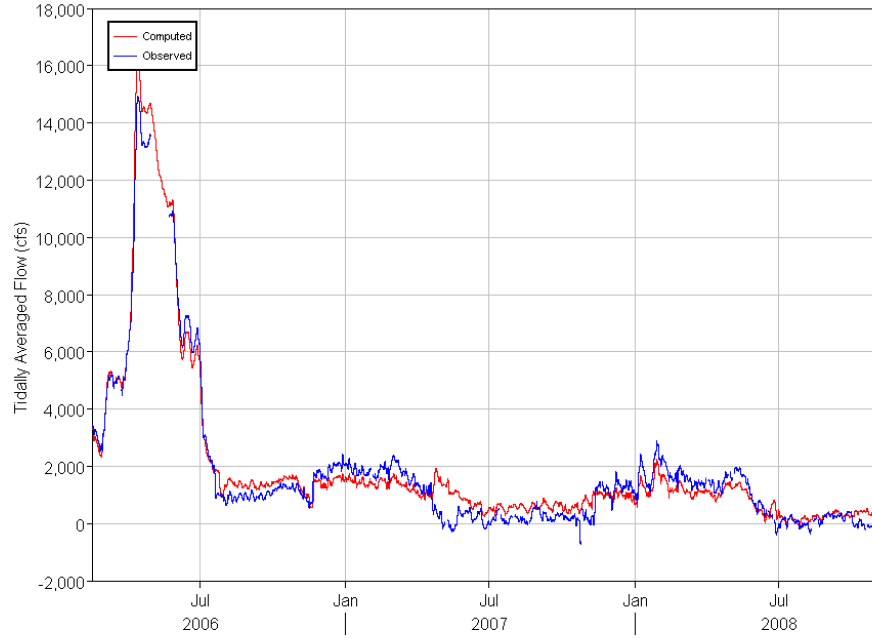
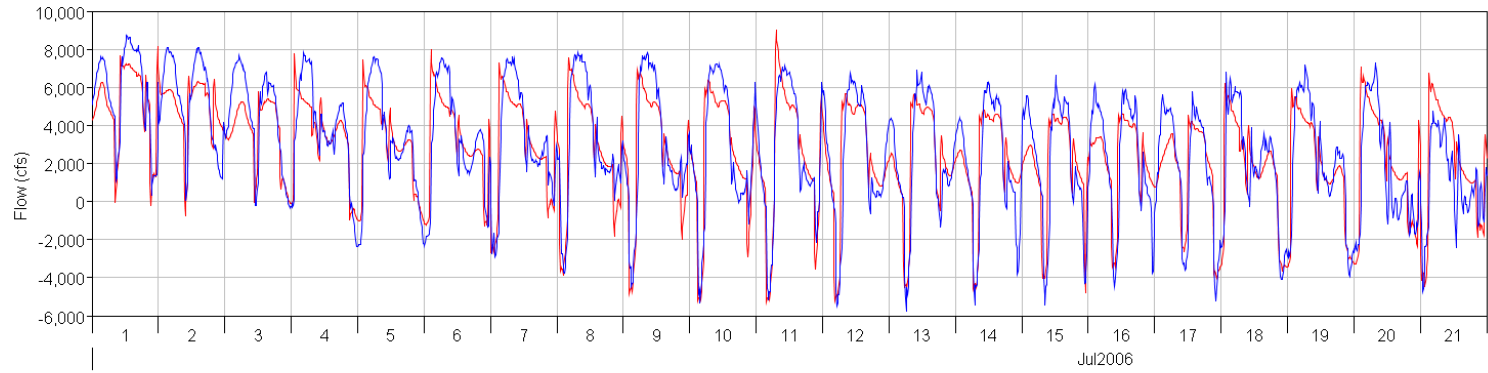
OH4 - Old River at Hwy4



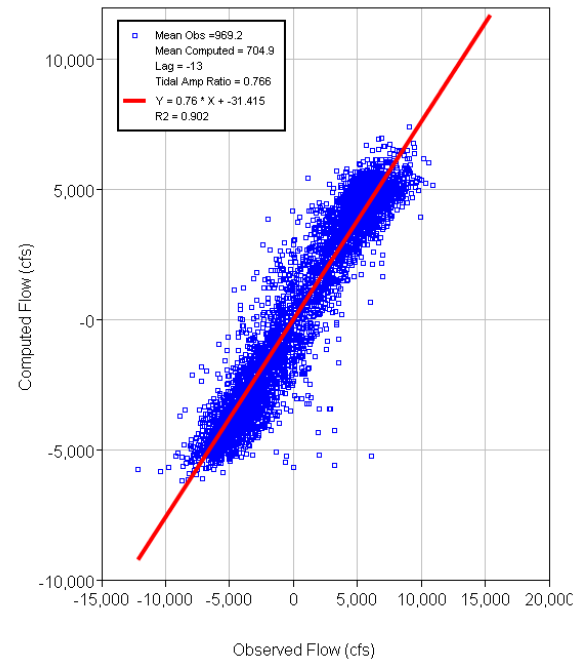
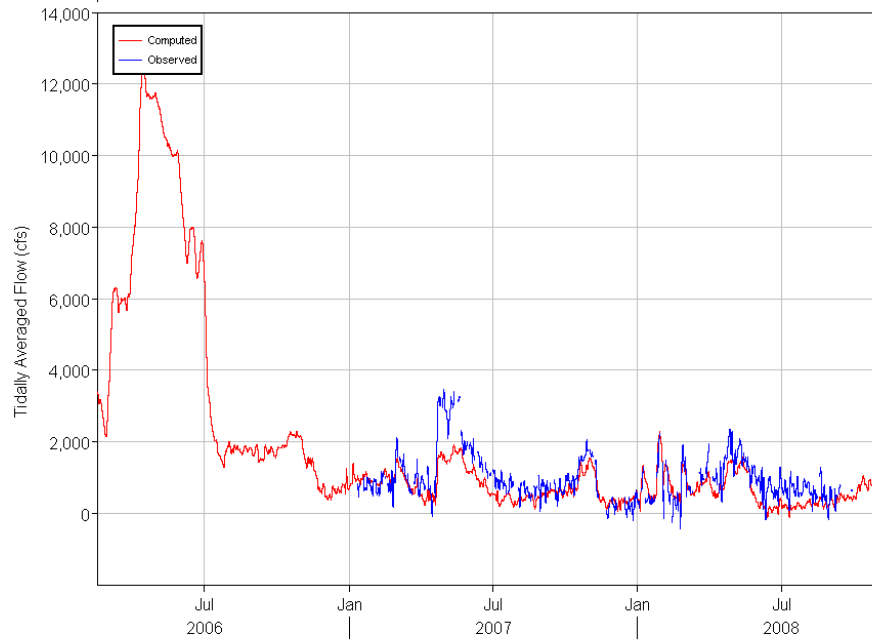
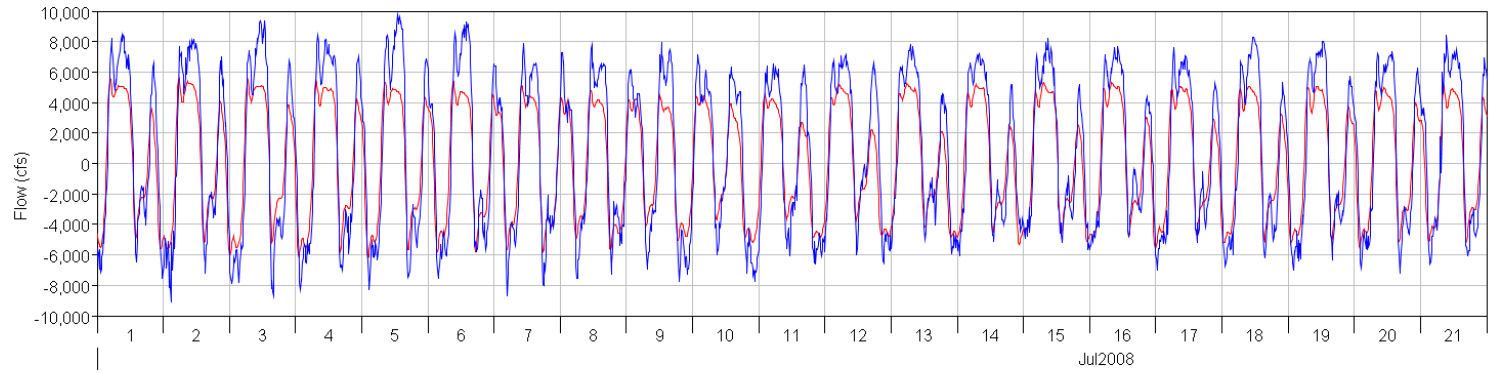
VCU - Victoria Canal



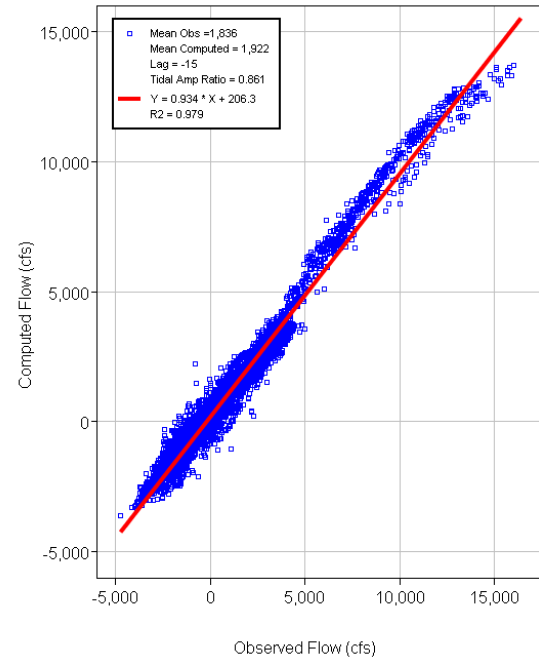
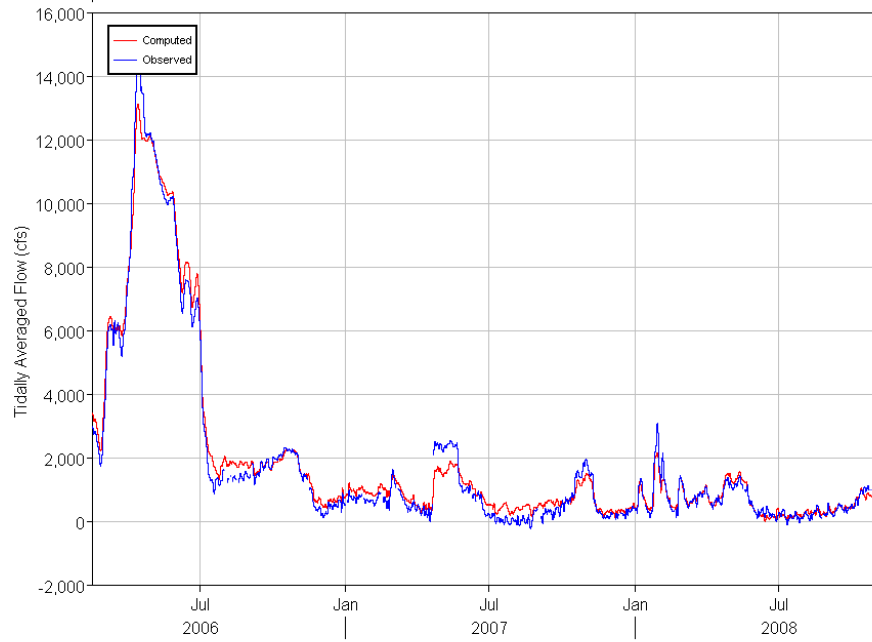
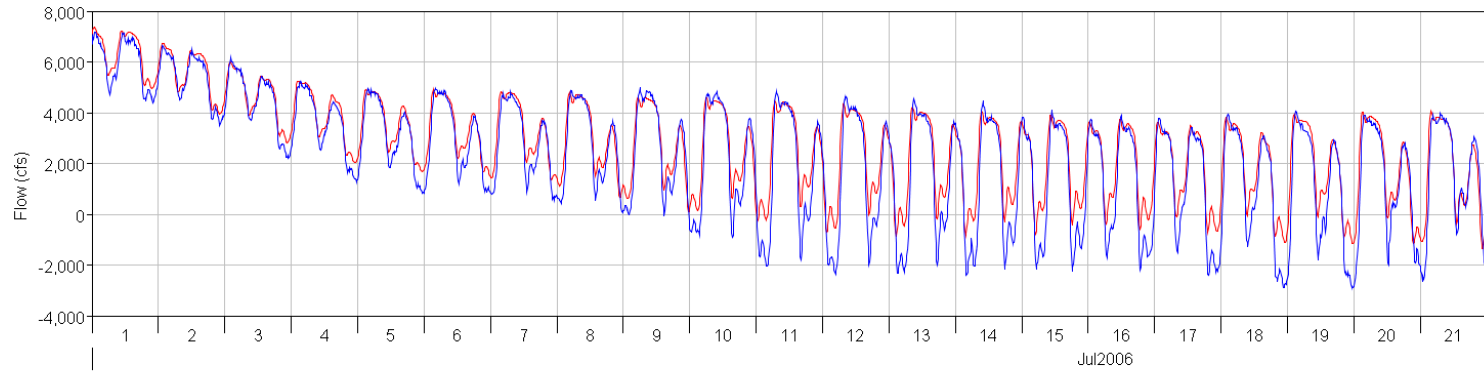
GLC - Grantline Canal near Tracy



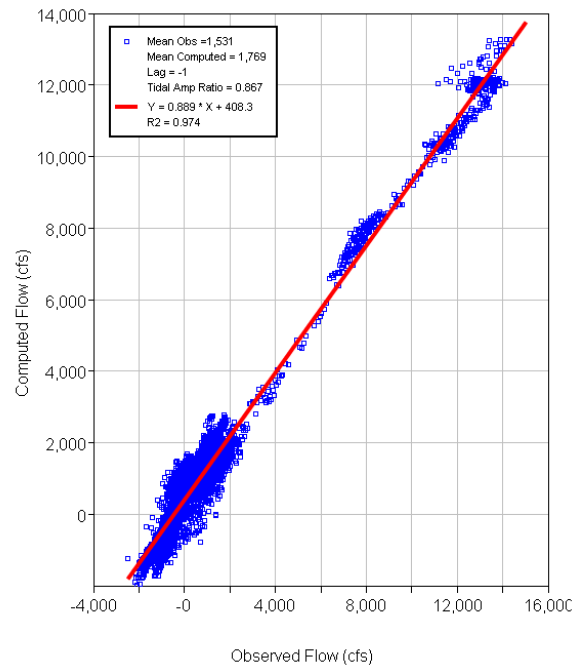
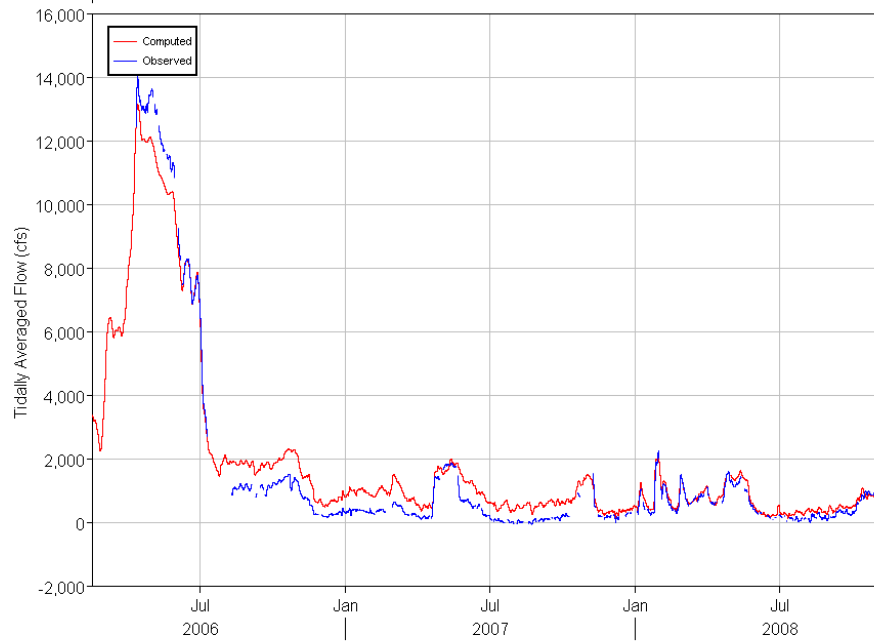
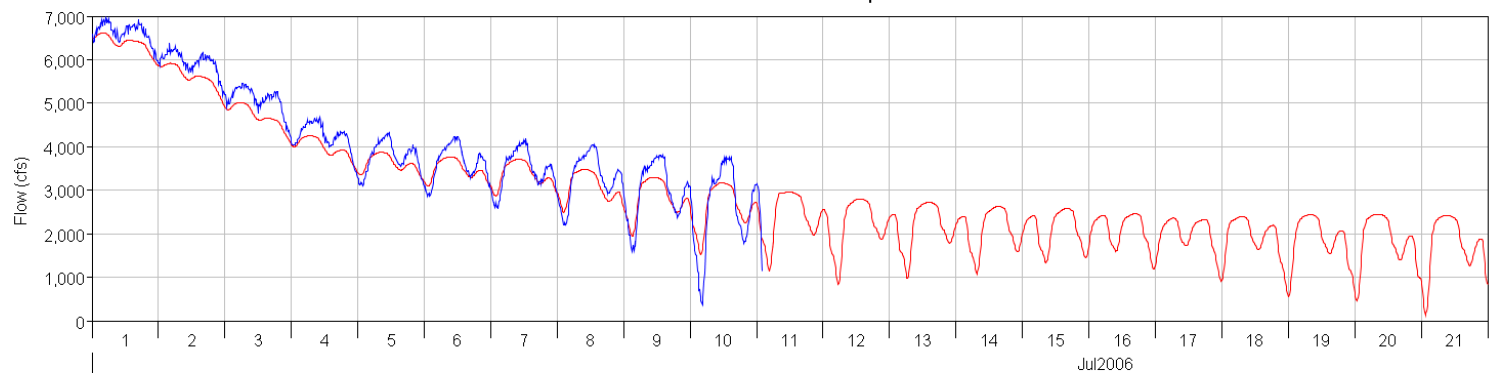
RRI - SJR at Rough-n-Ready



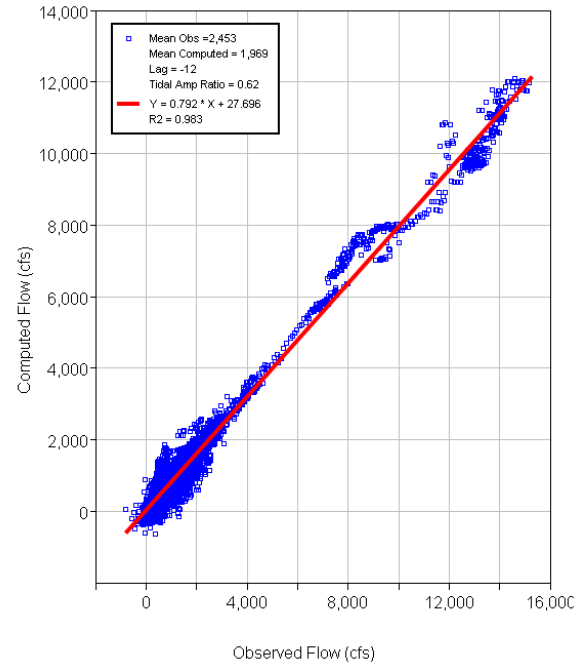
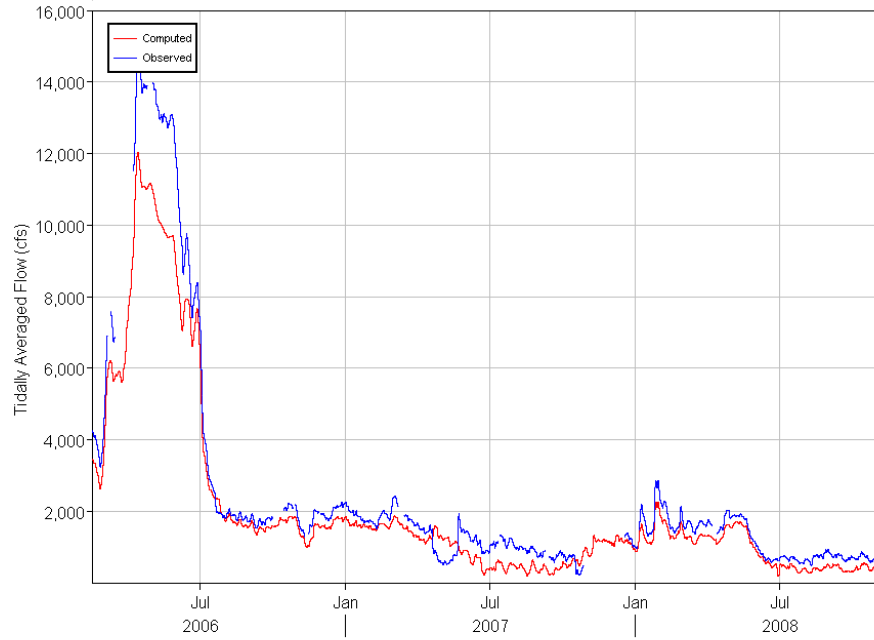
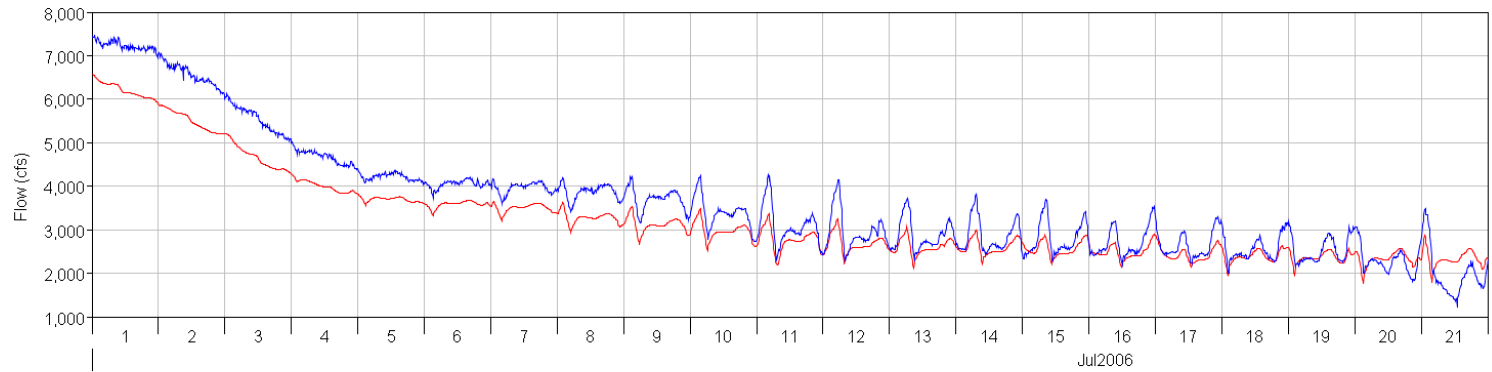
SJG - San Joaquin River at Garwood



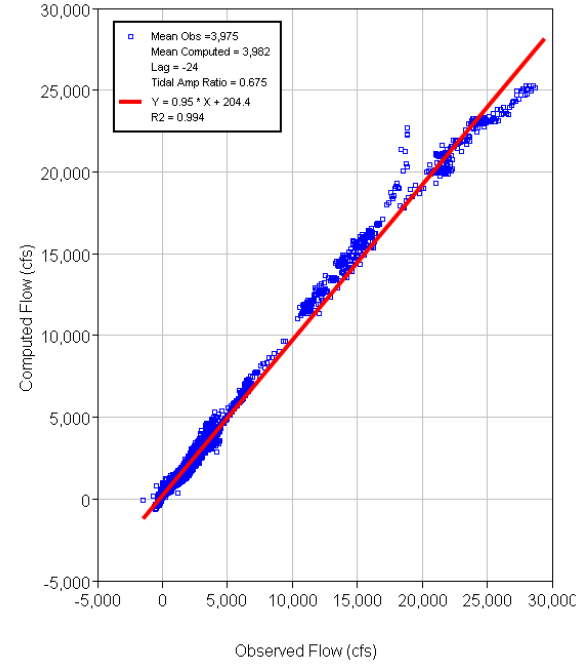
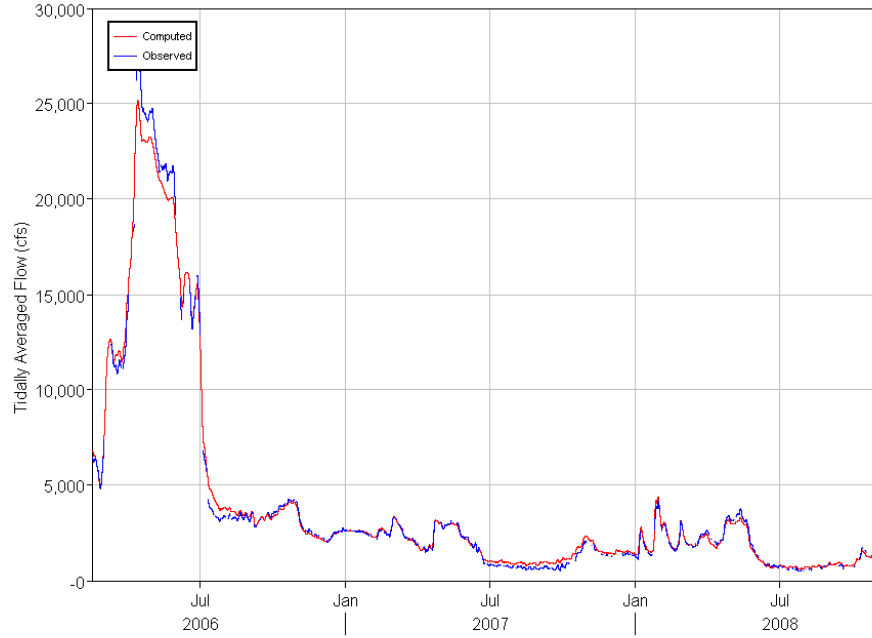
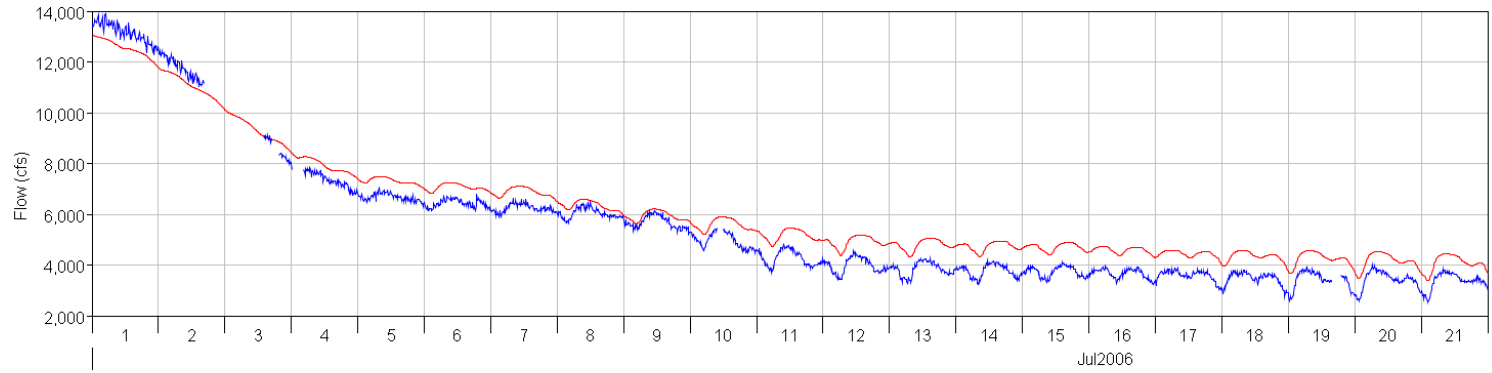
SJL - SJR near Lathrop



OH1 - Old River at Head

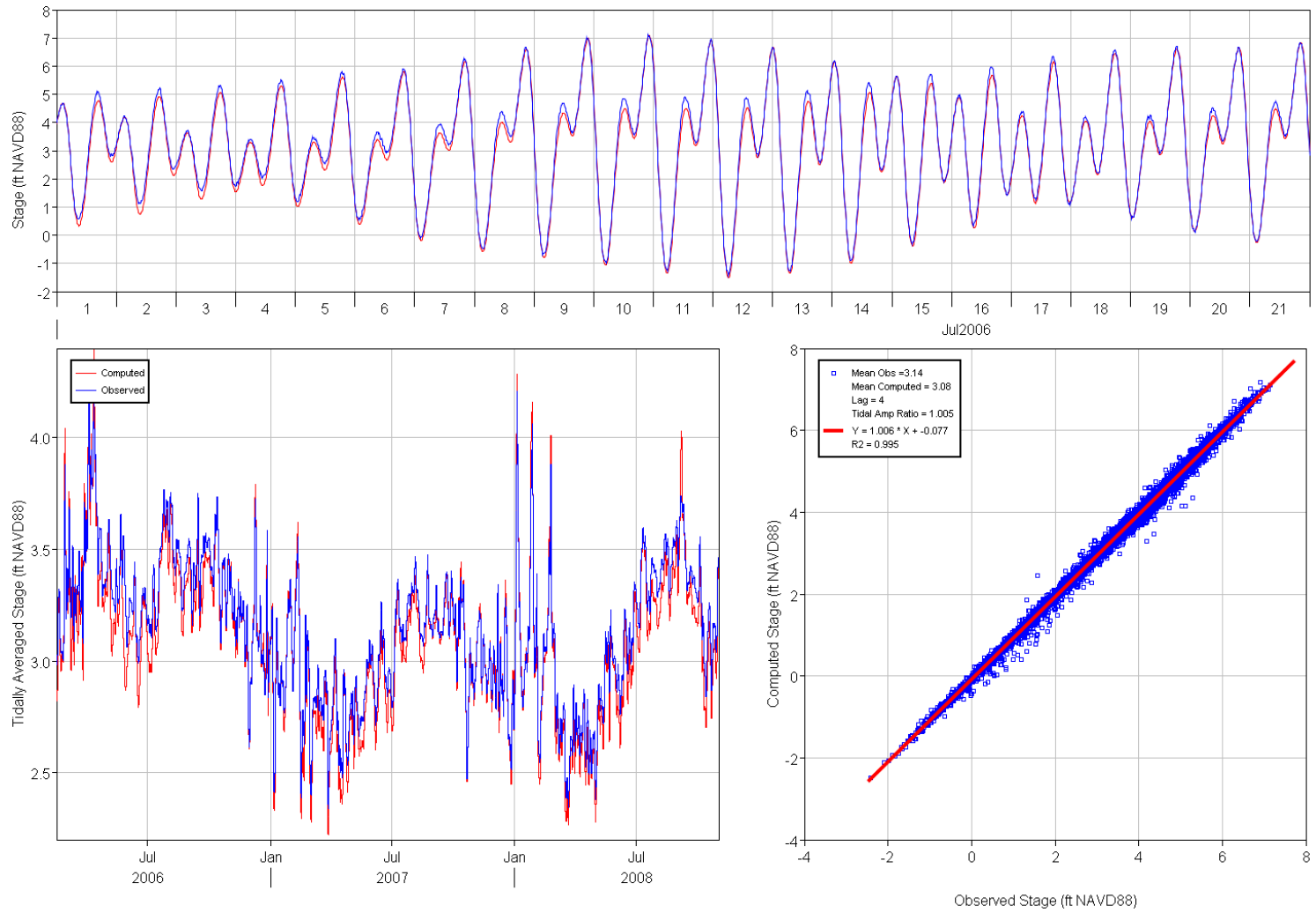


MSD - SJR at Mossdale

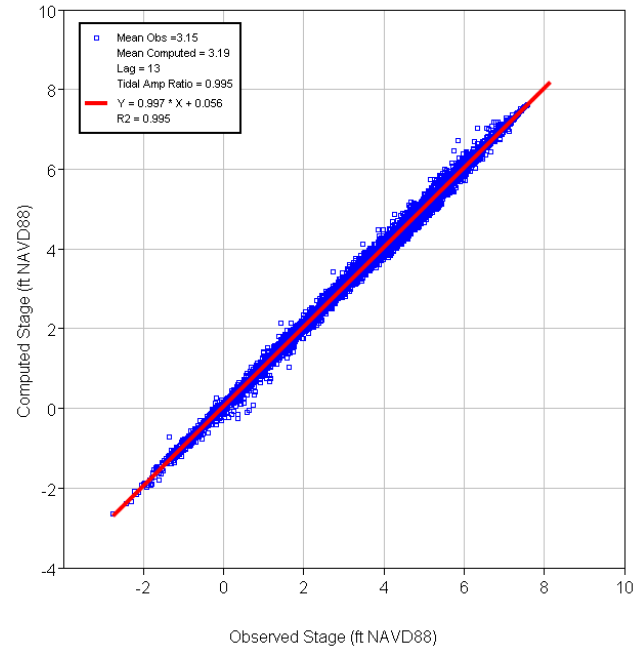
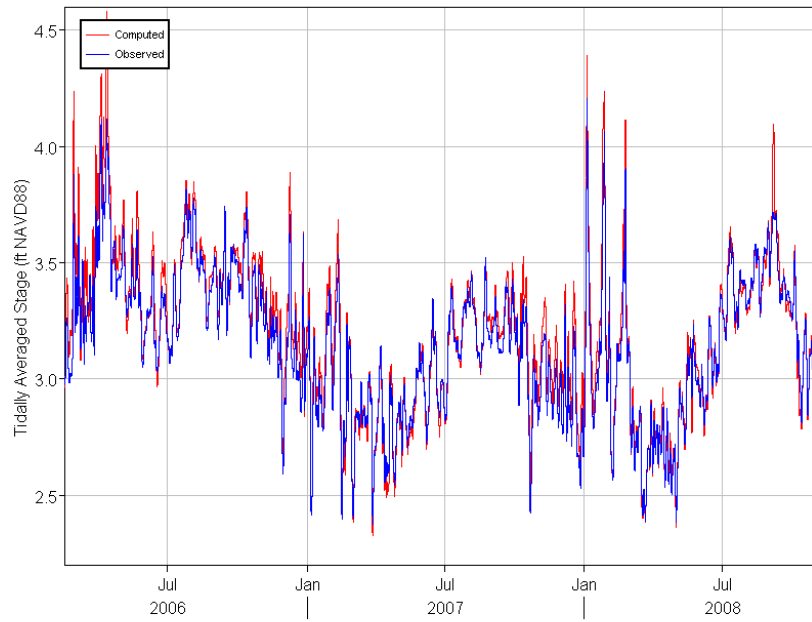
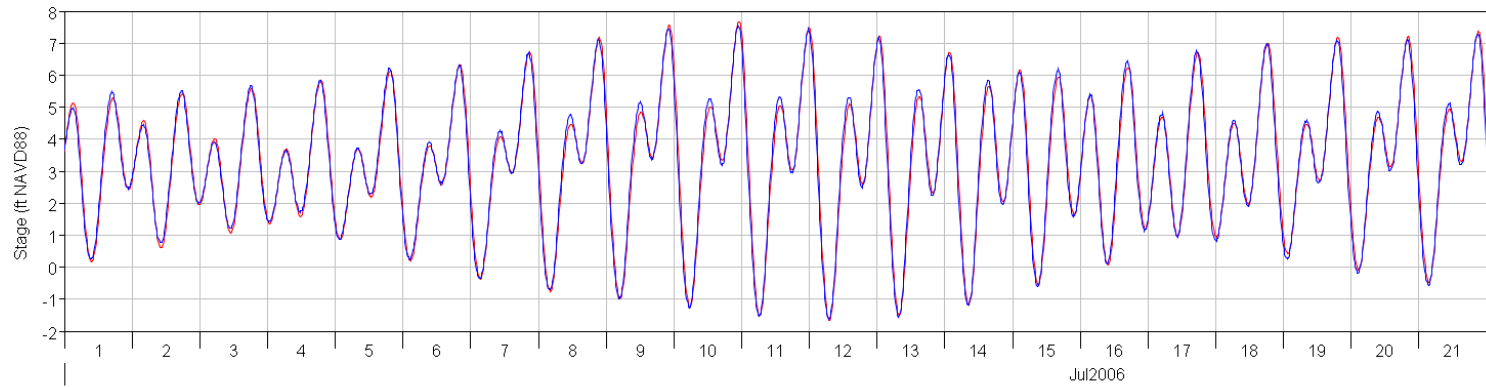


Appendix C: Contemporary San Francisco Estuary Model Individual Stage Station Plots

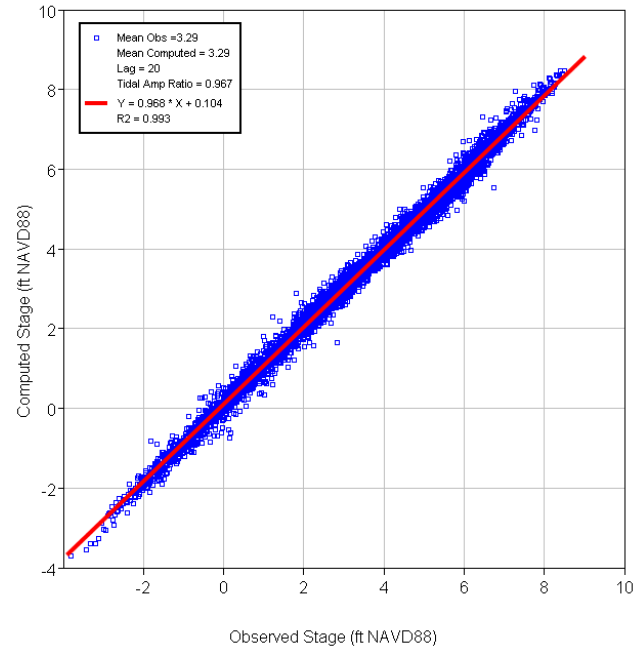
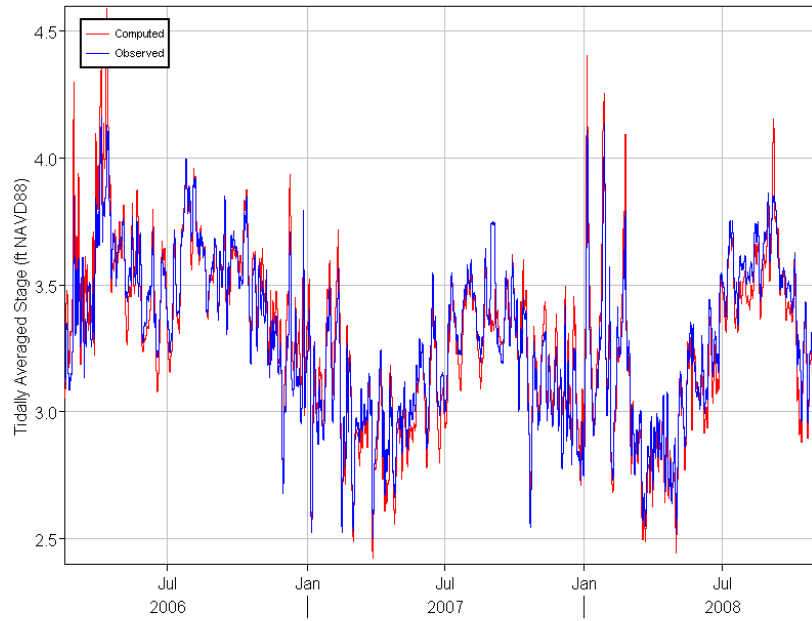
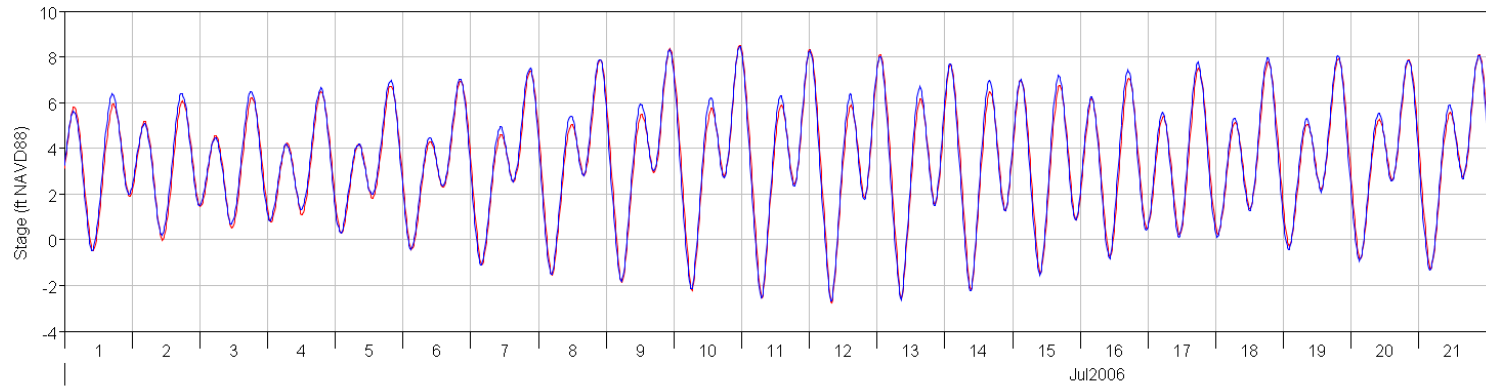
GGT - Golden Gate



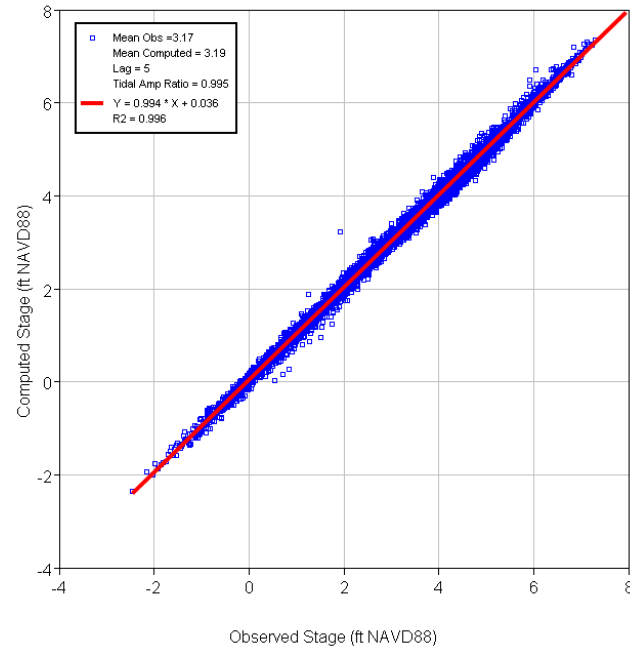
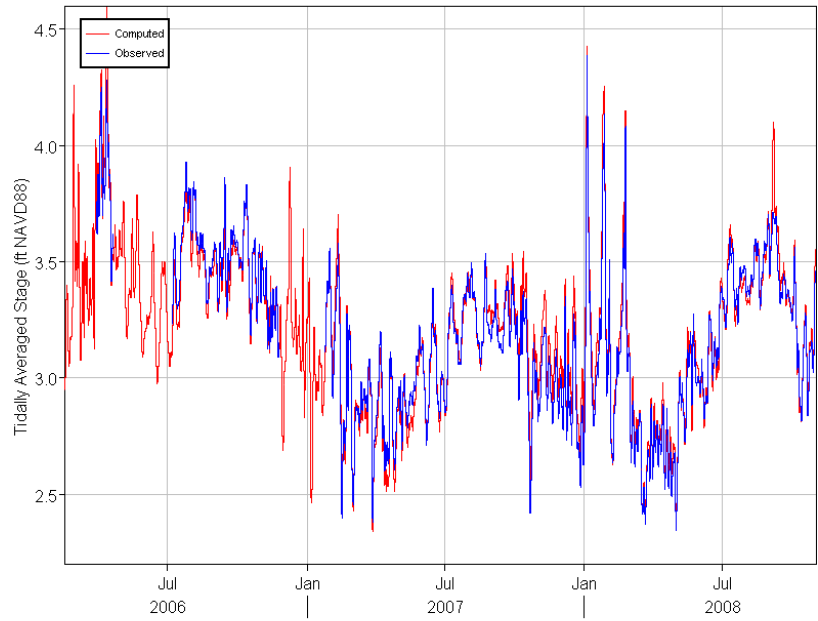
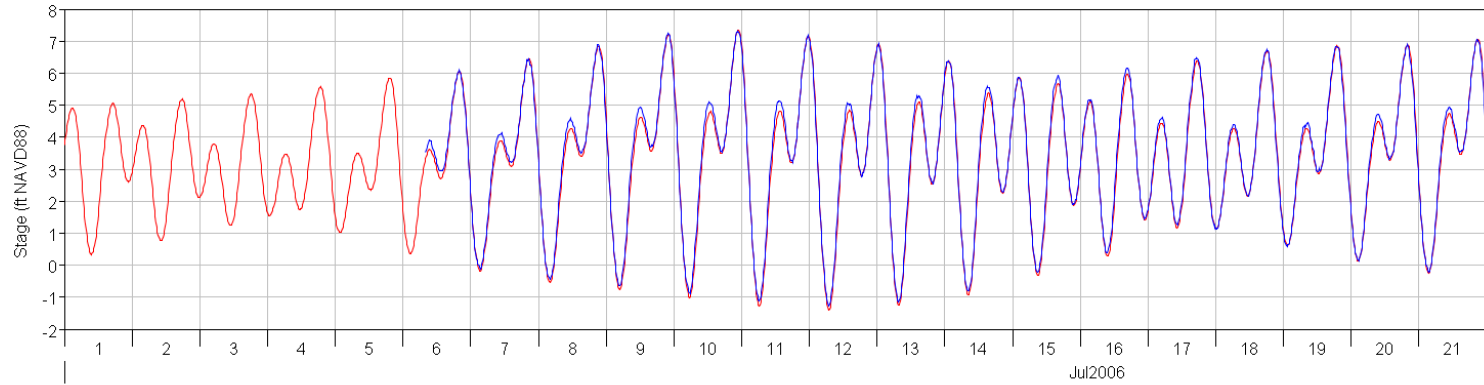
AMD - Alameda



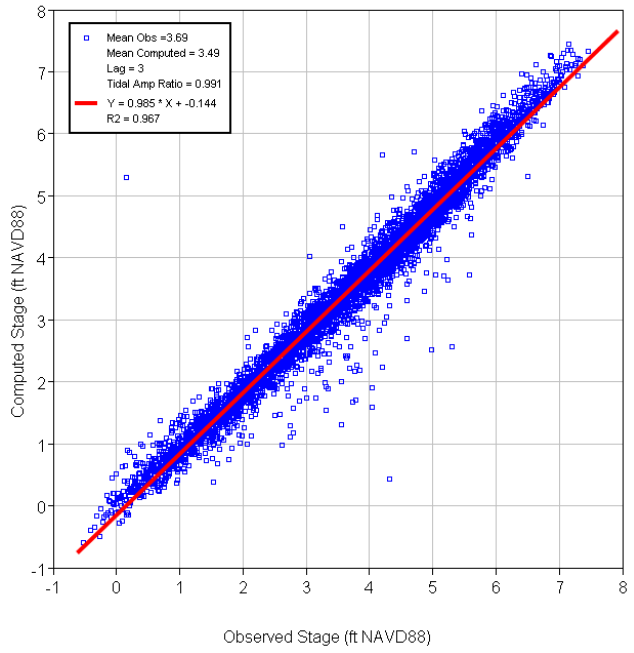
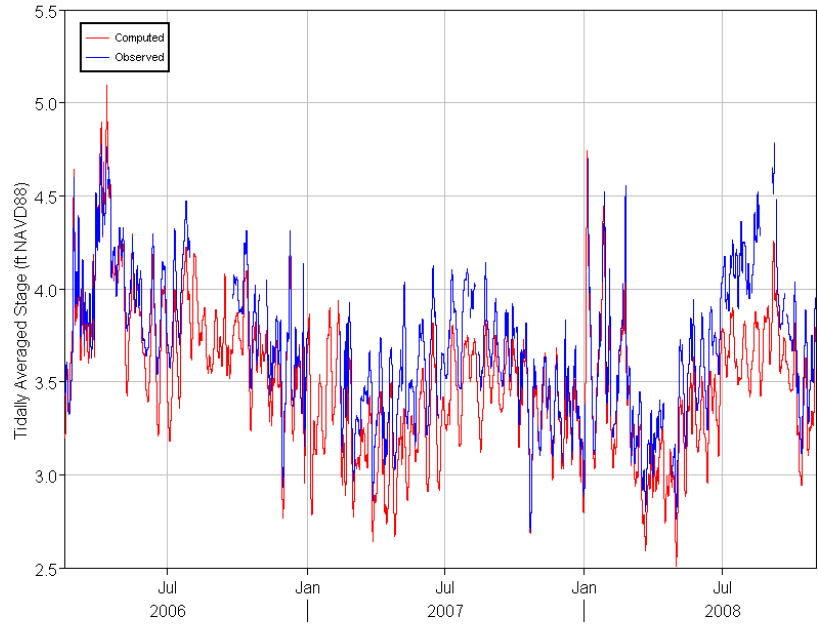
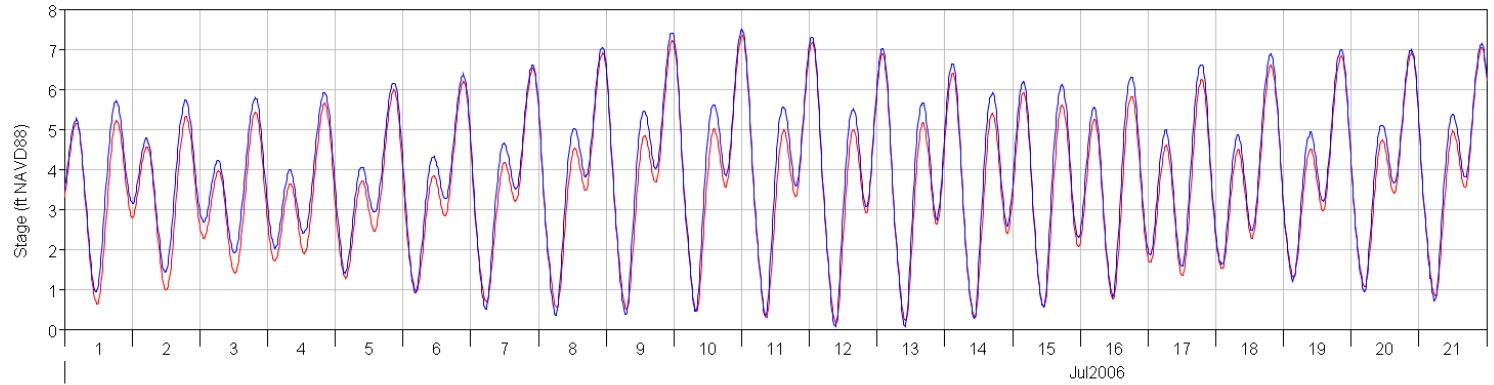
RWC - Redwood City



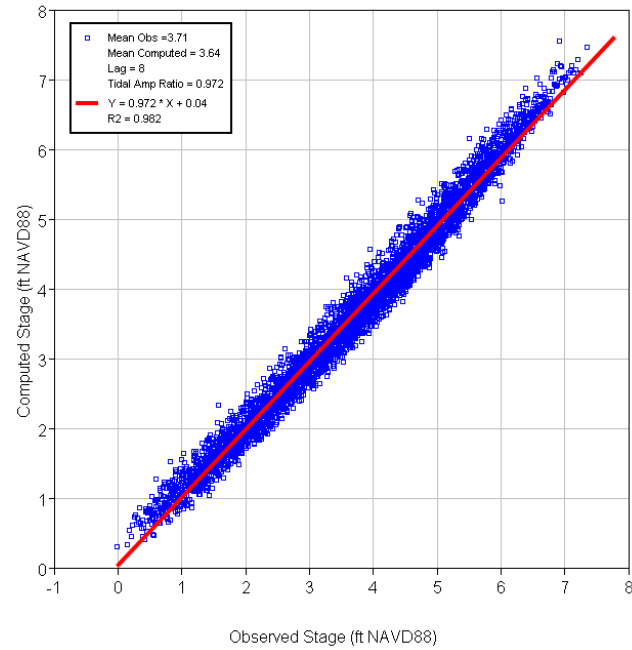
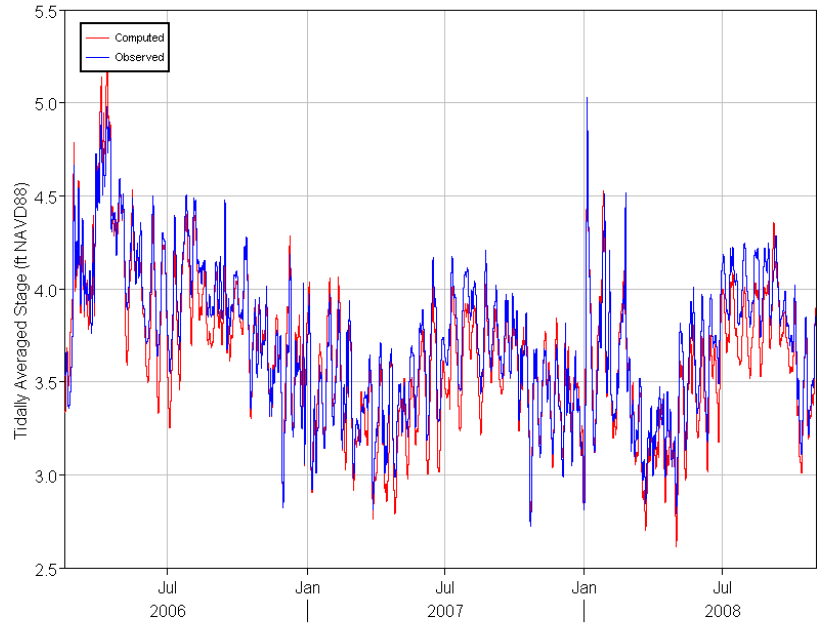
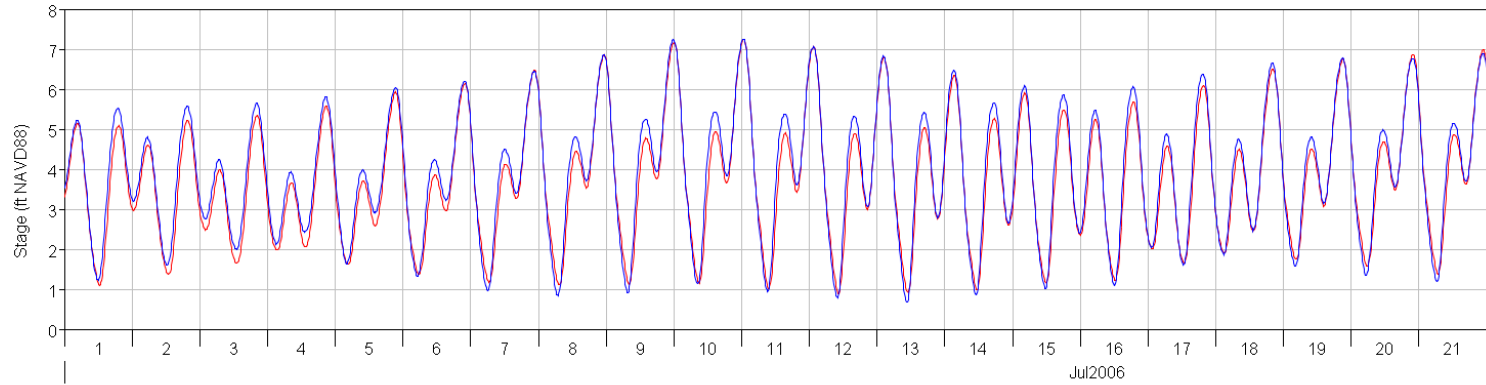
RMD - Richmond



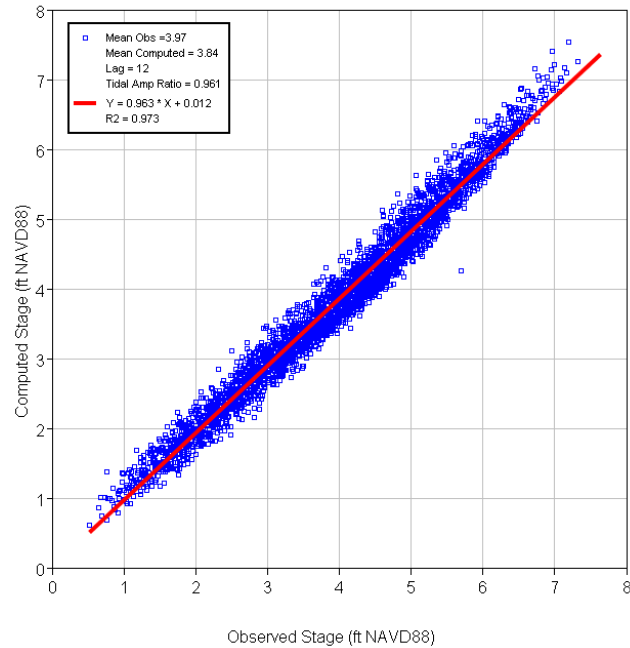
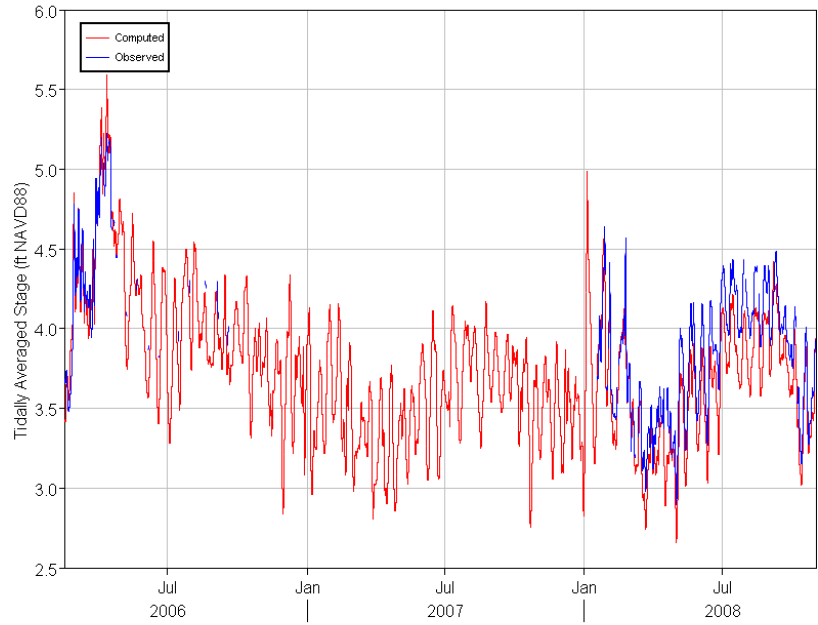
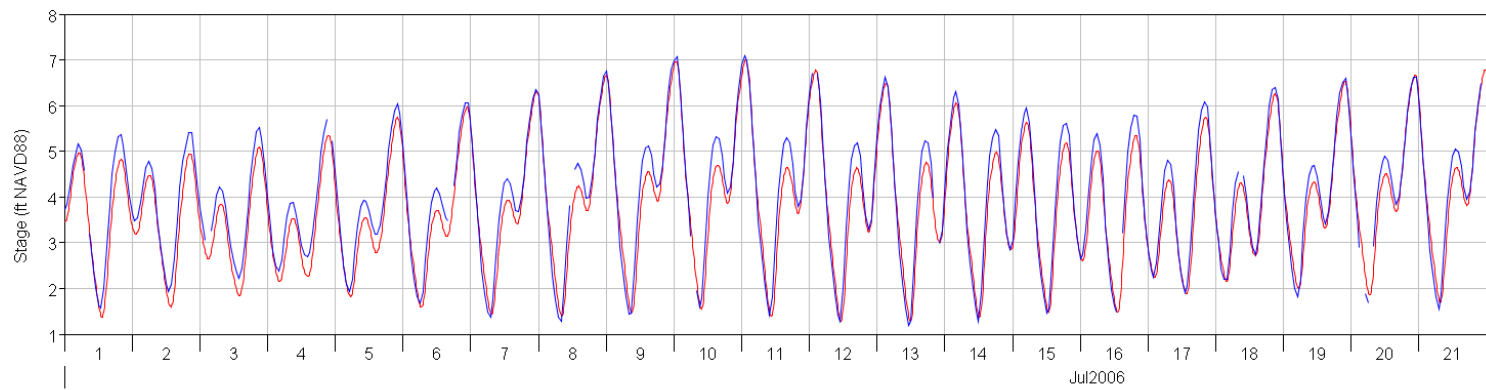
MRZ - Martinez



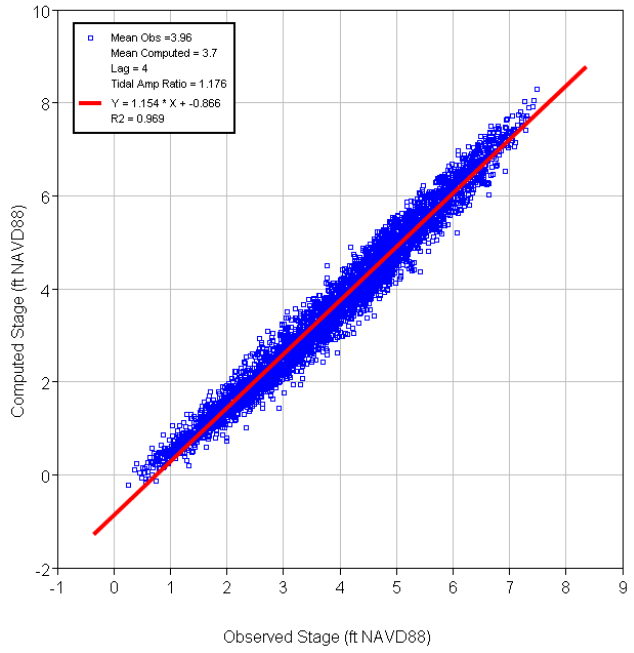
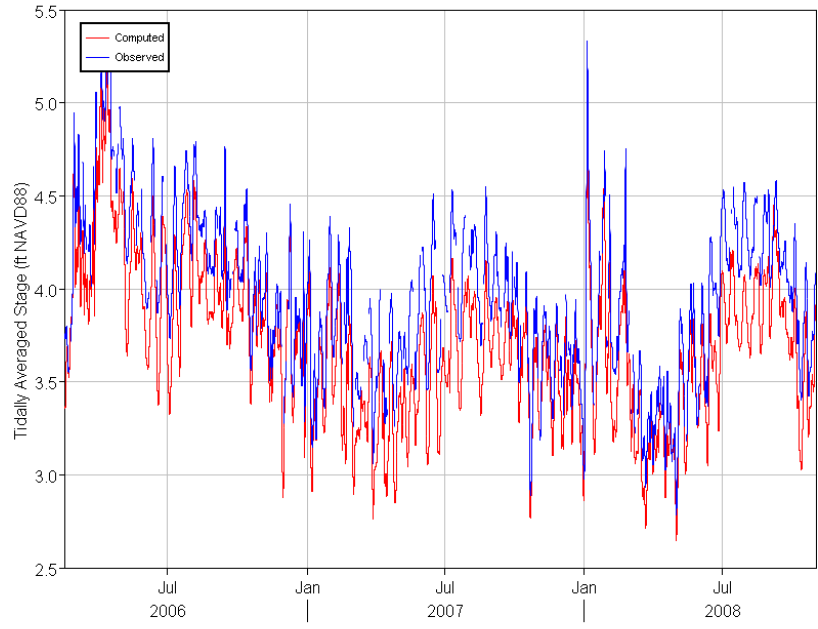
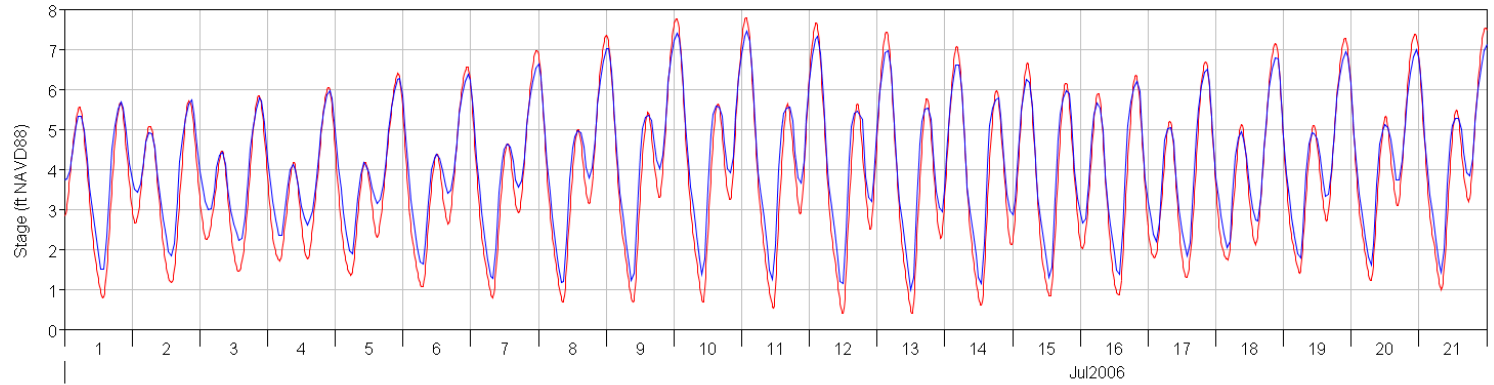
PCT - Port Chicago



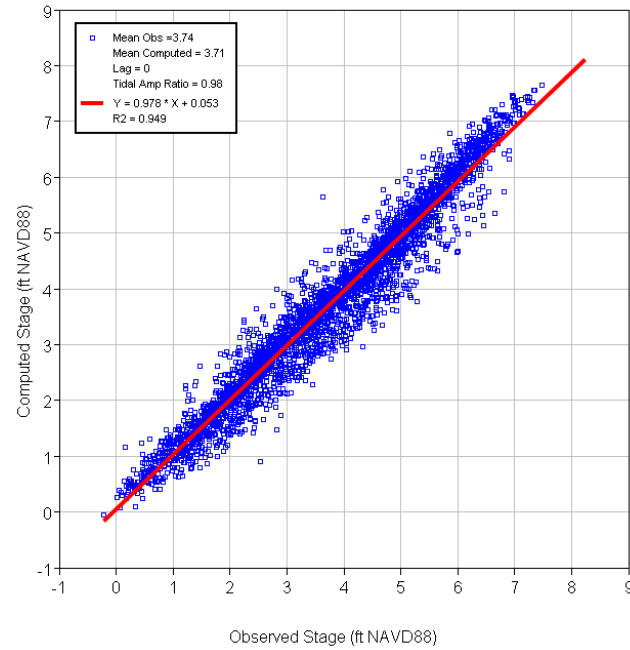
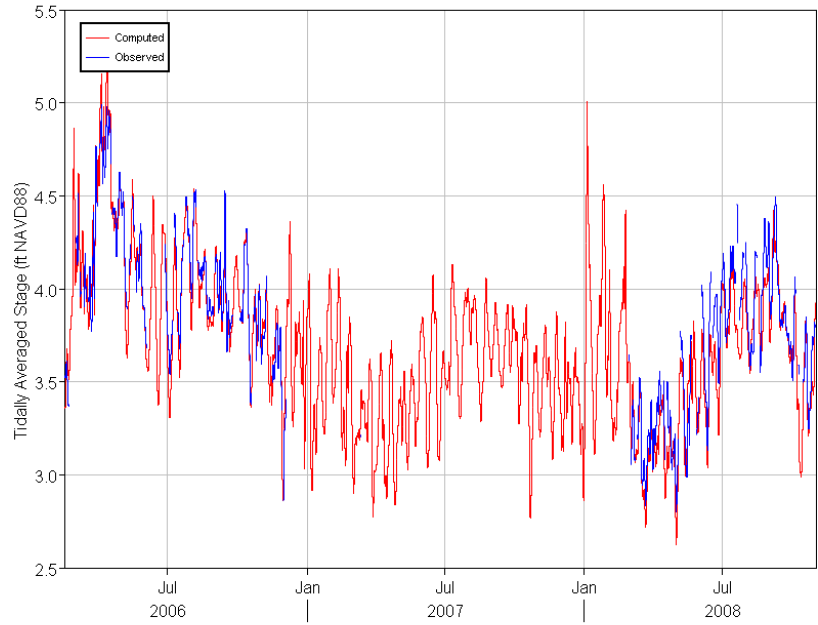
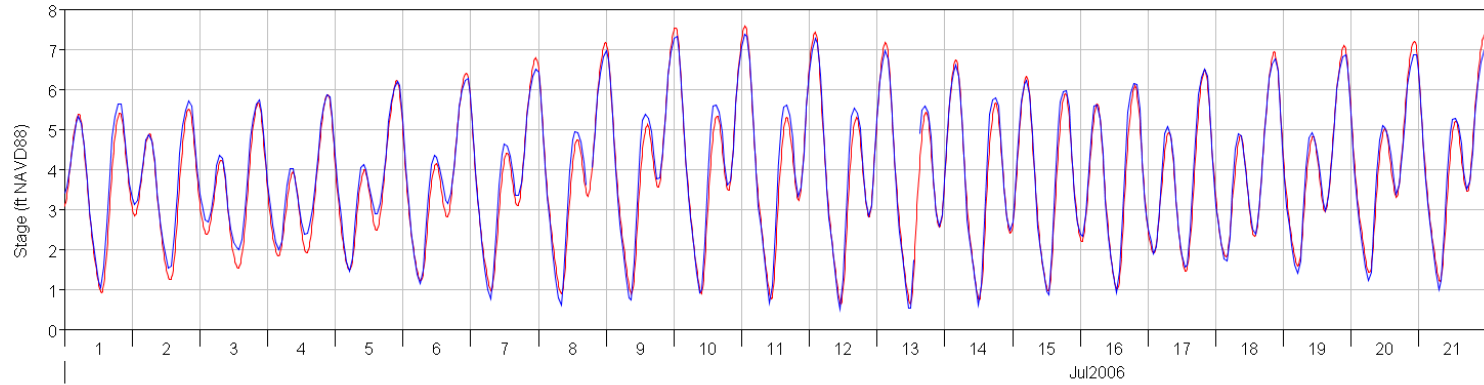
MAL - Mallard Island



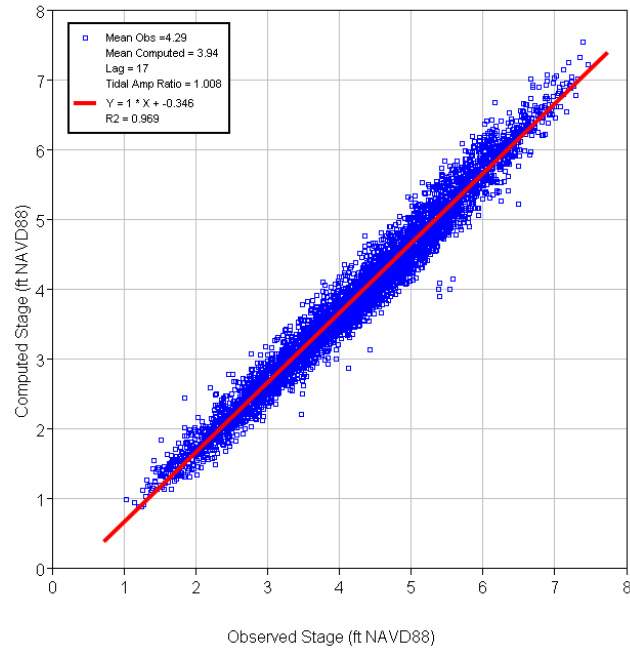
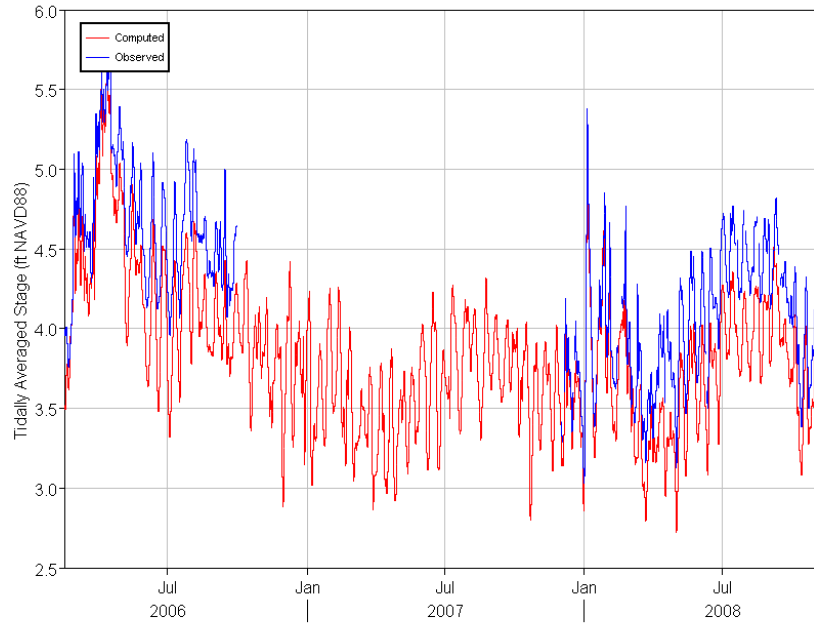
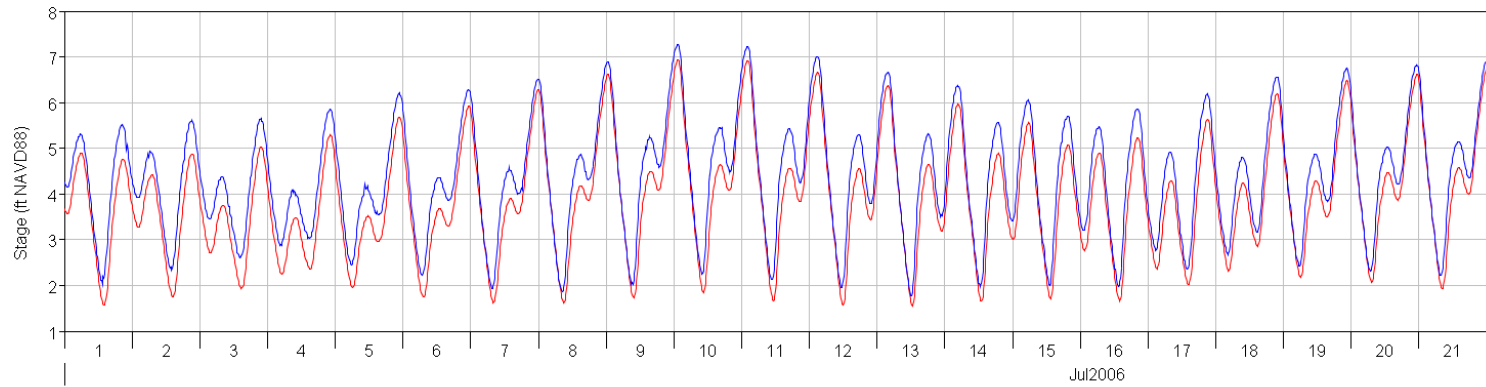
NSL - Montezuma SI at NSL



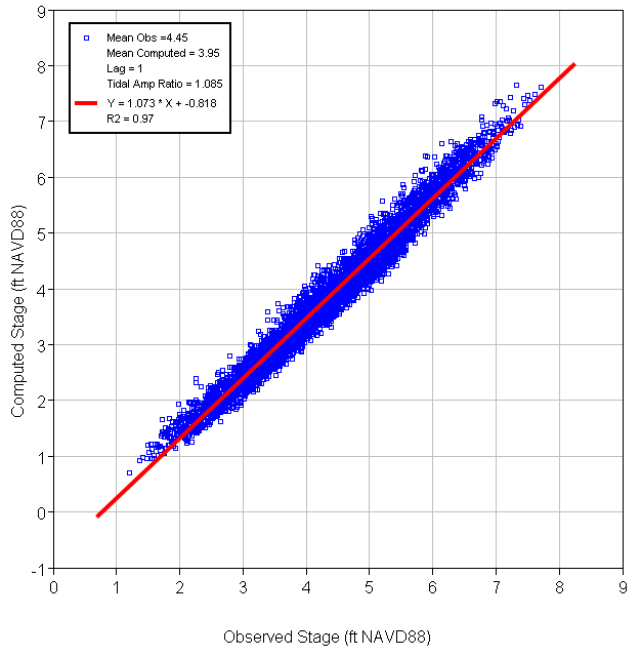
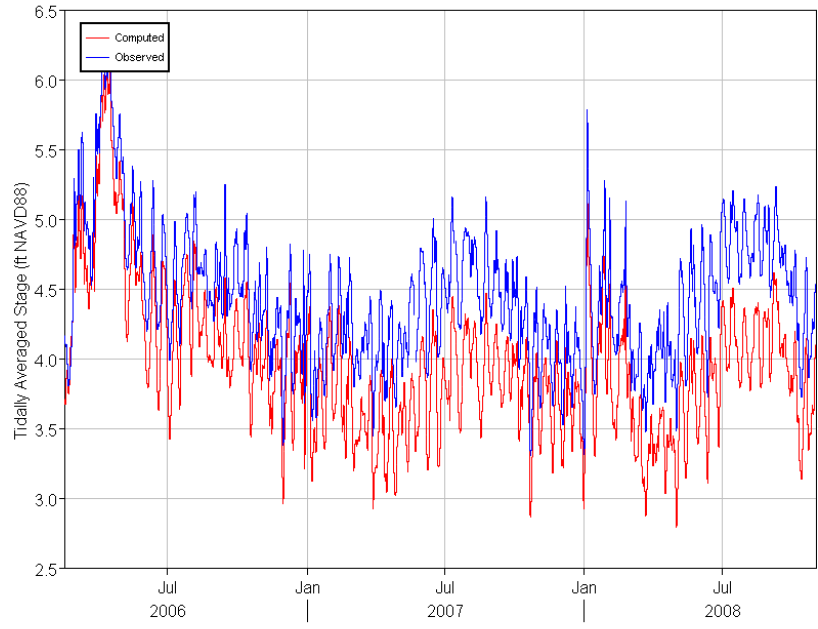
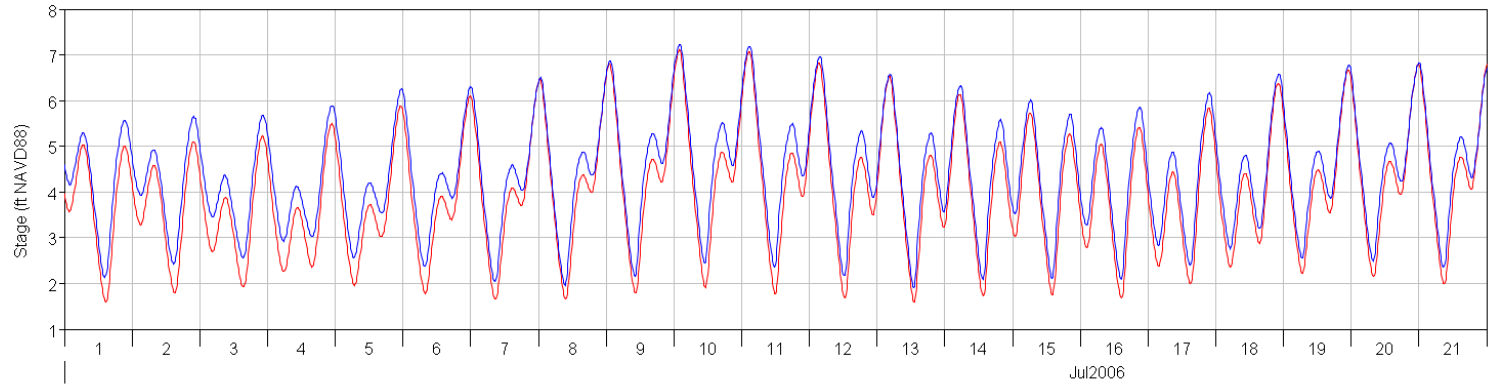
BDL - Beldon Landing



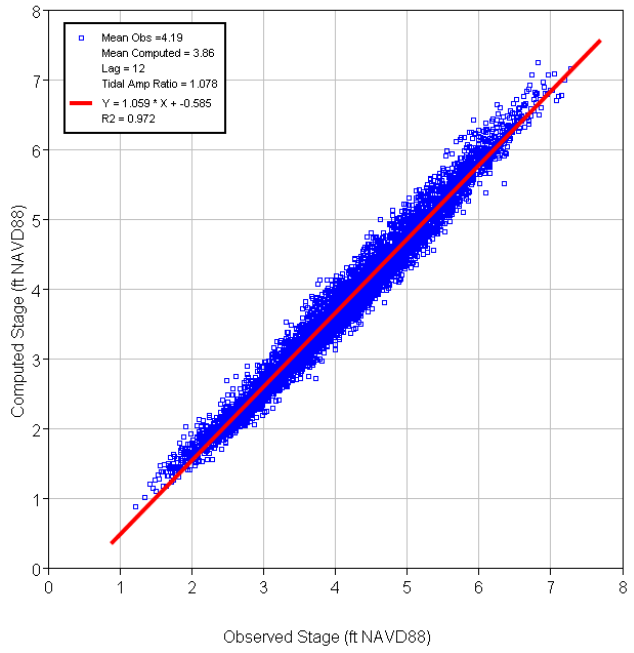
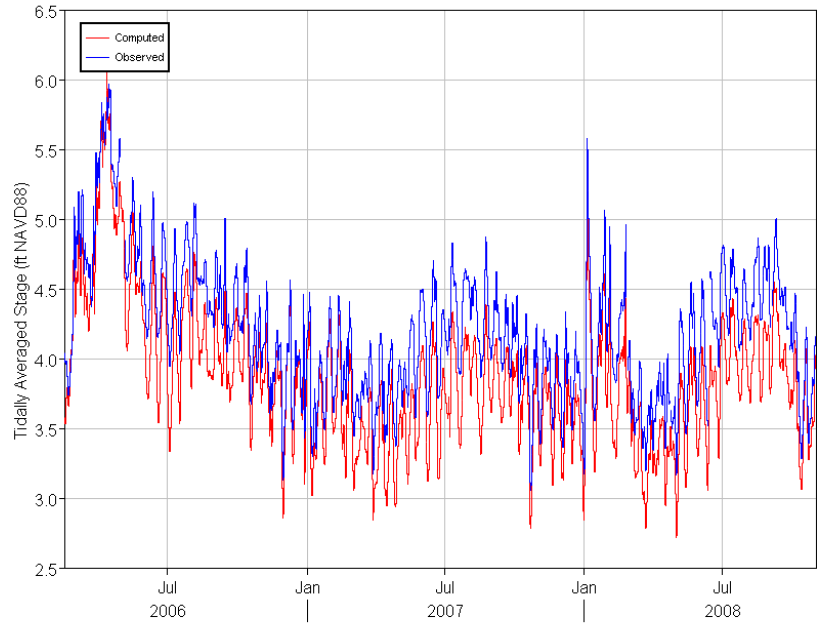
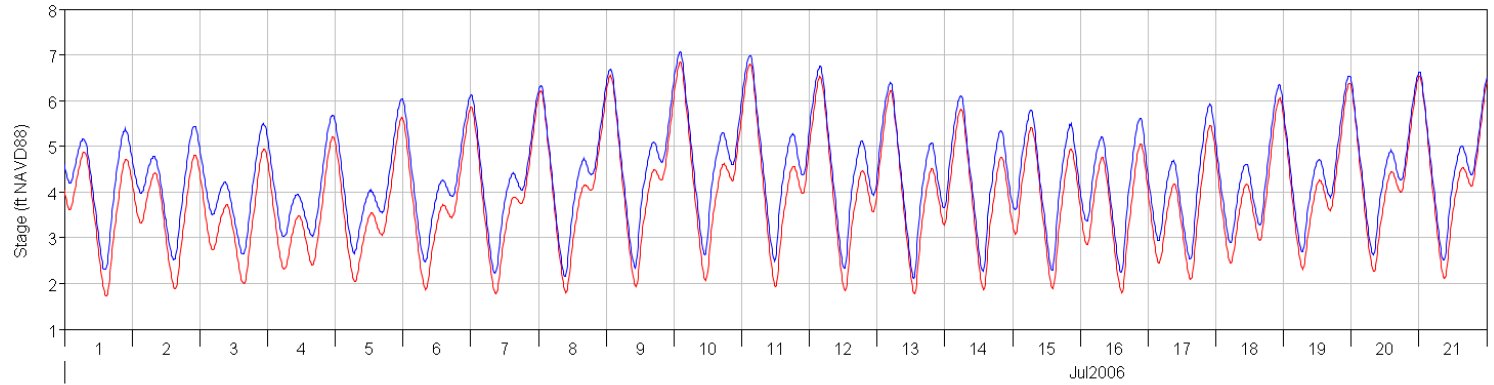
ANH - Antioch



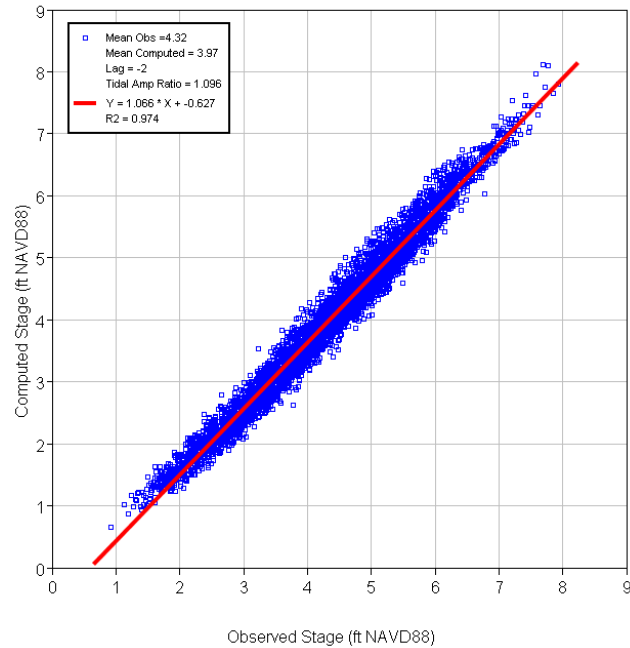
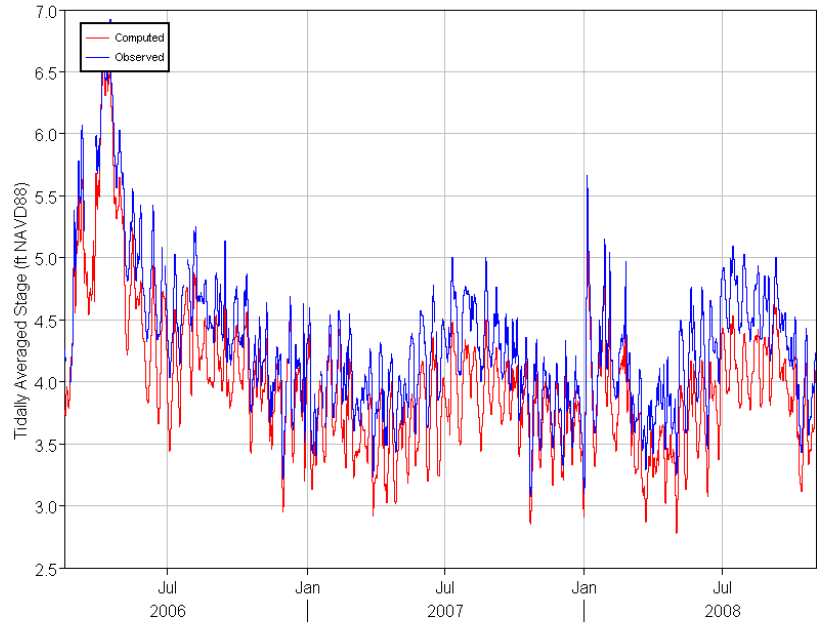
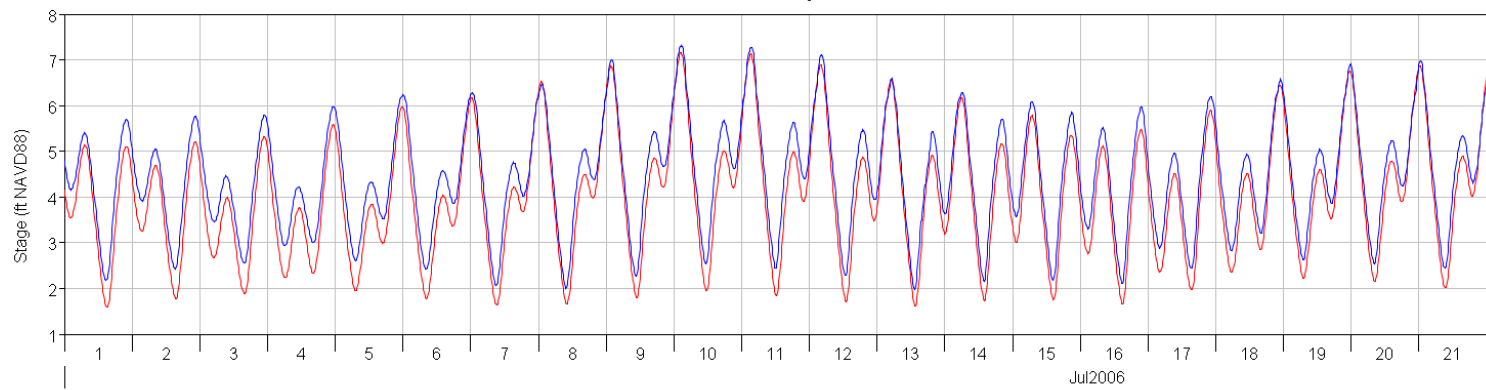
SRV - Sac River at Rio Vista



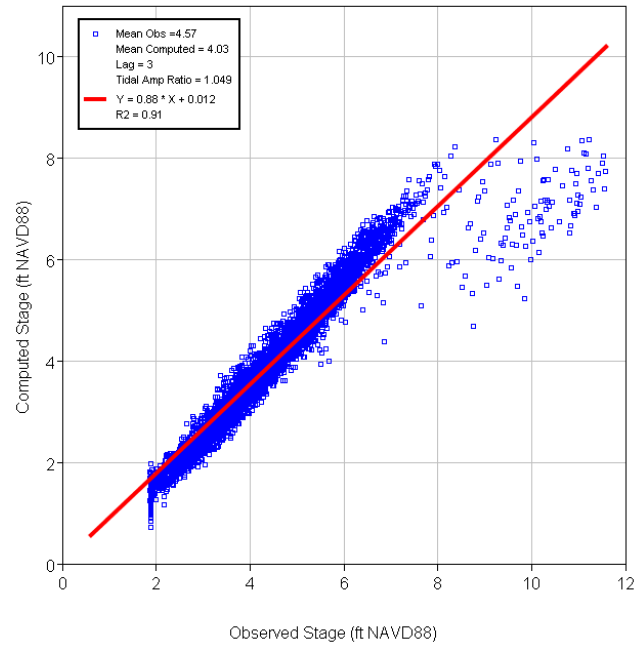
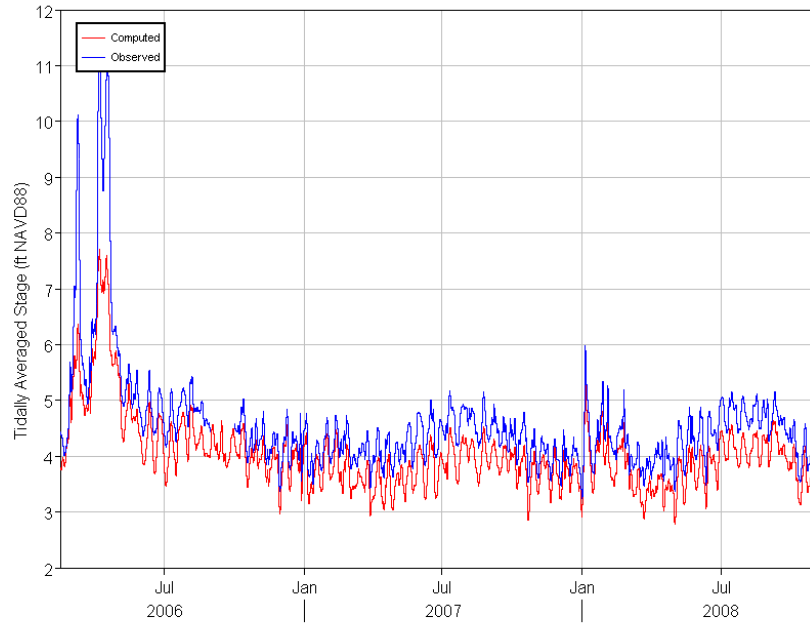
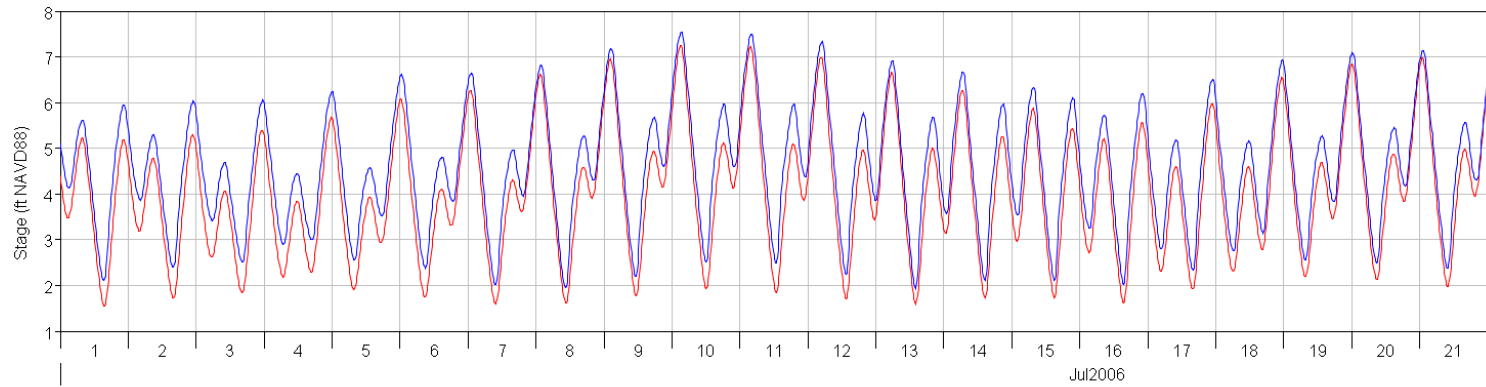
TSL - Threemile Slough



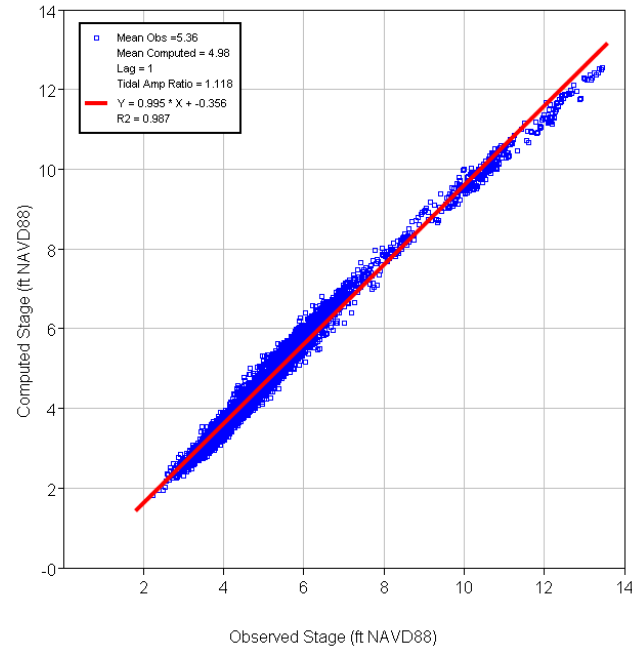
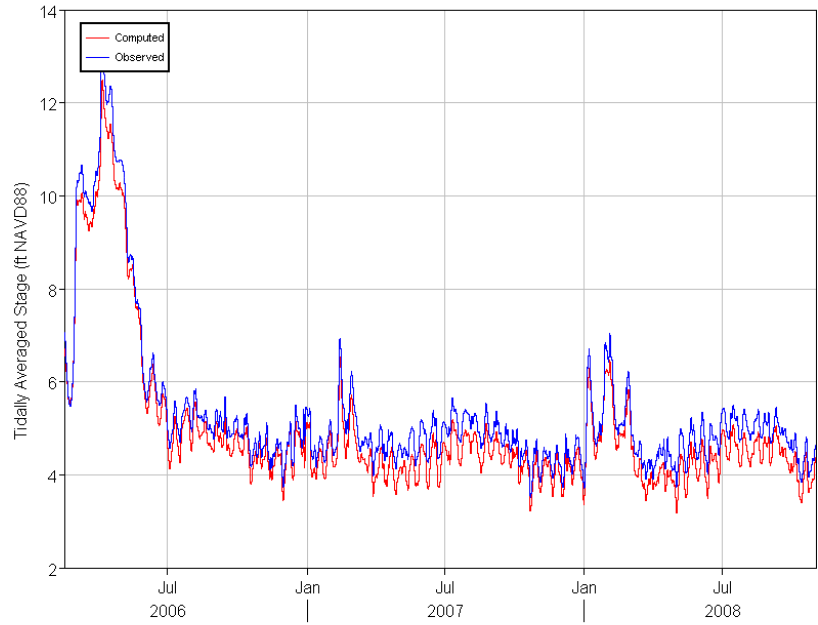
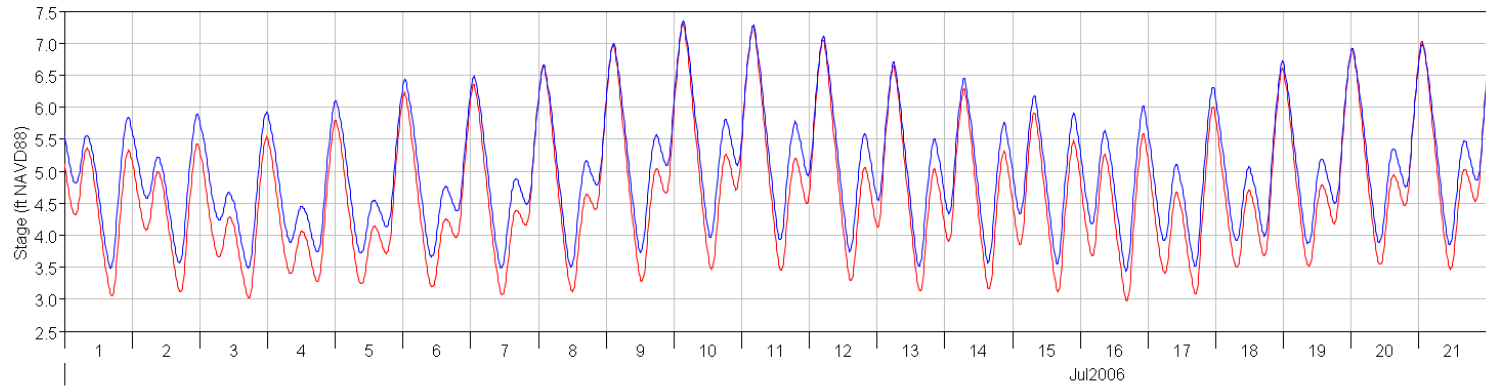
RYI - Cache SI at Ryer Island



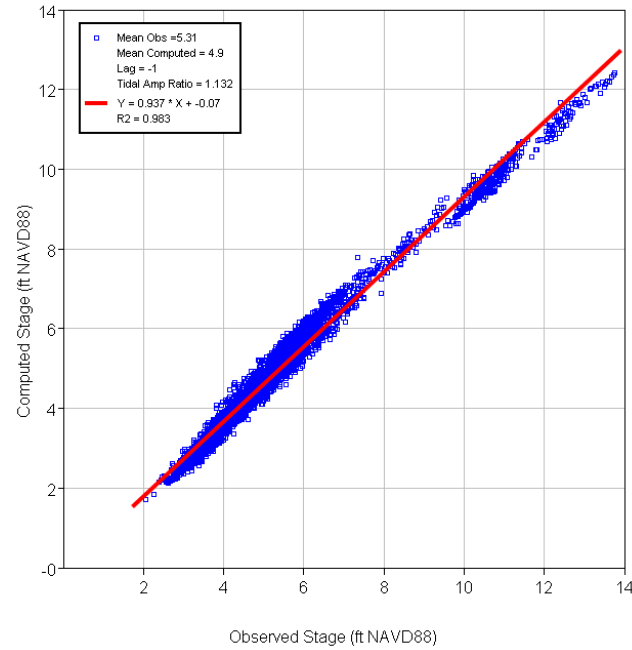
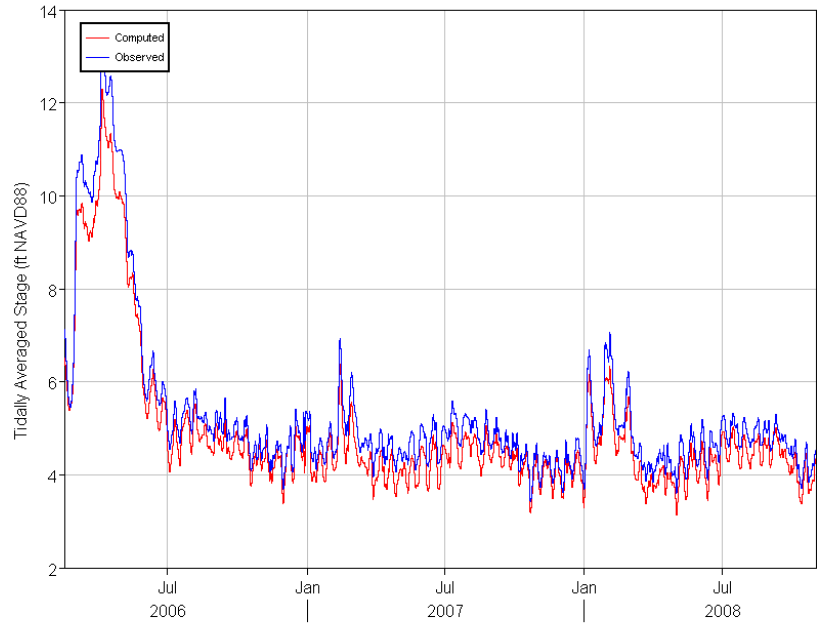
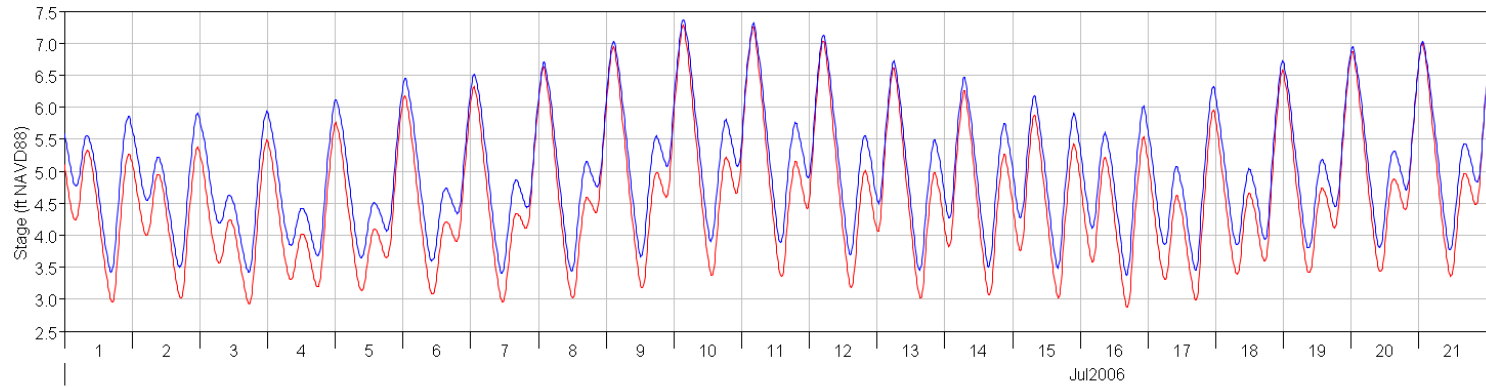
LIB - Liberty Island South



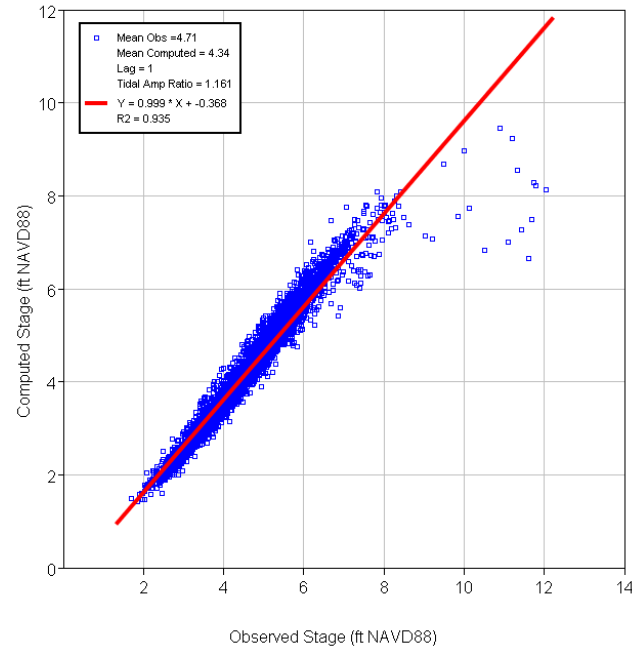
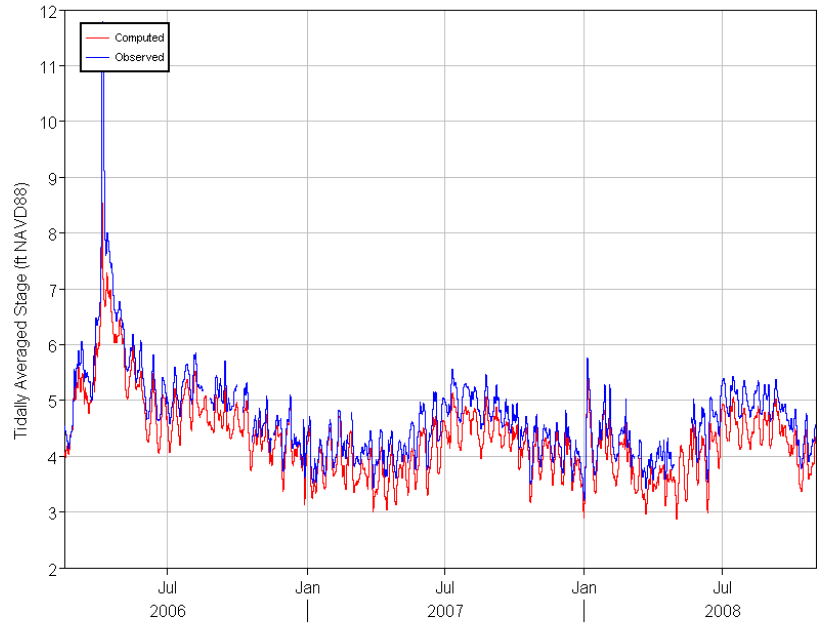
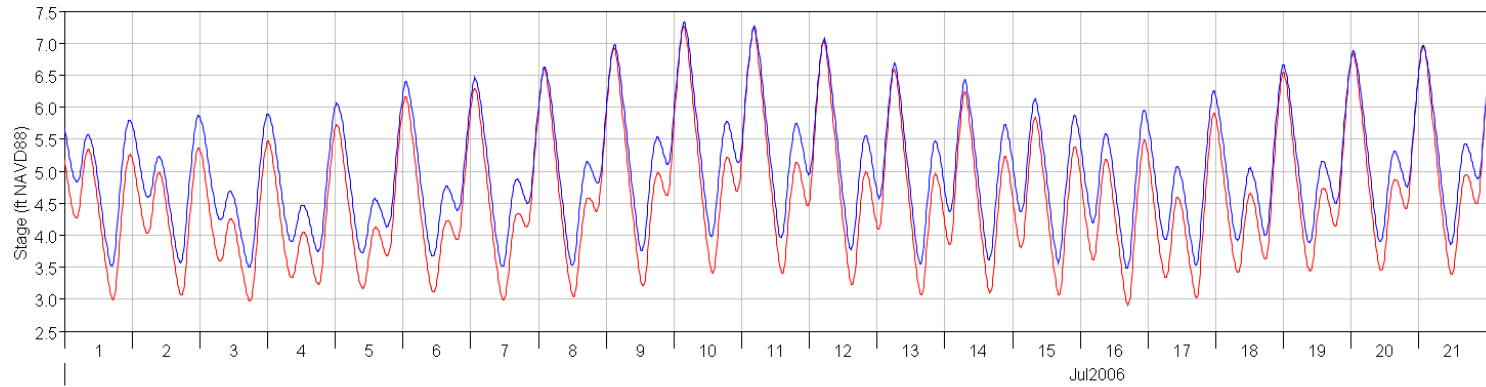
GES - Sacramento R below Georgiana SI



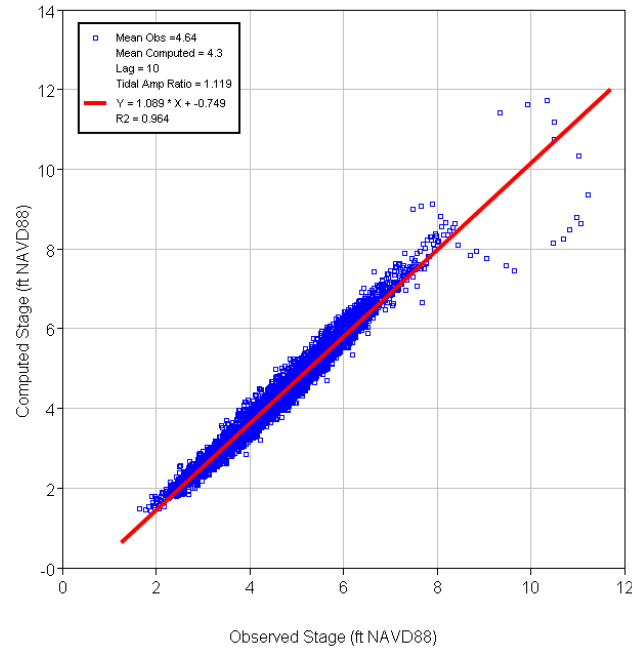
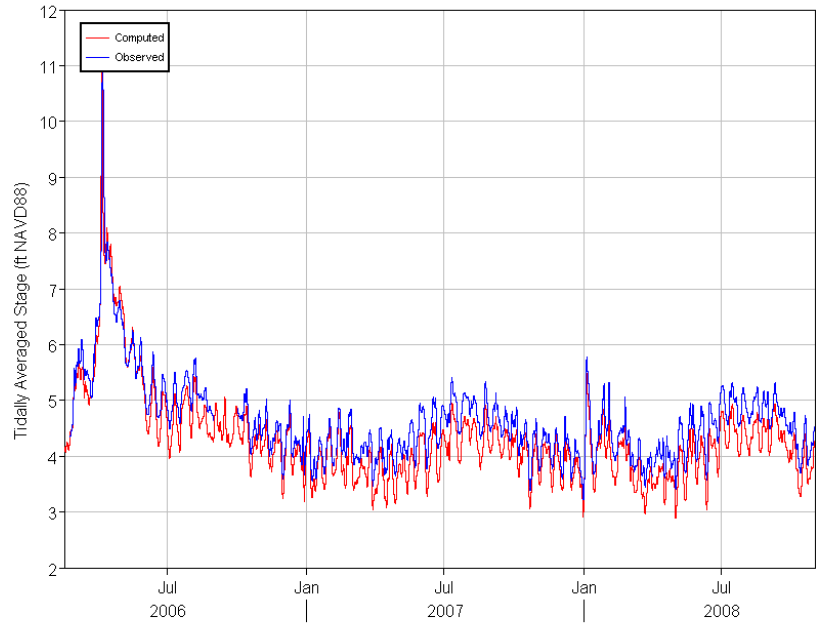
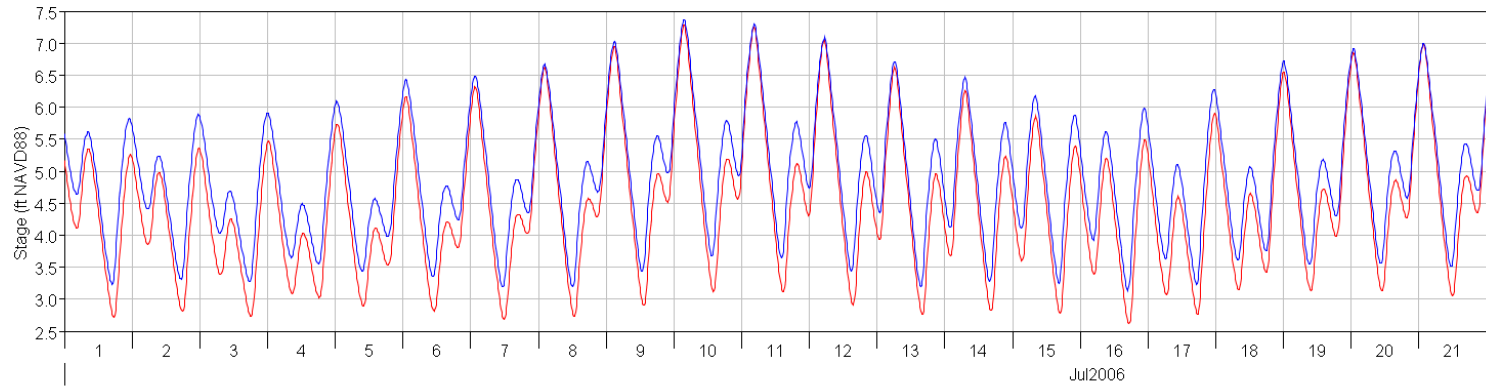
GSS - Georgiana Slough



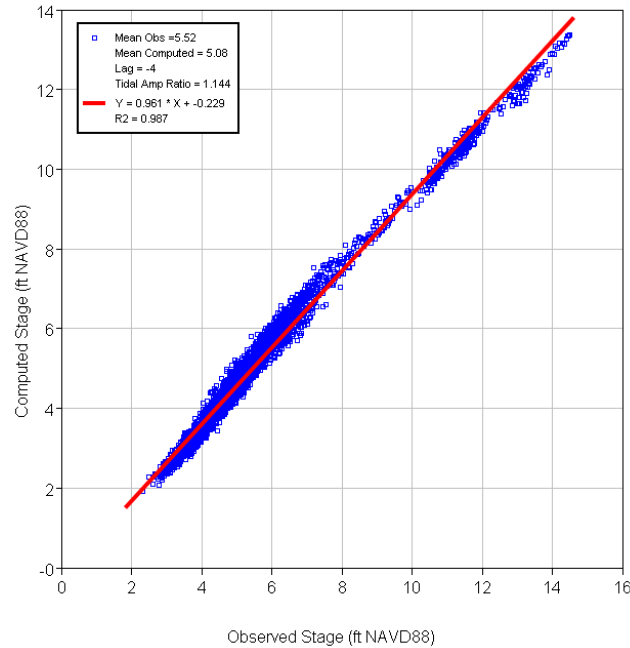
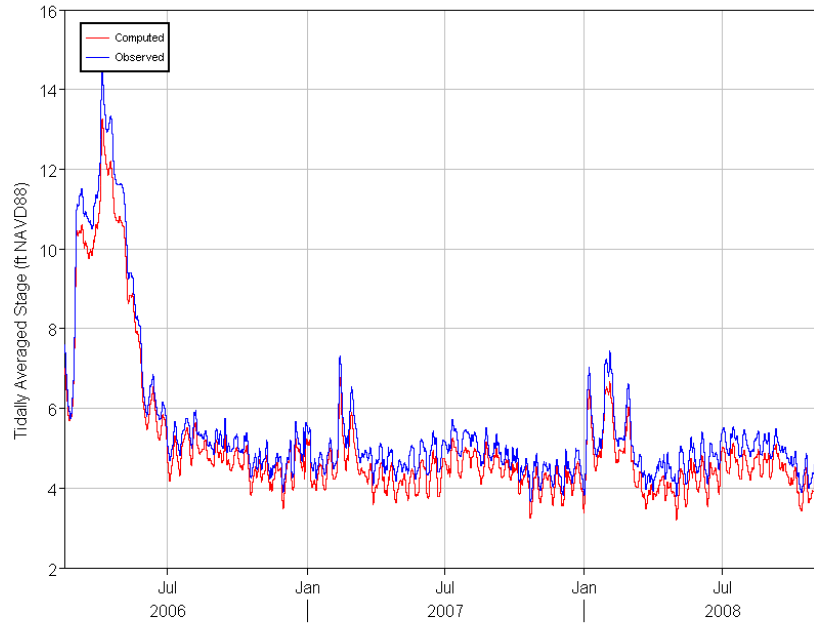
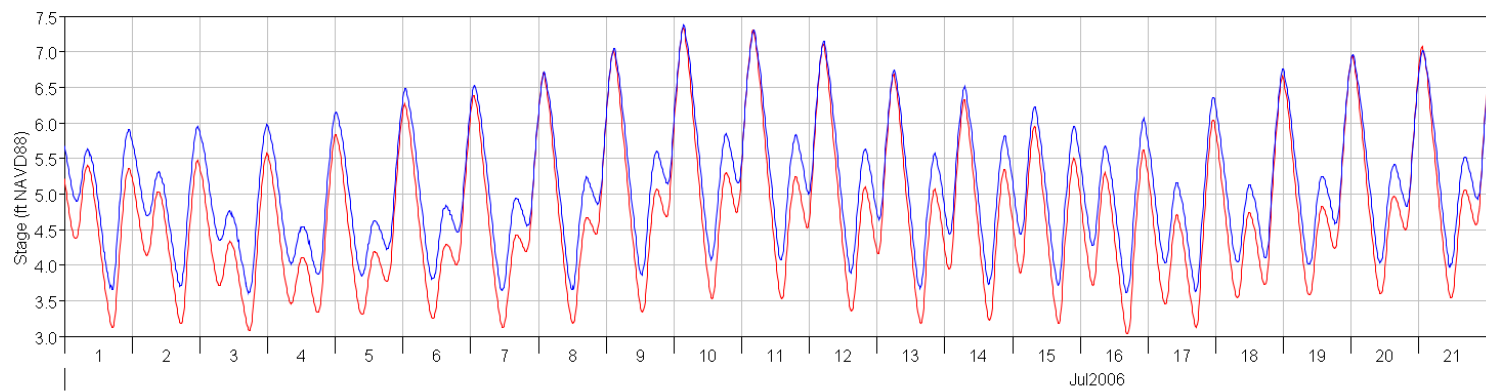
DCC - Delta Cross Channel



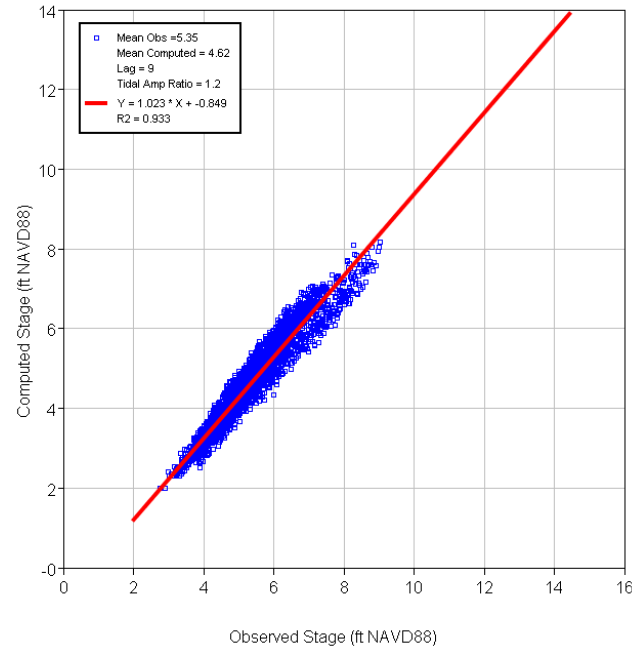
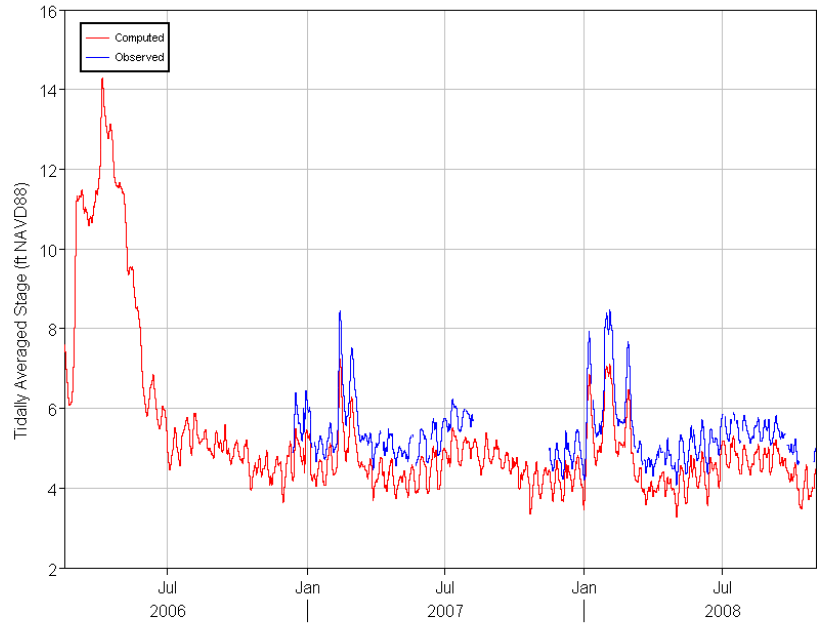
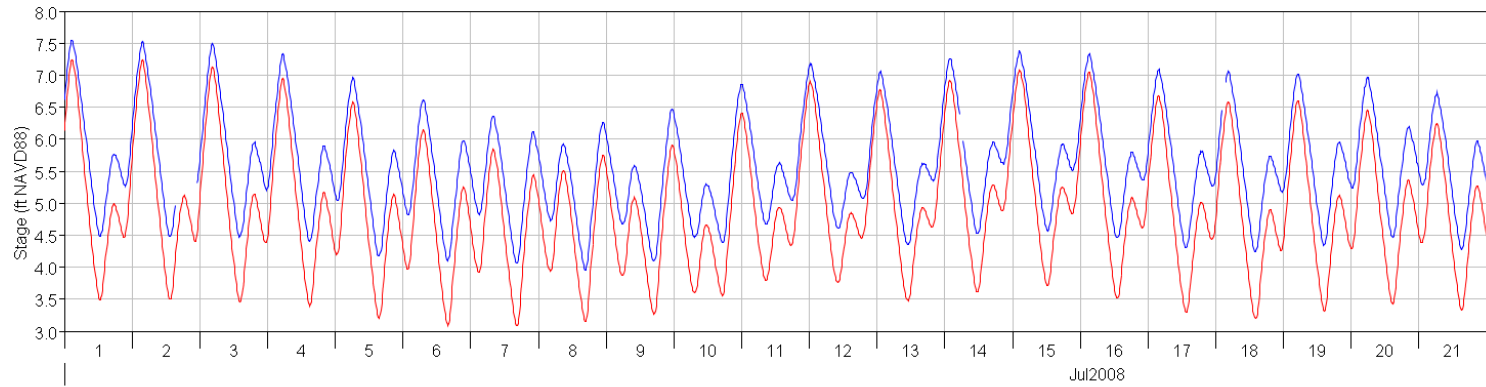
SMR - South Fork Mokelumne River



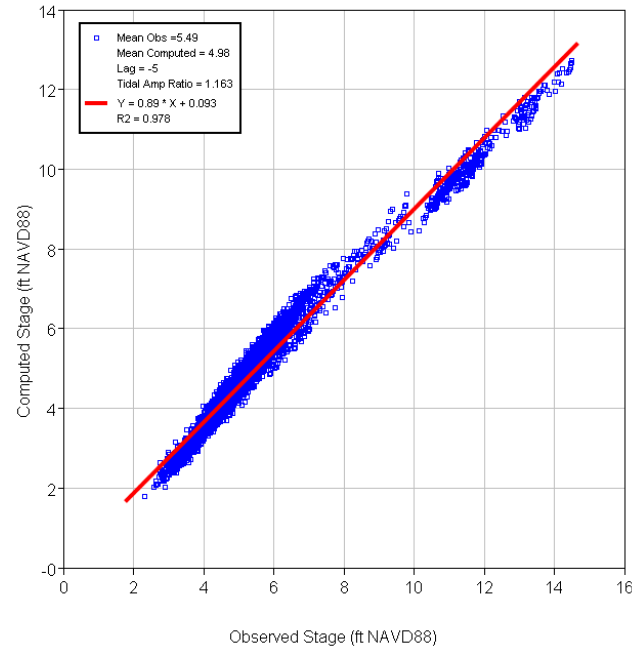
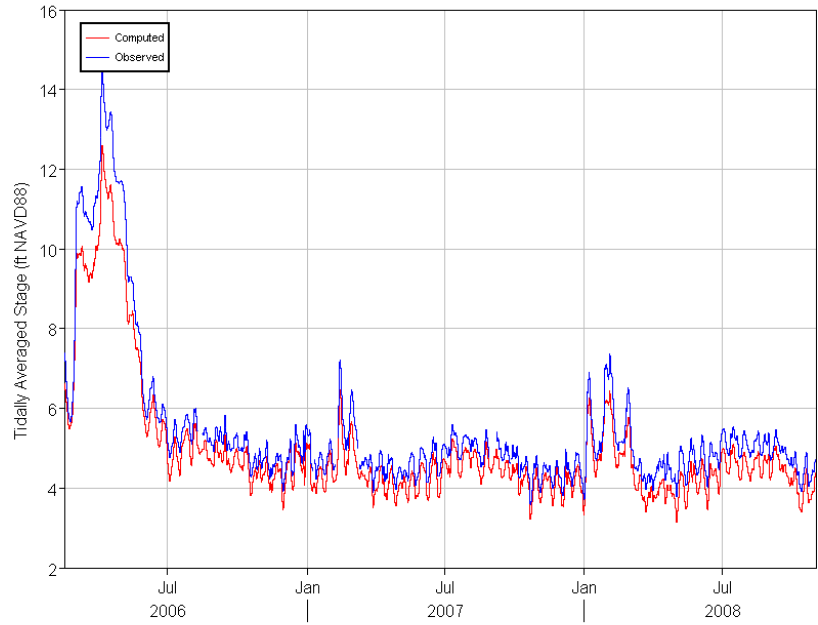
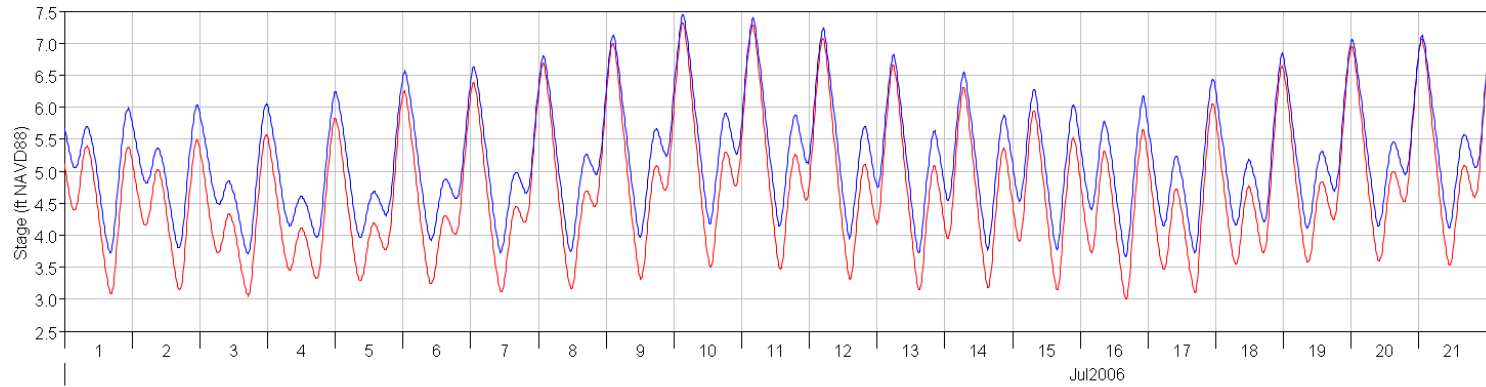
SDC - Sacramento R above DCC



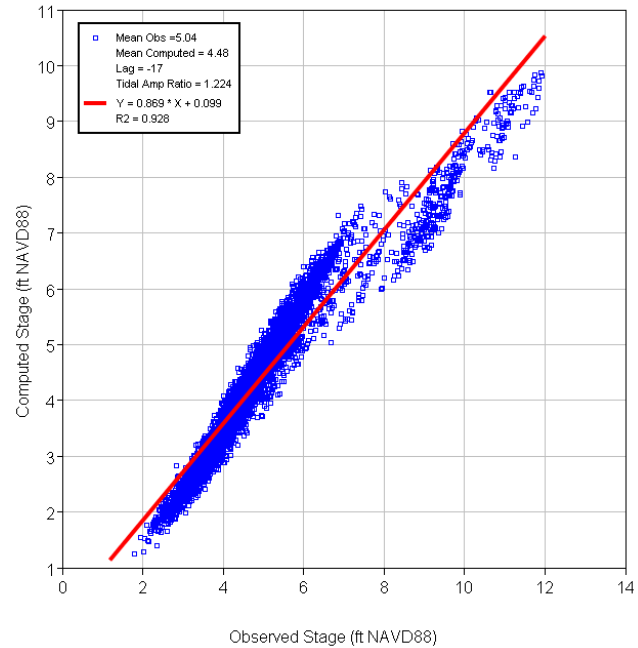
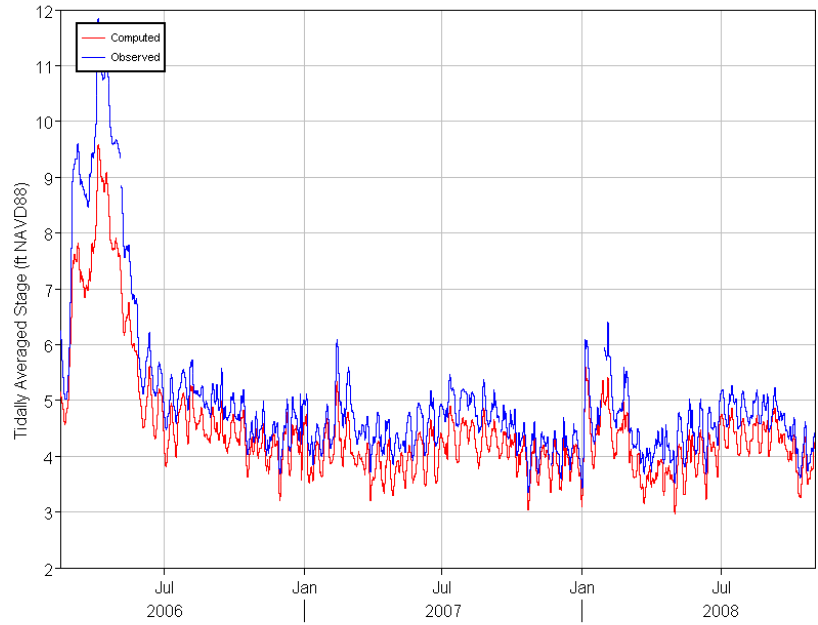
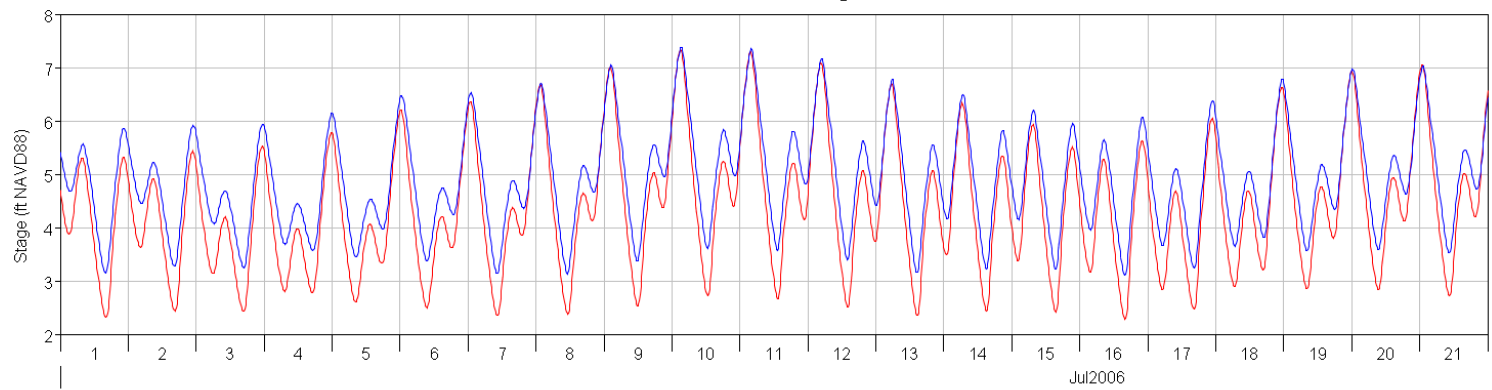
SUT - Sutter Slough



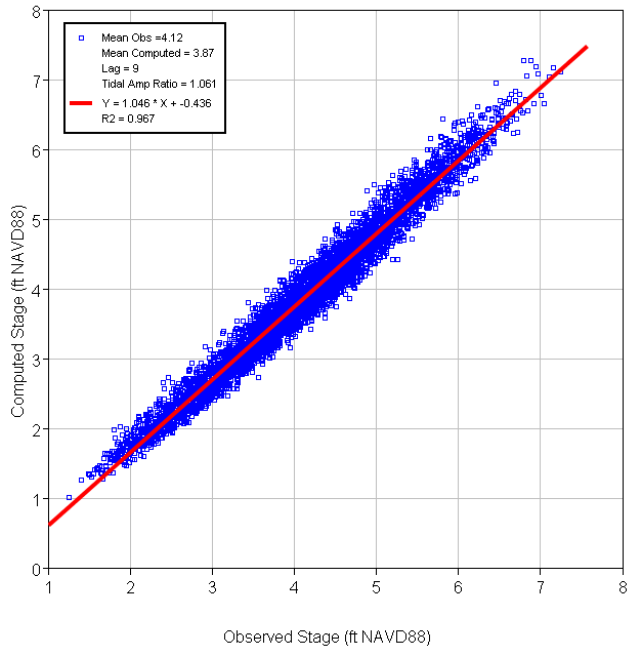
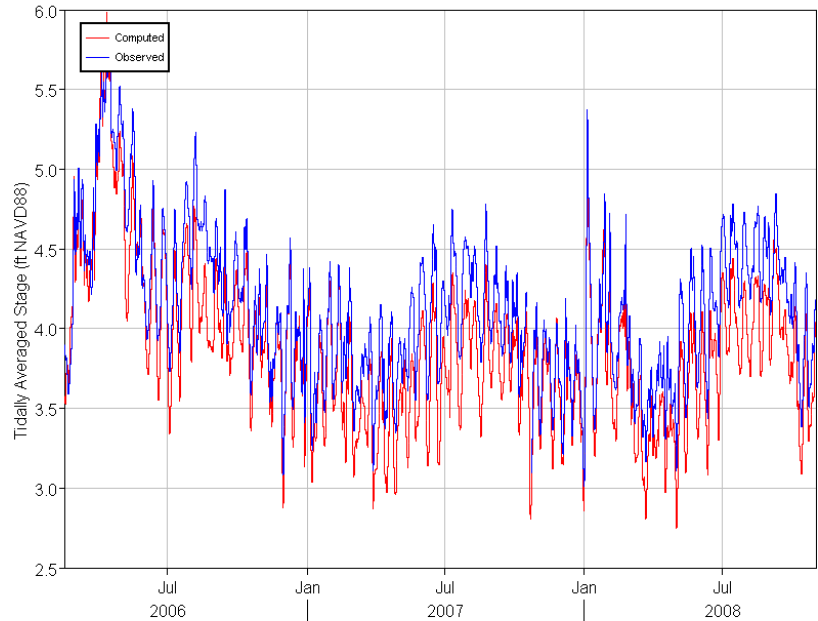
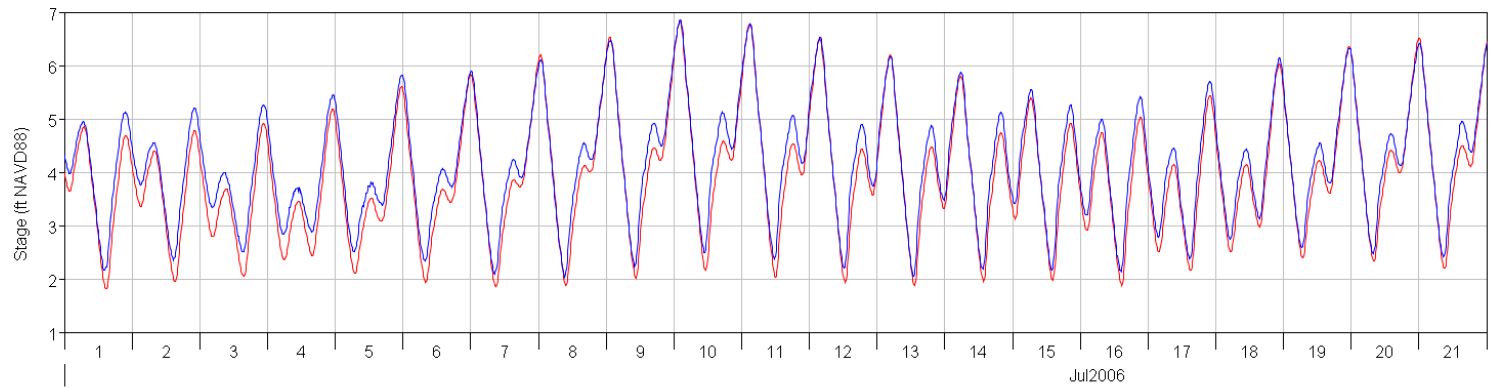
SSS - Steamboat Slough



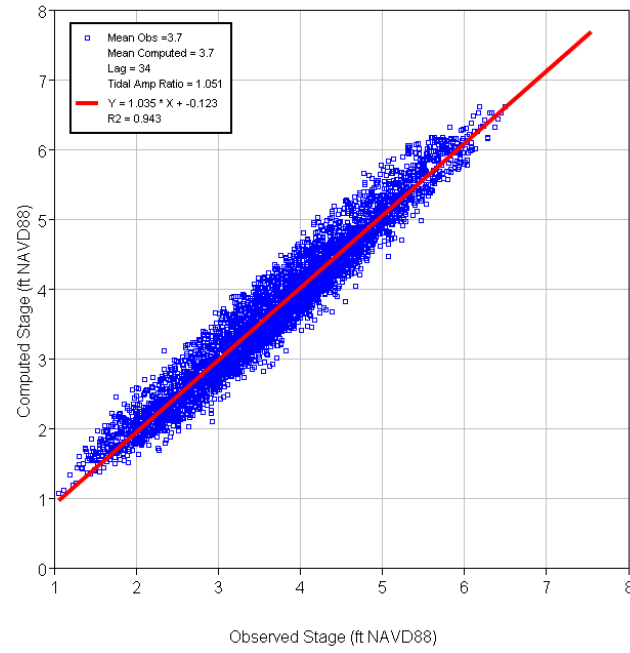
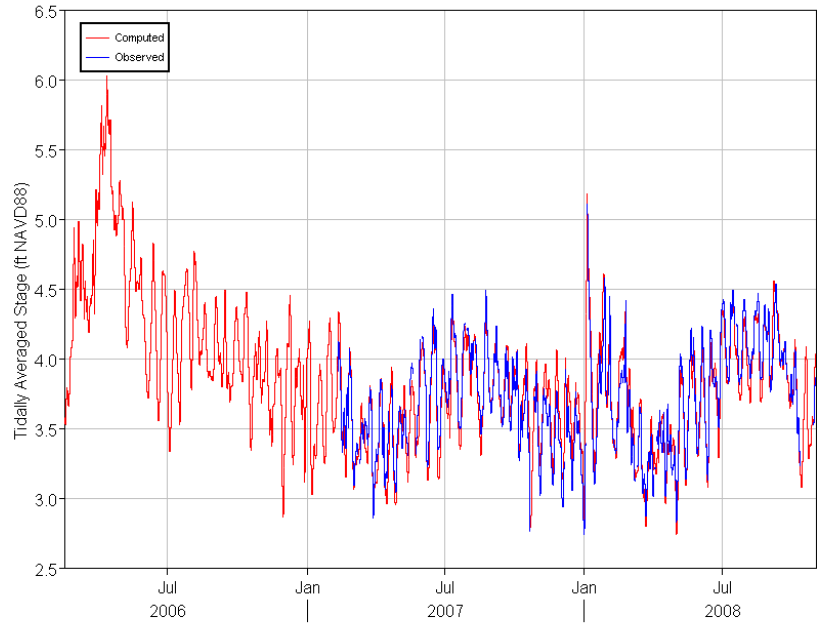
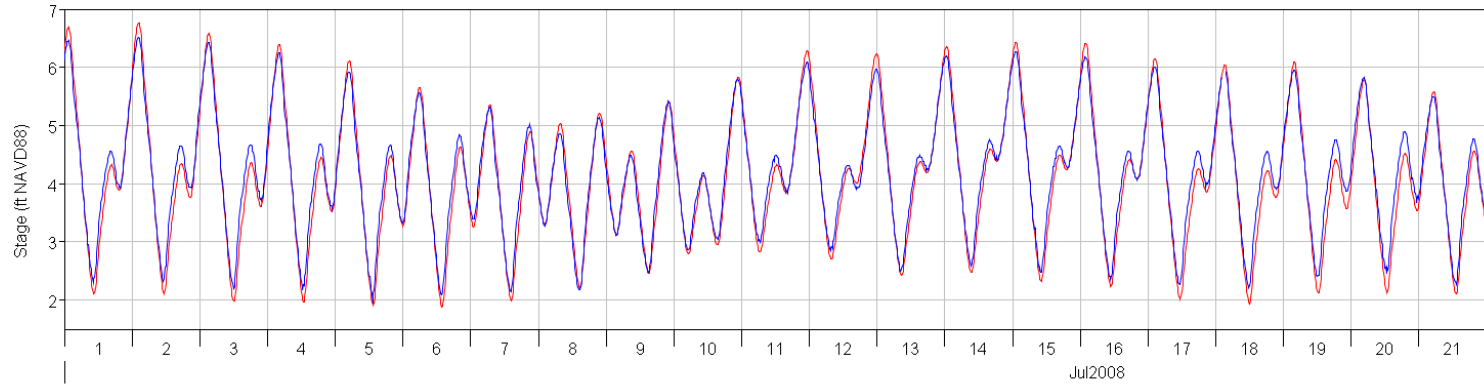
HWB - Miner Slough



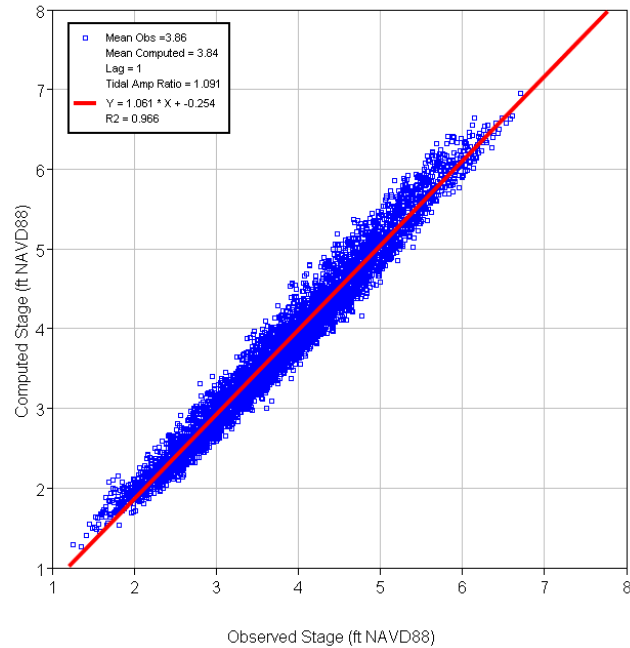
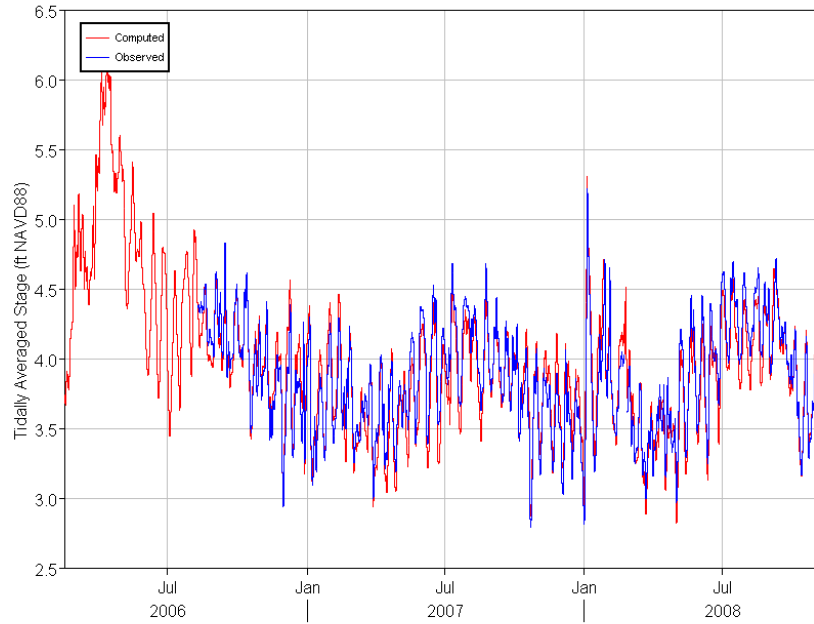
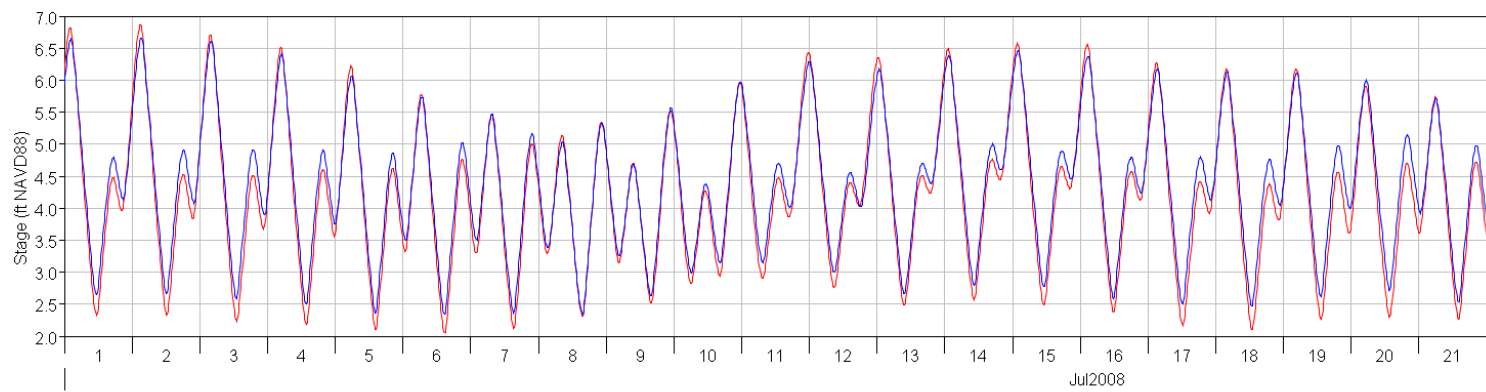
SJJ - SJR at Jersey Pt



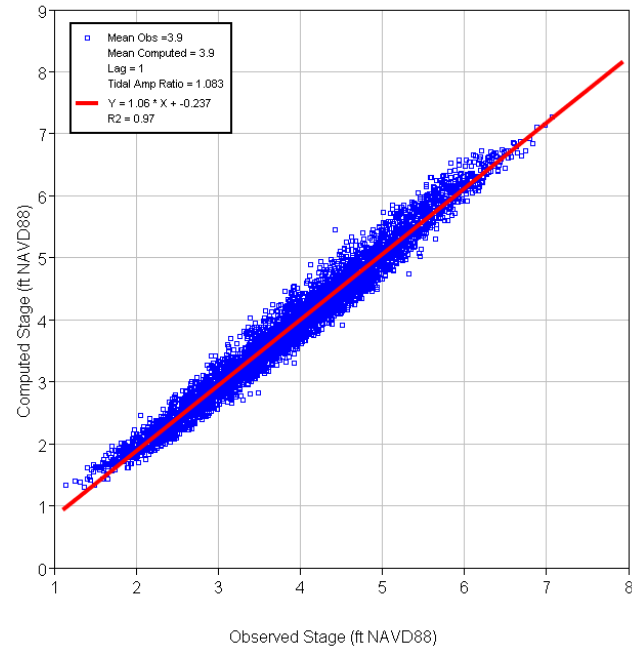
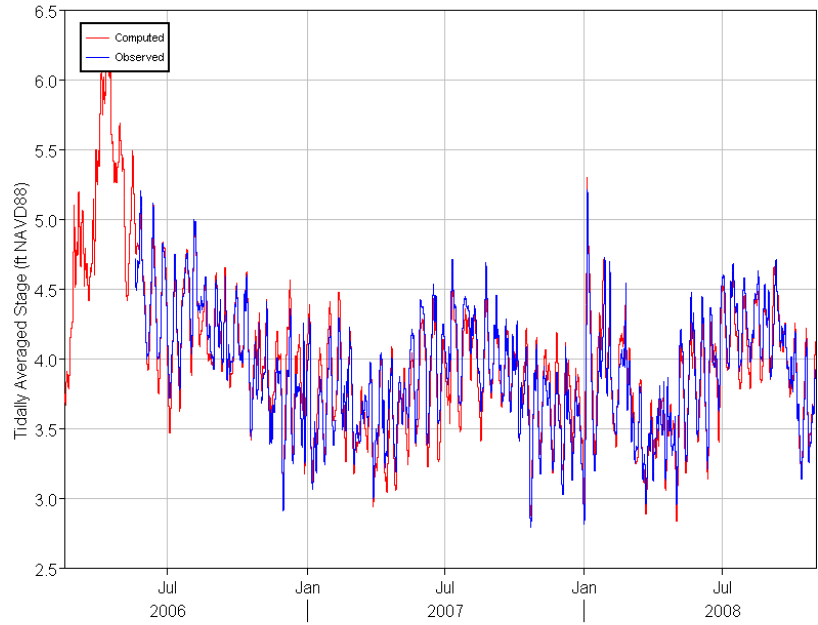
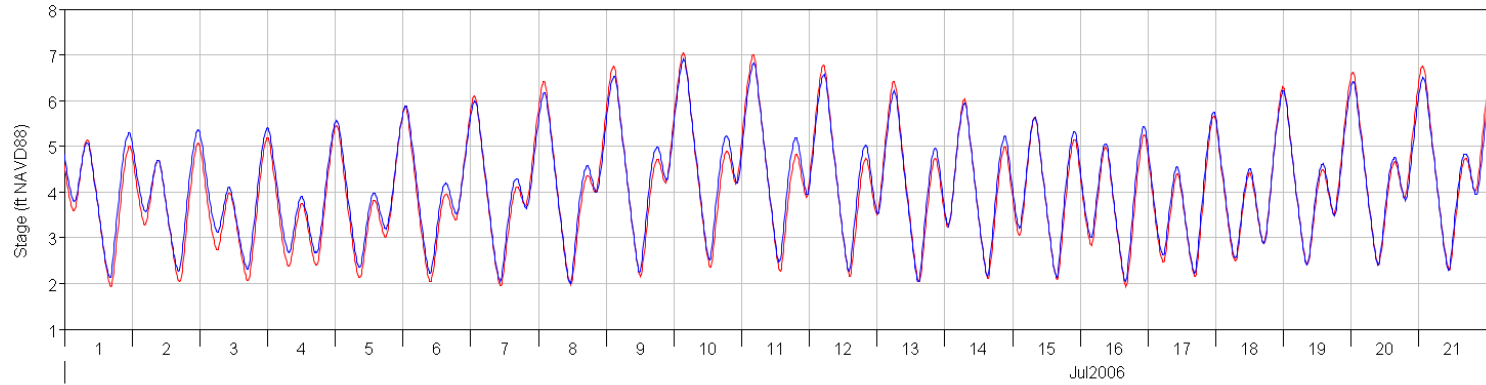
FAL - False River



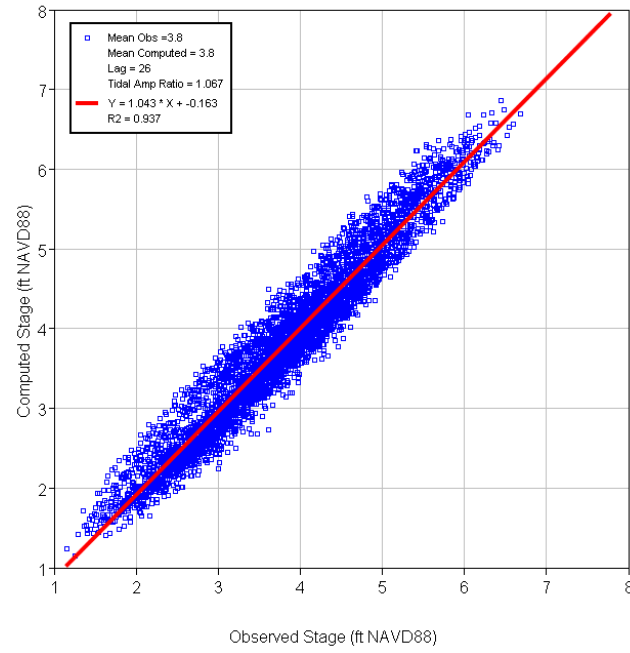
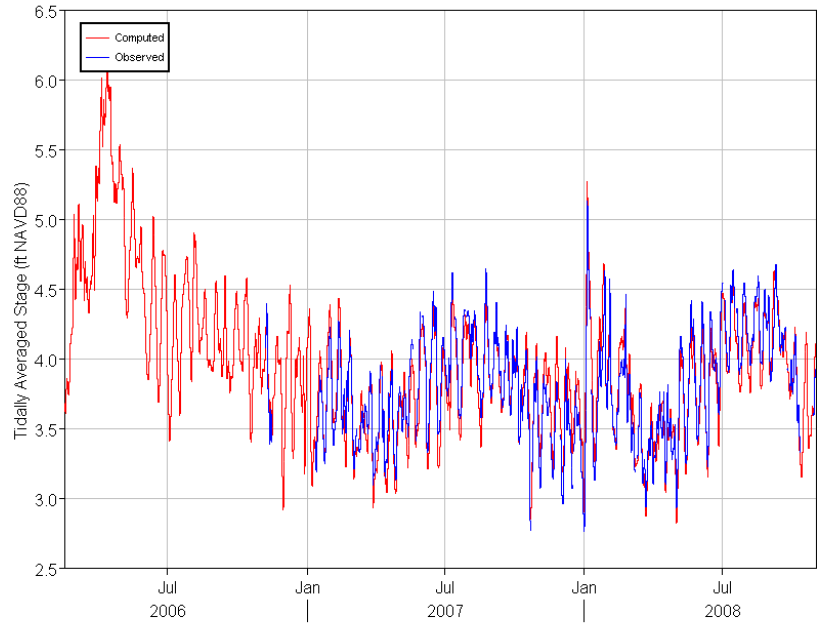
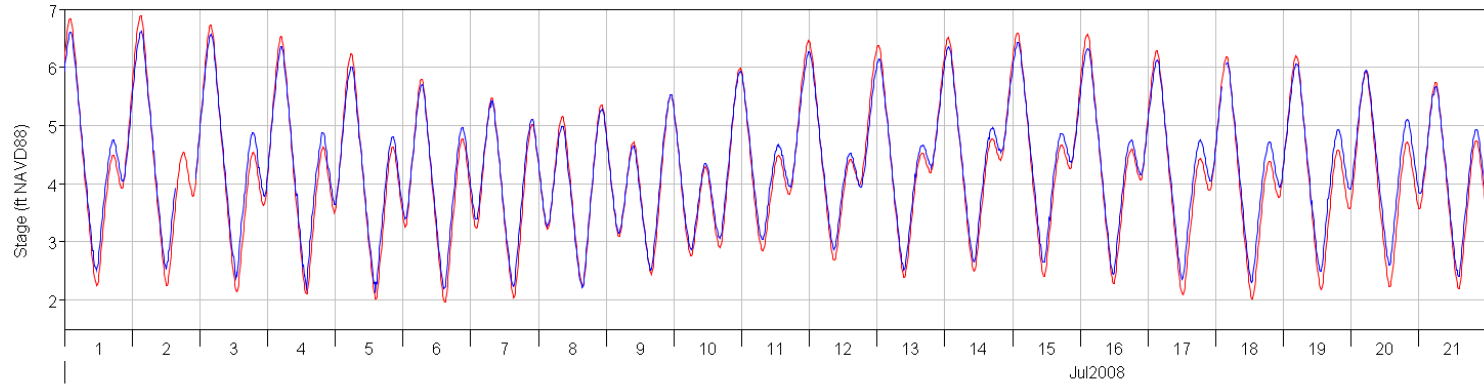
MOK - Mokelumne R at SJR



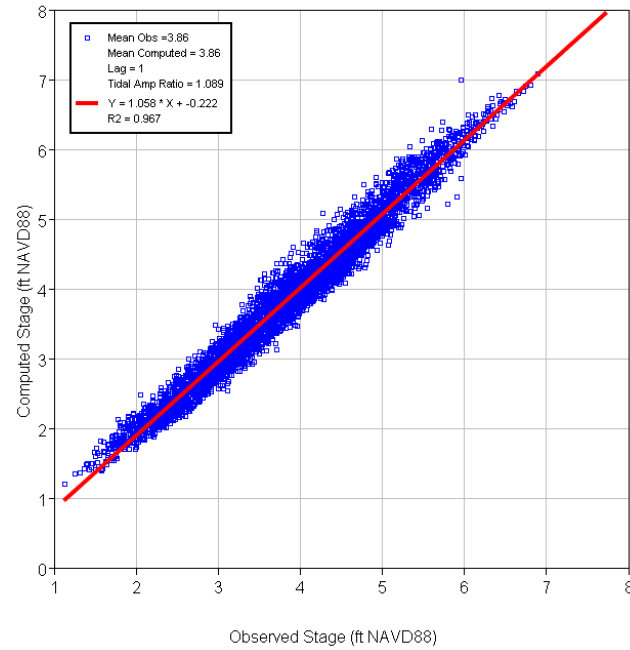
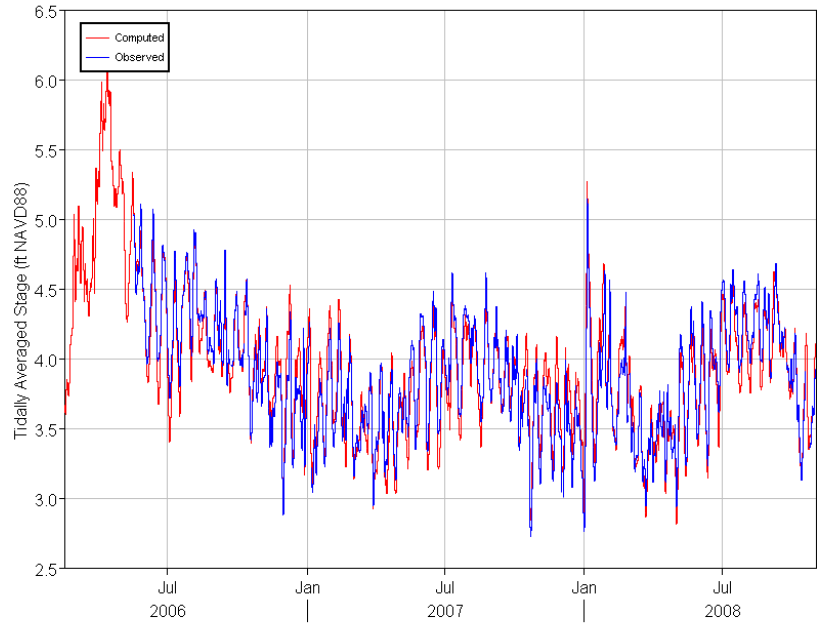
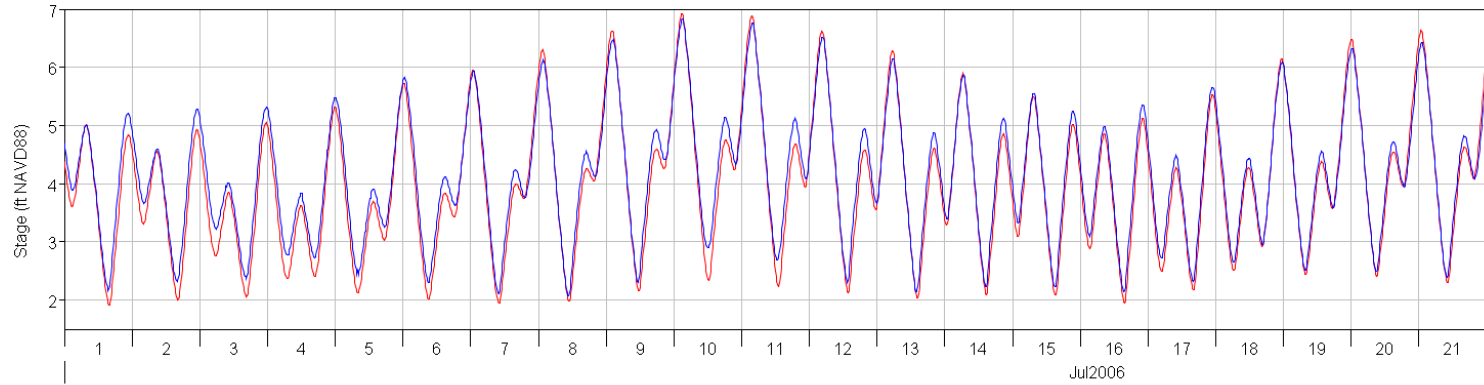
LPS - Little Potato Slough



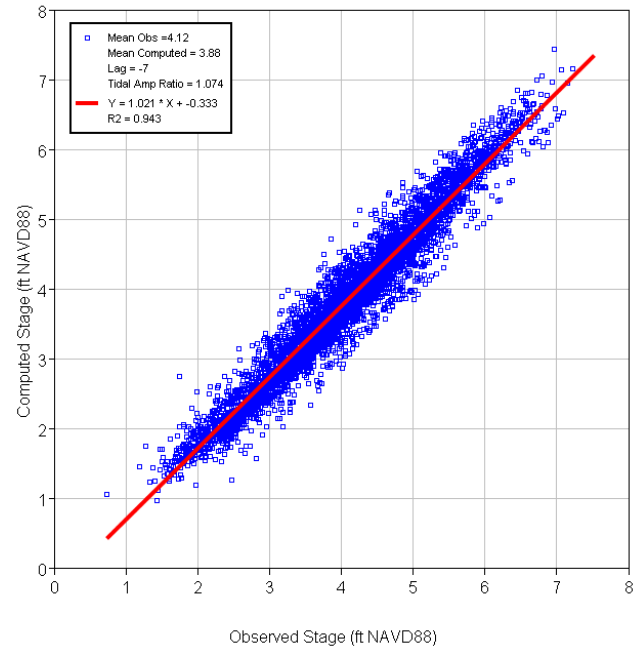
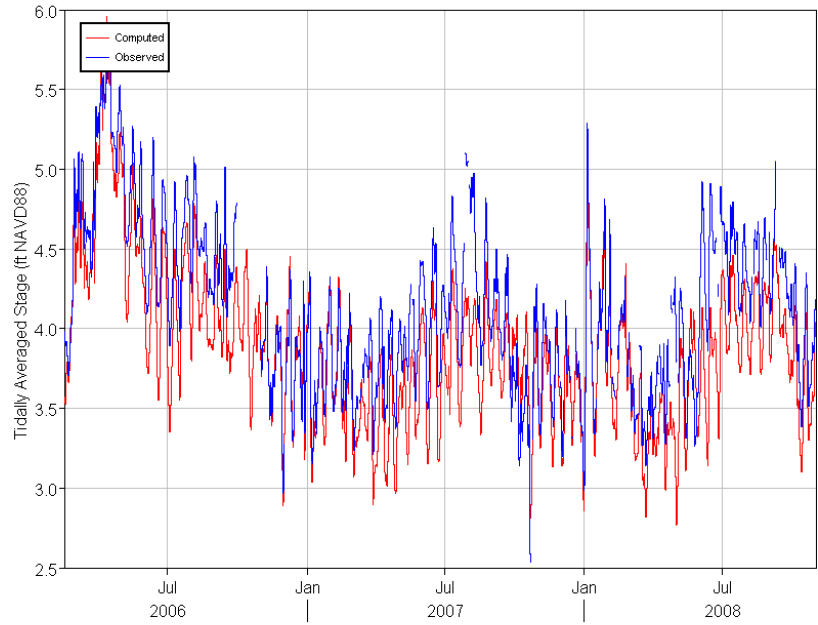
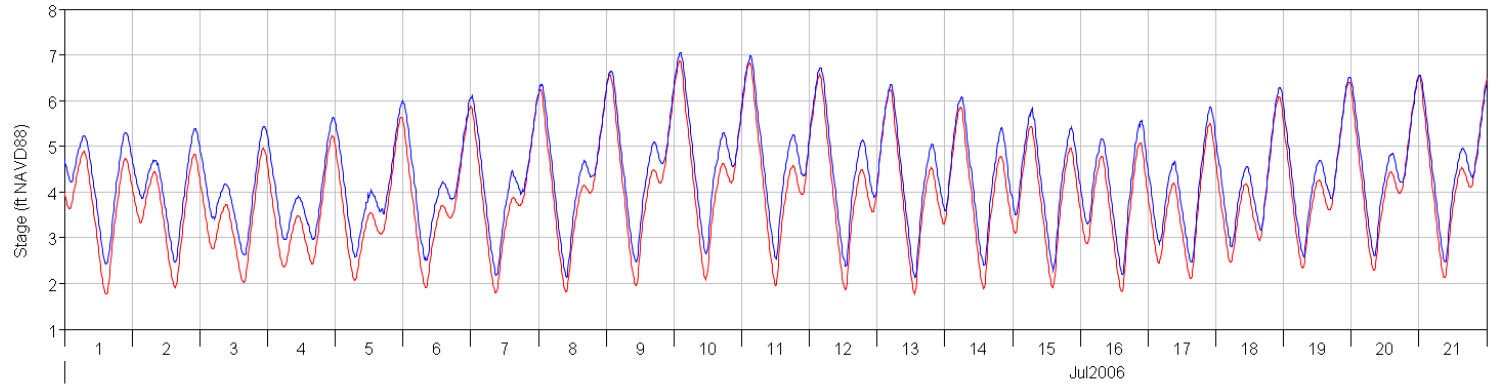
PRI - SJR at Prisoners Pt



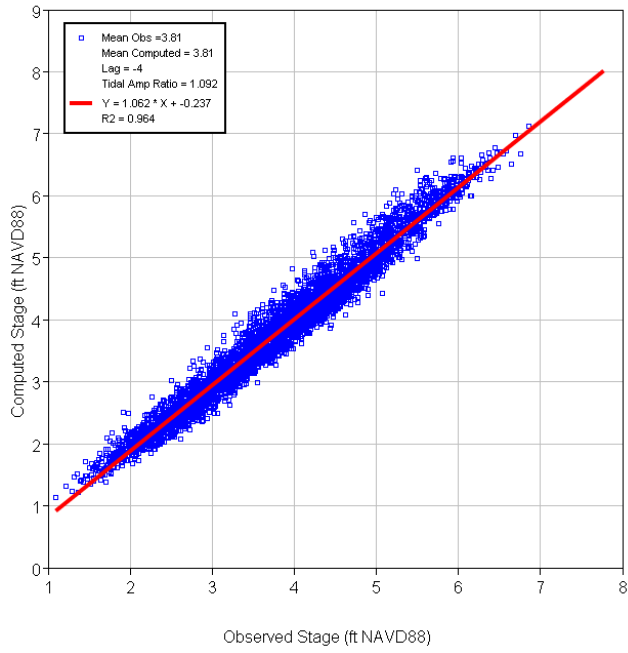
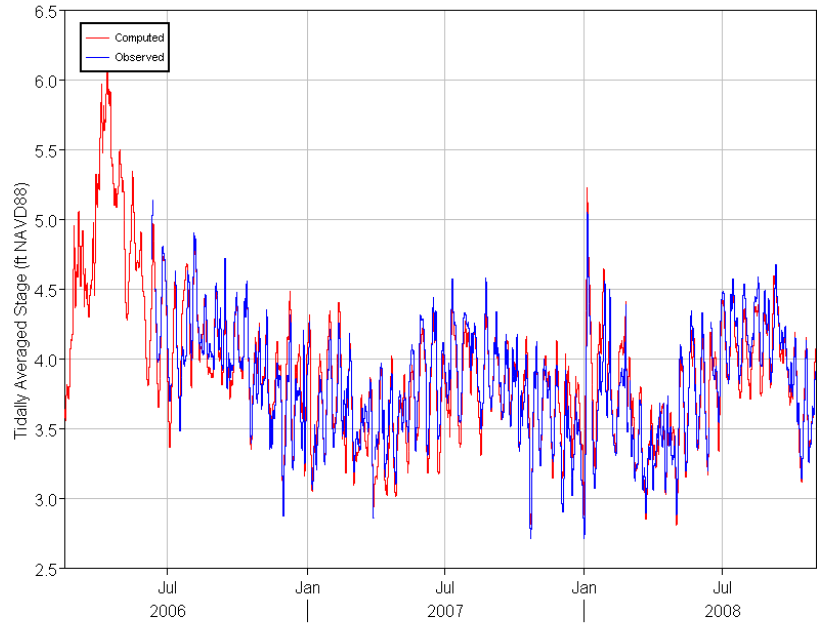
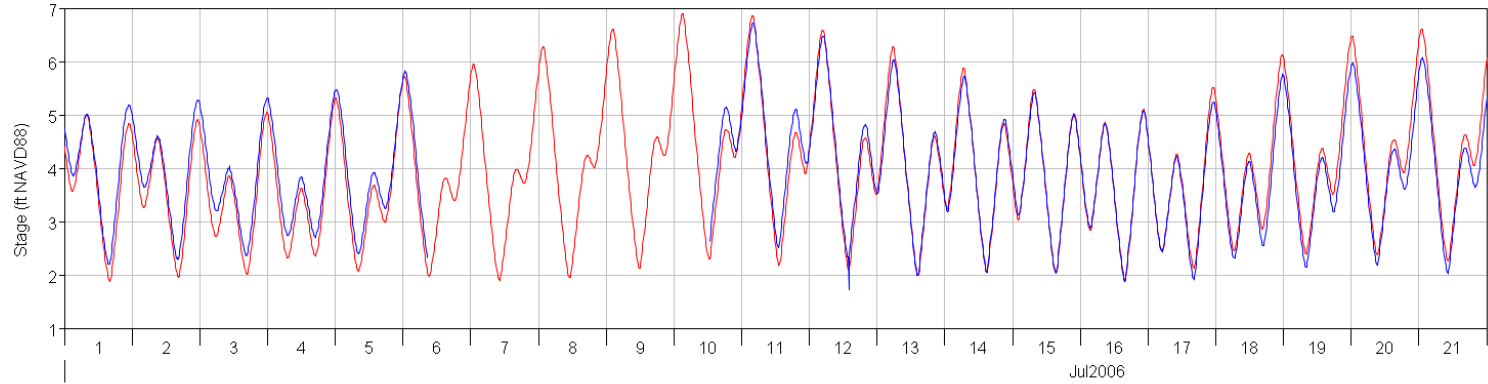
OSJ - Old River at Franks Tract



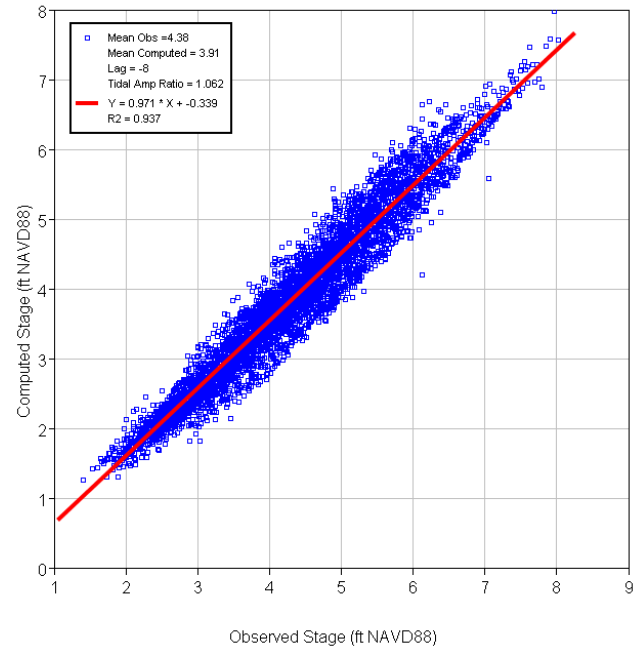
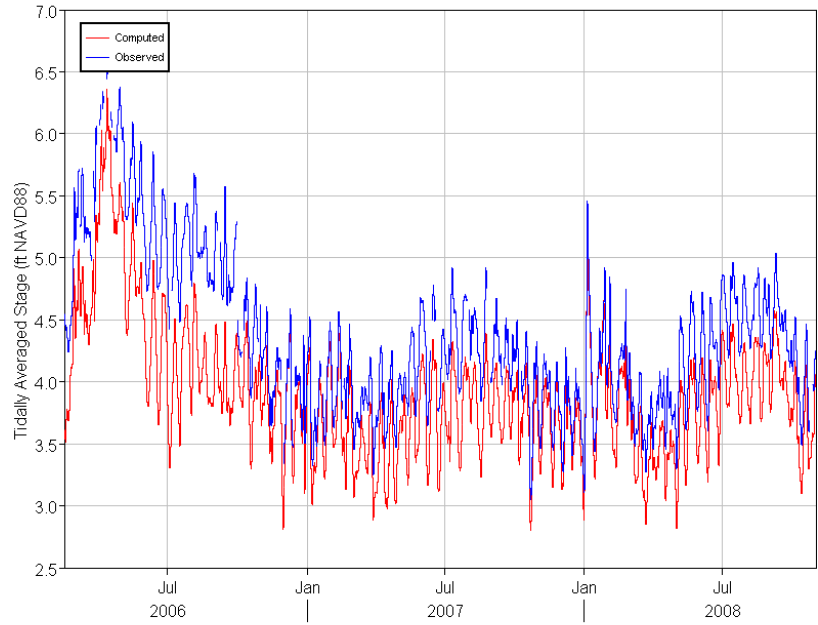
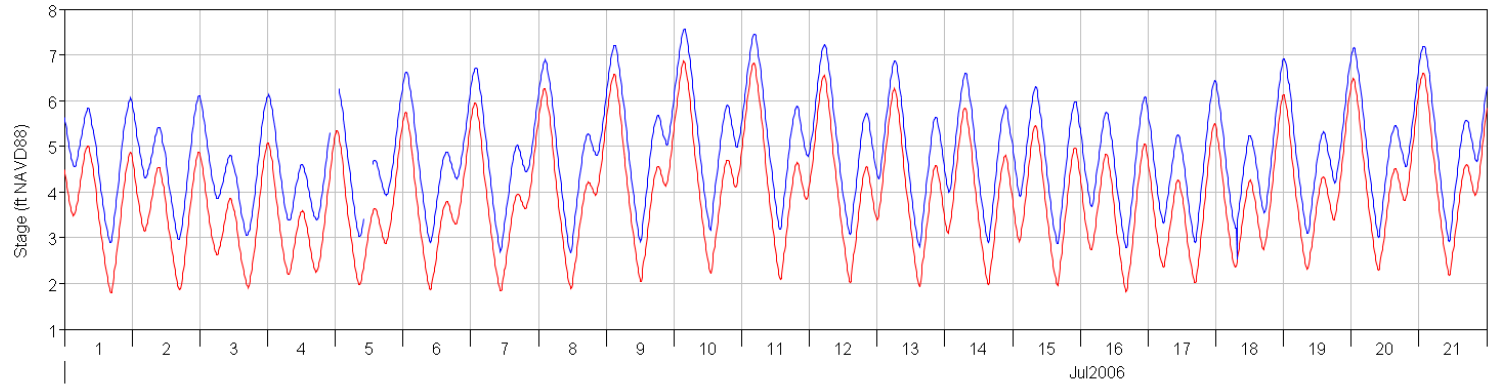
DSJ - Dutch Slough



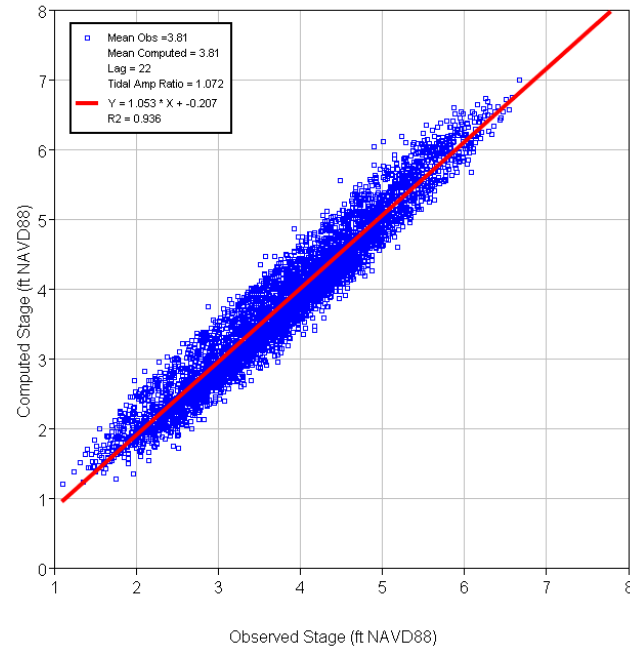
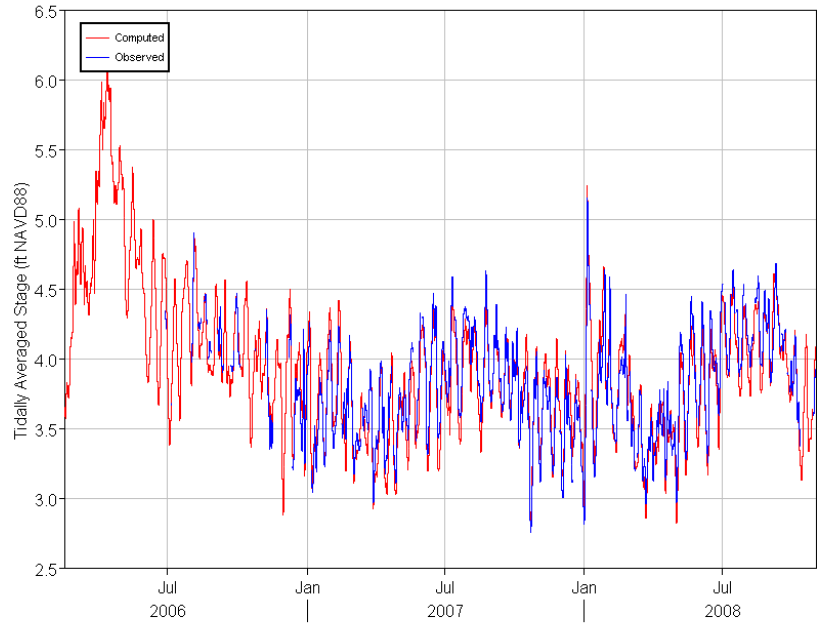
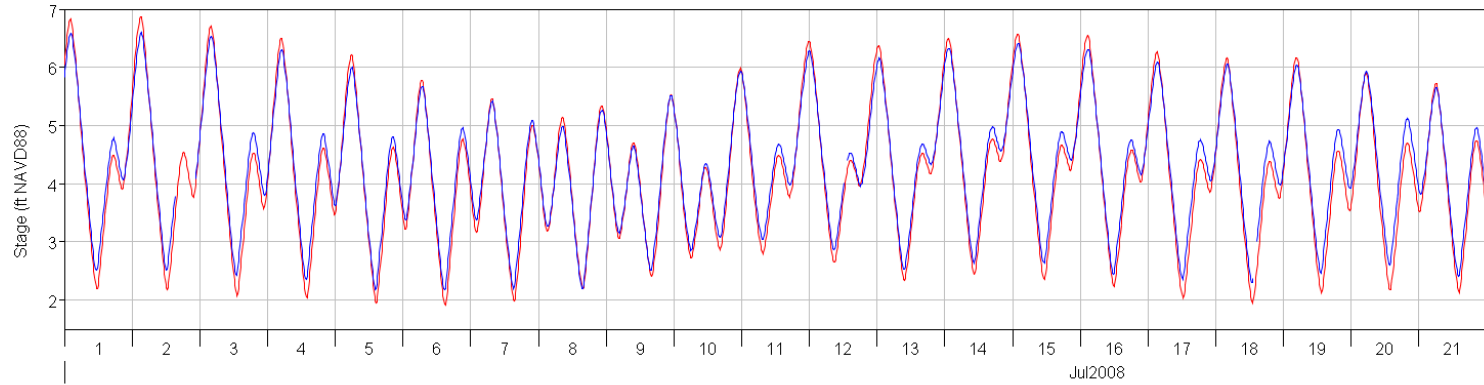
HOL - Holland Cut



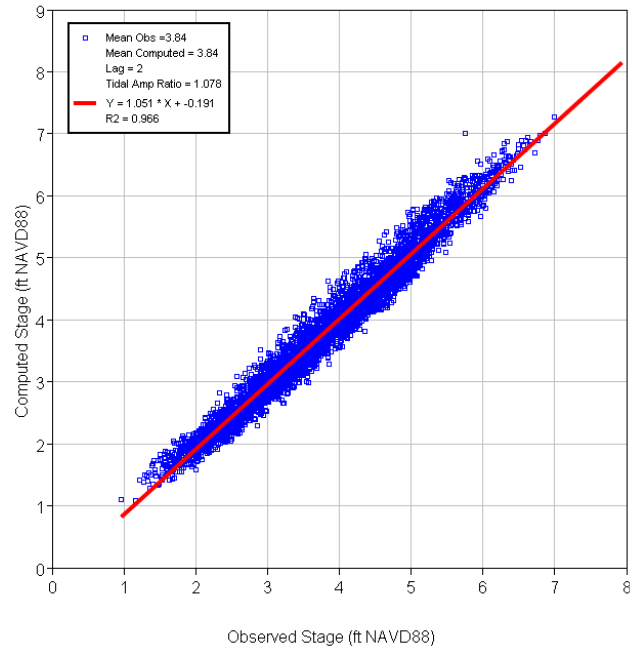
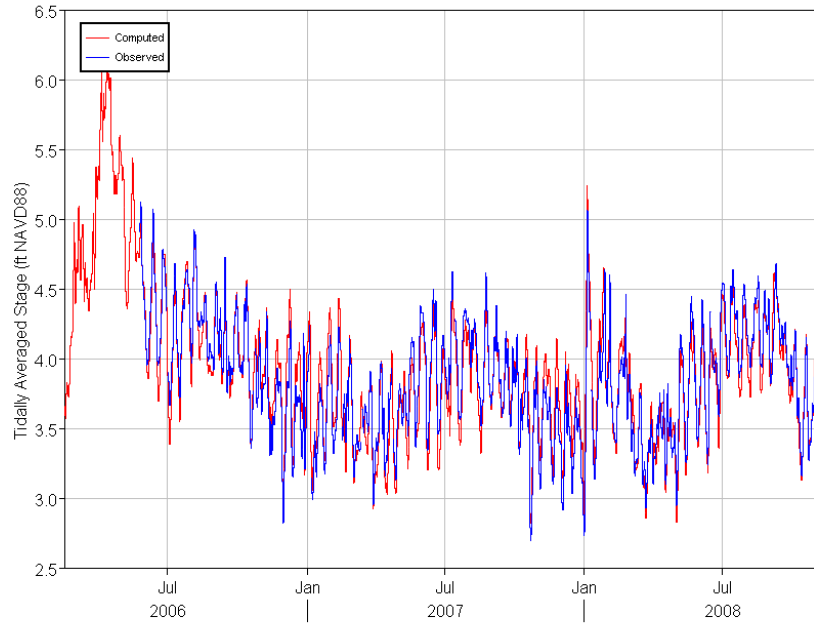
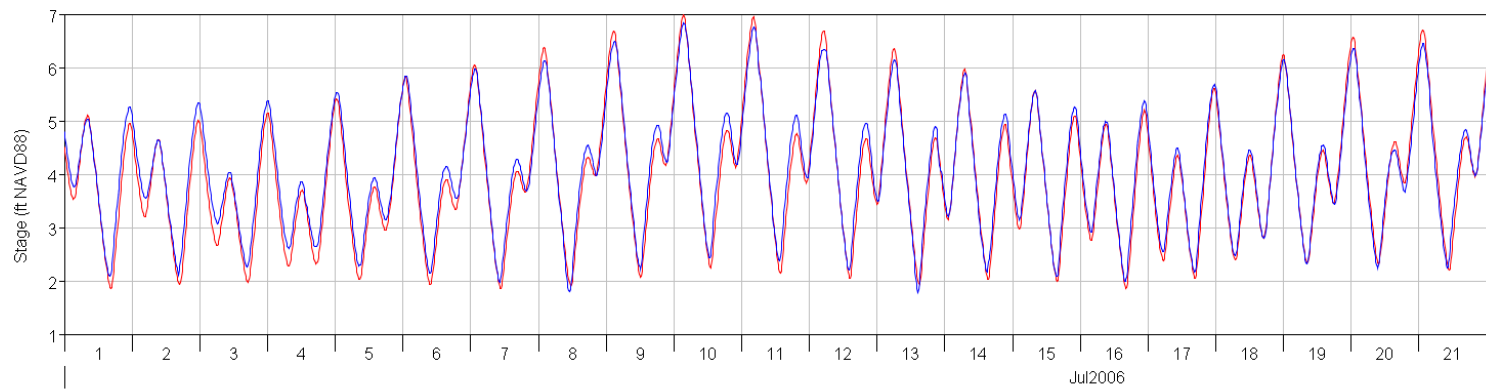
RSL - Rock Slough



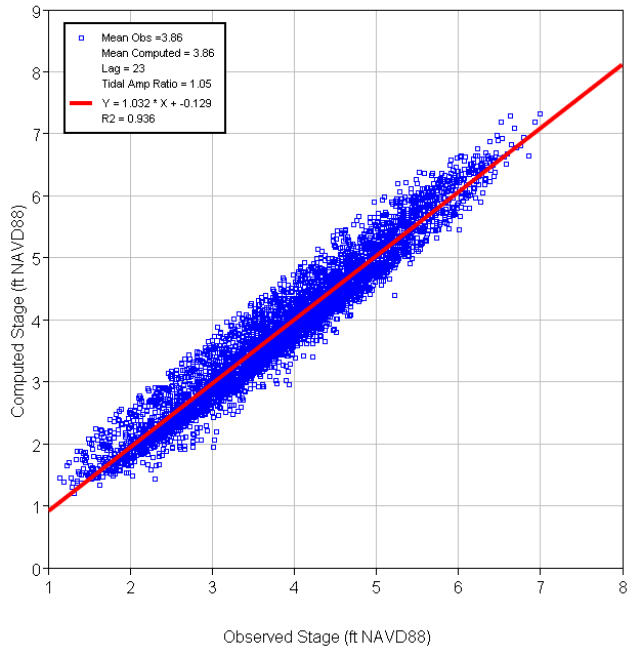
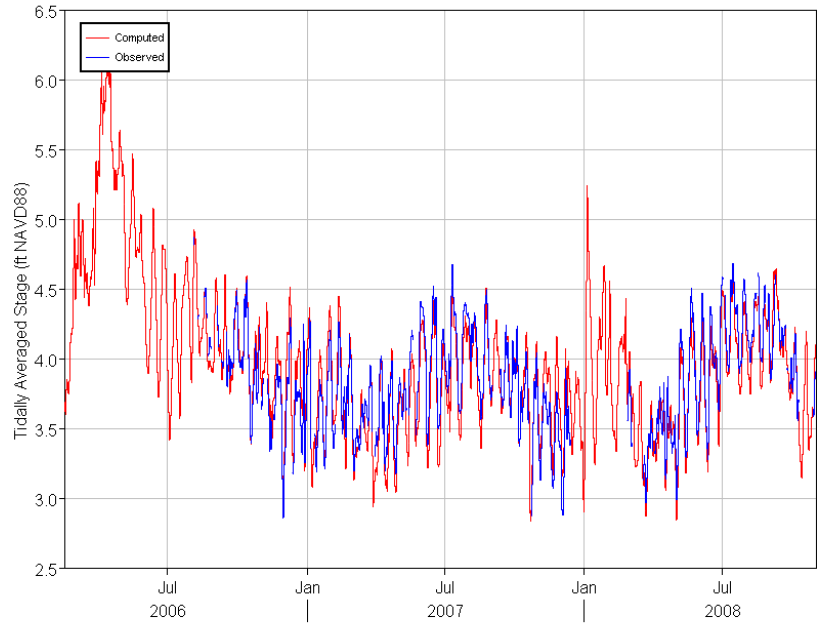
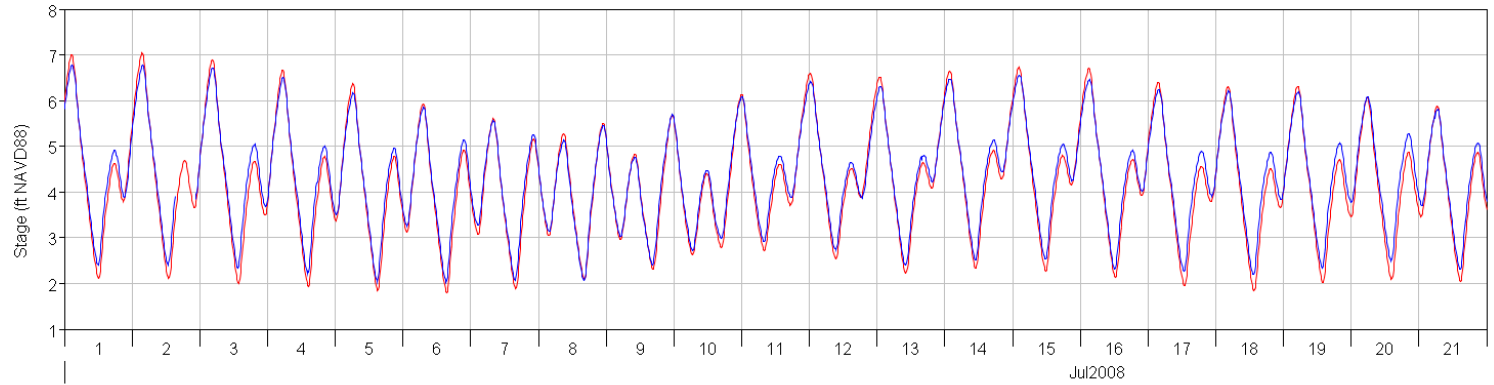
ORQ - Old River at Quimby



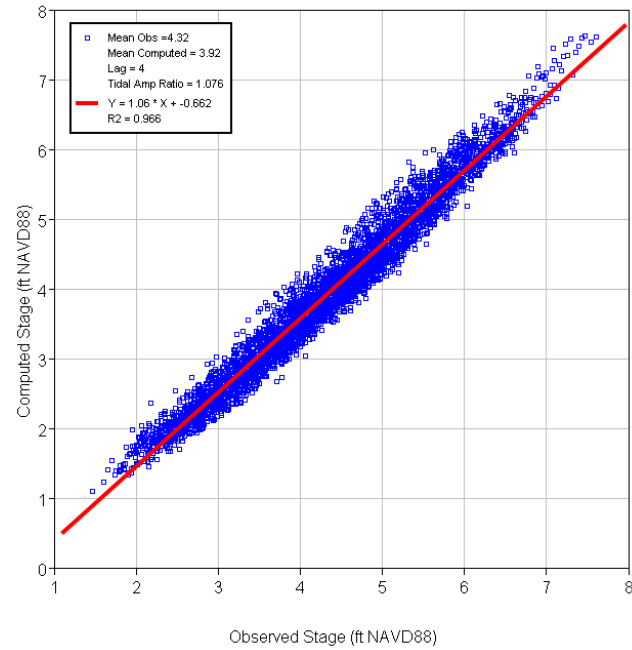
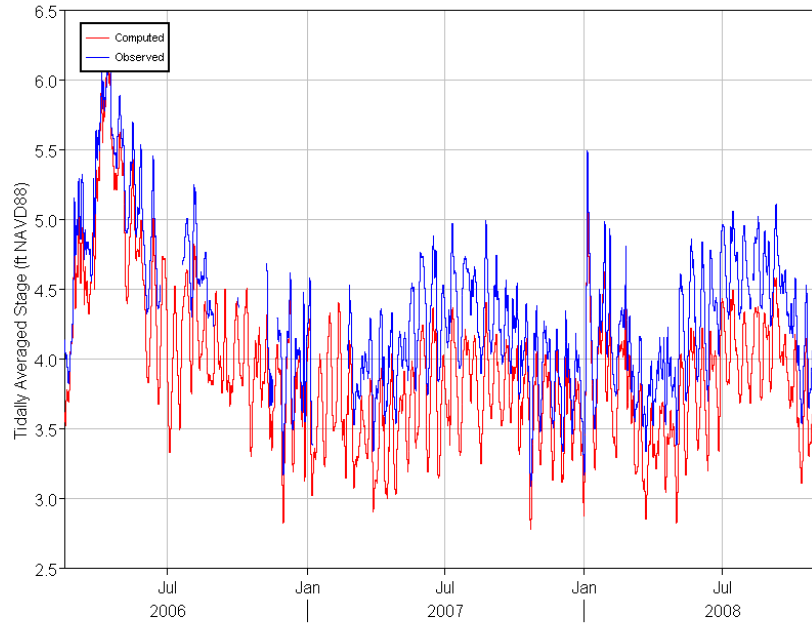
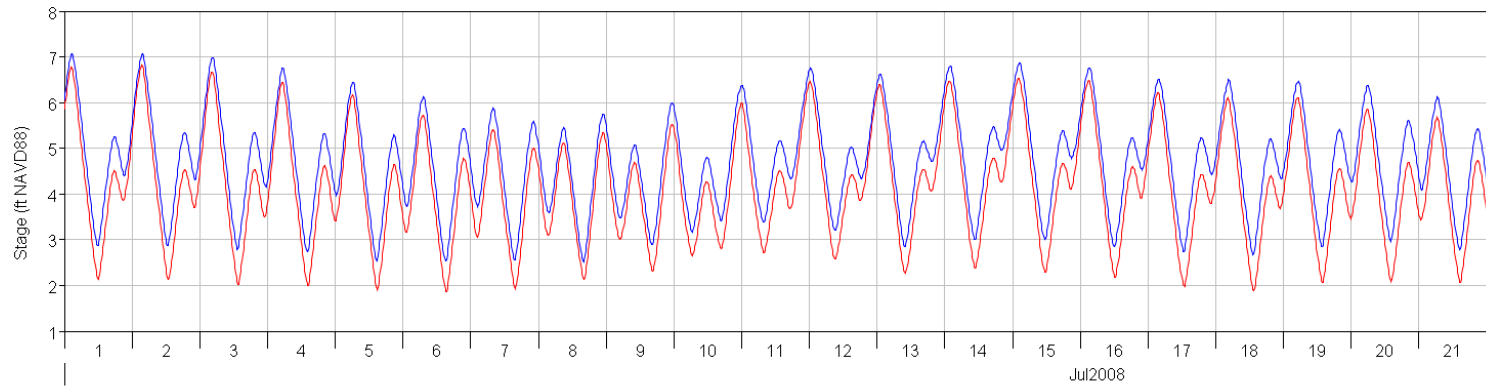
HLT - Middle River at Holt



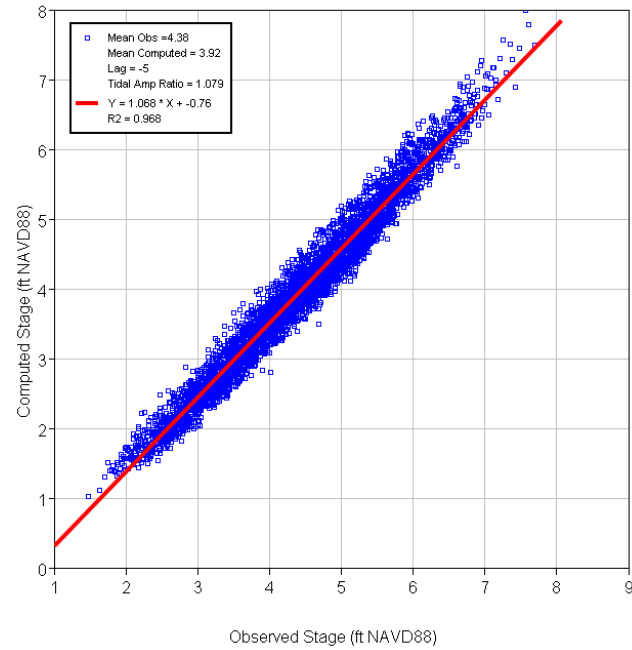
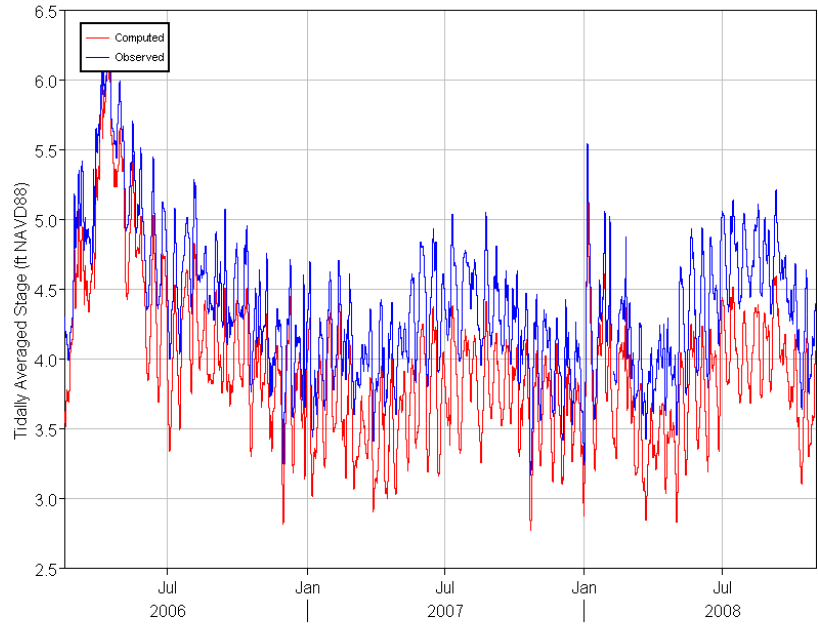
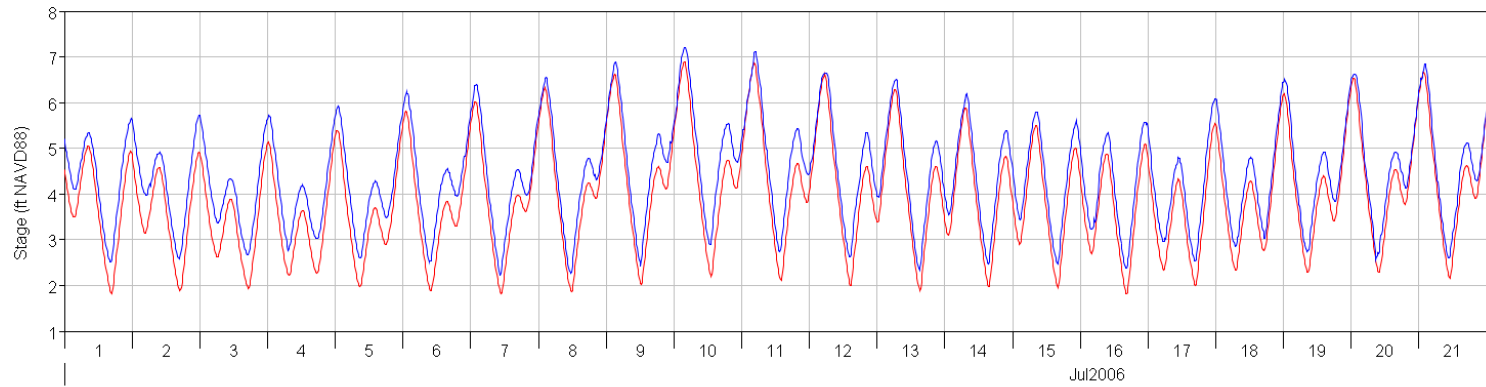
TRN - Turner Cut



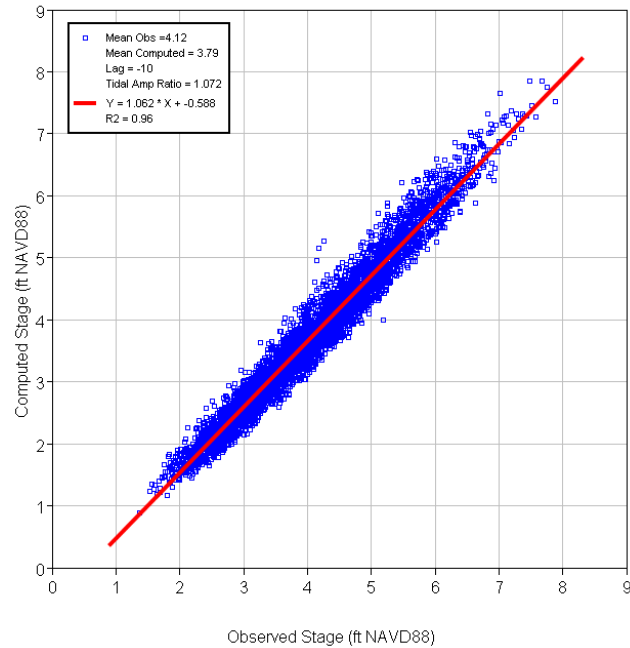
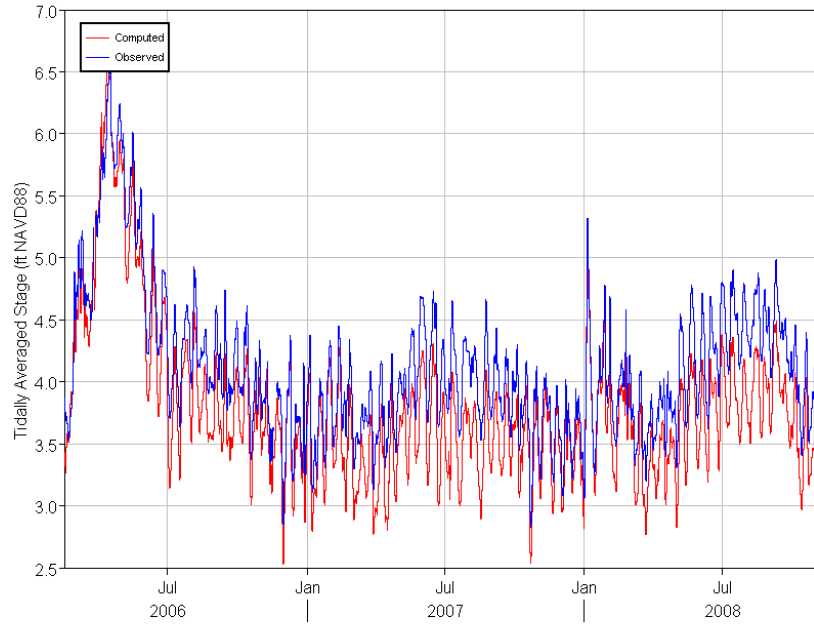
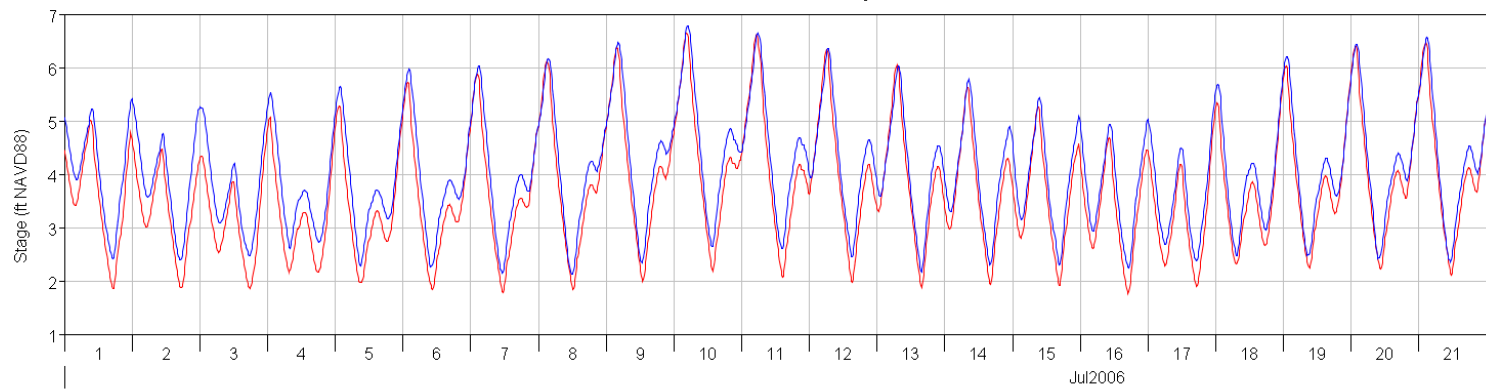
OBI - Old River at Bacon



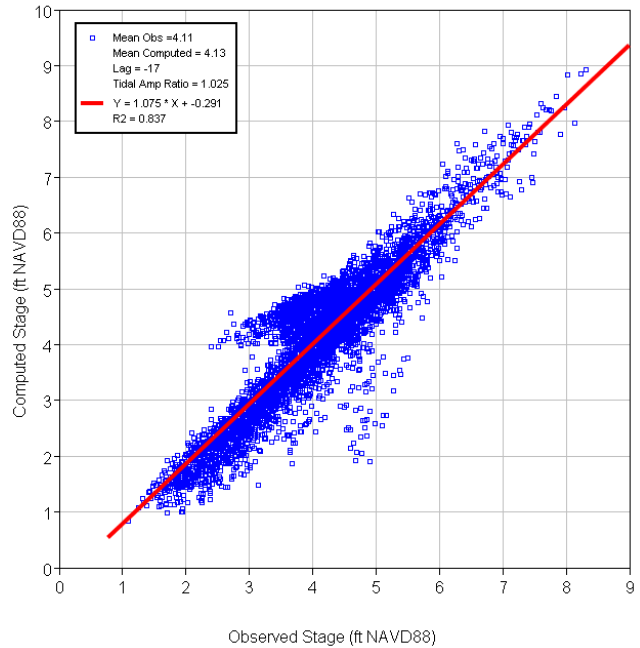
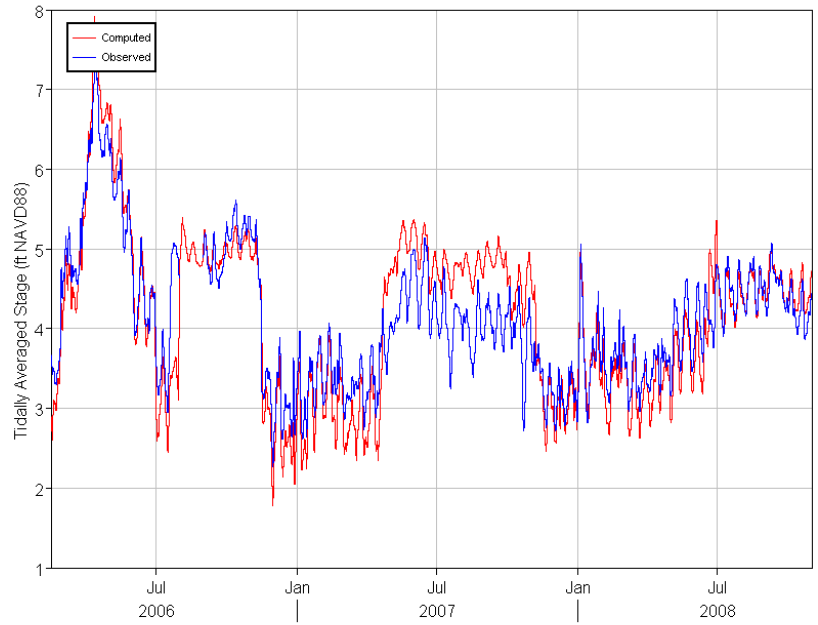
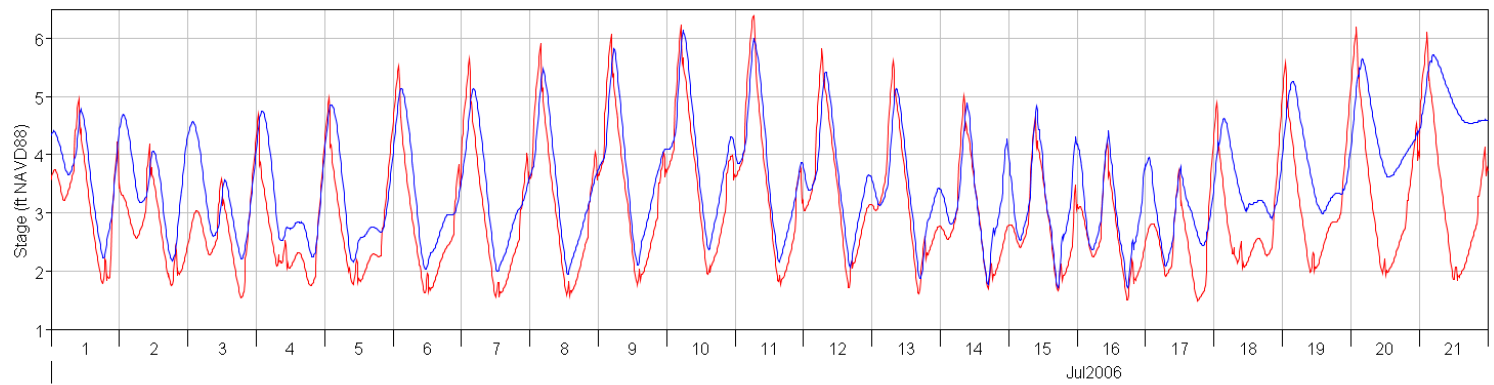
MDM - Middle River at Middle



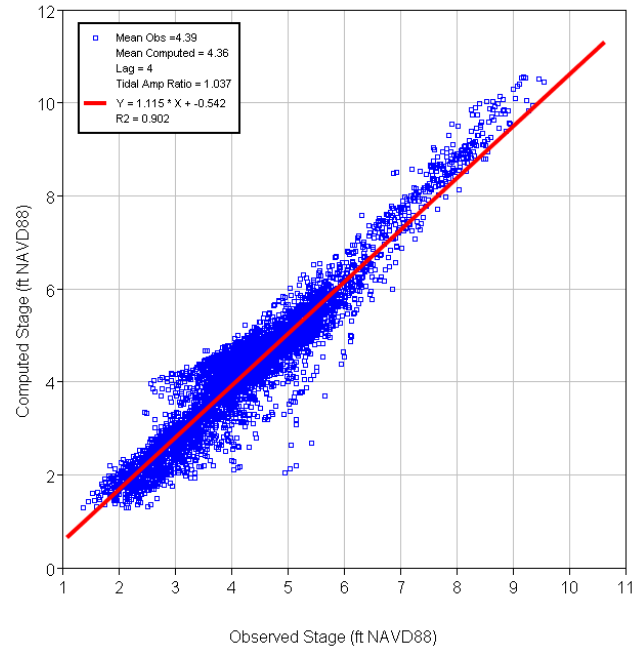
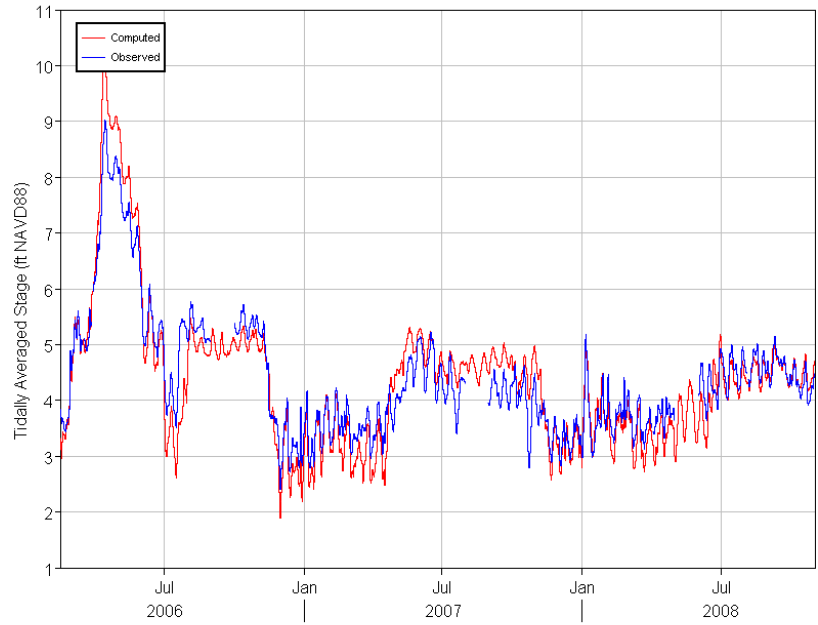
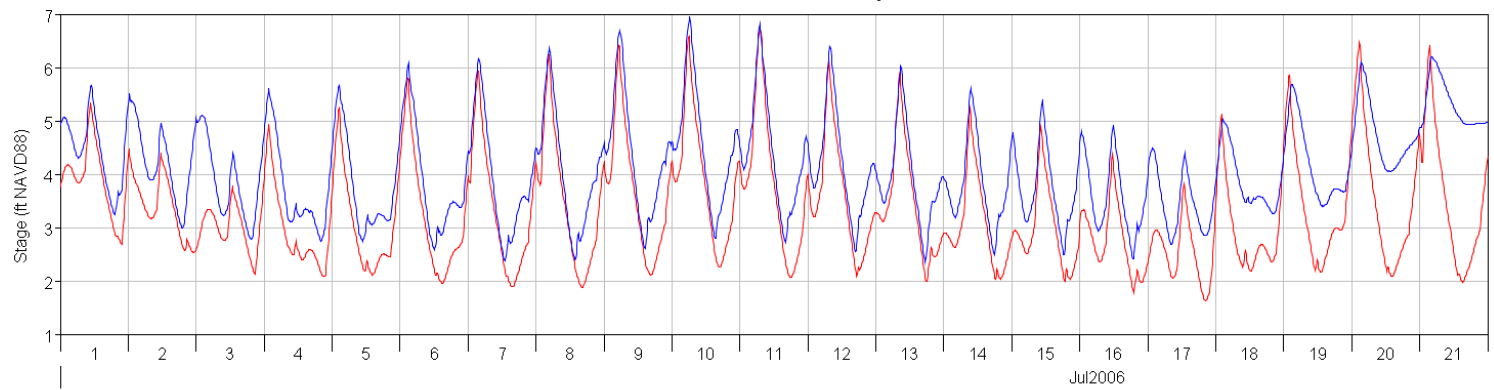
OH4 - Old River at Hwy4



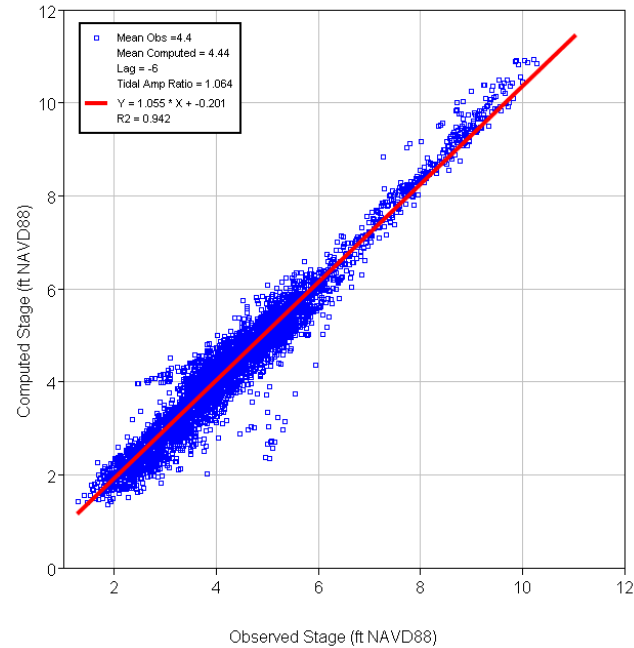
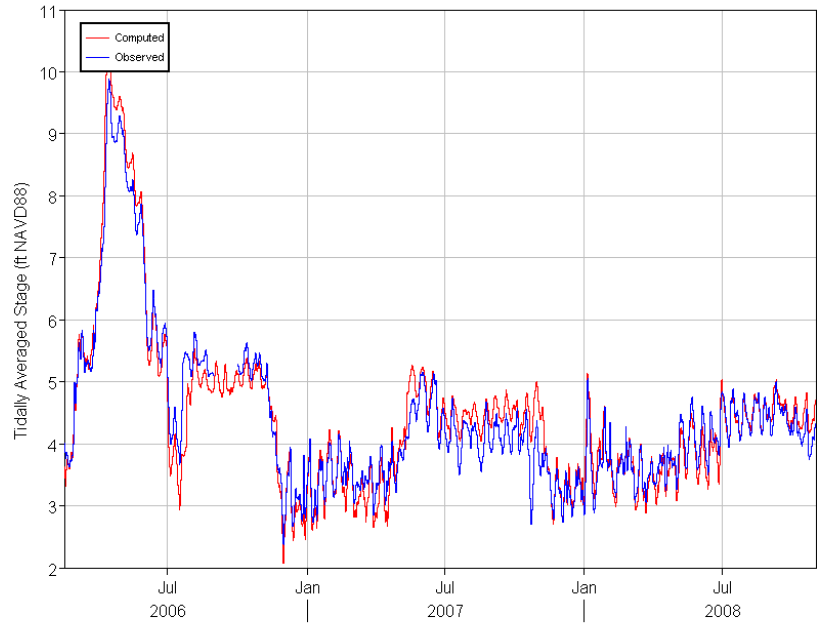
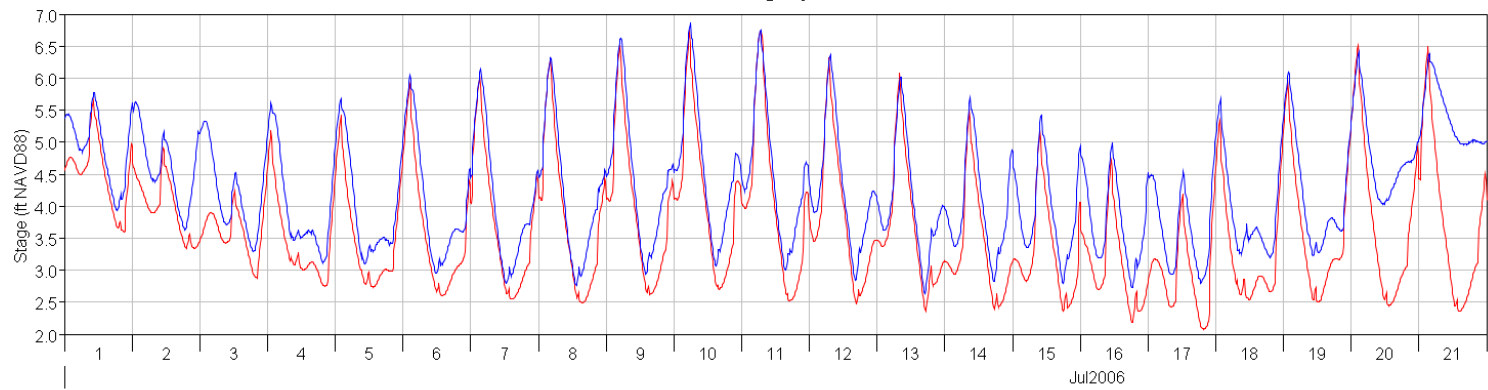
ODM - Old River at DMC



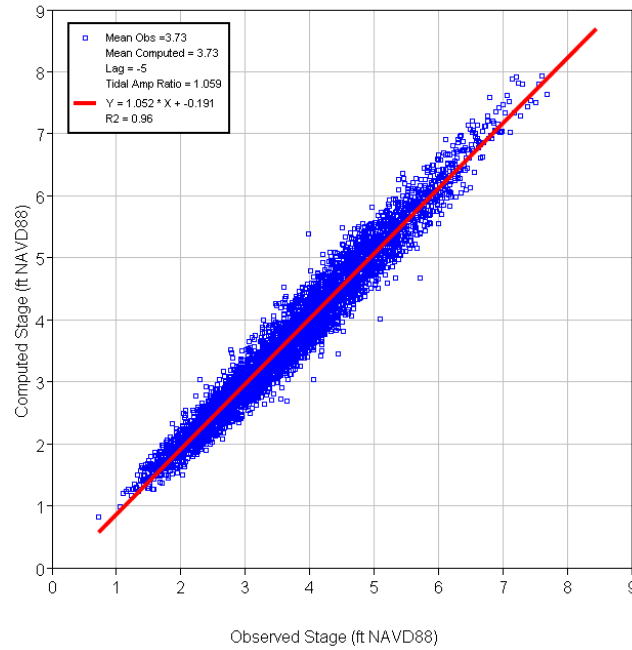
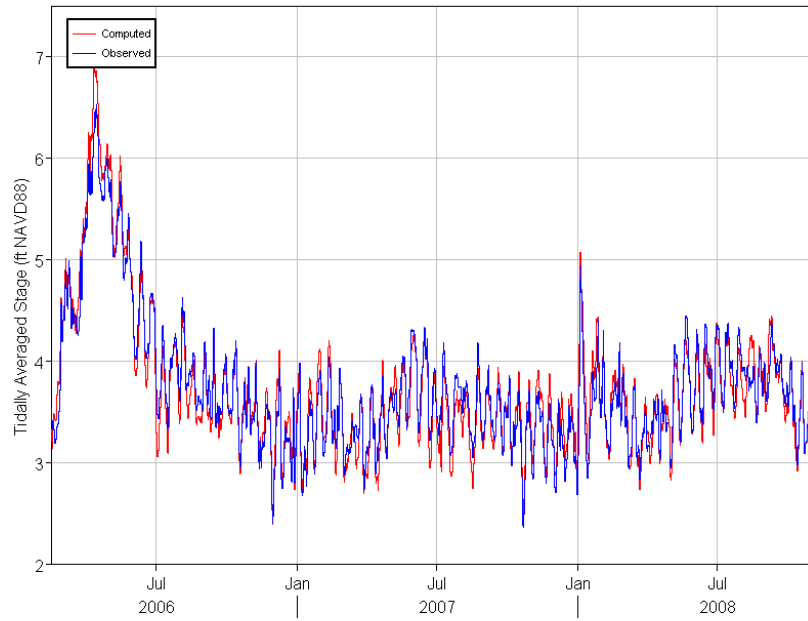
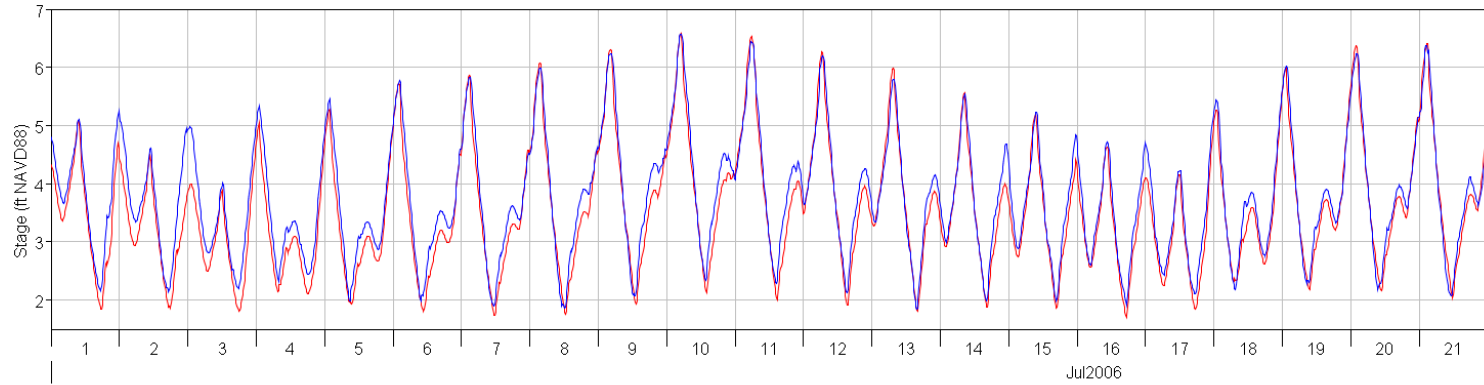
OLD - Old River at Tracy



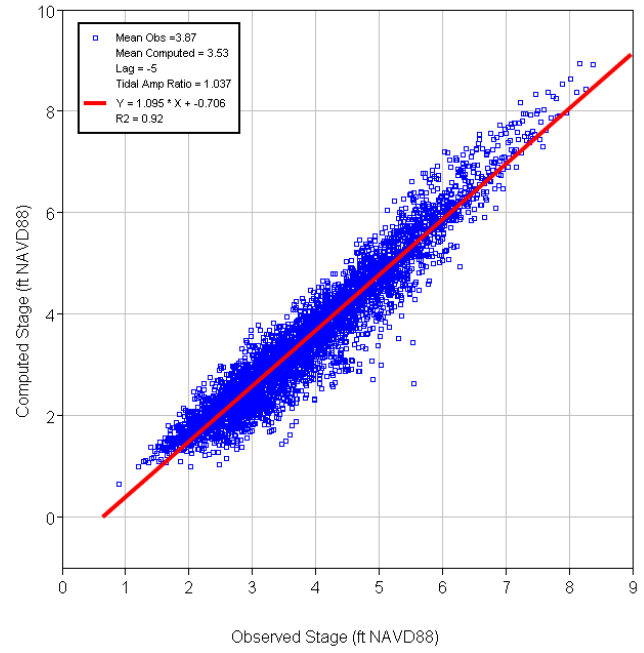
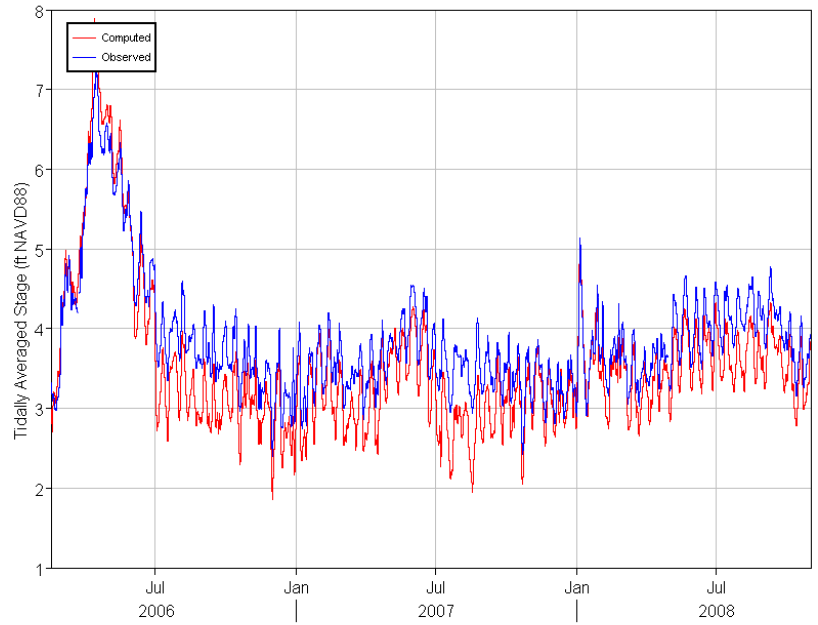
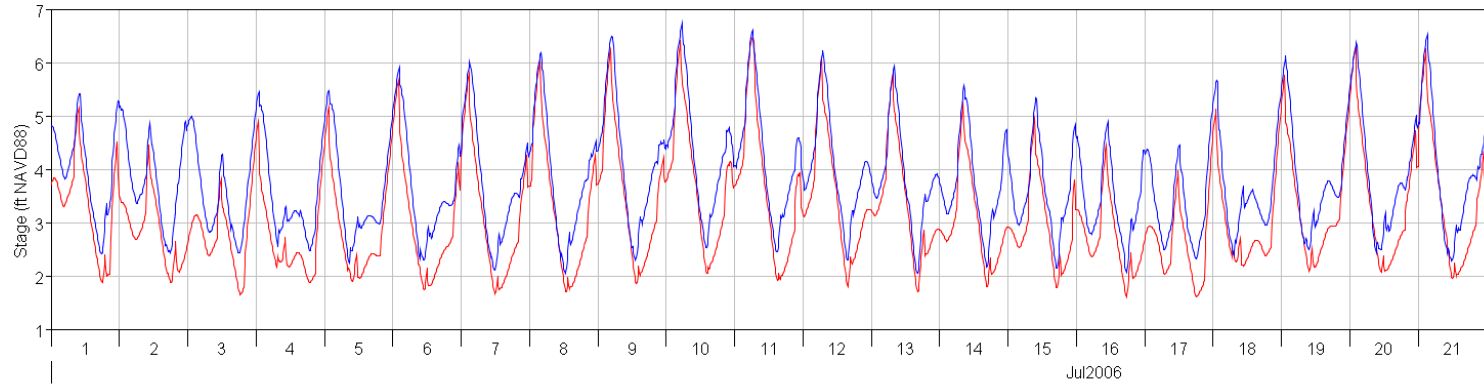
DGL - Doughty Cut



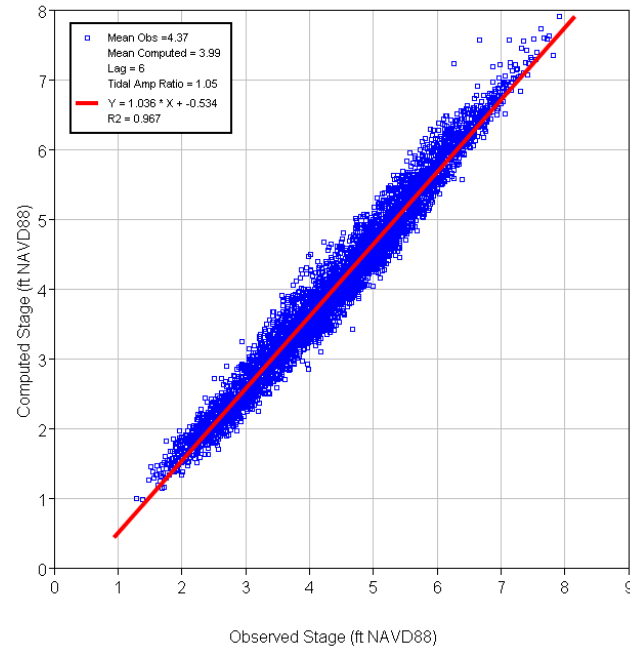
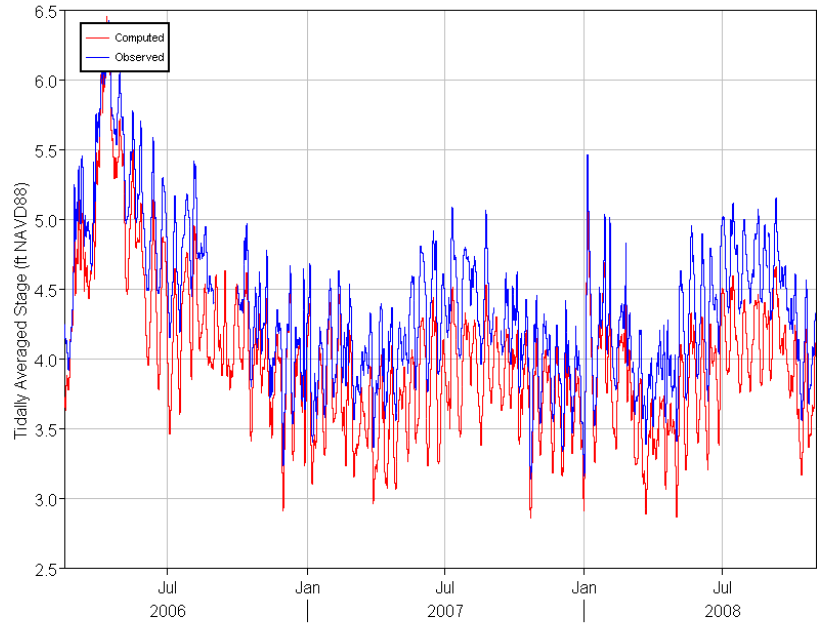
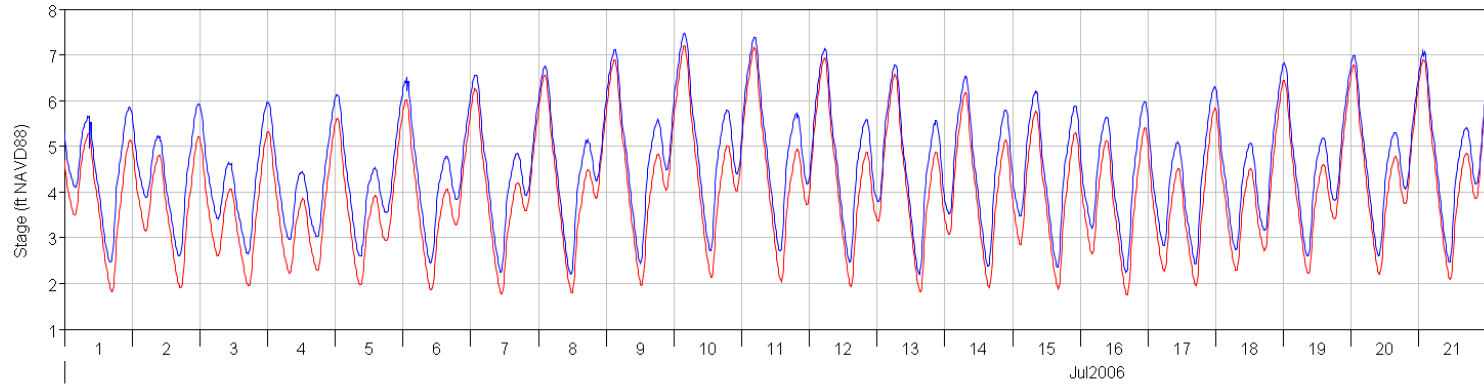
VCU - Victoria Canal



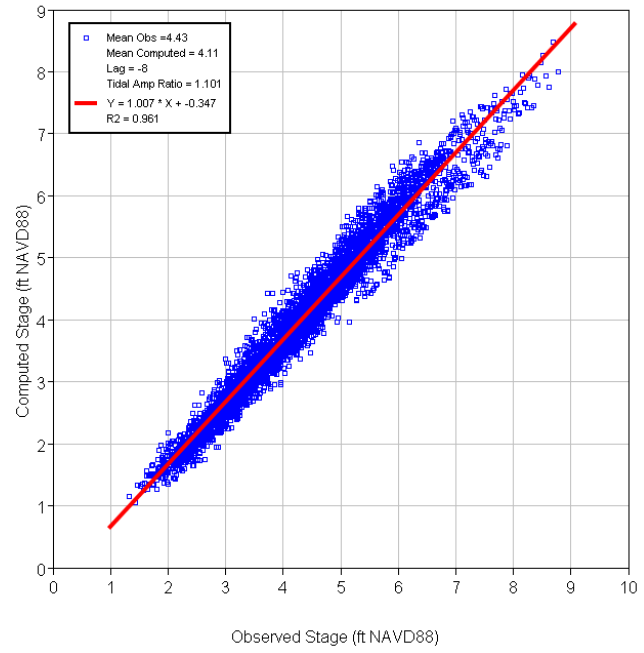
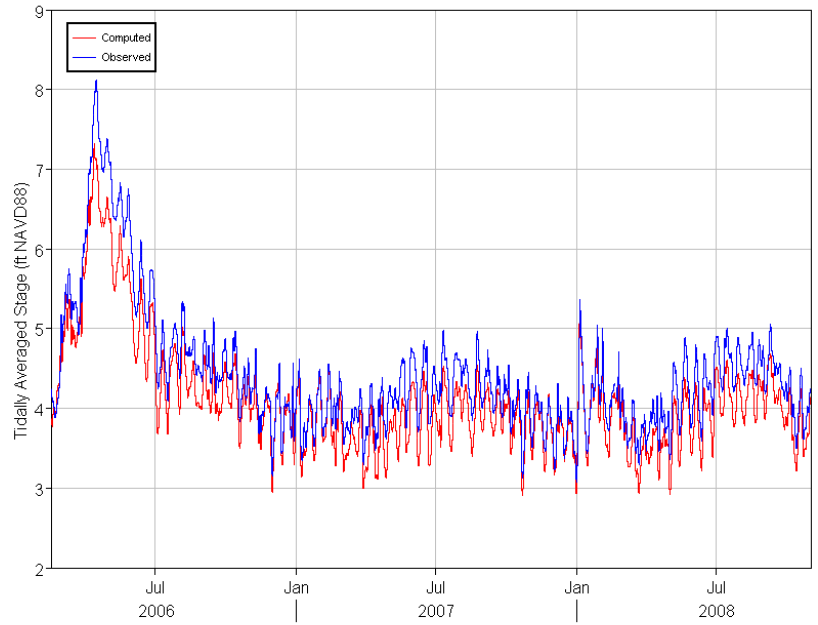
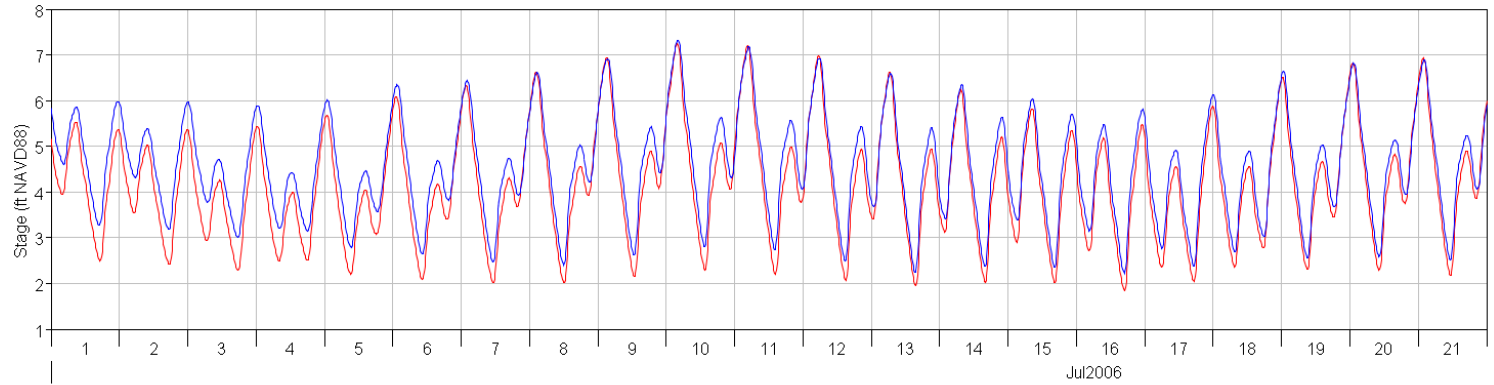
GLC - Grantline Canal near Tracy



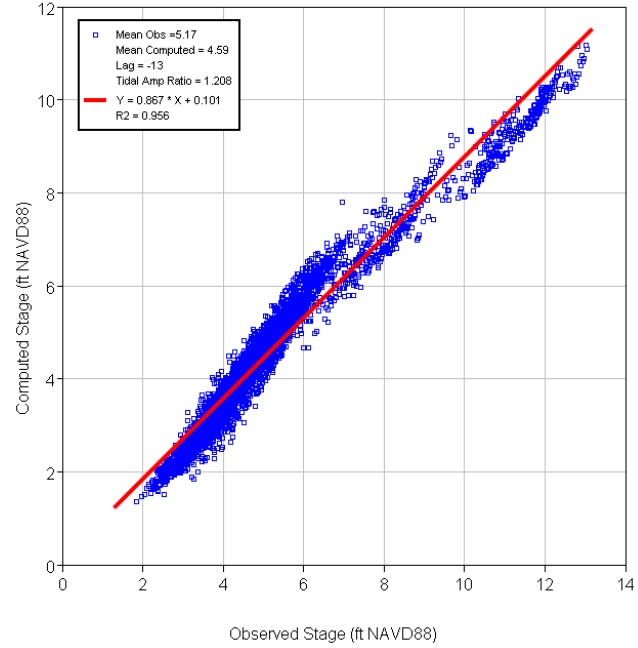
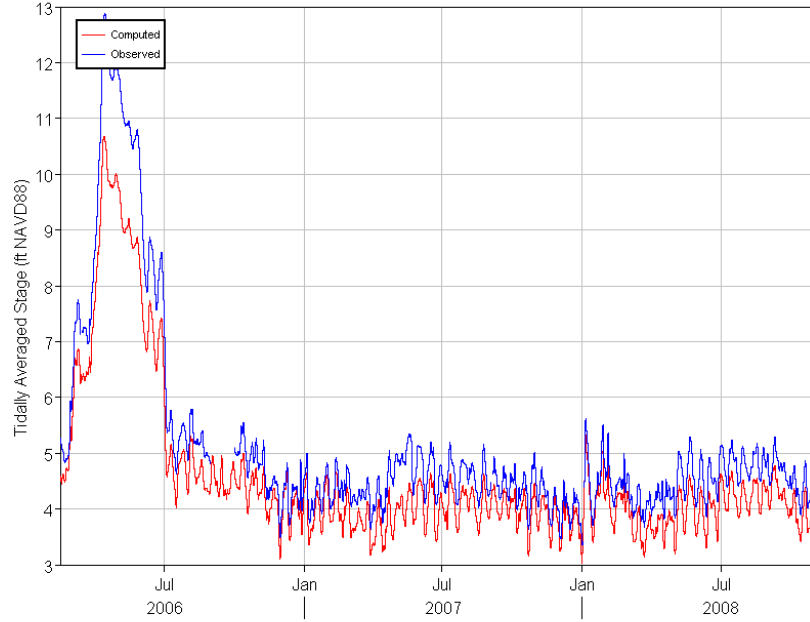
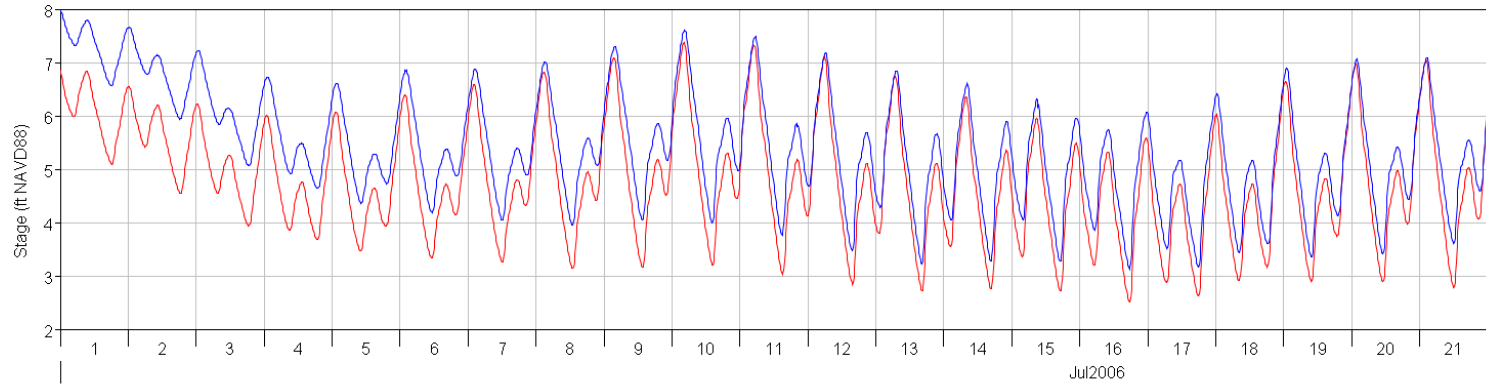
RRI - SJR at Rough-n-Ready



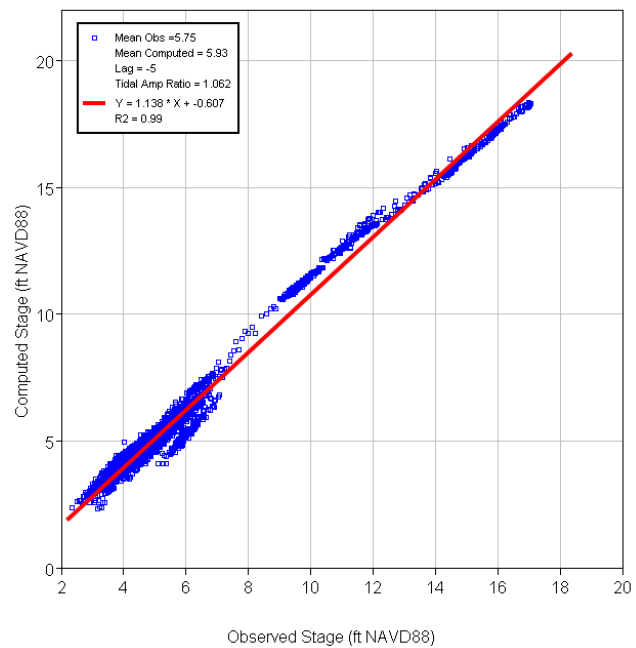
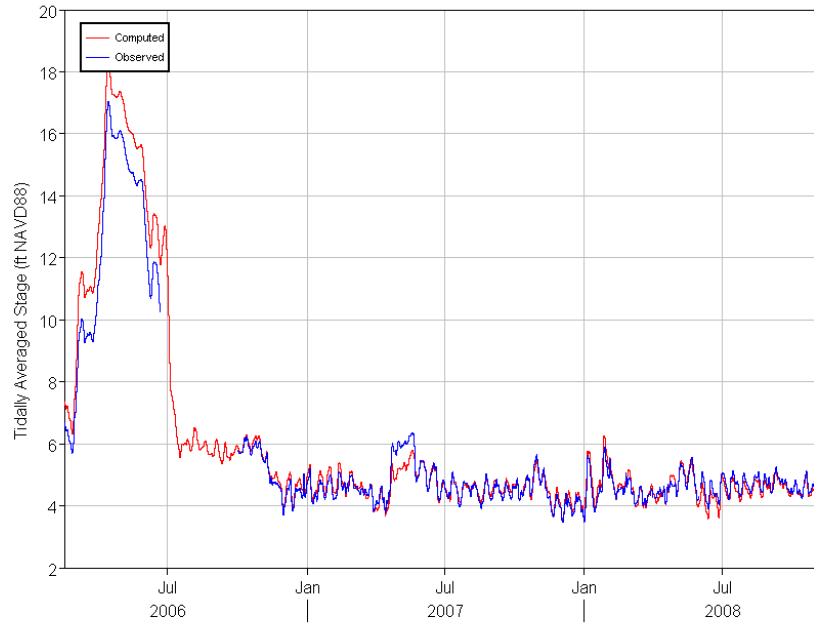
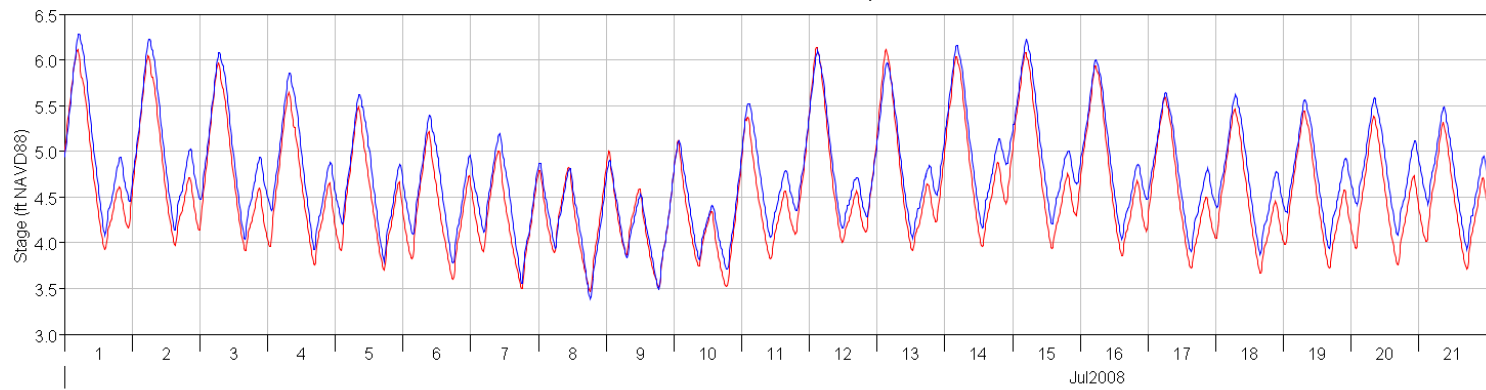
SJG - San Joaquin River at Garwood



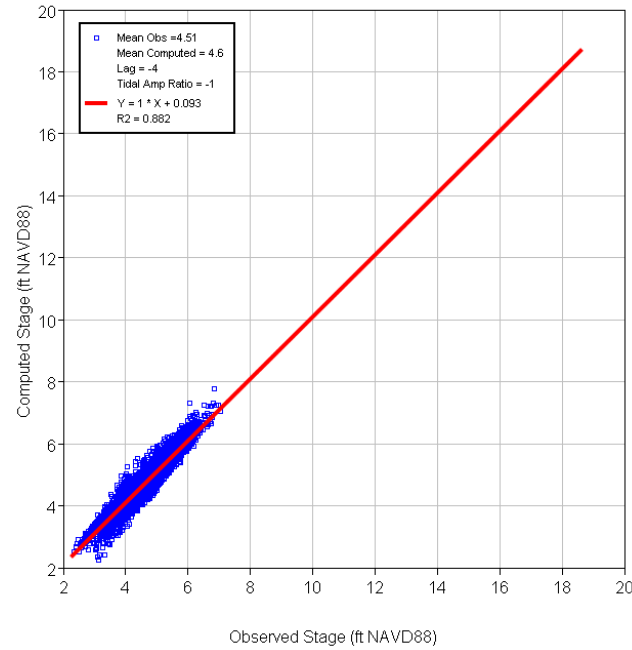
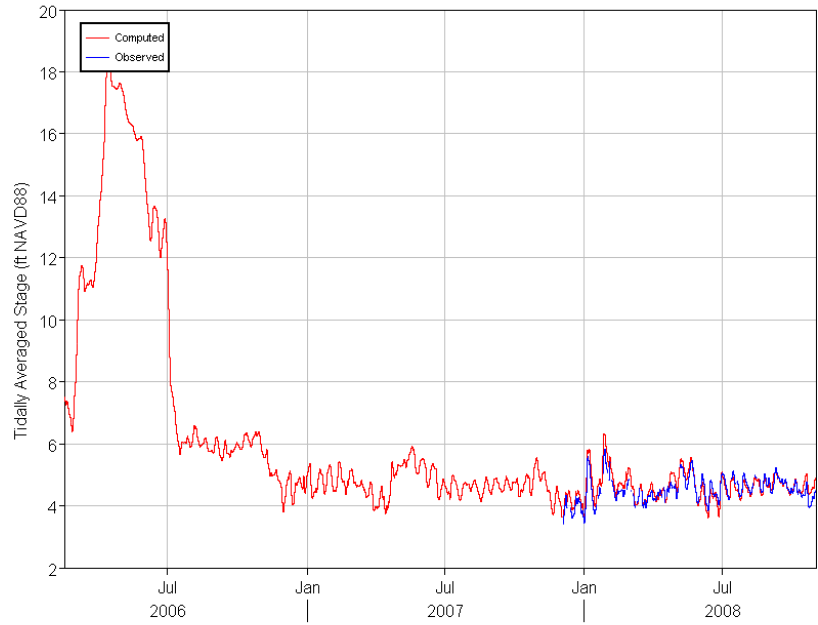
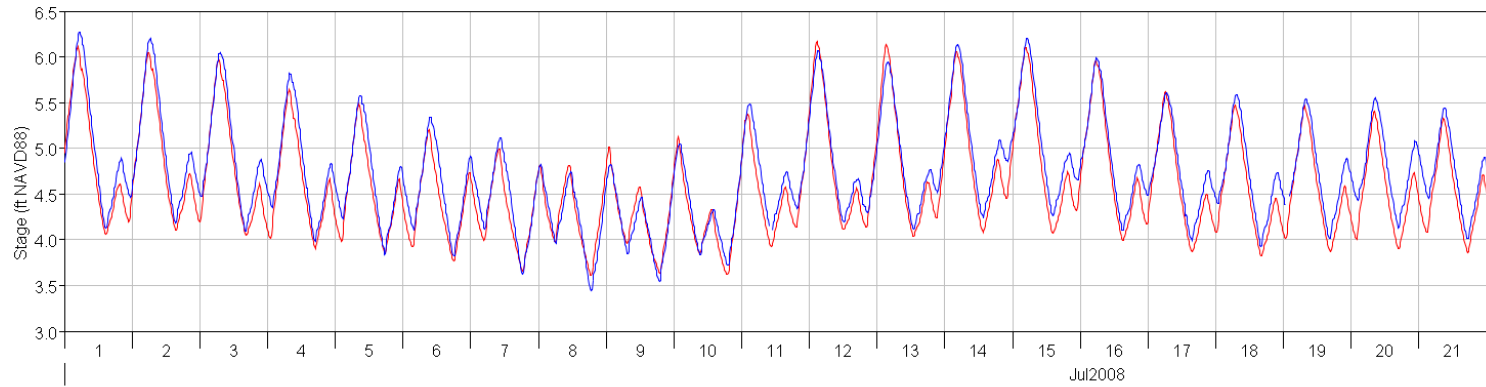
BDT - SJR at Brandt Bridge



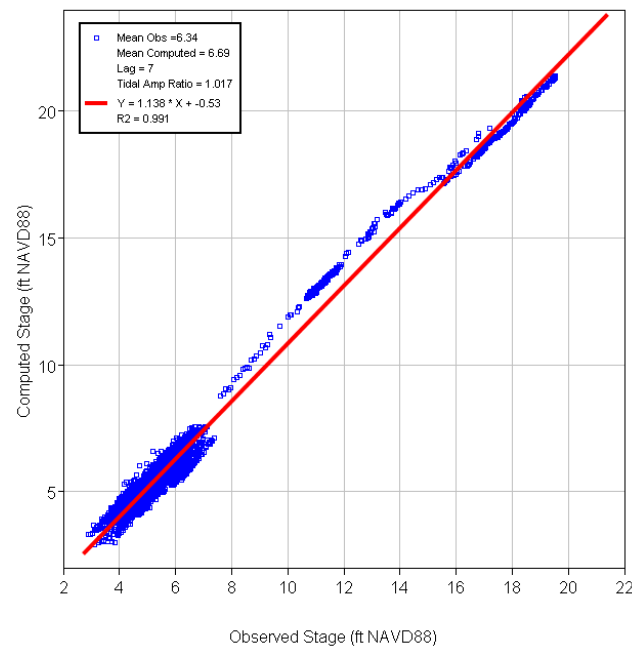
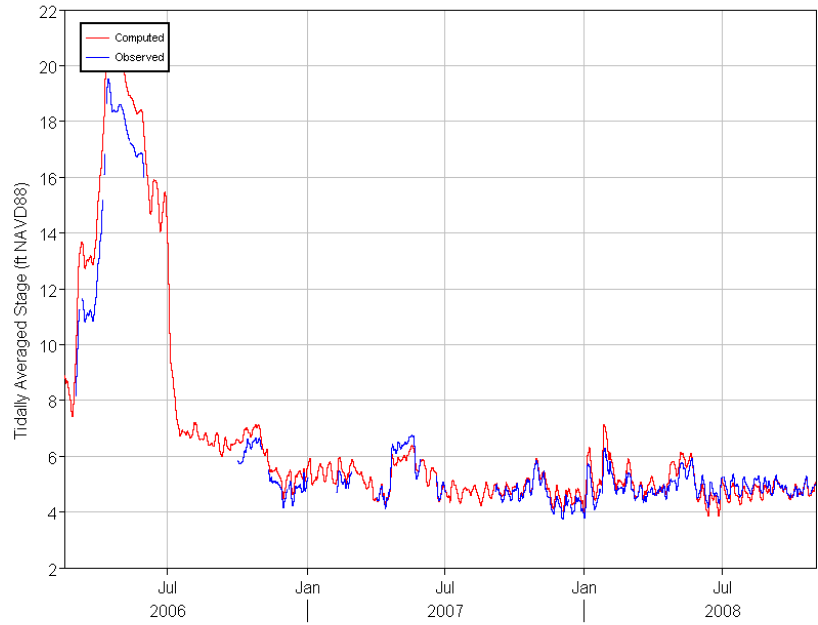
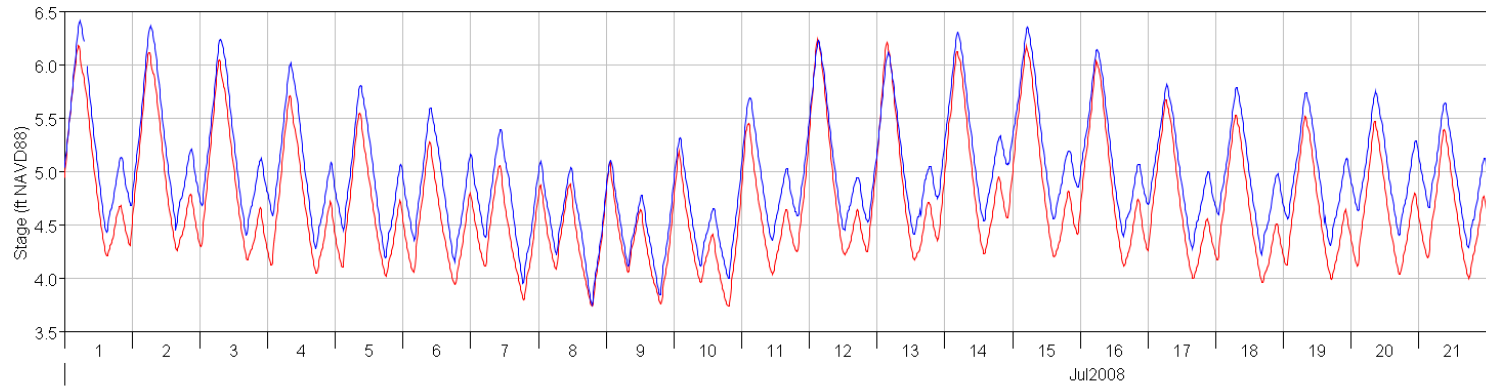
SJL - SJR near Lathrop



OH1 - Old River at Head



MSD - SJR at Mossdale



Appendix D: Individual Isohaline Regression Plots

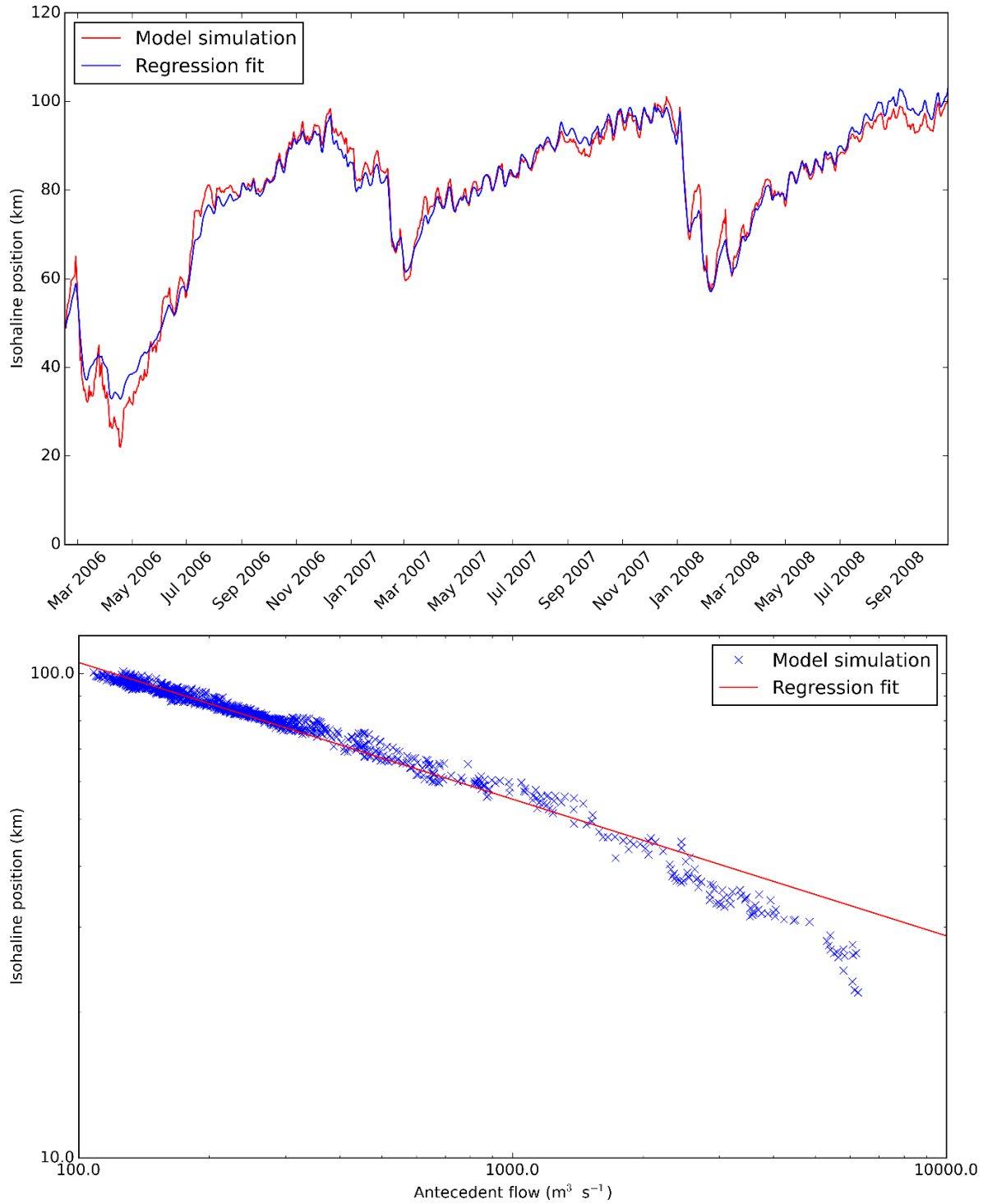


Figure 75 Contemporary system simulation 1 psu surface salinity regression and hydrodynamic model time series comparison (top) and regression fit (bottom). Model-calculated outflow at Martinez is used for the independent outflow variable, Q .

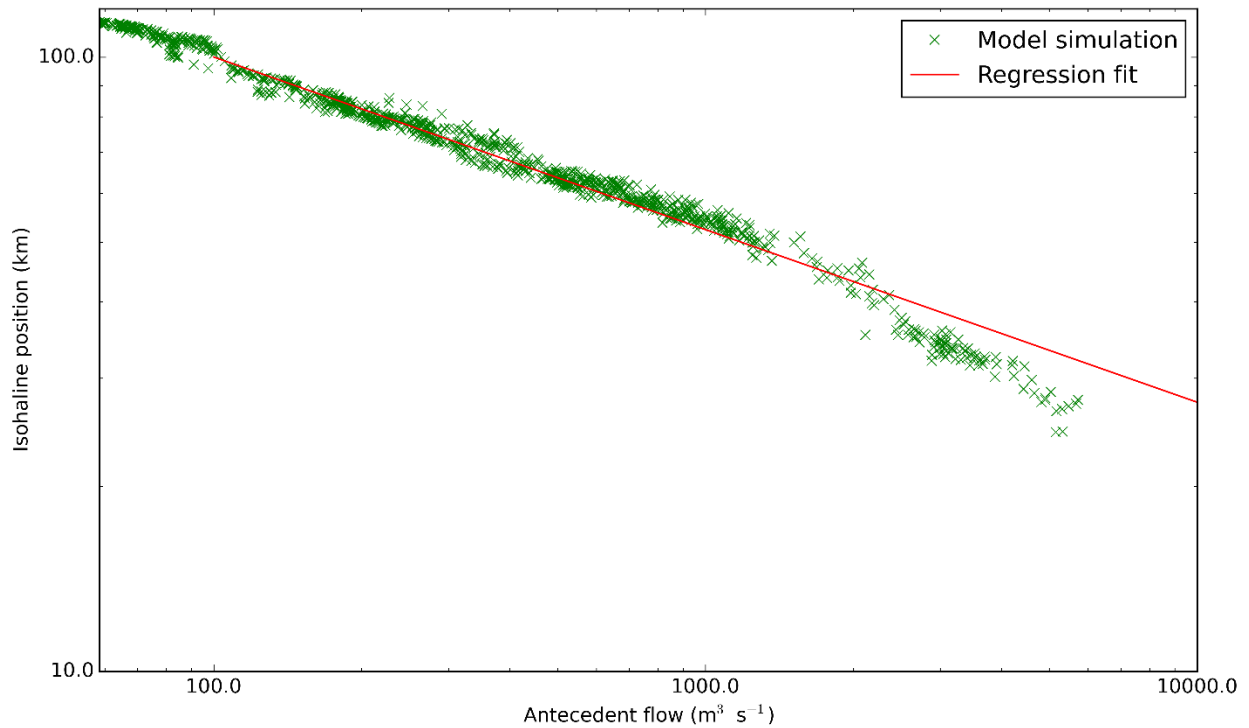
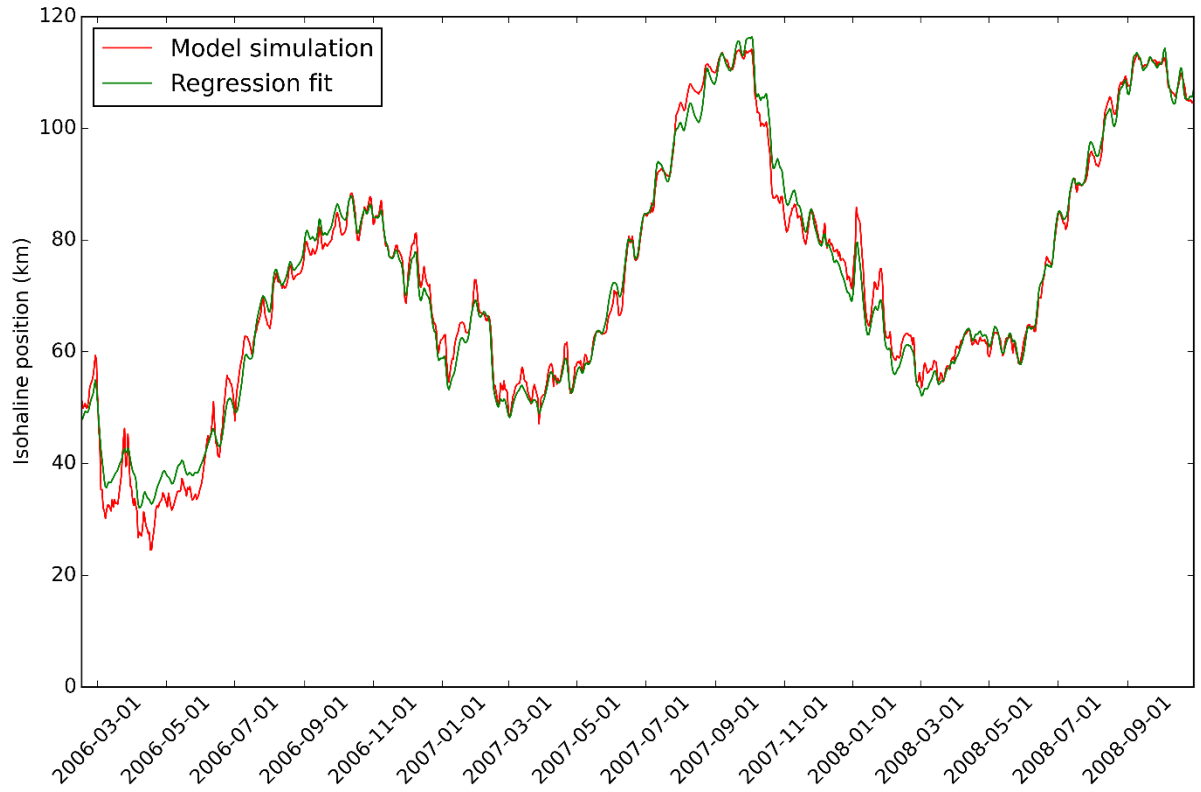


Figure 76 Pre-development system simulation 1 psu surface salinity regression and hydrodynamic model time series comparison (top) and regression fit (bottom). Model-calculated outflow at Martinez is used for the independent outflow variable, Q .

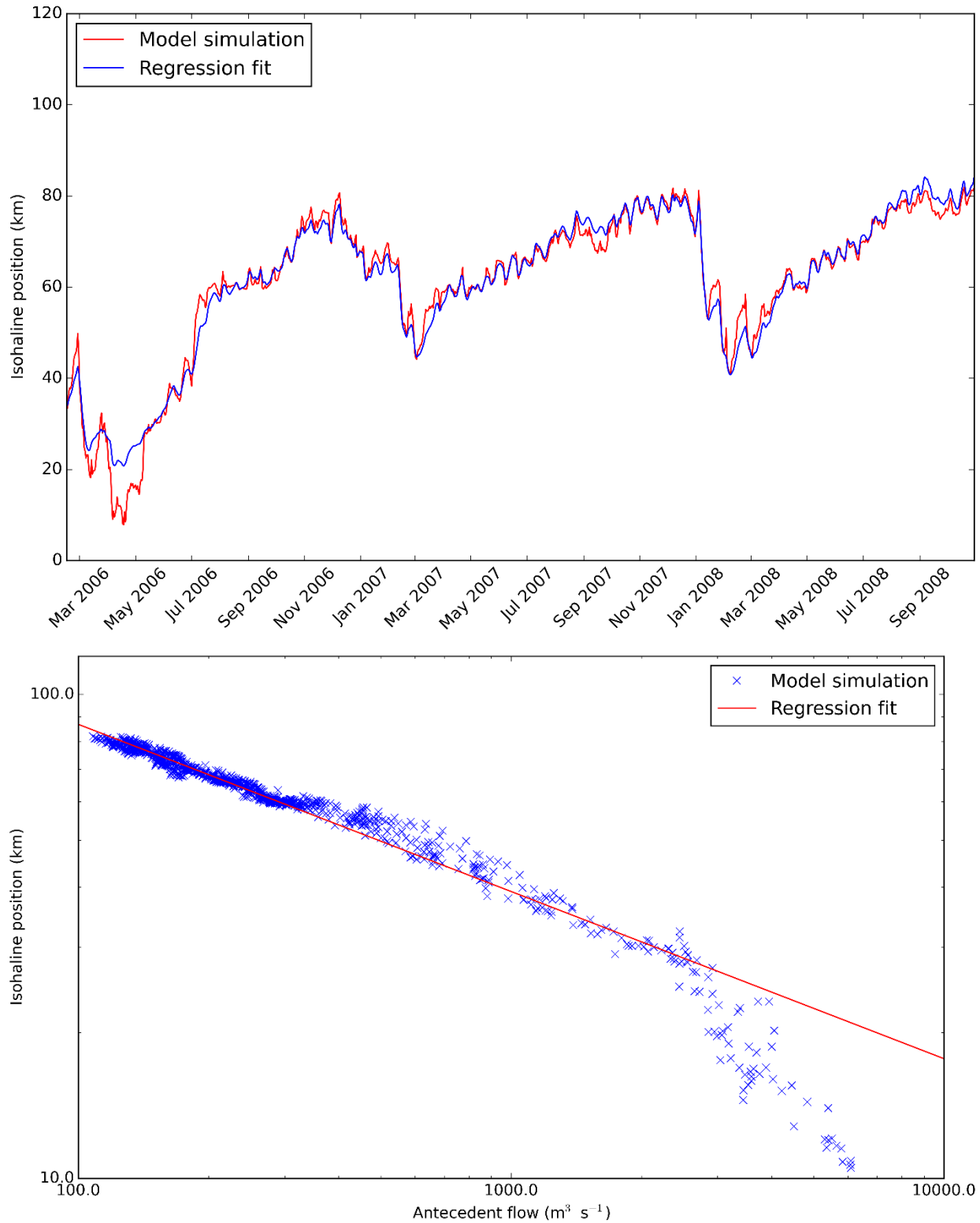


Figure 77 Contemporary system simulation 6 psu surface salinity regression and hydrodynamic model time series comparison (top) and regression fit (bottom). Model-calculated outflow at Martinez is used for the independent outflow variable, Q .

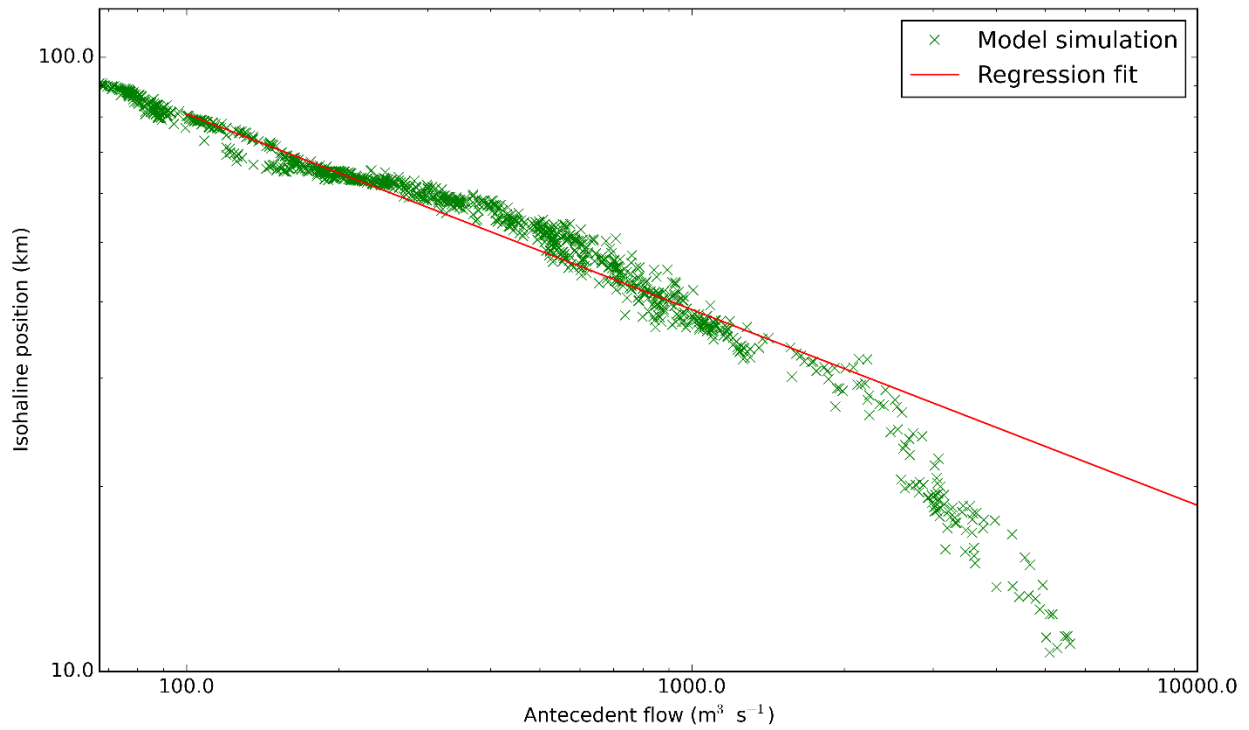
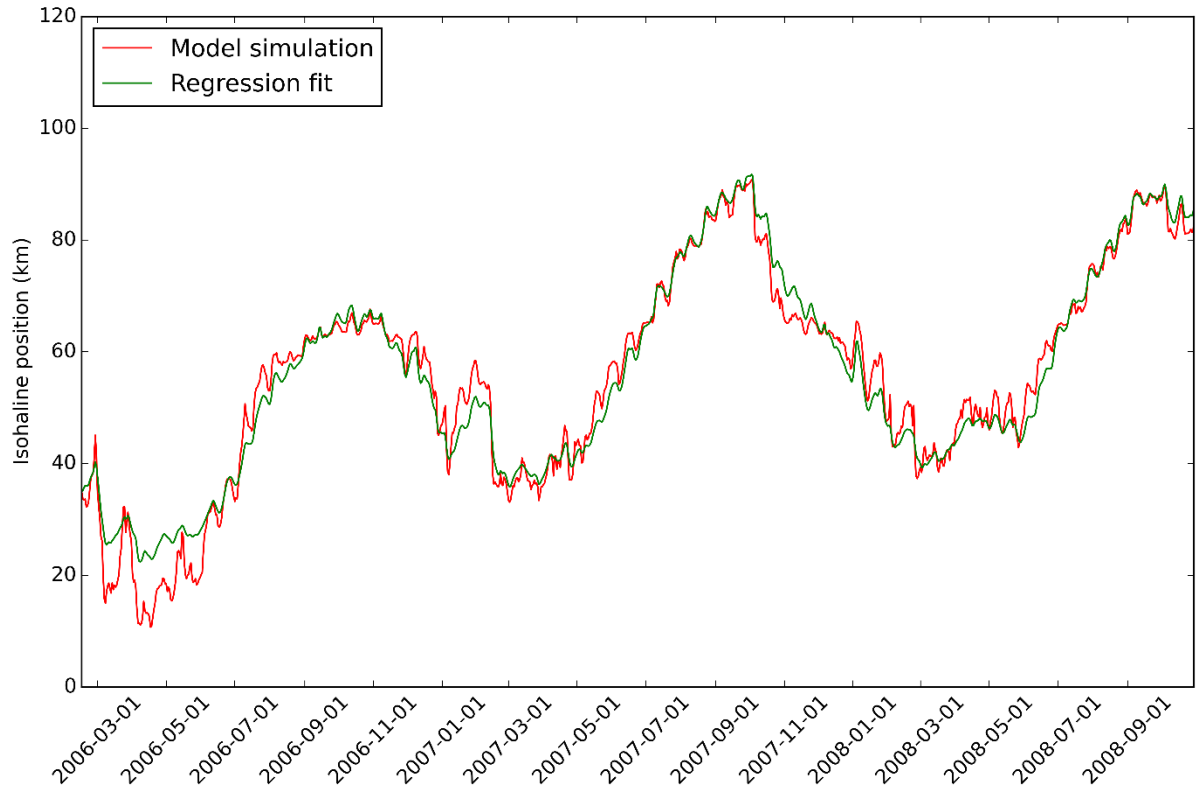


Figure 78 Pre-development system simulation 6 psu surface salinity regression and hydrodynamic model time series comparison (top) and regression fit (bottom). Model-calculated outflow at Martinez is used for the independent outflow variable, Q .

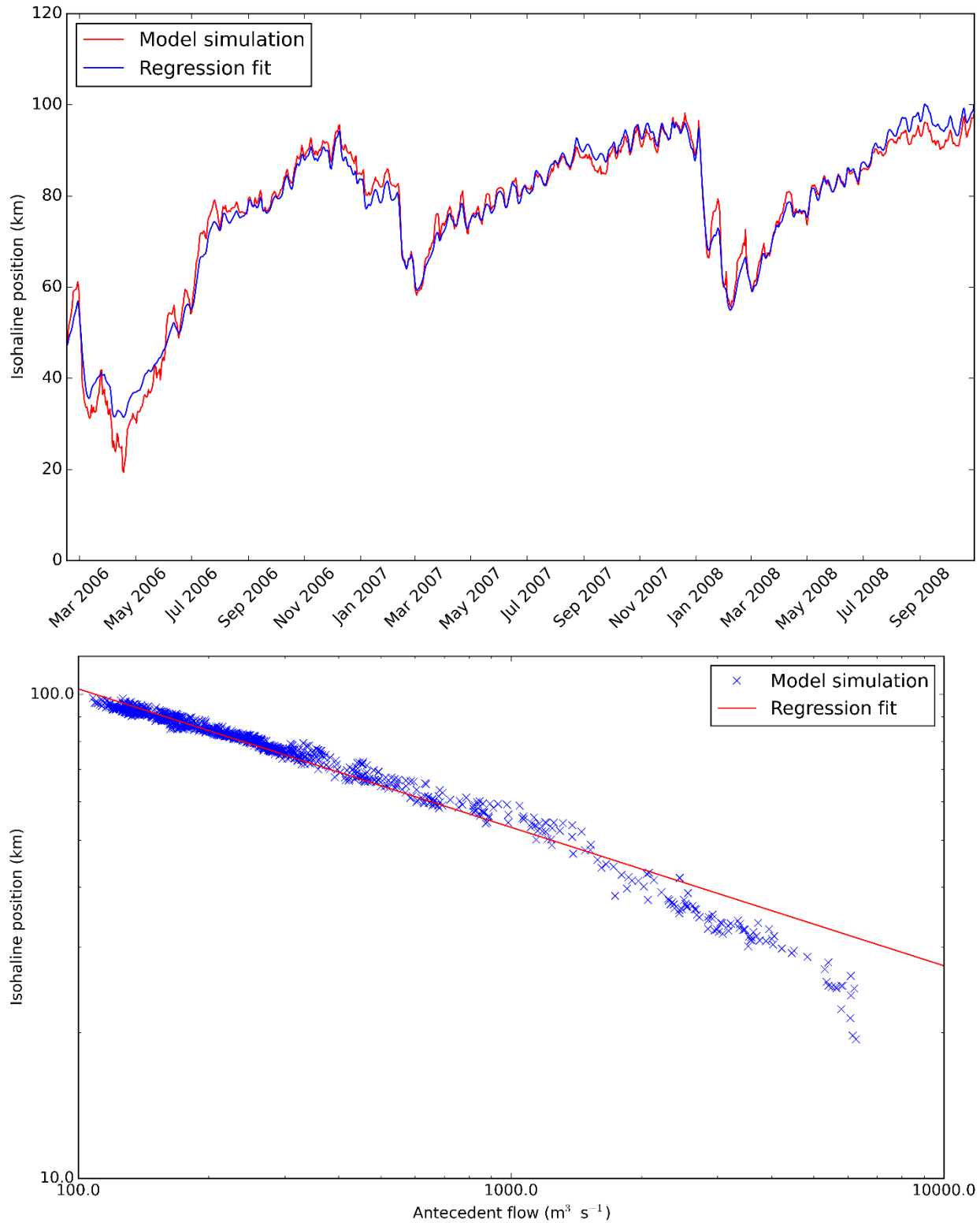


Figure 79 Contemporary system simulation 2.64 mS/cm surface EC regression and hydrodynamic model time series comparison (top) and regression fit (bottom). Model-calculated outflow at Martinez is used for the independent outflow variable, Q .

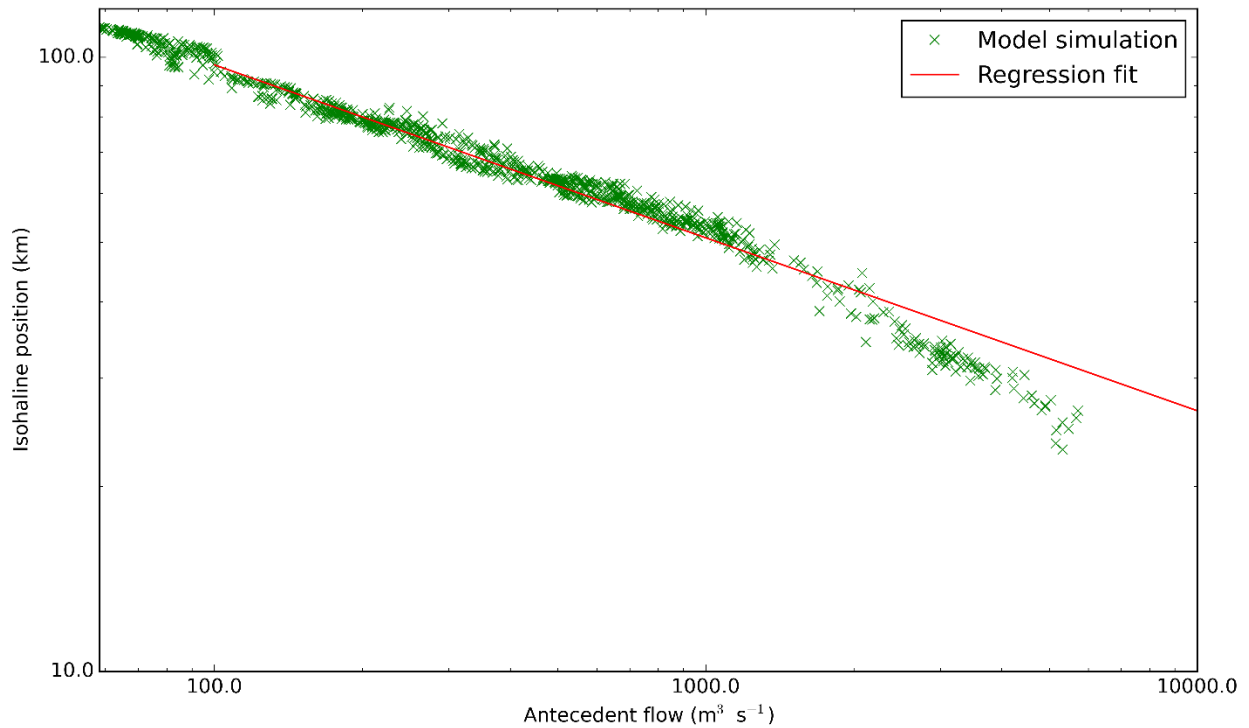
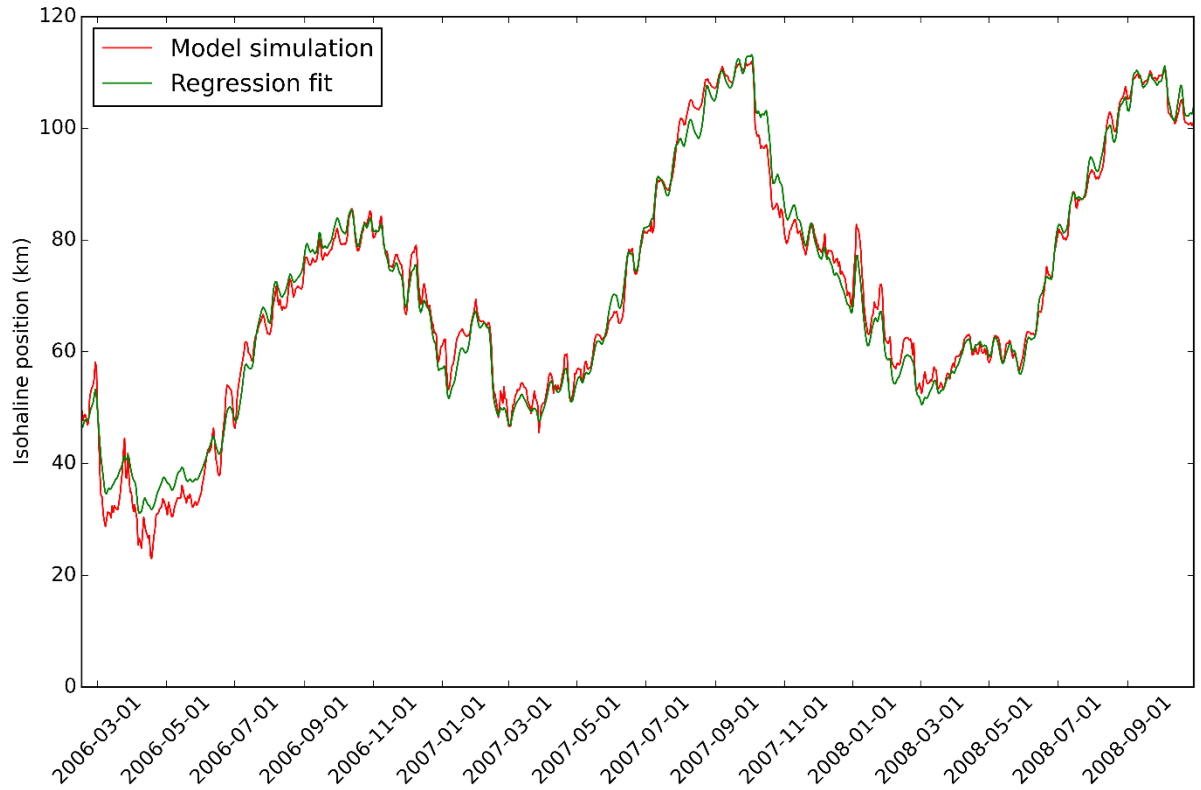


Figure 80 Pre-development system simulation 2.64 mS/cm surface EC regression and hydrodynamic model time series comparison (top) and regression fit (bottom). Model-calculated outflow at Martinez is used for the independent outflow variable, Q .